

N O T I C E

THIS DOCUMENT HAS BEEN REPRODUCED FROM
MICROFICHE. ALTHOUGH IT IS RECOGNIZED THAT
CERTAIN PORTIONS ARE ILLEGIBLE, IT IS BEING RELEASED
IN THE INTEREST OF MAKING AVAILABLE AS MUCH
INFORMATION AS POSSIBLE

(NASA-CR-169295) INVESTIGATIONS OF
FLOWFIELDS FOUND IN TYPICAL COMBUSTOR
GEOMETRIES Semiannual Status Report,
1 Feb. - 31 Jul. 1982 (Oklahoma State Univ.,
Stillwater.) 252 p HC A12/MF A01 CSCI 20D G3/34

N82-31643

Unclas
28848

INVESTIGATIONS OF FLOWFIELDS FOUND IN
TYPICAL COMBUSTOR GEOMETRIES

The Fourth Semi-Annual Status Report
to NASA-Lewis Research Center on
Grant NAG 3-74
Period: Feb. 1, 1982 to July 31, 1982



David G. Lilley

Principal Investigator

Professor
School of Mechanical and Aerospace Engineering
Oklahoma State University
Stillwater, OK 74078

NASA Technical Officer: Dr. J. D. Holdeman
Combustion Fundamentals Section

NASA Grants Officer: S. Szabo

INVESTIGATIONS OF FLOWFIELDS FOUND IN
TYPICAL COMBUSTOR GEOMETRIES

The Fourth Semi-Annual Status Report
to NASA-Lewis Research Center on
Grant NAG 3-74
Period: Feb. 1, 1982 to July 31, 1982

David G. Lilley

Principal Investigator

Professor
School of Mechanical and Aerospace Engineering
Oklahoma State University
Stillwater, OK 74078

NASA Technical Officer: Dr. J. D. Holdeman
Combustion Fundamentals Section

NASA Grants Officer: S. Szabo

ABSTRACT

Experimental and theoretical research is being undertaken on 2-D axisymmetric geometries under low speed, nonreacting, turbulent, swirling flow conditions. The flow enters the test section and proceeds into a larger chamber (the expansion ratio $D/d = 2$) via a sudden or gradual expansion (side-wall angle $\alpha = 90$ and 45 degrees). Inlet swirl vanes are adjustable to a variety of vane angles with values of $\phi = 0, 38, 45, 60$ and 70 degrees being emphasized.

This research is being funded by NASA Lewis Research Center and AF Wright Aeronautical Laboratories under Grant Number NAG 3-74 since July 1, 1980. The present document is the Fourth Semi-Annual Status Report and discussion is on those activities undertaken during the second half of the second year of the study. Section 1 of this document describes the recent activity, while Section 2 gives a brief summary of the present status and a list of recent publications. Appendices A through E contain an M.S. Thesis, two recent internal reports, and two recent AIAA papers.

TABLE OF CONTENTS

ABSTRACT.....	ii
1. <u>RECENT PROGRESS</u>	1
1.1 Time-Mean Velocity Measurements.....	1
1.2 Swirler Performance.....	2
1.3 Computational Studies.....	3
1.4 Hot-Wire Anemometry.....	5
1.5 Construction Activity.....	6
2. <u>PRESENT STATUS</u>	7
2.1 Summary.....	7
2.2 Publications.....	8
3. <u>APPENDICES</u>	
A. Five-Hole Pitot Probe Time-Mean Velocity Measurements in Confined Swirling Flows	
B. Annular Vane Swirler Performance	
C. Confined Swirling Flow Predictions: Effect of Swirl and Inlet Profile Assumptions	
D. Bluff-Body Flameholder Wakes: A Simple Numerical Solution	
E. Turbulence Measurements in a Confined Jet Using a Six-Orientation Hot-Wire Probe Technique	

1. RECENT PROGRESS

New features of the present year's study are: the turbulence measurements are being performed on swirling as well as nonswirling flow; and all measurements and computations are also being performed on a confined jet flowfield with realistic downstream blockage. Recent activity in the research program falls into three categories:

1. Time-mean flowfield characterization by five-hole pitot probe measurements and by flow visualization.
2. Turbulence measurements by a variety of single- and multi-wire hot-wire probe techniques.
3. Flowfield computations using the computer code developed during the previous year's research program.

During the last six months, students have drawn up six brief papers covering our studies.¹⁻⁶ They were supplied to the Contract Monitor with the April 1, 1982 newsletter. Three internal documents relating to degree requirements were successfully written, presented and approved by thesis committees.⁷⁻⁹ Hyung K. Yoon recently completed his M.S. Thesis,¹⁰ included here as Appendix A. Predictions resulting from very accurate inlet flow measurements⁵ (see Appendix B) are described and discussed in Ref. 11 (see Appendix C). Four ASME or AIAA conference papers were prepared for June 1982 meetings, the two most relevant of which are included in Appendices D and E.^{12,13}

1.1 Time-Mean Velocity Measurements

A recently completed M.S. Thesis¹⁰ investigated nonswirling and swirling flows (reaching higher swirl strengths than previously) in the test section. Later measurements included the effect of contraction nozzles of area ratio 2 and 4, located at two axial positions. The effects of several geometric

parameters on the flowfield were investigated including: side-wall expansion angle $\alpha = 90$ and 45 degrees, swirl vane angle $\phi = 0, 38, 45, 60,$ and 70 degrees, and contraction nozzle location $L/D = 1$ and 2 (if present). Data acquisition was via a five-hole pitot probe enabling three time-mean velocity components in the axial, radial and azimuthal directions to be measured. Velocities, yaw and pitch angles are extensively tabulated and plotted in a directly usable form. Artistic impressions of recirculation zones are then deducible. Full details are included in the M.S. Thesis included here as Appendix A.

Some results are now described briefly. The nonswirling confined jet possesses a corner recirculation zone extending to just beyond $x/D = 2$ with no central recirculation zone. The presence of a swirler shortens the corner recirculation zone and generates a central recirculation zone followed by a precessing vortex core. The effect of a gradual inlet expansion is to encourage the flow to remain close to the side wall and shorten the extent of the corner recirculation zone in all cases investigated. A contraction nozzle of area ratio 2 has little effect on weakly swirling and strongly swirling flows, which are dominated by forward flow and centrifugal forces, respectively. For the intermediate swirl case of $\phi = 45$ degrees, it encourages forward movement of otherwise slow-moving air and thereby shortens the central recirculating zone. A strong contraction nozzle of area ratio 4 has a more dramatic effect on the flowfields.

1.2 Swirler Performance

Five-hole pitot probe measurements have also been taken immediately downstream of the swirler, with expansion blocks removed, in contrast to earlier measurements which were made at the expansion plane located 3.2 cm further downstream. This study defines better the performance characteristics

of the swirler. Measurements of time-mean axial, radial and tangential velocities at the swirler exit plane for a range of blade swirl angles ϕ from 0 to 70 degrees show clearly the effects of centrifugal forces, recirculation zones, and blade stall on the combustor inlet velocity profiles. A brief paper⁵ describing these activities is included in Appendix B; more complete documentation is currently being drawn up. Results show that exit velocities are functions of radial and azimuthal parameters.

Assumptions of flat axial and swirl profiles with radial velocity equal to zero are progressively less realistic as the swirler blade angle increases. At moderate swirl $\phi = 45$ degrees, linearly increasing profiles of u and w with radius are appropriate with v nonzero. At strong swirl $\phi = 70$ degrees, even more spiked profiles are appropriate with most of the flow leaving the swirler near its outer edge. Nonaxisymmetry prevails in all swirl cases investigated.

1.3 Computational Studies

STARPIC is an advanced computer code developed earlier at Oklahoma State University to predict corresponding confined swirling flows to those studied experimentally. The calculation method includes a stairstep boundary representation of the expansion flow and a conventional $k-\epsilon$ turbulence model. The predictions include velocity profiles, recirculation zone characterization and mean streamline patterns. Currently, predictions are being made with the standard $k-\epsilon$ model and no downstream blockage. Predictions now include realistic inlet conditions for a complete range of swirl strengths (as described in Appendix B and other unpublished data), and results conform more realistically to measured flowfield velocities and streamline patterns. A full report¹¹ on these activities appears as Appendix C.

The appended report provides numerical predictions using various inlet velocity starting conditions for the case of swirl vane angle equal to 45 degrees. The validity of flowfield predictions resulting from the choice of inlet profiles is assessed by comparing the predicted velocity profiles with corresponding experimental velocity profiles. Results demonstrate that realistic predictions are forthcoming only from the inclusion of realistic axial, radial and swirl velocity profiles as inlet conditions, and that considerable errors occur if unrealistic idealized inlet conditions are used. Predictions are then exhibited for a range of swirl strengths ($\phi = 0, 38, 45, 60$ and 70 degrees) using measured inlet axial, radial and swirl velocity profiles in each case. The ensuing flowfields are characterized via velocity profiles and streamline patterns, and illustrate the large-scale effects of inlet swirl on flowfields.

Predictions of **downstream blockage** effects (two blockage sizes at two axial locations) have now been completed and these are being assessed in the light of the experimental data given in Appendix A. The amalgamation of a full report on these activities is currently underway.

Oblique to the main thrust of the present research program is application of the STARPIC code to MHD combustor flows, simple numerical solutions to the bluff-body flameholder wake problem, and prediction of 3-D turbulent flows. A brief research paper¹² on the second of these is included as Appendix D. There, numerical predictions are made of recirculation zones behind bluff-body flame stabilizers, showing quantitatively the effects of forebody geometry, blockage ratio, lateral position of the blockage and inlet swirl on the central recirculation zone. A simple transient Navier-Stokes solution algorithms and laminar flow simulation are used with 'free slip' and 'no slip' wall boundary conditions, thus illustrating how a basic approach may be used

to solve a sophisticated fluid dynamic problem. A 3-D turbulent version of this code is described in the research paper of Appendix D of the Third Semi-Annual Status Report. Turbulence is simulated by means the two-equation k- ϵ turbulence model; species diffusion and buoyancy are also included. Two applications of the code are presented to local destratification near the release structure of a reservoir and to the deflection of a jet entering normally into a uniform cross-flow. Predicted results exhibit good agreement with experimental data, showing that a useful characterization of fully three-dimensional flows is now available.

1.4 Hot-Wire Anemometry

Major attention has been given to application of the one-wire hot-wire technique in the present confined jet facility. Determination of all time-mean velocity components and all normal and shear Reynolds stresses results from the 6-orientation mean and fluctuating data at each flowfield location. The experiments are being performed to provide the information necessary for turbulence modeling development in the confined jet facility. Recently swirling flows have been investigated (with $\phi = 38$ and 45 degrees) and a research paper¹³ on the results, including the earlier nonswirling results, is included as Appendix E. Excellent cost-effective results are presented, with comparisons with independent data illustrating the reliability of the technique. Finally, a sensitivity analysis of the data reduction technique has been undertaken; it forms the major ingredient of an uncertainty analysis.

A new cross-wire probe is currently being used to make a more accurate evaluation of the turbulent shear stress than previously possible. This technique is being used for the nonswirling flow without downstream blockage, and is soon to be used with downstream blockage. These data will enable turbulent viscosity components to be deduced (from the turbulent stress vs.

mean velocity spatial gradients) and will aid the turbulence modeling aspects of the study.

A series of hot-wire measurements have been planned, using a three-wire, hot-wire probe with direct computer interface and data reduction. These measurements are to be performed by subcontractor Dynamics Technology, Inc., under the direction of Dr. Dennis K. McLaughlin. There, experiments are progressing behind schedule and recently a no-cost time extension to October 22, 1982 was agreed between them, Oklahoma State University and NASA Lewis Research Center. For this reason, no report on their activity is included in the present document, but copies will be distributed as soon as they are available.

1.5 Construction Activity

Dynamics Technology has been assembling for their subcontract and other activity a swirling jet facility which will duplicate the flowfield produced by the Oklahoma State University facility. However, it will be instrumented differently, with the three-wire hot-wire probe and its three-degree of freedom probe drive being major constituents. The complex probe drive, swirl pack and expansion blocks have been built by students at Oklahoma State University and loaned to the subcontractor for their experimentation.

2. PRESENT STATUS

2.1 Summary

During the second year of the present study, new features include:

1. Turbulence measurements are being performed on **swirling** as well as nonswirling flows.
2. The effect of size and location of a **downstream blockage** is being investigated.

Successful studies include:

1. Flow visualization.
2. Five-hole pitot probe measurements.
3. Single-wire and multi-wire hot-wire measurements.
4. Flowfield computations from realistic inlet conditions.

Proposed future studies include:

1. Expansion Ratio $D/d = 1.5$ - in addition to the $D/d = 2$ value currently being used, including flow visualization, time-mean velocity and normal and shear turbulent Reynolds stress measurements.
2. Corresponding Predictions - using advanced turbulence modeling developments.
3. Inlet Turbulence Level - effects to be clarified via flow visualization, and some time-mean and turbulent stress measurements, for a swirling flowfield.
4. Turbulence Length Scale - to be measured with one and/or two hot-wire probes, in nonswirling and one swirling flow.
5. Turbulence Model Developments - in the light of on-going activity both at Oklahoma State University and elsewhere.

The completion of these tasks, and the accomplishment of the goals and objectives of the grant will make a substantial contribution to the understanding and prediction capability of complex turbulent flows.

2.2 Publications

The following list of publications covers research conducted with the support of the grant, and does **not** include those listed in previous Semi-Annual Reports:

1. Abujelala, M. T., Confined Swirling Flow Predictions: Effect of Inlet Velocity Assumption. Proceedings of 13th Southwestern Graduate Research Conference in Applied Mechanics, held at the University of Oklahoma, Norman, OK, on April 16-17, 1982, pp. 267-273.
2. Busnaina, A. A., Turbulent Three-Dimensional Flowfield Predictions. Ibid, pp. 17-23.
3. Jackson, T. W., A Single Hot-Wire Technique for Swirling Flows. Ibid, pp. 260-266.
4. McKillop, B. E., Crossed Hot-Wire Anemometry in Turbulent Flows. Ibid, pp. 11-16.
5. Sander, G. F., Annular Vane Swirler Performance. Ibid, pp. 274-280.
6. Yoon, H. K., Five-Hole Pitot Probe Time-Mean Velocity Measurements in a Combustor Flowfield. Ibid, pp. 131-137.
7. Abujelala, M. T., Turbulence Models and Swirling Flow Prediction. Ph.D. Preliminary Write-Up, MAE, Oklahoma State University, June 1982.
8. Jackson, T. W., Turbulence Measurements in Axisymmetric Combustor Geometries. Ph.D. Preliminary Write-Up, MAE, Oklahoma State University, June 1982.
9. Busnaina, A. A., Transient Three-Dimensional Predictions of Turbulent Flows in Cylindrical and Cartesian Coordinate Systems. Ph.D. Qualifying Write-Up, MAE, Oklahoma State University, June 1982.

10. Yoon, H. K., Five-Hole Pitot-Probe Time-Mean Velocity Measurements in Confined Swirling Flows, M.S. Thesis, MAE, Oklahoma State University, July 1982.
11. Abujelala, M. T. and Lilley, D. G., Confined Swirling Flow Predictions: Effect of Swirl and Inlet Profile Assumptions, Report, MAE, Oklahoma State University, June 1982.
12. Vatistas, G. H., Lin, S., Kwok, C. K. and Lilley, D. G., Bluff-Body Flameholder Wakes: A Simple Numerical Solution. Paper AIAA-82-1177, Cleveland, OH, June 21-23, 1982.
13. Janjua, S. I., McLaughlin, D. K., Jackson, T. W. and Lilley, D. G., Turbulence Measurements in a Confined Jet Using a Six-Orientation Hot-Wire Probe Technique. Paper AIAA 82-1262, Cleveland, OH, June 21-23, 1982.

APPENDIX A

**FIVE-HOLE PITOT PROBE TIME-MEAN VELOCITY
MEASUREMENTS IN CONFINED SWIRLING FLOWS**

FIVE-HOLE PITOT PROBE TIME-MEAN VELOCITY
MEASUREMENTS IN CONFINED SWIRLING FLOWS

By

HYUNG KEE YOON

Bachelor of Engineering

Korea University

Seoul, Korea

1980

Submitted to the Faculty of the Graduate College
of the Oklahoma State University
in partial fulfillment of the requirements
for the Degree of
MASTER OF SCIENCE
July, 1982

Name: Hyung Kee Yoon

Date of Degree: July, 1982

Institution: Oklahoma State University Location: Stillwater, Oklahoma

Title of Study: FIVE-HOLE PITOT PROBE TIME-MEAN VELOCITY MEASUREMENTS
IN CONFINED SWIRLING FLOWS

Pages in Study: 151

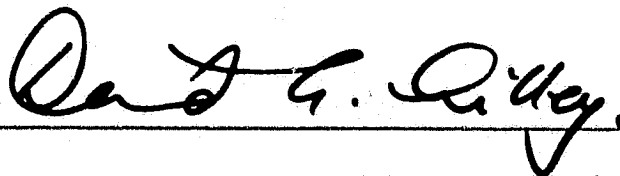
Candidate for Degree of Master of Science

Major Field: Mechanical Engineering

Scope and Method of Study: Nonswirling and swirling nonreacting flows are investigated in an axisymmetric test section with expansion ratio $D/d = 2$, which may be equipped with a contraction nozzle of area ratio 2 and 4. The effects of several geometric parameters on the flowfield are investigated including: side-wall expansion angle $\alpha = 90$ and 45 degrees, swirl vane angle $\phi = 0, 38, 45, 60,$ and 70 degrees, and contraction nozzle location $L/D = 1$ and 2 (if present). Data acquisition is via a five-hole pitot probe enabling three time-mean velocity components in the axial, radial and azimuthal directions to be measured. Velocities, yaw and pitch angles are extensively tabulated and plotted in a directly usable form. Artistic impressions of recirculation zones are then deducible.

Findings and Conclusions: The nonswirling confined jet possesses a corner recirculation zone extending to just beyond $x/D = 2$ with no central recirculation zone. The presence of a swirler shortens the corner recirculation zone and generates a central recirculation zone followed by a precessing vortex core. The effect of a gradual inlet expansion is to encourage the flow to remain close to the side wall and shorten the extent of the corner recirculation zone in all cases investigated. A contraction nozzle of area ratio 2 has little effect on weakly swirling and strongly swirling flows, which are dominated by forward flow and centrifugal forces, respectively. For the intermediate swirl case of $\phi = 45$ degrees, it encourages forward movement of otherwise slow-moving air and thereby shortens the central recirculating zone. A strong contraction nozzle of area ratio 4 has a more dramatic effect on the flowfields.

ADVISER'S APPROVAL



FIVE-HOLE PITOT PROBE TIME-MEAN VELOCITY
MEASUREMENTS IN CONFINED SWIRLING FLOWS

Thesis Approved:

David G. Ridley

Thesis Adviser

Pete W. Moore

A. J. Ghajjar

Dean of the Graduate College

ACKNOWLEDGMENTS

The author wishes to express his sincere gratitude to his major adviser, Dr. David G. Lilley for his guidance and encouragement. Appreciation is also extended to other committee members, Dr. Peter M. Moretti and Dr. Afshin J. Ghajar.

The author would like to extend a special thank you to Dr. Sherry Southard for reading the manuscripts, Miss Moonsook Choi for typing the rough draft, and Mrs. Barbara Vick for typing the final copy.

The author also wishes to gratefully acknowledge NASA Lewis Research Center for financial support under NASA Grant No. NAG 3-74.

This study is dedicated to the author's parents, Mr. In Shik and Mrs. Chil Sung Yoon, for their encouragement, prayer and love.

TABLE OF CONTENTS

Chapter	Page
I. INTRODUCTION	1
1.1 The Investigation of the Flowfield in a Confined Jet	1
1.2 Review of Previous Flowfield Measurement Studies	2
1.3 Flowfield Independence of Reynolds Number	4
1.4 The Scope and Significance of the Present Research	5
1.5 Outline of the Thesis	6
II. EXPERIMENTAL FACILITIES AND FIVE-HOLE PITOT PROBE INSTRUMENTATION	8
2.1 An Idealized Flowfield	8
2.2 Test Section	9
2.3 Five-Hole Pitot Probe Instrumentation	10
2.4 Swirler	12
III. MEASUREMENT AND REDUCTION OF DATA	14
3.1 Measurement Procedures	14
3.2 Calibrations	16
3.3 Data Reduction	17
IV. RESULTS	20
4.1 Effects of Swirl on Sudden Expansion Flows	20
4.2 Effects of Gradual Expansion on Flows	23
4.3 Effects of Contraction Nozzle on Flows	23
V. CLOSURE	27
5.1 Summary	27
5.2 Recommendations for Further Work	28
REFERENCES	31
APPENDIX A - TABLES	34
APPENDIX B - FIGURES	96
APPENDIX C - USER'S GUIDE TO FIVE-HOLE PITOT PROBE DATA REDUCTION COMPUTER PROGRAM	135

LIST OF TABLES

Table	Page
I. Nozzle Inlet Velocities and Reynolds Numbers	35
II. Velocity Data for Nonswirling Flow $\phi = 0^\circ$	36
III. Velocity Data for Swirl Vane Angle $\phi = 38^\circ$ [Side-Wall Expansion Angle $\alpha = 90^\circ$ Without Contraction Block] . . .	41
IV. Velocity Data for Swirl Vane Angle $\phi = 45^\circ$ [Side-Wall Expansion Angle $\alpha = 90^\circ$ Without Contraction Block] . . .	46
V. Velocity Data for Swirl Vane Angle $\phi = 60^\circ$ [Side-Wall Expansion Angle $\alpha = 90^\circ$ Without Contraction Block] . . .	51
VI. Velocity Data for Swirl Vane Angle $\phi = 70^\circ$ [Side-Wall Expansion Angle $\alpha = 90^\circ$ Without Contraction Block] . . .	56
VII. Velocity Data for Nonswirling Flow $\phi = 0^\circ$ [Side-Wall Expansion Angle $\alpha = 90^\circ$ with Contraction Block at $L/D = 1$]	61
VIII. Velocity Data for Nonswirling Flow $\phi = 0^\circ$ [Side-Wall Expansion Angle $\alpha = 90^\circ$ with Contraction Block at $L/D = 2$]	66
IX. Velocity Data for Swirl Vane Angle $\phi = 45^\circ$ [Side-Wall Expansion Angle $\alpha = 90^\circ$ with Contraction Block at $L/D = 1$]	71
X. Velocity Data for Swirl Vane Angle $\phi = 45^\circ$ [Side-Wall Expansion Angle $\alpha = 90^\circ$ with Contraction Block at $L/D = 2$]	76
XI. Velocity Data for Swirl Vane Angle $\phi = 70^\circ$ [Side-Wall Expansion Angle $\alpha = 90^\circ$ with Contraction Block at $L/D = 1$]	81
XII. Velocity Data for Swirl Vane Angle $\phi = 70^\circ$ [Side-Wall Expansion Angle $\alpha = 90^\circ$ with Contraction Block at $L/D = 2$]	86
XIII. Characteristics of Flowfields in Terms of the Effects of Swirl Vane Angle for Side-Wall Expansion Angle $\alpha = 90^\circ$.	91

Table		Page
XIV.	Sample Alphanumeric Headings	92
XV.	Sample Calibration Data	93
XVI.	Sample Measurement Data	94
XVII.	Sample Auxiliary Geometric Quantity Output	95

LIST OF FIGURES

Figure	Page
1. Typical Axisymmetric Gas Turbine Combustion Chamber	97
2. Schematic of Overall Flow Facility	98
3. Dynamic Pressure Conversion Characteristic	99
4. Contraction Block	100
5. Apparatus for Mean Velocity Measurements	101
6. Swirler	102
7. Velocity Components and Flow Direction Angles Associated with Five-Hole Pitot Measurements	103
8. Calibration Apparatus	104
9. Voltage Output Calibration Characteristic for Voltmeter . . .	105
10. Calibration Characteristics for Five-Hole Pitot Probe	106
11. Flowfield Independence of Reynolds Number for Side-Wall Ex- pansion Angle $\alpha = 90^\circ$ and Swirl Vane Angle $\phi = 45^\circ$ at Axial Station $x/D = 0.5$	107
12. Velocity Profiles for Side-Wall Expansion Angle $\alpha = 90^\circ$ Without Contraction Block	108
13. Velocity Profiles for Side-Wall Expansion Angle $\alpha = 45^\circ$ Without Contraction Block	113
14. Velocity Profiles for Swirl Vane Angle $\phi = 0^\circ$ with Contraction Block	118
15. Velocity Profiles for Swirl Vane Angle $\phi = 45^\circ$ with Contraction Block	120
16. Velocity Profiles for Swirl Vane Angle $\phi = 70^\circ$ with Contraction Block	122
17. Repeatability of Five-Hole Pitot Probe Measurement for Side- Wall Expansion Angle $\alpha = 90^\circ$ and Swirl Vane Angle $\phi = 45^\circ$ with Contraction Block at $L/D = 2$ at $x/D = 1.0$	124

Figure	Page
18. Velocity Profiles for Swirl Vane Angle $\phi = 0^\circ$ with Strong Contraction Nozzle	125
19. Velocity Profiles for Swirl Vane Angle $\phi = 45^\circ$ with Strong Contraction Nozzle	127
20. Velocity Profiles for Swirl Vane Angle $\phi = 70^\circ$ with Strong Contraction Nozzle	129
21. Artistic Impressions of Dividing Streamlines Without Contraction Block for Side-Wall Expansion Angle $\alpha = 90^\circ$ and Swirl Vane Angle: (a) $\phi = 0^\circ$, (b) $\phi = 45^\circ$, and (c) $\phi = 0^\circ$	131
22. Artistic Impressions of Dividing Streamlines with Contraction Block at $L/D = 2.0$ for Side-Wall Expansion Angle $\alpha = 90^\circ$ and Swirl Vane Angle: (a) $\phi = 0^\circ$, (b) $\phi = 45^\circ$, and (c) $\phi = 70^\circ$	132
23. Artistic Impressions of Dividing Streamlines with Strong Contraction Block at $L/D = 2.0$ for Side-Wall Expansion Angle $\alpha = 90^\circ$ and Swirl Vane Angle: (a) $\phi = 0^\circ$, (b) $\phi = 45^\circ$, and (c) $\phi = 70^\circ$	133
24. Flow Chart of Data Reduction Computer Program	134

NOMENCLATURE

C	velocity coefficient = $\rho V^2 / [2(P_C - P_W)]$
CRZ	corner recirculation zone
CRTZ	central recirculation zone
D	test section diameter
d	inlet nozzle diameter
G	axial flux of momentum
L	contraction block station
P	time-mean pressure
Re	Reynolds number
Q	volume flow rate
S	swirl number
$\underline{v} = (u, v, w)$	time-mean velocity (in x-, r-, θ -directions)
V, \bar{V}	time-mean vector velocity magnitude
x, r, θ	axial, radial, azimuthal cylindrical polar coordinates
α	side-wall expansion angle
β	yaw angle of probe = $\tan^{-1} (w/u)$
δ	pitch angle of probe = $\tan^{-1} [v/(u^2 + w^2)^{1/2}]$
ρ	density
ϕ	swirl vane angle = $\tan^{-1} (w_{in}/u_{in})$, assuming perfect vanes; general dependent variable $_{in}$

Subscripts

C central pitot pressure port

d relating to inlet nozzle diameter
in inlet conditions
N,S,E,W north, south, east, west pitot pressure ports
o value at inlet to flowfield
h swirl vane hub; expansion step height
p relating to probe sensing tip diameter
rms root-mean-squared quantity

Superscripts

 time mean average
' fluctuating quantity

CHAPTER I

INTRODUCTION

1.1 The Investigation of the Flowfield in a Confined Jet

A need for more thorough understanding of the fluid dynamics of the flow in a gas turbine combustor chamber has been recognized by designers in recent years. The flowfield is presently being investigated using various methods of approach, such as computer simulation (1-5), flow visualization (5-6) and time-mean velocity measurements (7-14) for both swirling and nonswirling flows.

Until recently, extensive and reliable experimental data for swirling flow have been unavailable, and more experimental data are needed. Such data together with combustion characteristics would be very useful to designers as well as to theoretical investigators who could compare the experimental data with the data obtained from the simulated mathematical methods.

Current research focuses on measuring time-mean velocity and investigating the extent of the recirculation zone (known to have great effects on flame stability and length) and the effects of geometric parameters on the flowfield in a confined can-type gas turbine combustor.

In order to study the flow phenomena in the combustor, it is necessary not only to know the static pressure and flow velocity, but also the flow direction. In addition, the sensing probe must be sufficiently

small to be capable of point measurement without appreciably affecting the flow in the passages by its presence. In these experiments, the five-hole pitot probe was used because it is acutely sensitive to flow, convenient to manipulate and relatively compact. Measurements were taken for nonswirling and swirling flow with and without a contraction block in an axisymmetrical confined jet facility simulating typical geometry. All flowfields were nonreacting.

1.2 Review of Previous Flowfield Measurement Studies

Lee and Ash (7) developed and calibrated a three-dimensional spherical pitot probe which would measure the static pressure and the magnitude and direction of the velocity vector for any arbitrary flow angle without needing to be adjusted. It was designed mainly for measuring the relative flow through rotating three-dimensional blade cascades.

An investigation of flow patterns in the gas turbine combustion chamber with a three-dimensional probe was done by Hiett and Powell (8) in the early nineteen sixties. They found that there is a large recirculation zone between the main flow along the centerline and the second flow along the chamber wall, and that there is a high temperature zone in this area.

Janjua (9) measured three velocity components and turbulence levels for nonswirling flows with the six-orientation hot-wire technique. An uncertainty analysis done on this technique reveals that turbulence intensities and shear stresses are extremely sensitive to some input parameters such as yaw factor and mean voltages.

Velocity distribution in a sudden expanding circular duct was

investigated by Moon and Rudinger (10) with a Laser-Doppler velocimeter. These experiments located both the dividing streamline, which separates the main flow from the recirculation region, and the point of the flow reversal in the recirculation region.

Chaturvedi (11) measured the mean velocity and pressure and the characteristics of the turbulence by using a stagnation tube and pitot probe in a can-type axisymmetric expansion combustor for isothermal nonswirling flowfields. His data will be compared with the current research results because of the close geometric similarity and experimental conditions. Furthermore, in his experiment a single and cross-hot wire were used to measure the longitudinal component of turbulence intensity, u'_{rms} , radial intensity, v'_{rms} , and turbulent shear stress, $\overline{u'v'}$.

Systematic research of swirl was done by Mathur and MacCallum (12). The test facilities which they used for the free jet consisted of two concentric tubes with supplies of air to both the central (primary) and annular (secondary) streams. They used a three-dimensional probe to measure the velocity components in the three-dimensional flow. They measured the pressure drop across the vane swirler by both experimental work and theoretical analysis. They also investigated the distribution of the static pressure along the axis of the jets and the variations of the velocity distributions in the tube according to the change of swirl vane angle in the free jet. Mathur and MacCallum (12) followed the same procedure in the experiments for the enclosed jets as for the free jets and observed similar physical characteristics for the flows according to geometric changes. They determined that a large central recirculation exists along the axis in the swirling free and confined jets. A combustion chamber of square cross-section was used.

Pratte and Keffer (14) have investigated a swirling jet having a moderate ratio of swirling to axial momentum. They showed that the flow achieved a self similarity for the mean velocities rather quickly while the normal turbulent intensities reached a self-similar state after a longer period of jet development. Also the entrainment rate and angle of spread for the swirling jet was found to be nearly twice that of the nonswirling free jet.

1.3 Flowfield Independence of Reynolds Number

Although the current experiments are being done under low speed and nonreacting conditions because of the limitations of the experimental facilities, the results can be applied to actual combustor hardware, which usually operate at higher Reynolds numbers than those used in the present test facility.

Moon and Rudinger (10) noticed that the location of the flow reversal is practically independent of the flow velocity over the range from about 40 to 90 m/s in the small tube. They also observed that, as the Reynolds number increases, the uncertainty in determining the reattachment point appears to decrease.

Rhode (5), who performed experiments to investigate the asymptotic invariance of Re_d on the flowfield, showed that there is little change in the flowfield for $Re_d \geq 47,000$, where Re_d is based on the nozzle inlet velocity and diameter. His study was done for $x/D = 2.5$, $\alpha = 90$ degrees, and $\phi = 38$ degrees. Because the flow was considered to be most sensitive to Re_d at a location slightly downstream of the recirculation zone and the recirculation zone was observed just before the axial station of 2.5. Also the central rather than corner recirculation zone was selected

since most of the combustion and flame stability occur there (17-19). Measurement traverses were repeated for the same conditions while increasing Re_d for each of the flowfields. In the present study the experiments were repeated using the same procedure as Rhode but for $x/D = 0.5$, $\alpha = 90$ degrees, and $\phi = 45$ degrees, where the most extensive and strongest turbulent reverse flows had been observed in previous experiments. The results indicate also the excellent consistency of velocity profiles independent of Reynolds numbers for $Re_d \geq 90,000$ at the axial location as shown later in Figure 11. The present study uses Reynolds numbers ranging from 53,000 to 220,000 as tabulated in Table I. For strong swirling flow with swirl vane angle $\phi = 70$ degrees, the Reynolds number is 53,000. This is not high enough to be sure that the flowfield is independent of Reynolds number, but 53,000 is the highest value which can be reached for $\phi = 70$ degrees in the current experimental facilities. In this study, a flowfield is assumed to be independent of Reynolds number for $Re_d \geq 53,000$.

1.4 The Scope and Significance of the Present Research

In the present study, a five-hole pitot probe was used to measure the magnitude and direction of the time-mean velocity in the combustor. Measurements have been carried out for sudden expansion and gradual expansion (side-wall expansion angle $\alpha = 90$ and 45 degrees) for nonswirling and swirling flows [swirl vane angle zero (swirler removed), 38, 45, 60, and 70 degrees]; and then with contraction block inserted at certain axial stations ($L/D = 1.0$ and 2.0). The raw data measured by a five-hole pitot probe are reduced by a FORTRAN computer program (which is described

in Appendix C) and plotted as axial, radial, and swirl velocity components by a plotting program using a complot plotter.

The current research is significant for the following reasons (23):

1. The magnitude and direction of the flow velocity is measured.
2. The extent of the corner and central recirculation zones is identified.
3. The effects of geometric parameters on the flowfields in the combustor chamber are determined.
4. Miscellaneous results such as the performance of the swirl vanes and the independence of the flowfields from the Reynolds number are provided.

The research is limited by the following factors:

1. The difficulty in investigating the exact reattachment points of the flows.
2. The low sensitivity of the probe to small velocities.

1.5 Outline of the Thesis

In the previous sections, the significance and scope of this study are introduced. Basic concepts are also given with reference to previous studies.

Chapter II describes the facilities and instrumentation employed. This chapter also explains the operation of the five-hole pitot probe, the concept of swirling flow, and the way a swirler performs.

The procedures of data measurements and reduction are described in Chapter III. A separate documentation in Appendix C contains a detailed description of the data reduction computer program and instructions for

its use. Descriptions of the calibrations of the voltmeter and the five-hole pitot probe are also included in this chapter.

Results for sudden expansion flows are discussed with emphasis on the extent of the recirculation zone in Section 4.1. Effects of geometric parameters such as a gradual expansion and a contraction nozzle are described in Sections 4.2 and 4.3.

Chapter V summarizes all of these results and suggests further research.

Appendix A and B include tables and figures, respectively. User's guide to five-hole pitot probe data reduction computer program is in Appendix C.

CHAPTER II

EXPERIMENTAL FACILITIES AND FIVE-HOLE

PITOT PROBE INSTRUMENTATION

2.1 An Idealized Flowfield

The test facility used to obtain a uniform flow of relatively low turbulence level is a wind tunnel designed and built at Oklahoma State University. The test section of the swirling confined-jet facility is a simulation of a typical axisymmetric can-type combustion chamber from a gas turbine engine as shown in Figure 1. A schematic of the facility is given in Figure 2. Since the actual gas turbine combustor is too complicated to be simulated in a laboratory, it is simplified, but the typical geometric features such as the presence of a sudden or gradual expansion block, a contraction nozzle, a swirler and a can-type shape of the flowfield domain are kept.

Ambient air enters the low-speed wind tunnel through an air filter consisting of a large box covered with foam rubber. Next a six-blade propeller fan, driven by a 5 h.p. varidrive motor which can be varied continuously from 1600 rpm to 3100 rpm, accelerates the air to the desired velocity.

The intensity of the turbulence caused by the driving fan is partially reduced by gradually expanding the flow into a stilling chamber containing numerous fine mesh screens. The turbulence intensity is further

reduced by passage through a turbulence management section. This section consists of a perforated aluminium plate (2 mm diameter holes) followed by a fine mesh screen, a 12.7 cm length of packed straws, and five more fine mesh screens. Most of the control of the turbulence occurs in this portion. The airflow, which is now relatively uniform and of low turbulence, then enters a contoured nozzle, which was designed to produce a minimum adverse pressure gradient on the boundary layer and thus avoid local separation and flow unsteadiness. The ratio of the area of the maximum cross section of the contour nozzle to that of the nozzle throat is approximately 22.5. The diameter of the nozzle throat is about 15 cm. There is a hole of 1 cm diameter just upstream of the nozzle throat for insertion of a standard pitot-static probe, so that the dynamic pressure can be measured upstream of the swirler. With the measured dynamic pressure, the corresponding nozzle throat velocity and Reynolds number are obtained from the dynamic pressure conversion characteristic shown in Figure 3.

2.2 Test Section

The test section is composed of a swirl vane assembly, an expansion or contraction block, a contraction nozzle, and a simplified can-type gas turbine combustion chamber. Details concerning the swirl vane assembly are given in Section 2.4.

The expansion or contraction block can be used optionally to give the simulated geometric characteristics desired for a certain expansion condition. The expansion blocks are interchangeable and those currently in use have expansion angles of 90 and 45 degrees. The expansion blocks have an inside diameter the same as that of the nozzle throat, and an

outside diameter approximately twice that of the nozzle throat, to match the test section inside diameter. The experimental results of Rhode (5) show that varying the expansion angle of the side wall does not affect the flowfield much except that the corner recirculation region decreases sharply as the expansion angle is decreased. The current study was conducted with side-wall expansion angles of $\alpha = 90$ and 45 degrees, to investigate the effects of both sudden and gradual expansions. A contraction block is used to simulate the confining wall of a real gas turbine combustor at the downstream end. The block was designed with a rounded profile that is one-quarter of a circle and a downstream cross-sectional area half that of the test section. The rounded upstream face is smoothly finished to reduce the surface shear stress. Details of the contraction block employed are given in Figure 4.

The test section used in this study is a straight, long circular plexiglass tube having a 30 cm inside diameter. Holes with 2.54 cm diameter are located along the length of the tube at distances which are multiples of $x/D = 0.5$, so that the pitot probe can be inserted into the flow and traverses made in the radial direction. It does not have film cooling holes or dilution air holes. The test section is carefully aligned with a low-power laser beam so that the centerlines of the test section and the wind tunnel coincide.

2.3 Five-Hole Pitot Probe Instrumentation

A five-hole pitot probe is one of the few instruments capable of measuring both the magnitude and the direction of fluid velocity simultaneously. The five-hole pitot probe used in this study is a model DC-125-12-CD manufactured by United Sensor and Control Corp. The

sensing head is hook-shaped to allow for probe shaft rotation without altering the probe tip location. Little information is available concerning the effects of turbulence on a pressure probe in a swirling flow. However, it is asserted that the five-hole pitot probe is accurate within approximately 5 percent for most of the measurements (5). This value may increase to 10 percent as the velocity magnitude falls below approximately 2.0 m/s because of the insensitivity of the probe to low dynamic pressure and the dependence of probe calibration on the probe Reynolds number.

There are three standard methods of operating the five-hole pitot probe:

1. To adjust the orientation of the probe in both pitch and yaw so that the probe is aligned with the local flow direction.
2. To determine the flow direction from the calibration relationship between probe pressures and flow direction while maintaining a fixed probe orientation.
3. To align the probe yaw angle with the flow yaw angle while deducing the pitch angle and total velocity coefficient calibration characteristics.

The third method was employed in this study because it used readily available orientation equipment and relatively simple data reduction procedures.

The instrumentation assembly, in addition to the five-hole pitot probe, is composed of a manual traverse mechanism, two five-way ball valves, a differential pressure transducer, a power supply, and an integrating digital voltmeter. The differential pressure transducer is model 590D from Datametrics, Inc. It has a differential pressure range of from

0 to $1.3 \times 10^3 \text{ N/m}^2$. The integrating voltmeter is the TSI model 1076. As auxiliary equipment, a model 631-B strobotac from General Radio, Inc. was used to check the fan speed and a micro-manometer along with a pitot-static probe was used to measure the dynamic pressure in the nozzle throat just upstream of the swirler. Also, a barometer/thermometer unit from Cenco Corporation was used for local pressure and temperature readings. Measurement apparatus are shown in Figure 5.

2.4 Swirler

Swirling jets are used as a means of controlling the length and stability of the flame in many combustor designs. The effects of the degree of swirl on the flowfields and combustion have been extensively investigated (5, 12, 19-21). A swirl number characterizes the degree of swirl. It is usually defined as the ratio of axial flux of tangential momentum to the axial flux of axial momentum (including a pressure contribution), nondimensionalized by use of the inlet nozzle radius. Thus:

$$S = \frac{G_{\theta}}{G_x d/2} \quad (2.1)$$

where:

G_{θ} = the axial flux of tangential momentum flux; and

G_x = the axial flux of axial momentum, including pressure contribution.

Often the pressure term is neglected, and the expression reduces to (20)

$$S = \frac{2}{3} \left(\frac{1 - Z^3}{1 - Z^2} \right) \tan \phi \quad (2.2)$$

where $Z = d_h/d$ for the case of an annular vane swirler idealized with

flat axial and flat swirl velocity profiles at the inlet. This is the case in the present study.

The swirler used currently was constructed at Oklahoma State University according to preliminary design plans from NASA. The schematic of the swirler is shown in Figure 6. It has ten adjustable vanes and a hub with a streamlined nose and a flat downstream face. The nose has a hyperbolic shape with a very smooth surface to reduce the pressure drop. The flat face and location of the hub is a simulation of an actual fuel injector. The flat blades are wedge-shaped to give a constant pitch-to-chord ratio of approximately one which should give good turning efficiency (21).

Mathur and MacCallum (12) thought that an overlap between the adjacent vanes is a determinant parameter to give a complete deflection of air. They found that a positive overlap is essential for effective directing of the air and a 30 degrees overlap is adequate for complete deflection. An approximately variable 20 degrees overlap is provided by the swirler used in this study. The positive axial velocity which was observed near to the hub might be the result of an insufficient overlap. An extensive study concerning the swirler performance is being conducted by Sander (24).

CHAPTER III

MEASUREMENT AND REDUCTION OF DATA

A schematic of the five-hole pitot probe is shown in Figure 7. To obtain all the components of the velocities in the axial, radial, and azimuthal directions at a given location in the model combustor, one must know the yaw angle β , the pitch angle δ , and the magnitude of the total velocity V at that point. The yaw angle β can be measured directly from the reading of the rotary vernier. The pitch angle δ and the total velocity V can be found from the corresponding calibration in a free jet.

With the above information, Rhode (5) wrote a data reduction computer program. This program reduces the raw pressure data from direct measurement into u , v , and w velocity component data.

3.1 Measurement Procedures

When using the five-hole pitot probe, one aligns the probe tip with the direction of the air flow in the horizontal plane and then reads the yaw angle β and the two differential pressures ($P_N - P_S$) and ($P_C - P_W$). These pressures are used to obtain the pitch angle δ in the vertical plane and the magnitude of total velocity vector from the calibration characteristics.

The first step in preparing to take measurements with the five-hole pitot probe is to measure the dynamic pressure of flow with a pitot-static probe at the nozzle throat just before the swirler. Then the

pressure transducer must be nulled for zero differential pressure. This is done by turning an adjustment screw on the transducer until the voltmeter reading for zero differential pressure (both ports open to atmosphere) is zero.

The next step in preparing for measurements is to adjust the position of the test section until the wind tunnel and test section axes coincide, and also to adjust the traverse mount until the probe zero point lies on the test section axis. Then the varidrive motor is set at the proper rpm to give the desired air velocity at the nozzle throat. The fan speed is checked regularly with a strobotac to keep the air velocity constant.

Before the production measurements are taken, the five-hole pitot probe rotary vernier must be set for zero yaw angle so that the x and θ axes of the measurement coordinate frame coincide with those of the test section. This is achieved by adjusting the yaw angle to be zero at the center of the test section inlet for nonswirling flow. Each radial traverse measurement begins at the centerline, which is identified with a low-power laser beam. The pressure and yaw angle data are read at 0.3 inch increments up to 5.7 inches from the centerline. In this study, 10 seconds time-mean data readings are used. To measure 10 seconds time-mean values, 30 to 40 seconds settling time is needed to allow transients to subside in the measuring apparatus.

The first measurement for each location is the yaw angle for a zero reading of $(P_W - P_E)$. This means that the probe tip is aligned with the flow direction in a horizontal plane. Then the five-way switching valves are set so that $(P_N - P_S)$ is sensed by the pressure transducer. Finally, the reading of $(P_C - P_W)$ is similarly measured.

3.2 Calibrations

Two kinds of calibration are employed to reduce the raw data from the direct measurements. One is the calibration of the voltmeter, which determines a relationship between the voltmeter output and the magnitude of velocity. The other is the calibration of the five-hole pitot probe, which consists of two calibration characteristics: pitch angle δ versus differential pressure ratio $(P_N - P_S)/(P_C - P_W)$, and velocity coefficient

$$C = \rho V^2 / [2(P_C - P_W)] \quad (3.1)$$

versus pitch angle δ .

Proper calibration is extremely critical to the accuracy of the experimental work. The calibration of the five-hole pitot probe is based on the investigation, which concluded that the calibration coefficients are independent of Re_p , which is based on probe tip diameter (5). The investigation determined that this conclusion is true for $Re_p \geq 1090$, or a local velocity of 5.4 m/s. Low velocity might cause some calibration error. However, the investigation also shows that this calibration error affects the velocity measurements typically by less than 6 percent for $Re_p \geq 400$, corresponding to a local velocity greater than 2.0 m/s. In this study, all calibrations are conducted at air velocity of 4.6 m/s.

A schematic of the calibration facilities is given in Figure 8. The jet employed for calibrations is a free jet with a contoured nozzle which has a 3.5 cm diameter throat. Compressed air is used for the calibrating jet and its mass flow rate is controlled by a small pressure regulator and a Fisher and Porter model 10A1735A rotameter. The five-hole pitot probe is rotated by the rotary table model BH-9 from Troyke Manufacturing Co., whose rotary vernier is readable to ± 0.5 minutes of arc.

The calibration procedure of the voltmeter consists of reading the micro-manometer with a pitot static probe for a known air flow rate. The volume flow rate is incremented by $0.5 \text{ ft}^3/\text{min}$ [$1 \text{ ft}^3/\text{min} = 0.000472 \text{ m}^3/\text{s}$] over the range $0.5 \leq Q \leq 9.0$. As shown in Figure 9, there exists a linear relationship between the velocity magnitude and the pressure reading.

The first step to calibrate the five-hole pitot probe is to set the probe tip in the horizontal plane so that the yaw is aerodynamically nulled. This condition can be maintained by frequently checking the zero reading for $(P_W - P_E)$ during the whole calibration proceeding. The next step consists of reading the voltage output from the pressure transducer for differential pressures $(P_N - P_S)$ and $(P_C - P_W)$. These data are measured at 5 degrees increments in δ over the range $-55 \leq \delta \leq 55$.

Figure 10 shows the calibration characteristics from which the pitch angle δ and the velocity coefficient C are obtained, respectively. The calibration is conducted two times to be sure that the measurements are exact and that they remain the same. Even if the measurements are taken by different observers and at different times, the consistency is splendid. Most of the discrepancies lie within 2-3 percent, and the maximum is within 10 percent.

3.3 Data Reduction

It is difficult to define in a word what turbulence is. According to Hinze's (22) definition, "Turbulent fluid motion is an irregular condition of flow in which the various quantities show a random variation with time and space coordinates, so that statistically distinct values can be discerned." The vector velocity of turbulent flow consists of

a time-mean velocity and a fluctuating velocity component. As mentioned in the previous section, the differential pressure readings from the five-hole pitot probe are utilized directly to obtain the square of the vector velocity in the velocity coefficient. With the information from the five-hole pitot probe measurements alone, it is impossible to express the square of the vector velocity $\overline{V^2}$ as the sum of the square of the magnitude of the time-mean velocity \overline{V}^2 and the time-mean fluctuation term $\overline{V'^2}$, as given by

$$\overline{V^2} = \overline{V}^2 + \overline{V'^2} \quad (3.2)$$

Obtaining the fluctuation term $\overline{V'^2}$ depends on other methods of measurement. But the available data for the term $\overline{V'^2}$ is not thought to be reliable. Furthermore, an established theory for the effect of turbulence in swirl flows on pressure probes is unavailable. So even though some discrepancy is to be expected, the reduced velocity is taken to be the time-mean velocity magnitude \overline{V} which is written without the overbar onward. In this study, all properties of the acting fluid are assumed to be those of ambient air.

With the measurement data of the differential pressure ratio $(P_N - P_S)/(P_C - P_W)$, the corresponding pitch angle δ is obtained with a cubic spline interpolation technique from the calibration characteristics shown in Figure 10(a). The velocity coefficient C is determined from this value by using the corresponding calibration characteristic in Figure 10(b). The magnitude of the velocity vector is calculated by

$$V = \left[\frac{2}{\rho} (P_C - P_W) \cdot C \right]^{1/2} \quad (3.3)$$

The velocity components are easily calculated by elementary geometry using the measured yaw angle β , the derived pitch angle δ , and the total velocity V .

All data used in this investigation were reduced with the FORTRAN data reduction computer program written by Rhode (5). Full details of the data reduction procedure are given in Appendix C, including a program listing, sample input and output, and a user's guide.

CHAPTER IV

RESULTS

Nonswirling and swirling nonreacting flows are investigated in an axisymmetric test section with expansion ratio $D/d = 2$, which may be equipped with a contraction nozzle of area ratio 2 and 4. Velocity measurements are made with the five-hole pitot probe as described in Chapter III. An analysis is made of the effects of various geometric parameters on the extent of the recirculation zones in the flowfield. These parameters include side-wall expansion angle $\alpha = 90$ and 45 degrees, swirl vane angle $\phi = 0, 38, 45, 60,$ and 70 degrees, and contraction nozzle location $L/D = 1$ and 2 (if present). The nozzle inlet velocities and Reynolds numbers employed in this study are high enough to ensure that the flowfields are investigated under conditions independent of Reynolds number variation. All nozzle inlet velocities and Reynolds numbers employed are listed in Table I. Flow characteristics are tabulated in terms of normalized $u, v,$ and w velocity components, yaw angle β and pitch angle δ in Tables II through XII. Axial and swirl velocity profiles for all flows studied are shown in Figures 12 through 16 and 18 through 20.

4.1 Effects of Swirl on Sudden Expansion

Flows

Swirling flows result from the application of a spiraling motion, with a swirl velocity component being imparted to the flow via the use

of swirl vanes. A swirl number S characterizes the degree of swirl. The swirl vane angles employed in this study are 0 (swirler removed), 38, 45, 60, and 70 degrees. These correspond to swirl numbers S of 0, 0.52, 0.67, 1.15, and 1.83, under the definition of swirl number introduced in Section 2.4. Figure 12 parts a through e show the axial and swirl velocity profiles for $\phi = 0, 38, 45, 60,$ and 70 degrees, respectively, with side-wall expansion angle $\alpha = 90$ degrees.

The nonswirling flow investigated is obtained with the swirler removed. Figure 12(a) shows an uniform axial velocity entering the test section. The corner recirculation zone extends to just beyond $x/D = 2.0$. The measurements for a corresponding flow taken with a stagnation tube and pitot tube by Chaturvedi (11). He found the reattachment point to be at $x/D = 2.3$ which is in good agreement with the present study. Moon and Rudinger (10) measured the reattachment point with both theoretical and experimental methods in a similar circular test section with an expansion ratio $D/d = 1.43$, which is different from the present study [with $D/d = 2$]. The result yielded a value of $x/D = 1.25$ as a reattachment point, which corresponds to an attachment point approximately eight step-heights downstream. This is in good agreement with the present study.

The velocity profiles for swirling flows shown in Figure 12 parts b through e reveal that the flow entering through the swirl vanes is not uniform and has steep velocity gradients in the radial direction especially at high swirl numbers. Furthermore, a considerable back flow around the hub is observed for $\phi = 70$ degrees, as shown in Figure 12(e). For all values of swirl vane angle used in this study, the corner recirculation zone is not seen at $x/D = 0.5$ the closest axial location to the expansion block; instead, the maximum axial velocity is observed close

to the top wall at $x/D = 0.5$. The effects result from the strong centrifugal forces present in the incoming swirling flow.

The central recirculation zone and precessing vortex core are now discussed. The precessing vortex core is defined as the region of high swirl, low axial velocity flow along the axis, which has a relatively constant small diameter. In flow visualization studied, it is seen to precess along the axis of the test section. The central recirculation zone is defined as the wide reverse flow region encountered near the inlet. Artistic impressions are given later in Figure 21 in which lines have been drawn connecting the radial positions of zero axial velocity. In case of the vortex core, that region is drawn along the zero axial velocity boundary in the downstream direction after the central recirculation region. The size of the central recirculation zone increases with the increasing swirl vane angle until a certain value of swirl vane angle is reached (around 40 degrees). Then its length begins to decrease under stronger swirl conditions. The results are tabulated in Table XIII. The core vortex was present at all values of swirl vane angle used in this investigation. In contrast to the central recirculation zone, the vortex core gets larger and larger continuously as the swirl vane angle increases.

The swirl velocity peaks sharply around the edge of the expansion block before becoming more uniform farther downstream as shown in Figure 12 parts b through e. A considerably nonuniform swirl velocity profile is observed at $x/D = 0.5$. Thereafter, relatively steady and uniform velocity profiles are seen, except for the region around the axis. The radial location where the maximum swirl velocity occurs goes up as the swirl vane angle increases. This trend is caused by the increase of

centrifugal effects. The swirl velocity along the axis is found to be zero as expected because of symmetry.

4.2 Effects of Gradual Expansion on Flows

Gradual expansion flows with $\alpha = 45$ degrees were measured at two axial stations of $x/D = 0.5$ and 1.0 for swirl vane angles of $0, 38, 45, 60,$ and 70 degrees. Only the upstream flowfield needed to be thoroughly investigated in these cases, since inlet expansion effects affect this region the most, and their influence rapidly diminishes in the downstream direction (5, 13). Measurements were not taken at the inlet in this geometry because the presence of the expansion block interferes with probe positioning.

The corresponding sequence of axial and swirl velocity profiles to a sudden expansion is given in Figure 13 parts a through e for $\alpha = 45$ degrees. Velocity profiles for a gradual expansion follow a similar trend to those for a sudden expansion. The major effect of a gradual inlet expansion is to encourage the air to flow along the side sloping wall, shorten the corner recirculation zone and accelerate axial velocities close to the top wall. Influence on the central recirculation zone for the swirl flow cases is minimal.

4.3 Effects of Contraction Nozzle on Flows

It is best to interpret the data obtained when the contraction block is inserted at different axial stations on the flowfields by comparing them to the data obtained without the contraction block. The measurements were taken at axial locations ranging from the inlet plane to the axial station just upstream of the station where the contraction block

was located. The effect of a contraction nozzle was investigated with the contraction block at $L/D = 1$ and 2 for a range of swirl strengths $\phi = 0, 45,$ and 70 degrees with sudden expansion $\alpha = 90$ degrees only. Figures 14, 15, and 16 present these velocity profiles with $L/D = 1$ and 2 in parts a and b, respectively.

Figure 14 shows that the contraction block generally affects the flowfield very little under nonswirling conditions. Furthermore, as the block is moved farther in the downstream direction, its effect on the flowfield decreases. The only effect that can be noticed from the velocity profiles is decreased in length of the corner recirculation region due to the nozzle effect.

Figure 15(a) shows the axial and swirl velocity profiles for the intermediate swirling flow of $\phi = 45$ degrees with a contraction block at $L/D = 1$. Significant positive axial velocities are observed along the center line. This situation is in striking contrast to that of the intermediate swirling flow without the contraction block, in which case the central recirculation zone spreads extensively along the centerline to $x/D = 1.5$ with vortex core following it in the test section. Slightly larger swirl velocities are seen in Figure 15(a) with contraction block at $L/D = 1$ than in Figure 12(c) without contraction block. Velocity profiles shown in Figure 15(b), for $\phi = 45$ degrees with contraction block at $L/D = 2$, follow a trend similar to the corresponding flow without the contraction block at the first two axial stations of $x/D = 0$ and 0.5 . But the axial velocities have quite different profiles at two axial stations of $x/D = 1.0$ and 1.5 being affected by the proximity of the contraction nozzle. At the axial station of $x/D = 1.0$, reverse flow is not observed at all, and considerable positive axial velocities are measured

near the axis. A rather uniform velocity profile is obtained at $x/D = 1.5$. The effect of the contraction block on the swirl velocity profiles is negligible. The presence of a contraction block, in the intermediate swirling flowfield, results in the existence of positive axial velocities near the axis.

For strong swirling flows of $\phi = 70$ degrees, the axial and swirl velocity profiles are shown in Figure 16. A contraction block does not affect the flowfield much except at the axial station immediately upstream of the block.

In comparison with corresponding cases without downstream blockages, Figure 16(a) shows a wider central recirculation zone when $L/D = 1$ and Figure 16(b) shows a narrower precessing vortex core when $L/D = 2$. The swirl velocity profiles do not change significantly with or without presence of downstream blockages.

In summary, a nozzle has most effect on the intermediate swirl case $\phi = 45$ degrees. Its contraction effect in this case is strong enough to overwhelm the swirling recirculation region.

However, a contraction has little effect on weakly swirling and strongly swirling flows, which are dominated by forward flow and centrifugal forces, respectively.

Since the most drastic change in the velocity profile was observed at $x/D = 1.0$ for intermediate swirling flow of $\phi = 45$ degrees with a contraction block at $L/D = 2$, the measurements were repeated to ensure confidence in them. The new results, obtained at a slightly higher Reynolds number, confirm the previous results. Both sets of results are shown in

Figure 17, and seem to be very consistent.

The effect of a stronger contraction nozzle was investigated for a range of swirl lengths $\phi = 0, 45$ and 70 degrees with side-wall expansion angle $\alpha = 90$ degrees. The contraction nozzle, of area ratio 4 with 45 degree sloping upstream face, is located at $L/D = 1$ and 2 . Figures 18, 19, and 20 show these velocity profiles with $L/D = 1$ and 2 in parts a and b, respectively.

Figure 18 shows that the flowfield with a strong contraction nozzle changes very little as compared to the corresponding flowfield with a weak contraction nozzle shown in Figure 14.

Figure 19 shows the axial and swirl velocity profiles for a swirl vane angle $\phi = 45$ degrees. The presence of a strong contraction nozzle generates the high positive axial velocity near the axis. However, it decelerates the axial velocity close to the top wall. The central recirculation zone is smaller and located in an annular region, which excludes the axis. The swirl velocity profiles show narrower and stronger core swirl velocity gradients than previously.

For swirl vane angle $\phi = 70$ degrees, the axial and swirl velocity profiles are given in Figure 20. It shows that the axial velocity near the axis is highly positive and the central recirculation region extends only to less than $x/D = 1.0$, much less than its corresponding case with the weak contraction block. At the axial station $x/D = 1.0$, forward flow occurs across the whole test section. This situation is in sharp contrast to that of a weak contraction nozzle, in which case the contraction block affects the flowfield very little under strong swirling conditions. Swirl velocity profiles given in Figure 20 show the narrower strong core swirl velocity gradient, as also observed in the

swirl vane angle $\phi = 45$ degree case.

The above observances are summarized as follows. The effect of a weak contraction nozzle of area ratio 2 is confined to intermediate swirling flow case, while a strong contraction nozzle of area ratio 4 affects both intermediate and strong swirling flow cases. Artistic impressions for a weak contraction nozzle and a strong contraction nozzle with emphasis on the recirculation zones are given in Figures 20 and 23, for a range of swirl strengths with blockage located at $L/D = 2$.

CHAPTER V

CLOSURE

5.1 Summary

This study is five-hole pitot probe time-mean velocity measurements in confined swirling flows under low speed and nonreacting conditions. Three velocity components normalized with the inlet axial velocity are tabulated along with yaw and pitch angles. This provides an extensive data base for later verification of a theoretical simulation of the complex turbulent flowfield.

The extent of the recirculation zone for sudden expansion flows with $\alpha = 90$ degrees is characterized for swirl vane angles $\phi = 0, 38, 45, 60,$ and 70 degrees. For a nonswirling flow, the corner recirculation zone extends to just beyond 2 with no central recirculation zone. The presence of a swirler shortens the corner recirculation zone and generates a central recirculation zone followed by a precessing vortex core. The largest central recirculation zone was shown to be in the intermediate swirling flow case of $\phi = 38$ degrees; the strongest precessing core vortex was found to be in the strongest swirling flow considered with $\phi = 70$ degrees.

Effects of a gradual inlet expansion of $\alpha = 45$ degrees are investigated for the same swirl vane angles as employed for a sudden inlet expansion. Velocity profiles for a gradual expansion follow a similar

trend to those for a sudden expansion. The only major effect of a gradual inlet expansion is to encourage the flow to remain close to the sloping side wall and shorten the extent of the corner recirculation zone in all cases investigated.

Effects of the presence of a contraction nozzle at $L/D = 1$ and 2 are investigated for $\phi = 0, 45,$ and 70 degrees. A contraction nozzle has little effect on weakly swirling and strongly swirling flows, which are dominated by forward flow and centrifugal forces, respectively. For the intermediate swirl case of $\phi = 45$ degrees, it encourages forward movement of otherwise slow-moving air and thereby shortens the central recirculation zone. A strong contraction nozzle of area ratio 4 has a more dramatic effect on the flowfields.

5.2 Recommendations for Further Work

The five-hole pitot probe technique is a useful cost-effective tool to investigate turbulent swirling recirculating confined flow. It enables time-mean axial, radial and swirl velocities to be deduced at any location in the flowfield. It is strongly recommended for use to obtain further flowfield measurements in the test facility at Oklahoma State University. It has, however, some inherent problems:

1. Weak sensitivity to small velocities, which might permit large relative errors.
2. Turbulence effects on the measurement of time-mean data cannot be easily accounted for.
3. The measurement of normal and shear turbulent stresses is not possible.

It is recommended that further work be done on the repeatability,

reliability, and accuracy of this technique. Results may be compared with hot-wire and laser doppler anemometers measurements in corresponding flow situations.

REFERENCES

- (1) Rhode, D. L., D. G. Lilley, and D. K. McLaughlin. "On the Prediction of Swirling Flowfields Found in Axisymmetric Combustor Geometries." Proceedings, ASME Symposium on Fluid Mechanics of Combustion Systems. Boulder, Colo., June 22-24, 1981, pp. 257-266. See Also: ASME Journal of Fluids Engineering, 1982 (in press).
- (2) Lilley, D. G. "Prospects for Computer Modeling in Ramjet Combustors." AIAA Paper No. 80-1189. Hartford, Conn., June 30-July 2, 1980.
- (3) Serag-Eldin, M. A. and D. B. Spalding. "Computations of Three Dimensional Gas Turbine Combustion Chamber Flow." Transaction ASME, Journal of Engineering for Power, Vol. 101 (July, 1979), pp. 326-336.
- (4) Novick, A. S., G. A. Miles, and D. G. Lilley. "Numerical Simulation of Combustor Flow Fields." Journal of Energy, Vol. 3, No. 2 (March-April, 1979), pp. 95-105.
- (5) Rhode, D. L. "Predictions and Measurements of Isothermal Flowfields in Axisymmetric Combustor Geometries." Ph.D. Thesis (December, 1981), Oklahoma State University.
- (6) Bird, J. D. "Visualization of Flowfields by Use of a Tuft Grid Technique." Journal of Aeronautical Science, Vol. 19 (1952), pp. 481-485.
- (7) Lee, J. C. and J. E. Ash. "A Three-Dimensional Spherical Pitot Probe." Transactions, ASME (April, 1956), pp. 603-608.
- (8) Hiatt, G. F. and G. E. Powell. "Three-Dimensional Probe for Investigation of Flow Patterns." The Engineer (January, 1962), pp. 165-170.
- (9) Janjua, S. I. "Turbulence Measurements in a Complex Flowfield Using a Six-Orientation Hot-Wire Probe Technique." M.S. Thesis (December, 1981), Oklahoma State University.
- (10) Moon, L. F. and G. Rudinger. "Velocity Distribution in an Abruptly Expanding Circular Duct," Journal of Fluids Engineering (March, 1977), pp. 226-230.

- (11) Chaturvedi, M. C. "Flow Characteristics of Axisymmetric Expansions." Proceedings, Journal of the Hydraulics Division, ASCE, Vol. 89, No. HY3 (1963), pp. 61-92.
- (12) Mathur, M. L. and N. R. L. MacCallum. "Swirling Air Jets Issuing from Vane Swirlers. Part 1: Free Jets; Part 2: Enclosed Jets." Journal of the Inst. of Fuel, Vol. 40 (May, 1967), pp. 238-245.
- (13) Rhode, D. L., D. G. Lilley, and D. K. McLaughlin. "Mean Flowfields in Axisymmetric Combustor Geometries with Swirl." AIAA Paper No. 82-0177, Orlando, Florida, January 11-14, 1982.
- (14) Pratte, B. D. and J. F. Keffer. "The Swirling Turbulent Jet." Journal of Basic Engineering, Vol. 94 (December, 1972), pp. 739-748.
- (15) Back, L. H. and E. J. Roschke. "Shear Layer Flow Regimes and Wave Instabilities and Reattachment Lengths Downstream of an Abrupt Circular Channel Expansion." Journal of Applied Mechanics Vol. 94 (September, 1972), pp. 677-681.
- (16) McMahon, H. M., D. D. Hester, and J. G. Palfery. "Vortex Shedding from a Turbulent Jet in a Cross-Wind." Journal of Fluid Mechanics, Vol. 48 (1971), pp. 73-80.
- (17) Lilley, D. G. "Flowfield Modeling in Practical Combustors: A Review." Journal of Energy, Vol. 3 (July-August, 1979), pp. 193-210.
- (18) Krall, K. M. and E. M. Sparrow. "Turbulent Heat Transfer in the Separated, Reattached, and Redevelopment Regions of a Circular Tube." Journal of Heat Transfer (February, 1966), pp. 131-136.
- (19) Kerr, N. M. and D. Fraser. "Swirl. Part 1: Effect on Axisymmetrical Turbulent Jets." Journal of Institute of Fuel, Vol. 38 (December, 1965), pp. 527-538.
- (20) Beer, J. M. and N. A. Chigier. Combustion Aerodynamics. London: Applied Science; and New York: Halsted-Wiley, 1972.
- (21) Supta, A. K., D. G. Lilley, and N. Syred. Swirl Flows. Abacus Press, Tunbridge Wells, England, 1982 (in press).
- (22) Hinze, J. O. Turbulence: An Introduction to Its Mechanism and Theory. McGraw-Hill Book Company, Inc., 1959.
- (23) Yoon, H. K. "Five-Hole Pitot Probe Time-Mean Velocity Measurements In Combustor Flowfield." Thirteenth Southwestern Graduate Research Conference in Applied Mechanics, Norman, Oklahoma, April 16-17, 1982, pp. 131-137.

- (24) Sander, G. F. "Annular Vane Swirler Performance." Thirteenth Southwestern Graduate Research Conference in Applied Mechanics, Norman, Oklahoma, April 16-17, 1962, pp. 274-280.
- (25) Gurtis, F. G. Applied Numerical Analysis 2nd Edition. Addison-Wesley Publishing Company, Massachusetts, May, 1980.

APPENDIX A

TABLES

TABLE I
NOZZLE INLET VELOCITIES AND REYNOLDS NUMBERS

ϕ	$\alpha = 90^\circ$		$\alpha = 45^\circ$		$\alpha = 90^\circ, L/D = 1, 2$	
	U_{in} (m/s)	Re_d	U_{in} (m/s)	Re_d	U_{in} (m/s)	Re_d
0°	15.7	150,000	15.5	154,000	22.3	220,000
38°	10.5	100,000	10.6	105,000		
45°	12.6	120,000	14.9	148,000	13.5	134,000
60°	8.84	84,000	9.58	95,000		
70°	5.57	53,000	6.25	62,000	6.8	67,500

ORIGINAL PAGE IS
OF POOR QUALITY.

TABLE II

VELOCITY DATA FOR NONSWIRLING FLOW $\phi = 0^\circ$

J	Y	1	2	3	4	5	6
20	0.14478	0.0	1.80E+02	1.80E+02	0.0	0.0	3.57E+02
19	0.13716	0.0	1.80E+02	1.80E+02	0.0	0.0	3.57E+02
18	0.12954	0.0	1.80E+02	1.80E+02	3.58E+02	0.0	3.57E+02
17	0.12192	0.0	1.80E+02	1.80E+02	3.58E+02	3.60E+02	3.58E+02
16	0.11430	0.0	1.80E+02	1.80E+02	3.58E+02	3.60E+02	3.58E+02
15	0.10668	0.0	1.80E+02	3.60E+02	3.58E+02	3.60E+02	3.58E+02
14	0.09906	0.0	1.80E+02	3.60E+02	3.58E+02	3.60E+02	3.58E+02
13	0.09144	0.0	3.60E+02	3.60E+02	3.58E+02	3.60E+02	3.58E+02
12	0.08382	0.0	3.60E+02	3.60E+02	3.59E+02	3.60E+02	3.58E+02
11	0.07620	0.0	3.60E+02	3.60E+02	3.59E+02	3.60E+02	3.58E+02
10	0.06858	3.60E+02	3.60E+02	3.60E+02	3.60E+02	3.60E+02	3.58E+02
9	0.06096	3.60E+02	3.60E+02	3.60E+02	3.60E+02	3.60E+02	3.58E+02
8	0.05334	3.60E+02	3.60E+02	3.60E+02	3.60E+02	3.60E+02	3.59E+02
7	0.04572	3.60E+02	3.60E+02	3.60E+02	3.60E+02	3.60E+02	3.59E+02
6	0.03810	3.60E+02	3.60E+02	3.60E+02	3.60E+02	3.60E+02	3.59E+02
5	0.03048	3.60E+02	3.60E+02	3.60E+02	3.60E+02	3.60E+02	3.59E+02
4	0.02286	3.60E+02	3.60E+02	3.60E+02	3.60E+02	3.60E+02	3.60E+02
3	0.01524	3.60E+02	3.60E+02	3.60E+02	3.60E+02	3.60E+02	3.60E+02
2	0.00762	3.60E+02	3.60E+02	3.60E+02	3.60E+02	3.60E+02	3.60E+02
1	0.0	3.60E+02	3.60E+02	3.60E+02	3.60E+02	3.60E+02	3.60E+02

(a) $\gamma = 7^\circ$ Angle

ORIGINAL PAGE IS
OF POOR QUALITY

TABLE II (Continued)

J	Y	1	2	3	4	5	6
	X =	0.0	0.14935	0.25845	0.4478C	0.5565C	0.74625
20	0.14478	0.0	-3.00E+01	-2.52E+01	0.0	0.0	2.97E+00
19	0.13716	0.0	-4.79E+01	-3.71E+01	0.0	0.0	3.50E+01
18	0.12954	0.0	0.0	-3.65E+01	0.0	0.0	2.47E+01
17	0.12192	0.0	-5.79E+01	-2.72E+01	5.50E+01	4.08E+01	2.04E+01
16	0.11430	0.0	-4.92E+01	-3.00E+01	4.42E+01	3.59E+01	2.29E+01
15	0.10668	0.0	-4.39E+01	4.25E+01	3.24E+01	2.13E+01	2.13E+01
14	0.09506	0.0	0.0	2.09E+01	2.49E+01	1.35E+01	1.58E+01
13	0.09144	0.0	2.24E+01	1.45E+01	1.80E+01	1.10E+01	1.49E+01
12	0.08382	0.0	8.83E+00	8.21E+00	1.22E+01	8.79E+00	1.44E+01
11	0.07620	0.0	5.09E+00	6.05E+00	5.87E+00	5.37E+00	1.10E+01
10	0.06858	4.96E+00	3.18E+00	4.29E+00	7.74E+00	7.40E+00	1.07E+01
9	0.06096	3.15E+00	1.33E+00	3.07E+00	6.20E+00	5.56E+00	8.12E+00
8	0.05334	1.57E+00	3.69E-01	1.75E+00	4.89E+00	4.43E+00	7.05E+00
7	0.04572	8.47E-01	-1.49E-01	7.98E-01	3.91E+00	3.53E+00	6.03E+00
6	0.03810	5.08E-01	-5.05E-01	1.39E-01	3.00E+00	2.32E+00	5.12E+00
5	0.03048	3.84E-01	-6.36E-01	-2.50E-01	2.52E+00	1.93E+00	4.60E+00
4	0.02286	3.50E-01	-9.34E-01	-5.98E-01	2.17E+00	1.09E+00	3.88E+00
3	0.01524	4.76E-01	-9.06E-01	-8.47E-01	1.63E+00	7.31E-01	2.91E+00
2	0.00762	5.64E-01	-1.07E+00	-7.13E-01	1.36E+00	6.74E-02	2.40E+00
1	0.0	8.79E-01	-1.06E+00	-9.35E-01	1.47E+00	-3.58E-01	1.70E+00

(5) Pitch Angle

ORIGINAL PAGE IS
OF POOR QUALITY

Table II (Continued)

J	Y	1	2	3	4	5	6
20	0.48511	0.0	-7.45E-02	-1.30E-01	0.0	0.0	2.91E-02
19	0.45957	0.0	-9.90E-02	-1.59E-01	0.0	0.0	4.63E-02
18	0.43404	0.0	-7.74E-02	-1.23E-01	2.93E-02	0.0	5.49E-02
17	0.40851	0.0	-6.64E-02	-1.17E-01	5.57E-02	8.57E-02	1.33E-01
16	0.38298	0.0	-5.82E-02	-8.33E-02	1.05E-01	1.19E-01	1.41E-01
15	0.35745	0.0	-6.94E-02	9.60E-02	1.60E-01	1.92E-01	1.92E-01
14	0.33191	0.0	0.0	2.09E-01	2.37E-01	3.10E-01	2.39E-01
13	0.30638	0.0	1.20E-01	3.16E-01	3.18E-01	3.71E-01	2.64E-01
12	0.28085	0.0	3.38E-01	4.69E-01	4.11E-01	4.39E-01	2.98E-01
11	0.25532	0.0	6.19E-01	6.29E-01	5.00E-01	4.42E-01	3.64E-01
10	0.22979	1.01E+00	8.70E-01	7.85E-01	6.05E-01	5.11E-01	3.93E-01
9	0.20425	1.01E+00	1.02E+00	8.74E-01	6.97E-01	5.88E-01	4.62E-01
8	0.17872	9.96E-01	1.04E+00	9.66E-01	7.70E-01	6.39E-01	5.08E-01
7	0.15319	9.94E-01	1.04E+00	1.01E+00	8.49E-01	7.29E-01	5.64E-01
6	0.12766	9.96E-01	1.04E+00	1.03E+00	9.04E-01	7.74E-01	6.04E-01
5	0.10213	9.95E-01	1.04E+00	1.04E+00	9.25E-01	8.14E-01	6.45E-01
4	0.07660	9.94E-01	1.04E+00	1.04E+00	9.47E-01	8.53E-01	6.92E-01
3	0.05106	9.96E-01	1.04E+00	1.04E+00	9.53E-01	8.80E-01	7.12E-01
2	0.02553	9.95E-01	1.04E+00	1.04E+00	9.58E-01	8.88E-01	7.28E-01
1	0.0	9.95E-01	1.04E+00	1.04E+00	9.61E-01	8.96E-01	7.38E-01

(c) u/u_0

ORIGINAL PAGE IS
OF POOR QUALITY

TABLE II (Continued)

J	Y	I = X = 0.0	2	3	4	5	6
20	0.48511	C.0	-4.30E-02	-6.11E-02	0.0	C.0	1.51E-03
19	0.45957	0.0	-1.09E-01	-1.20E-01	0.0	C.0	3.25E-02
18	0.43404	0.0	0.0	-9.10E-02	0.0	0.0	4.38E-02
17	0.40851	0.0	-1.06E-01	-5.98E-02	7.95E-02	7.38E-02	4.94E-02
16	0.36298	0.0	-6.73E-02	-4.81E-02	1.02E-01	8.61E-02	5.95E-02
15	0.35745	C.0	-6.69E-02	8.80E-02	1.01E-01	7.49E-02	7.49E-02
14	0.33191	0.0	0.0	8.01E-02	1.10E-01	7.42E-02	6.75E-02
13	0.30638	0.0	4.97E-02	8.16E-02	1.03E-01	7.24E-02	7.03E-02
12	0.28085	0.0	5.25E-02	6.77E-02	8.90E-02	6.79E-02	7.64E-02
11	0.25532	0.0	5.51E-02	6.66E-02	6.71E-02	7.30E-02	7.05E-02
10	0.22979	8.77E-02	4.84E-02	5.89E-02	8.23E-02	6.64E-02	7.41E-02
9	0.20425	5.55E-02	2.37E-02	4.65E-02	7.57E-02	5.72E-02	6.59E-02
8	0.17872	2.73E-02	6.69E-03	2.96E-02	6.59E-02	4.55E-02	6.28E-02
7	0.15319	1.47E-02	-2.70E-03	1.41E-02	5.80E-02	4.50E-02	5.56E-02
6	0.12766	8.83E-03	-5.18E-03	2.49E-03	4.74E-02	3.14E-02	5.42E-02
5	0.10213	6.66E-03	-1.16E-02	-4.52E-03	4.07E-02	2.74E-02	5.19E-02
4	0.07660	6.06E-03	-1.70E-02	-1.08E-02	3.58E-02	1.63E-02	4.69E-02
3	0.05106	8.28E-03	-1.65E-02	-1.54E-02	2.70E-02	1.12E-02	3.62E-02
2	0.02553	9.80E-03	-1.95E-02	-1.29E-02	2.28E-02	1.04E-03	3.05E-02
1	0.0	1.53E-02	-1.53E-02	-1.70E-02	2.46E-02	-5.60E-03	2.18E-02

(d) v/u_0

ORIGINAL PAGE IS
OF POOR QUALITY

TABLE II (Continued)

	1	2	3	4	5	6
I =	0.0	0.50042	1.00000	1.50042	2.00000	2.50042
X =	0.0	0.50042	1.00000	1.50042	2.00000	2.50042
Y						
20	0.48511	0.0	2.60E-07	4.53E-07	0.0	-1.53E-03
19	0.45557	0.0	3.45E-07	5.56E-07	0.0	-2.43E-03
18	0.43404	0.0	2.70E-07	4.29E-07	-1.02E-03	0.0
17	0.40651	0.0	2.32E-07	4.07E-07	-1.95E-03	-5.16E-07
16	0.38298	0.0	2.03E-07	2.90E-07	-3.68E-03	-7.18E-07
15	0.35745	0.0	2.42E-07	-5.78E-07	-5.58E-03	-1.16E-06
14	0.33191	0.0	0.0	-1.26E-06	-8.29E-03	-1.87E-06
13	0.30638	0.0	-7.25E-07	-1.91E-06	-1.11E-02	-2.24E-06
12	0.28085	0.0	-2.03E-06	-2.83E-06	-7.17E-03	-2.65E-06
11	0.25532	0.0	-3.73E-06	-3.79E-06	-8.73E-03	-2.66E-06
10	0.22979	-6.09E-06	-5.24E-06	-4.73E-06	-3.65E-06	-3.08E-06
9	0.20425	-6.06E-06	-6.13E-06	-5.26E-06	-4.20E-06	-3.54E-06
8	0.17872	-6.00E-06	-6.26E-06	-5.82E-06	-4.64E-06	-3.85E-06
7	0.15319	-5.99E-06	-6.26E-06	-6.11E-06	-5.11E-06	-4.39E-06
6	0.12766	-6.00E-06	-6.27E-06	-6.19E-06	-5.45E-06	-4.66E-06
5	0.10213	-5.99E-06	-6.27E-06	-6.25E-06	-5.57E-06	-4.90E-06
4	0.07650	-5.99E-06	-6.28E-06	-6.26E-06	-5.70E-06	-5.14E-06
3	0.05106	-6.00E-06	-6.28E-06	-6.26E-06	-5.74E-06	-5.30E-06
2	0.02553	-6.00E-06	-6.28E-06	-6.26E-06	-5.77E-06	-5.35E-06
1	0.0	-5.99E-06	-6.29E-06	-6.26E-06	-5.79E-06	-5.40E-06

(c) w/u_0

ORIGINAL PAGE IS
OF POOR QUALITY

TABLE III

VELOCITY DATA FOR SWIRL VANE ANGLE $\phi = 38^\circ$ [SIDE-WALL
EXPANSION ANGLE $\alpha = 90^\circ$ WITHOUT CONTRACTION BLOCK]

J	Y	1	2	3	4	5	6
	X =	0.0	0.14935	0.29845	0.45237	0.60329	0.75413
20	0.14478	0.0	1.90E+01	2.93E+01	6.23E+01	5.78E+01	5.25E+01
19	0.13716	0.0	1.94E+01	3.50E+01	5.80E+01	6.20E+01	6.02E+01
18	0.12954	0.0	1.94E+01	4.02E+01	5.80E+01	6.20E+01	6.08E+01
17	0.12192	0.0	1.96E+01	4.94E+01	5.80E+01	6.14E+01	6.12E+01
16	0.11430	0.0	2.12E+01	5.72E+01	5.80E+01	6.14E+01	6.16E+01
15	0.10668	0.0	2.60E+01	6.54E+01	5.90E+01	6.14E+01	6.22E+01
14	0.09906	0.0	3.92E+01	7.36E+01	6.20E+01	6.14E+01	6.30E+01
13	0.09144	0.0	7.92E+01	7.98E+01	6.10E+01	6.20E+01	6.44E+01
12	0.08382	0.0	1.16E+02	8.54E+01	6.30E+01	6.32E+01	6.62E+01
11	0.07620	0.0	1.28E+02	8.98E+01	6.50E+01	6.50E+01	6.80E+01
10	0.06858	2.64E+01	1.34E+02	9.18E+01	6.70E+01	6.70E+01	7.04E+01
9	0.05096	3.01E+01	1.36E+02	9.46E+01	6.90E+01	7.04E+01	7.32E+01
8	0.05334	3.00E+01	1.38E+02	9.58E+01	7.20E+01	7.36E+01	7.58E+01
7	0.04572	2.43E+01	1.40E+02	9.72E+01	7.50E+01	7.64E+01	7.90E+01
6	0.03810	3.56E+02	1.42E+02	9.96E+01	7.80E+01	8.00E+01	8.18E+01
5	0.03048	0.0	1.46E+02	1.02E+02	8.30E+01	8.34E+01	8.54E+01
4	0.02286	0.0	1.50E+02	1.05E+02	8.90E+01	8.58E+01	8.92E+01
3	0.01524	0.0	1.59E+02	1.12E+02	9.10E+01	8.90E+01	9.20E+01
2	0.00762	0.0	1.69E+02	1.20E+02	9.80E+01	8.90E+01	9.36E+01
1	0.0	0.0	1.78E+02	1.45E+02	1.06E+02	7.54E+01	8.30E+01

(a) Yaw Angle

ORIGINAL PAGE IS
OF POOR QUALITY

TABLE III (Continued)

	1	2	3	4	5	6
I =	0.0	0.14935	0.25845	0.45237	0.60325	0.75413
X =	0.0	0.14935	0.25845	0.45237	0.60325	0.75413
J	Y					
20	0.14478	0.0	2.32E+01	7.23E-01	1.22E+01	1.10E+01
19	0.13716	0.0	2.04E+01	-7.21E+00	-1.20E+00	2.76E+00
18	0.12954	0.0	2.06E+01	-1.14E+01	-3.99E+00	-1.81E+00
17	0.12192	0.0	1.91E+01	-1.70E+01	-4.73E+00	-2.47E+00
16	0.11430	0.0	1.77E+01	-1.55E+01	-6.13E+00	-2.81E+00
15	0.10668	0.0	1.53E+01	-2.30E+01	-6.01E+00	-3.15E+00
14	0.09906	0.0	1.77E+01	-2.26E+01	-7.35E+00	-3.98E+00
13	0.09144	0.0	-3.79E+01	-2.15E+01	-6.67E+00	-4.80E+00
12	0.08382	0.0	2.00E+01	-1.86E+01	-7.31E+00	-5.28E+00
11	0.07620	0.0	7.69E+00	-1.65E+01	-6.74E+00	-6.71E+00
10	0.06858	1.14E+01	5.78E+00	-1.46E+01	-7.17E+00	-7.90E+00
9	0.06096	1.18E+01	4.41E+00	-1.43E+01	-7.49E+00	-5.67E+00
8	0.05334	9.70E+00	4.76E+00	-1.35E+01	-7.75E+00	-1.16E+01
7	0.04572	1.00E+01	3.36E+00	-1.33E+01	-8.63E+00	-1.40E+01
6	0.03810	0.0	2.97E+00	-1.44E+01	-1.05E+01	-1.69E+01
5	0.03048	0.0	2.97E+00	-1.77E+01	-1.35E+01	-2.09E+01
4	0.02286	0.0	2.97E+00	-2.15E+01	-1.79E+01	-2.68E+01
3	0.01524	0.0	2.97E+00	-3.08E+01	-2.41E+01	-3.71E+01
2	0.00762	0.0	7.42E-01	-4.60E+01	-4.42E+01	0.0
1	0.0	0.0	1.26E+00	0.0	5.11E+01	0.0

(b) Pitch Angle

ORIGINAL PAGE IS
OF POOR QUALITY

TABLE III (Continued)

	1	2	3	4	5	6
I =	0.0	0.50042	1.00000	1.50042	2.00000	2.50042
X =	0.0	0.50042	1.00000	1.50042	2.00000	2.50042
Y						
J	0.48511	0.0	6.83E-01	5.12E-01	2.15E-01	2.70E-01
19	0.45957	0.0	9.06E-01	5.85E-01	2.73E-01	2.57E-01
18	0.43404	0.0	9.79E-01	4.54E-01	2.79E-01	2.56E-01
17	0.40851	0.0	9.32E-01	3.60E-01	2.87E-01	2.62E-01
16	0.38258	0.0	7.71E-01	2.68E-01	2.86E-01	2.64E-01
15	0.35745	0.0	5.12E-01	1.85E-01	2.83E-01	2.66E-01
14	0.33191	0.0	2.38E-01	1.20E-01	2.59E-01	2.67E-01
13	0.30638	0.0	2.13E-02	7.41E-02	2.69E-01	2.62E-01
12	0.28085	0.0	-1.12E-01	3.49E-02	2.54E-01	2.54E-01
11	0.25532	0.0	-2.32E-01	1.59E-03	2.39E-01	2.35E-01
10	0.22979	1.46E+00	-2.84E-01	-1.49E-02	2.18E-01	2.14E-01
9	0.20425	1.57E+00	-3.13E-01	-3.85E-02	1.98E-01	1.79E-01
8	0.17872	1.64E+00	-3.25E-01	-4.94E-02	1.69E-01	1.46E-01
7	0.15319	9.25E-01	-3.19E-01	-5.99E-02	1.34E-01	1.15E-01
6	0.12766	1.15E-01	-3.17E-01	-7.61E-02	9.81E-02	7.92E-02
5	0.10213	0.0	-3.06E-01	-8.72E-02	5.05E-02	4.63E-02
4	0.07660	0.0	-3.04E-01	-8.83E-02	6.12E-03	2.41E-02
3	0.05106	0.0	-2.93E-01	-8.98E-02	-4.40E-03	4.15E-03
2	0.02553	0.0	-3.02E-01	-6.43E-02	-1.85E-02	2.02E-03
1	0.0	0.0	-2.86E-01	-5.38E-02	-1.21E-02	3.12E-02

(c) u/u₀

ORIGINAL PAGE IS
OF POOR QUALITY.

TABLE III (Continued)

	1	2	3	4	5	6		
J	20	0.48511	0.0	3.19E-01	7.41E-03	9.98E-02	5.83E-02	1.84E-02
Y	19	0.45957	0.0	3.58E-01	9.03E-02	1.08E-02	2.64E-02	4.08E-03
	18	0.43404	0.0	3.91E-01	1.31E-01	3.67E-02	1.72E-02	1.53E-02
	17	0.40851	0.0	3.43E-01	1.69E-01	4.48E-02	2.36E-02	2.38E-02
	16	0.38298	0.0	2.63E-01	1.76E-01	5.79E-02	2.71E-02	2.82E-02
	15	0.35745	0.0	1.56E-01	1.89E-01	5.78E-02	3.06E-02	3.15E-02
	14	0.33191	0.0	9.80E-02	1.77E-01	7.12E-02	3.88E-02	3.76E-02
	13	0.30638	0.0	-8.85E-02	1.65E-01	6.49E-02	4.69E-02	4.37E-02
	12	0.28085	0.0	9.38E-02	1.46E-01	7.17E-02	5.21E-02	5.84E-02
	11	0.25532	0.0	5.11E-02	1.35E-01	6.67E-02	6.53E-02	6.37E-02
	10	0.22979	3.28E-01	4.17E-02	1.24E-01	7.01E-02	7.61E-02	7.33E-02
	9	0.20425	3.79E-01	3.36E-02	1.22E-01	7.28E-02	9.09E-02	9.28E-02
	8	0.17872	3.23E-01	3.64E-02	1.17E-01	7.43E-02	1.06E-01	1.03E-01
	7	0.15319	1.79E-01	2.45E-02	1.13E-01	8.05E-02	1.22E-01	1.18E-01
	6	0.12766	0.0	2.09E-02	1.18E-01	8.75E-02	1.38E-01	1.31E-01
	5	0.10213	0.0	1.92E-02	1.30E-01	9.95E-02	1.54E-01	1.44E-01
	4	0.07660	0.0	1.81E-02	1.31E-01	1.13E-01	1.67E-01	1.63E-01
	3	0.05106	0.0	1.63E-02	1.40E-01	1.13E-01	1.79E-01	1.79E-01
	2	0.02553	0.0	3.99E-03	1.33E-01	1.29E-01	0.0	0.0
	1	0.0	0.0	6.29E-03	0.0	0.0	1.53E-01	0.0

(d) v/u_0

ORIGINAL PAGE IS
OF POOR QUALITY

TABLE III (Continued)

	1	2	3	4	5	6
I =	0.0	0.50042	1.00000	1.50042	2.00000	2.50042
K =	0.0	0.50042	1.00000	1.50042	2.00000	2.50042
Y						
J	0.48511	0.0	2.35E-01	2.67E-01	4.10E-01	4.29E-01
	0.45957	0.0	3.19E-01	4.09E-01	4.36E-01	4.83E-01
	0.43404	0.0	3.45E-01	4.18E-01	4.46E-01	4.81E-01
	0.40851	0.0	3.32E-01	4.20E-01	4.60E-01	4.80E-01
	0.38298	0.0	2.99E-01	4.16E-01	4.57E-01	4.84E-01
	0.35745	0.0	2.50E-01	4.05E-01	4.71E-01	4.88E-01
	0.33191	0.0	1.94E-01	4.09E-01	4.87E-01	4.90E-01
	0.30638	0.0	1.12E-01	4.12E-01	4.85E-01	4.93E-01
	0.28085	0.0	2.32E-01	4.33E-01	4.98E-01	5.03E-01
	0.25532	0.0	2.99E-01	4.56E-01	5.12E-01	5.03E-01
	0.22979	7.24E-01	2.99E-01	4.75E-01	5.13E-01	5.05E-01
	0.20425	9.11E-01	3.02E-01	4.75E-01	5.17E-01	5.03E-01
	0.17872	9.46E-01	2.92E-01	4.86E-01	5.19E-01	4.96E-01
	0.15319	4.18E-01	2.69E-01	4.74E-01	5.00E-01	4.76E-01
	0.12766	-7.65E-03	2.46E-01	4.50E-01	4.61E-01	4.49E-01
	0.10213	0.0	2.09E-01	3.97E-01	4.11E-01	4.00E-01
	0.07660	0.0	1.73E-01	3.20E-01	3.51E-01	3.29E-01
	0.05106	0.0	1.13E-01	2.18E-01	2.52E-01	2.38E-01
	0.02553	0.0	6.19E-02	1.11E-01	1.32E-01	1.15E-01
	0.0	0.0	9.59E-03	3.77E-02	4.23E-02	1.20E-01

(c) v/u_0

ORIGINAL PAGE IS
OF POOR QUALITY

TABLE IV

VELOCITY DATA FOR SWIRL VANE ANGLE $\phi = 45^\circ$ [SIDE-WALL
EXPANSION ANGLE $\alpha = 90^\circ$ WITHOUT CONTRACTION BLOCK]

J	I	1	2	3	4	5	6
	X =	0.0	0.1493E	0.2554E5	0.44780	0.59690	0.74625
20	0.147d	0.0	2.00E+01	3.28E+01	6.20E+01	6.30E+01	5.65E+01
19	0.15716	0.0	2.40E+01	3.86E+01	6.38E+01	6.20E+01	5.75E+01
18	0.12954	0.0	2.72E+01	4.56E+01	6.14E+01	6.20E+01	5.88E+01
17	0.12192	0.0	3.16E+01	5.32E+01	6.04E+01	6.14E+01	5.98E+01
16	0.11430	0.0	4.20E+01	6.04E+01	6.00E+01	6.10E+01	5.98E+01
15	0.10658	0.0	6.60E+01	6.80E+01	6.00E+01	6.10E+01	6.08E+01
14	0.09906	0.0	9.52E+01	7.48E+01	6.08E+01	6.16E+01	6.18E+01
13	0.09144	0.0	1.18E+02	8.12E+01	6.20E+01	6.24E+01	6.32E+01
12	0.08382	0.0	1.26E+02	8.64E+01	6.32E+01	6.40E+01	6.46E+01
11	0.07620	0.0	1.29E+02	9.00E+01	6.54E+01	6.56E+01	6.64E+01
10	0.06858	2.58E+01	1.30E+02	9.36E+01	6.70E+01	6.80E+01	6.86E+01
9	0.06096	2.72E+01	1.30E+02	9.56E+01	6.94E+01	7.12E+01	7.14E+01
8	0.05334	2.66E+01	1.30E+02	9.82E+01	7.22E+01	7.50E+01	7.48E+01
7	0.04572	2.82E+01	1.30E+02	1.00E+02	7.60E+01	7.84E+01	7.74E+01
6	0.03810	2.56E+01	1.32E+02	1.03E+02	7.96E+01	8.28E+01	8.12E+01
5	0.03048	3.60E+01	1.33E+02	1.06E+02	8.44E+01	8.52E+01	8.50E+01
4	0.02286	1.01E+02	1.38E+02	1.10E+02	9.00E+01	9.16E+01	8.96E+01
3	0.01524	1.53E+02	1.44E+02	1.17E+02	9.70E+01	9.66E+01	9.52E+01
2	0.00762	1.75E+02	1.56E+02	1.31E+02	1.06E+02	1.04E+02	1.02E+02
1	0.0	1.97E+02	1.76E+02	1.67E+02	1.49E+02	1.77E+02	1.30E+02

(a) Yaw Angle

ORIGINAL PAGE IS
OF POOR QUALITY

TABLE IV (Continued)

	I	2	3	4	5	6		
X =	0.0	0.14935	C.2964E	C.4478C	C.5965C	0.74625		
Y								
J	20	0.14478	C.0	1.89E+00	2.13E+00	1.12E+01	5.73E+00	4.90E+00
	19	0.13716	0.0	-2.33E+00	-3.71E+00	2.85E+00	2.84E+00	2.36E+00
	18	0.12954	0.0	-8.42E+00	-8.33E+00	3.66E-01	-1.99E-01	3.23E-01
	17	0.12192	0.0	-1.24E+01	-1.20E+01	-2.20E-01	-8.47E-01	-1.52E-01
	16	0.11430	0.0	-1.89E+01	-1.52E+01	-9.37E-01	-1.15E+00	-6.15E-01
	15	0.10668	0.0	-2.75E+01	-1.61E+01	-1.41E+00	-1.52E+00	-5.13E-01
	14	0.09906	0.0	-4.15E+00	-1.60E+01	-1.63E+00	-1.81E+00	-1.35E+00
	13	0.09144	0.0	3.55E+00	-1.65E+01	-2.08E+00	-2.82E+00	-2.05E+00
	12	0.08382	0.0	4.93E+00	-1.64E+01	-2.98E+00	-3.48E+00	-2.12E+00
	11	0.07620	0.0	5.12E+00	-1.54E+01	-3.54E+00	-4.24E+00	-2.94E+00
	10	0.05858	1.18E+01	4.65E+00	-1.41E+01	-4.26E+00	-5.77E+00	-3.79E+00
	9	0.06096	1.18E+01	3.47E+00	-1.42E+01	-5.09E+00	-6.99E+00	-4.49E+00
	8	0.05354	1.06E+01	2.61E+00	-1.38E+01	-6.65E+00	-7.75E+00	-5.37E+00
	7	0.04572	8.11E+00	9.32E-01	-1.43E+01	-8.00E+00	-9.81E+00	-7.07E+00
	6	0.03610	1.49E+01	-7.38E-01	-1.60E+01	-1.11E+01	-1.09E+01	-7.90E+00
	5	0.03048	-8.50E-01	-3.94E+00	-1.82E+01	-1.43E+01	-1.52E+01	-8.50E+00
	4	0.02286	-5.10E+01	-6.18E+00	-2.12E+01	-2.17E+01	-1.84E+01	-1.20E+01
	3	0.01524	-3.10E+01	-1.08E+01	-3.06E+01	-3.06E+01	-2.56E+01	-1.85E+01
	2	0.00762	-3.57E+01	-1.72E+01	-3.82E+01	-4.33E+01	-4.50E+01	-2.75E+01
	1	0.0	-2.86E+01	-1.17E+01	0.0	0.0	5.04E+01	-4.13E+01

(b) Pitch Angle

ORIGINAL PAGE IS
OF POOR QUALITY

TABLE IV (Continued)

	1	2	3	4	5	6
I =	0.0	0.50042	1.00000	1.50042	2.00000	2.50042
X =						
J						
Y						
20	0.48511	0.0	9.12E-01	6.92E-01	2.60E-01	2.44E-01
19	0.45957	0.0	8.54E-01	6.03E-01	2.61E-01	2.67E-01
18	0.43404	0.0	7.44E-01	4.76E-01	2.89E-01	2.80E-01
17	0.40851	0.0	5.64E-01	3.65E-01	3.04E-01	2.89E-01
16	0.38298	0.0	3.36E-01	2.72E-01	3.16E-01	2.94E-01
15	0.35745	0.0	1.05E-01	1.94E-01	3.23E-01	2.98E-01
14	0.33191	0.0	-4.67E-02	1.34E-01	3.18E-01	2.95E-01
13	0.30638	0.0	-1.73E-01	7.67E-02	3.11E-01	2.88E-01
12	0.28085	0.0	-2.51E-01	3.16E-02	3.00E-01	2.76E-01
11	0.25532	0.0	-2.97E-01	1.66E-06	2.80E-01	2.56E-01
10	0.22979	1.68E+00	-3.11E-01	-3.40E-02	2.60E-01	2.28E-01
9	0.20425	1.82E+00	-3.11E-01	-5.32E-02	2.31E-01	1.92E-01
8	0.17372	1.93E+00	-3.07E-01	-7.97E-02	1.96E-01	1.49E-01
7	0.15319	1.34E+00	-2.91E-01	-9.70E-02	1.46E-01	1.10E-01
6	0.12766	4.05E-01	-2.67E-01	-1.15E-01	9.98E-02	6.46E-02
5	0.10213	1.70E-01	-2.37E-01	-1.29E-01	4.79E-02	6.33E-03
4	0.07060	-1.62E-02	-2.16E-01	-1.42E-01	1.23E-06	1.08E-02
3	0.05106	-1.39E-01	-1.94E-01	-1.42E-01	-3.45E-02	-3.12E-02
2	0.02553	-1.36E-01	-1.73E-01	-1.42E-01	-5.06E-02	-3.97E-02
1	0.0	-1.30E-01	-1.83E-01	-1.04E-01	-4.32E-02	-1.01E-01

(c) u/u_0

ORIGINAL PAGE IS
OF POOR QUALITY

TABLE IV (Continued)

J	I =	1	2	3	4	5	6
	X =	0.0	0.50042	1.00000	1.50042	2.00000	2.50042
20	Y	0.0	3.20E-02	3.06E-02	1.10E-01	5.39E-02	4.77E-02
19		0.0	-3.80E-02	-5.01E-02	2.94E-02	2.83E-02	2.38E-02
18		0.0	-1.24E-01	-9.97E-02	3.86E-03	-2.07E-03	3.30E-03
17		0.0	-1.46E-01	-1.30E-01	-2.36E-03	-8.92E-03	-1.60E-03
16		0.0	-1.55E-01	-1.50E-01	-1.03E-02	-1.23E-02	-6.47E-03
15		0.0	-1.35E-01	-1.50E-01	-1.59E-02	-1.63E-02	-9.68E-03
14		0.0	-2.12E-02	-1.46E-01	-1.86E-02	-1.95E-02	-1.44E-02
13		0.0	2.29E-02	-1.49E-01	-2.41E-02	-3.06E-02	-2.19E-02
12		0.0	3.69E-02	-1.48E-01	-3.46E-02	-3.83E-02	-2.27E-02
11		0.0	4.22E-02	-1.44E-01	-4.16E-02	-4.60E-02	-3.13E-02
10		3.90E-01	3.56E-02	-1.36E-01	-4.96E-02	-6.15E-02	-4.00E-02
9		4.29E-01	2.55E-02	-1.38E-01	-5.84E-02	-7.32E-02	-4.68E-02
8		4.05E-01	2.16E-02	-1.37E-01	-7.47E-02	-7.85E-02	-5.46E-02
7		2.17E-01	7.30E-03	-1.35E-01	-8.46E-02	-9.43E-02	-6.86E-02
6		1.19E-01	-5.13E-03	-1.45E-01	-1.09E-01	-5.94E-02	-7.25E-02
5		-3.12E-03	-2.38E-02	-1.57E-01	-1.25E-01	-1.23E-01	-7.14E-02
4		-1.05E-01	3.15E-02	-1.61E-01	-1.54E-01	-1.29E-01	-8.56E-02
3		-9.37E-02	4.57E-02	-1.78E-01	-1.68E-01	-1.54E-01	-1.05E-01
2		-5.79E-02	5.85E-02	-1.72E-01	-1.71E-01	-1.59E-01	-1.11E-01
1		-7.42E-02	3.80E-02	0.0	0.0	1.22E-01	-9.88E-02

(d) v/u_0

ORIGINAL PAGE IS
OF POOR QUALITY

TABLE IV (Continued)

	1	2	3	4	5	6		
I =	0.0	0.50042	1.00000	1.50042	2.00000	2.50042		
X =	0.0	0.50042	1.00000	1.50042	2.00000	2.50042		
Y								
J	20	0.46511	C.0	3.22E-C1	4.46E-01	4.90E-01	4.78E-01	4.64E-01
	19	0.45957	0.0	3.80E-01	4.81E-01	5.30E-01	5.03E-01	4.86E-01
	18	0.43404	0.0	3.82E-01	4.86E-01	5.31E-01	5.26E-01	5.01E-01
	17	0.40851	0.0	3.47E-C1	4.88E-01	5.35E-01	5.30E-01	5.19E-01
	16	0.38298	0.0	3.02E-01	4.79E-01	5.47E-01	5.31E-01	5.20E-01
	15	0.35745	0.0	2.36E-01	4.81E-01	5.59E-01	5.38E-01	5.30E-01
	14	0.33191	0.0	2.88E-01	4.92E-01	5.69E-01	5.45E-01	5.38E-01
	13	0.30638	0.0	3.26E-01	4.95E-01	5.86E-01	5.51E-01	5.46E-01
	12	0.28085	0.0	3.46E-01	5.02E-01	5.93E-01	5.65E-01	5.56E-01
	11	0.25532	0.0	3.66E-01	5.23E-01	6.11E-01	5.65E-01	5.59E-01
	10	0.22979	8.10E-01	3.74E-01	5.41E-01	6.13E-01	5.64E-01	5.62E-01
	9	0.20425	9.37E-01	3.73E-C1	5.42E-01	6.14E-01	5.65E-01	5.64E-01
	8	0.17872	9.68E-01	3.61E-01	5.53E-01	6.10E-01	5.57E-01	5.60E-01
	7	0.15319	7.18E-01	3.42E-01	5.39E-01	5.85E-01	5.34E-01	5.40E-01
	6	0.12766	1.94E-01	2.96E-C1	4.92E-01	5.44E-01	5.12E-01	5.16E-01
	5	0.10213	1.23E-01	2.51E-01	4.61E-01	4.89E-01	4.53E-01	4.76E-01
	4	0.07660	6.35E-02	1.95E-01	3.91E-01	3.87E-01	3.88E-01	4.03E-01
	3	0.05106	7.08E-02	1.39E-01	2.73E-01	2.81E-01	2.69E-01	3.12E-01
	2	0.02553	1.28E-02	7.62E-02	1.66E-01	1.74E-01	1.55E-01	2.08E-01
	1	0.0	-4.08E-02	1.28E-C2	2.35E-02	2.55E-02	4.93E-03	8.55E-02

(e) w/u_0

ORIGINAL PAGE IS
OF POOR QUALITY

TABLE V

VELOCITY DATA FOR SWIRL VANE ANGLE $\phi = 60^\circ$ [SIDE-WALL
EXPANSION ANGLE $\alpha = 90^\circ$ WITHOUT CONTRACTION BLOCK]

J	Y	1	2	3	4	5	6
20	0.1478	0.0	4.10E+01	5.24E+01	6.48E+01	6.26E+01	6.60E+01
19	0.13716	0.0	4.24E+01	5.38E+01	6.46E+01	6.26E+01	6.62E+01
18	0.12554	0.0	4.36E+01	5.72E+01	6.44E+01	6.32E+01	6.72E+01
17	0.12192	0.0	4.64E+01	6.12E+01	6.50E+01	6.38E+01	6.88E+01
16	0.11430	0.0	5.26E+01	6.50E+01	6.50E+01	6.50E+01	7.04E+01
15	0.10608	0.0	6.10E+01	6.84E+01	6.56E+01	6.60E+01	7.22E+01
14	0.09906	0.0	7.24E+01	7.14E+01	6.64E+01	6.78E+01	7.36E+01
13	0.09144	0.0	8.54E+01	7.38E+01	6.78E+01	6.94E+01	7.54E+01
12	0.08382	0.0	9.48E+01	7.58E+01	6.92E+01	7.12E+01	7.76E+01
11	0.07620	0.0	1.02E+02	7.76E+01	7.14E+01	7.38E+01	7.98E+01
10	0.06858	3.56E+01	1.05E+02	7.90E+01	7.44E+01	7.64E+01	8.24E+01
9	0.06096	3.42E+01	1.07E+02	8.14E+01	7.76E+01	7.90E+01	8.52E+01
8	0.05334	3.78E+01	1.08E+02	8.32E+01	8.12E+01	8.16E+01	8.78E+01
7	0.04572	7.94E+01	1.09E+02	8.60E+01	8.50E+01	8.50E+01	9.08E+01
6	0.03810	1.17E+02	1.10E+02	9.02E+01	8.84E+01	8.86E+01	9.56E+01
5	0.03048	1.04E+02	1.11E+02	9.44E+01	9.28E+01	9.34E+01	1.00E+02
4	0.02286	9.22E+01	1.14E+02	1.01E+02	9.72E+01	9.86E+01	1.06E+02
3	0.01524	9.40E+01	1.18E+02	1.04E+02	1.03E+02	1.05E+02	1.13E+02
2	0.00762	5.90E+01	1.31E+02	1.13E+02	1.11E+02	1.13E+02	1.36E+02
1	0.0	1.10E+02	1.68E+02	1.39E+02	1.28E+02	1.35E+02	1.66E+02

(a) Yaw Angle

ORIGINAL PAGE IS
OF POOR QUALITY

TABLE V (Continued)

J	Y	I	2	3	4	5	6
20	0.14478	0.0	2.17E+01	1.01E+01	9.00E+00	6.38E+00	1.10E+01
19	0.13716	0.0	1.40E+01	3.30E+00	3.07E+00	2.86E+00	5.31E+00
18	0.12954	0.0	1.04E+01	-2.70E+00	1.20E+00	2.65E+00	1.87E+00
17	0.12192	0.0	9.60E+00	-3.78E+00	6.62E-01	2.06E+00	1.42E+00
16	0.11430	0.0	6.55E+00	-4.36E+00	1.53E-01	1.44E+00	9.89E-01
15	0.10608	0.0	1.33E+00	-4.77E+00	3.27E-01	7.92E-01	7.66E-01
14	0.09906	0.0	-3.23E+00	-4.51E+00	1.42E-01	2.37E-01	3.17E-02
13	0.09144	0.0	-6.11E+00	-4.31E+00	-2.08E-01	-1.68E-01	-3.18E-01
12	0.08382	0.0	-5.84E+00	-3.87E+00	-6.00E-01	-1.05E+00	-1.09E+00
11	0.07620	0.0	-5.78E+00	-3.42E+00	-1.27E+00	-1.59E+00	-1.73E+00
10	0.06858	7.13E+00	-4.58E+00	-2.55E+00	-2.09E+00	-2.60E+00	-2.33E+00
9	0.06096	4.84E+00	-4.39E+00	-2.34E+00	-2.12E+00	-3.72E+00	-3.34E+00
8	0.05334	-2.82E-01	-4.12E+00	-2.78E+00	-3.79E+00	-4.81E+00	-4.42E+00
7	0.04572	-5.34E+00	-4.19E+00	-3.70E+00	-4.85E+00	-5.86E+00	-6.09E+00
6	0.03810	4.50E+00	-5.04E+00	-5.31E+00	-6.74E+00	-8.66E+00	-7.53E+00
5	0.03048	-2.29E+01	-6.14E+00	-7.84E+00	-8.70E+00	-1.15E+01	-1.11E+01
4	0.02286	-3.46E+01	-7.81E+00	-1.23E+01	-1.27E+01	-1.58E+01	-1.62E+01
3	0.01524	-3.84E+01	-1.34E+01	-1.79E+01	-1.79E+01	-2.30E+01	-2.47E+01
2	0.00762	-4.44E+01	-2.71E+01	-2.83E+01	-2.68E+01	-3.66E+01	-3.82E+01
1	0.0	-5.74E+01	-4.06E+01	-5.79E+01	-5.13E+01	-5.59E+01	0.0

(b) Pitch Angle

ORIGINAL PAGE IS
OF POOR QUALITY

TABLE V (Continued)

	I	2	3	4	5	6
X	0.0	0.50042	1.00000	1.50042	2.00000	2.50042
J						
Y						
20	0.46511	0.0	8.09E-01	5.92E-01	3.54E-01	3.93E-01
19	0.45957	0.0	7.85E-01	5.92E-01	3.82E-01	4.07E-01
18	0.43434	0.0	7.28E-01	5.27E-01	3.91E-01	4.02E-01
17	0.40851	0.0	6.58E-01	4.69E-01	3.91E-01	4.05E-01
16	0.35258	0.0	5.14E-01	4.06E-01	3.99E-01	3.59E-01
15	0.35745	0.0	3.66E-01	3.51E-01	3.95E-01	3.87E-01
14	0.33191	0.0	2.09E-01	3.06E-01	3.90E-01	3.68E-01
13	0.30638	0.0	5.75E-02	2.73E-01	3.75E-01	3.46E-01
12	0.28085	0.0	-6.38E-02	2.44E-01	3.55E-01	3.20E-01
11	0.25532	0.0	-1.64E-01	2.19E-01	3.22E-01	2.80E-01
10	0.22979	2.59E+00	-2.29E-01	1.97E-01	2.72E-01	2.37E-01
9	0.20425	2.70E+00	-2.65E-01	1.58E-01	2.15E-01	1.92E-01
8	0.17872	1.39E+00	-2.89E-01	1.23E-01	1.51E-01	1.44E-01
7	0.15319	8.13E-02	-2.96E-01	6.98E-02	8.32E-02	6.30E-02
6	0.12706	-1.50E-01	-2.91E-01	3.27E-03	2.50E-02	2.15E-02
5	0.10213	-4.51E-02	-2.82E-01	6.43E-02	-4.00E-02	4.72E-02
4	0.07600	-7.61E-03	-2.69E-01	1.28E-01	8.88E-02	1.03E-01
3	0.05106	-1.38E-02	-2.34E-01	1.33E-01	1.28E-01	1.41E-01
2	0.02553	-2.51E-02	-2.11E-01	1.41E-01	1.47E-01	1.39E-01
1	0.0	-3.06E-02	-1.55E-01	1.16E-01	1.27E-01	1.37E-01

(c) u/u_0

ORIGINAL PAGE IS
OF POOR QUALITY

TABLE V (Continued)

J	Y	1	2	3	4	5	6
20	0.43511	0.0	4.28E-01	1.72E-01	1.32E-01	5.55E-02	1.59E-01
19	0.45957	0.0	2.65E-01	5.77E-02	4.78E-02	4.41E-02	8.02E-02
18	0.43404	0.0	1.85E-01	4.60E-02	1.89E-02	4.12E-02	2.86E-02
17	0.40851	0.0	1.61E-01	6.44E-02	1.07E-02	3.30E-02	2.26E-02
16	0.38298	0.0	9.72E-02	7.33E-02	2.52E-03	2.38E-02	1.60E-02
15	0.35745	0.0	1.76E-02	7.96E-02	5.45E-03	1.32E-02	1.26E-02
14	0.33191	0.0	-3.91E-02	7.55E-02	2.41E-03	4.02E-03	5.29E-04
13	0.30638	0.0	-7.67E-02	7.37E-02	3.60E-03	2.88E-03	5.42E-03
12	0.23085	0.0	-7.80E-02	6.72E-02	1.40E-02	1.82E-02	1.88E-02
11	0.25532	0.0	-8.28E-02	6.10E-02	2.23E-02	2.80E-02	3.02E-02
10	0.22979	3.98E-01	7.60E-02	5.40E-02	3.68E-02	4.57E-02	4.09E-02
9	0.20425	2.76E-01	6.96E-02	4.30E-02	5.46E-02	6.54E-02	5.83E-02
8	0.17872	-8.68E-01	6.65E-02	5.04E-02	6.53E-02	6.31E-02	7.45E-02
7	0.15319	-4.13E-02	6.77E-02	6.46E-02	8.10E-02	5.76E-02	5.61E-02
6	0.12706	2.59E-02	7.66E-02	8.73E-02	1.06E-01	1.34E-01	1.11E-01
5	0.10213	-8.09E-02	8.48E-02	1.15E-01	1.25E-01	1.63E-01	1.44E-01
4	0.07000	-1.37E-01	9.13E-02	1.46E-01	1.60E-01	1.55E-01	1.81E-01
3	0.05106	-1.56E-01	1.19E-01	1.73E-01	1.81E-01	2.32E-01	2.12E-01
2	0.02553	-1.57E-01	1.65E-01	1.57E-01	2.05E-01	2.68E-01	2.36E-01
1	0.0	-1.43E-01	1.71E-01	2.45E-01	2.55E-01	2.86E-01	0.0

(d) v/u_0

ORIGINAL PAGE IS
OF POOR QUALITY

TABLE V (Continued)

J	Y	I	2	3	4	5	6
	X =	0.0	0.50042	1.00000	1.50042	2.00000	2.50042
20	0.48511	0.0	7.04E-01	7.68E-01	7.53E-01	7.57E-01	7.46E-01
19	0.65957	0.0	7.17E-01	8.08E-01	8.04E-01	7.84E-01	7.89E-01
18	0.43404	0.0	6.93E-01	8.18E-01	8.16E-01	7.55E-01	8.09E-01
17	0.40851	0.0	6.91E-01	8.53E-01	8.38E-01	8.22E-01	8.47E-01
16	0.38256	0.0	6.72E-01	8.71E-01	8.55E-01	8.56E-01	8.75E-01
15	0.35745	0.0	6.61E-01	8.87E-01	8.70E-01	8.69E-01	9.00E-01
14	0.33191	0.0	6.60E-01	9.08E-01	8.92E-01	9.01E-01	9.17E-01
13	0.30638	0.0	7.14E-01	9.38E-01	9.18E-01	9.21E-01	9.44E-01
12	0.28085	0.0	7.60E-01	9.65E-01	9.35E-01	9.39E-01	9.65E-01
11	0.25532	0.0	8.00E-01	9.98E-01	9.57E-01	9.65E-01	9.85E-01
10	0.22979	1.85E+00	8.42E-01	1.02E+00	9.74E-01	9.79E-01	9.97E-01
9	0.20425	1.84E+00	8.67E-01	1.04E+00	9.79E-01	9.87E-01	9.96E-01
8	0.17872	1.08E+00	8.78E-01	1.03E+00	9.76E-01	9.77E-01	9.63E-01
7	0.15319	4.34E-01	8.78E-01	9.58E-01	9.51E-01	9.48E-01	9.01E-01
6	0.12766	2.94E-01	8.19E-01	9.39E-01	8.94E-01	8.61E-01	8.38E-01
5	0.10213	1.86E-01	7.35E-01	8.36E-01	8.17E-01	7.95E-01	7.24E-01
4	0.07650	1.58E-01	6.09E-01	6.57E-01	7.03E-01	6.83E-01	6.00E-01
3	0.05106	1.57E-01	4.43E-01	5.18E-01	5.46E-01	5.27E-01	4.24E-01
2	0.02553	1.58E-01	2.42E-01	3.38E-01	3.79E-01	3.34E-01	2.07E-01
1	0.0	8.60E-02	4.14E-02	1.00E-01	1.60E-01	1.36E-01	3.04E-02

(e) w/u₀

ORIGINAL PAGE IS
OF POOR QUALITY.

TABLE VI

VELOCITY DATA FOR SWIRL VANE ANGLE $\phi = 70^\circ$ [SIDE-WALL
EXPANSION ANGLE $\alpha = 90^\circ$ WITHOUT CONTRACTION BLOCK]

J	Y	1	2	3	4	5	6
	X =	0.0	0.14935	0.29845	0.44780	0.59690	0.74625
20	0.14478	0.0	2.90E+01	6.58E+01	6.94E+01	6.70E+01	5.58E+01
19	0.13716	0.0	3.98E+01	6.76E+01	7.02E+01	6.86E+01	5.84E+01
18	0.12954	0.0	4.94E+01	6.86E+01	7.08E+01	6.94E+01	6.14E+01
17	0.12192	0.0	5.96E+01	7.00E+01	7.18E+01	7.10E+01	6.36E+01
16	0.11430	0.0	7.12E+01	7.14E+01	7.22E+01	7.28E+01	6.58E+01
15	0.10668	0.0	8.14E+01	7.32E+01	7.44E+01	7.46E+01	6.80E+01
14	0.09906	0.0	8.98E+01	7.48E+01	7.58E+01	7.70E+01	6.98E+01
13	0.09144	0.0	9.60E+01	7.64E+01	7.80E+01	7.94E+01	7.22E+01
12	0.08382	0.0	9.98E+01	7.86E+01	8.04E+01	8.18E+01	7.44E+01
11	0.07620	0.0	1.02E+02	8.06E+01	8.32E+01	8.44E+01	7.70E+01
10	0.06858	4.38E+01	1.03E+02	8.32E+01	8.60E+01	8.70E+01	7.96E+01
9	0.06096	4.28E+01	1.03E+02	8.64E+01	8.92E+01	9.04E+01	8.26E+01
8	0.05334	6.30E+01	1.03E+02	9.00E+01	9.26E+01	9.37E+01	8.54E+01
7	0.04572	1.12E+02	1.05E+02	9.46E+01	9.58E+01	9.70E+01	8.86E+01
6	0.03810	1.24E+02	1.07E+02	9.90E+01	9.98E+01	1.01E+02	9.26E+01
5	0.03048	1.13E+02	1.09E+02	1.03E+02	1.04E+02	1.05E+02	9.64E+01
4	0.02286	1.08E+02	1.11E+02	1.07E+02	1.08E+02	1.10E+02	1.02E+02
3	0.01524	1.04E+02	1.14E+02	1.10E+02	1.13E+02	1.17E+02	1.09E+02
2	0.00762	1.08E+02	1.20E+02	1.17E+02	1.21E+02	1.27E+02	1.22E+02
1	0.0	1.27E+02	1.36E+02	1.34E+02	1.41E+02	1.59E+02	1.64E+02

(a) Yaw Angle

ORIGINAL PAGE IS
OF POOR QUALITY

TABLE VI (Continued)

	I	2	J	4	5	6
X	0.0	0.1493E	0.25E4E	0.447E0	0.5565C	0.74625
Y						
20	0.14478	0.0	1.56E+C1	1.07E+01	8.46E+00	6.45E+00
19	0.13716	0.0	4.60E+00	3.21E+0C	3.91E+00	1.27E+00
18	0.12954	0.0	-2.13E+00	-2.90E+00	5.53E-01	-2.13E-01
17	0.12192	0.0	-6.80E+00	-3.61E+0C	-6.47E-02	-1.48E+00
16	0.11430	0.0	-5.49E+CC	-4.67E+00	-1.20E+00	-2.04E+0C
15	0.10668	0.0	-1.05E+01	-5.37E+00	-1.75E+00	-2.74E+00
14	0.09906	0.0	-1.12E+01	-6.01E+00	-2.80E+00	-3.77E+00
13	0.09144	0.0	-1.03E+01	-6.07E+00	-3.87E+00	-4.44E+00
12	0.08382	0.0	-9.67E+00	-6.13E+00	-5.02E+00	-5.05E+00
11	0.07620	0.0	-8.78E+00	-6.44E+0C	-6.20E+00	-6.09E+00
10	0.05858	1.20E+00	-8.13E+00	-7.39E+00	-7.49E+00	-7.03E+00
9	0.06096	-3.71E+CC	-7.57E+00	-8.35E+0C	-8.91E+00	-7.81E+00
8	0.05334	-2.38E+01	-8.24E+00	-9.60E+0C	-1.07E+01	-5.57E+00
7	0.04572	-1.76E+01	-8.85E+00	-1.11E+01	-1.30E+01	-1.14E+01
6	0.03810	-9.40E+0C	-1.07E+01	-1.37E+01	-1.59E+01	-1.34E+01
5	0.03048	-1.22E+01	-1.24E+01	-1.64E+01	-1.96E+01	-1.61E+01
4	0.02286	-2.35E+01	-1.69E+01	-2.19E+01	-2.59E+01	-2.21E+01
3	0.01524	-3.24E+01	-2.46E+01	-2.85E+01	-3.41E+01	-2.90E+01
2	0.00762	-4.36E+01	-3.46E+01	-4.11E+01	-4.72E+01	-3.93E+01
1	0.0	-5.48E+01	-5.41E+01	0.0	0.0	0.0

(b) Pitch Angle

ORIGINAL PAGE IS
OF POOR QUALITY

TABLE VI (Continued)

J	Y	I	2	3	4	5	6
20	0.46511	0.0	1.62E+00	5.15E-01	4.38E-01	4.78E-01	5.96E-01
19	0.45957	0.0	1.30E+00	4.91E-01	4.48E-01	4.67E-01	5.98E-01
18	0.43404	0.0	9.77E-01	5.01E-01	4.35E-01	4.60E-01	5.94E-01
17	0.40851	0.0	6.75E-01	4.79E-01	4.23E-01	4.36E-01	5.78E-01
16	0.39298	0.0	3.89E-01	4.52E-01	4.19E-01	4.05E-01	5.50E-01
15	0.35745	0.0	1.73E-01	4.17E-01	3.75E-01	3.69E-01	5.15E-01
14	0.33191	0.0	4.11E-01	3.84E-01	3.46E-01	3.17E-01	4.84E-01
13	0.30638	0.0	-1.29E-01	3.51E-01	2.95E-01	2.63E-01	4.38E-01
12	0.28065	0.0	-2.16E-01	2.99E-01	2.39E-01	2.07E-01	3.88E-01
11	0.25512	0.0	-2.70E-01	2.50E-01	1.71E-01	1.43E-01	3.27E-01
10	0.22979	3.47E+00	3.02E-01	1.80E-01	1.01E-01	7.70E-02	2.61E-01
9	0.20425	2.77E+00	3.05E-01	9.44E-02	2.02E-02	-1.02E-02	1.81E-01
8	0.17872	6.03E-01	3.19E-01	4.60E-06	-6.35E-02	-9.02E-02	1.09E-01
7	0.15319	-3.34E-01	3.26E-01	-1.10E-01	-1.33E-01	-1.59E-01	3.13E-02
6	0.12766	-4.76E-01	3.55E-01	-1.96E-01	-2.07E-01	-2.19E-01	5.31E-02
5	0.10213	-2.88E-01	3.51E-01	-2.48E-01	-2.49E-01	-2.76E-01	1.13E-01
4	0.07650	-1.39E-01	3.16E-01	-2.63E-01	-2.64E-01	-2.91E-01	1.79E-01
3	0.05106	-9.55E-02	2.62E-01	-2.42E-01	-2.59E-01	-3.02E-01	2.10E-01
2	0.02553	-8.68E-02	2.13E-01	-2.05E-01	-2.21E-01	-2.64E-01	2.25E-01
1	0.0	-1.07E-01	1.54E-01	-2.08E-01	-2.34E-01	-2.38E-01	1.35E-01

(c) u/u_0

ORIGINAL PAGE IS
OF POOR QUALITY.

TABLE VI (Continued)

J	I	2	3	4	5	6
	I =	0.50042	1.00000	1.50042	2.00000	2.50042
	X =	0.0				
Y						
20	0.48511	0.0	5.18E-01	2.35E-01	1.85E-01	1.38E-01
19	0.45957	0.0	1.36E-01	7.23E-02	9.03E-02	2.84E-02
18	0.43404	0.0	-5.58E-02	-6.96E-02	1.28E-02	-4.87E-03
17	0.40851	0.0	-1.59E-01	-8.83E-02	-1.53E-03	-3.46E-02
16	0.38298	0.0	-2.02E-01	-1.16E-01	-2.87E-02	-4.87E-02
15	0.35745	0.0	-2.14E-01	-1.36E-01	-4.27E-02	-6.65E-02
14	0.33191	0.0	-2.33E-01	-1.54E-01	-6.90E-02	-9.28E-02
13	0.30638	0.0	-2.24E-01	-1.59E-01	-9.61E-02	-1.11E-01
12	0.28085	0.0	-2.17E-01	-1.62E-01	-1.26E-01	-1.29E-01
11	0.25532	0.0	-2.04E-01	-1.73E-01	-1.57E-01	-1.57E-01
10	0.22979	1.01E-01	-1.98E-01	-1.98E-01	-1.91E-01	-1.82E-01
9	0.20425	-2.45E-01	-1.55E-01	-2.21E-01	-2.27E-01	-2.00E-01
8	0.17872	-5.86E-01	-2.02E-01	-2.45E-01	-2.65E-01	-2.36E-01
7	0.15319	-2.83E-01	-2.07E-01	-2.70E-01	-3.05E-01	-2.63E-01
6	0.12766	-1.40E-01	-2.31E-01	-3.06E-01	-3.46E-01	-2.83E-01
5	0.10213	-1.31E-01	-2.38E-01	-3.25E-01	-3.78E-01	-3.01E-01
4	0.07660	-1.92E-01	-2.63E-01	-3.70E-01	-4.24E-01	-3.42E-01
3	0.05106	-2.44E-01	-2.55E-01	-3.82E-01	-4.49E-01	-3.66E-01
2	0.02553	-2.70E-01	-2.96E-01	-3.99E-01	-4.69E-01	-3.59E-01
1	0.0	-2.51E-01	-2.55E-01	0.0	0.0	0.0

(d) v/u_0

ORIGINAL PAGE IS
OF POOR QUALITY

TABLE VI (Continued)

J	I	1	2	3	4	5	6
	X =	0.0	0.5C042	1.CC000	1.50042	2.00000	2.50042
20	0.38511	0.0	8.98E-01	1.16E+00	1.16E+00	1.13E+00	8.77E-01
19	0.45557	0.0	1.C8E+00	1.19E+00	1.24E+00	1.19E+00	9.72E-01
18	0.43404	0.0	1.14E+00	1.28E+00	1.25E+00	1.22E+00	1.C5E+00
17	0.40851	0.0	1.15E+00	1.32E+00	1.29E+00	1.27E+00	1.16E+00
16	0.38298	0.0	1.14E+00	1.34E+00	1.30E+00	1.31E+00	1.22E+00
15	0.35745	0.0	1.15E+00	1.38E+00	1.34E+00	1.34E+00	1.27E+00
14	0.33191	0.0	1.18E+00	1.41E+00	1.37E+00	1.37E+00	1.31E+00
13	0.30638	0.0	1.23E+00	1.45E+00	1.39E+00	1.41E+00	1.36E+00
12	0.23085	0.0	1.25E+00	1.48E+00	1.42E+00	1.44E+00	1.39E+00
11	0.25532	0.0	1.29E+00	1.51E+00	1.44E+00	1.46E+00	1.42E+00
10	0.22979	3.33E+00	1.35E+00	1.51E+00	1.45E+00	1.47E+00	1.42E+00
9	0.20425	2.57E+00	1.36E+00	1.50E+00	1.45E+00	1.46E+00	1.39E+00
8	0.17872	1.18E+00	1.36E+00	1.45E+00	1.40E+00	1.39E+00	1.36E+00
7	0.15319	8.26E-01	1.29E+00	1.37E+00	1.31E+00	1.29E+00	1.28E+00
6	0.12766	7.01E-01	1.16E+00	1.24E+00	1.20E+00	1.17E+00	1.17E+00
5	0.10213	5.36E-01	1.02E+00	1.07E+00	1.03E+00	1.00E+00	1.00E+00
4	0.07660	4.18E-01	8.06E-01	8.83E-01	8.33E-01	7.92E-01	8.16E-01
3	0.05106	3.72E-01	5.87E-01	6.50E-01	6.11E-01	5.87E-01	6.03E-01
2	0.02553	2.70E-01	3.72E-01	4.09E-01	3.74E-01	3.51E-01	3.55E-01
1	0.0	1.41E-01	1.48E-01	2.17E-01	1.89E-01	1.89E-01	3.57E-02

(e) w/u_0

ORIGINAL PAGE IS
OF POOR QUALITY

TABLE VII

VELOCITY DATA FOR NONSWIRLING FLOW $\phi = 0^\circ$
[SIDE-WALL EXPANSION ANGLE $\alpha = 90^\circ$
WITH CONTRACTION BLOCK AT $L/D = 1$]

J	Y	I =	1	2
	X =	0.0	0.14935	
20	0.14478	0.0		1.80E+02
19	0.13716	0.0		1.80E+02
18	0.12954	0.0		1.84E+02
17	0.12192	0.0		1.85E+02
16	0.11430	0.0		1.87E+02
15	0.10668	0.0		1.87E+02
14	0.09906	0.0		3.60E+02
13	0.09144	0.0		3.60E+02
12	0.08382	0.0		3.60E+02
11	0.07620	0.0		3.60E+02
10	0.06858	3.60E+02		3.60E+02
9	0.06096	3.60E+02		3.60E+02
8	0.05334	3.60E+02		3.60E+02
7	0.04572	3.60E+02		3.60E+02
6	0.03810	3.60E+02		3.60E+02
5	0.03048	3.60E+02		3.60E+02
4	0.02286	3.60E+02		3.60E+02
3	0.01524	3.60E+02		3.60E+02
2	0.00762	3.60E+02		3.60E+02
1	0.0	3.60E+02		3.60E+02

(a) Yaw Angle

ORIGINAL PAGE IS
OF POOR QUALITY

TABLE VII (Continued)

J	Y	X	Z
20	0.14478	0.0	-8.38E-01
19	0.13716	0.0	-1.25E+01
18	0.12954	0.0	-3.57E+01
17	0.12192	0.0	0.0
16	0.11430	0.0	0.0
15	0.10668	0.0	-5.61E+01
14	0.09906	0.0	0.0
13	0.09144	0.0	-2.69E+01
12	0.08382	0.0	8.73E+00
11	0.07620	0.0	8.64E+00
10	0.06858	2.79E+00	4.47E+00
9	0.06096	1.91E+00	2.73E+00
8	0.05334	7.83E-01	1.50E+00
7	0.04572	2.69E-01	9.48E-01
6	0.03810	2.07E-01	7.78E-01
5	0.03048	1.42E-01	7.23E-01
4	0.02286	3.26E-01	8.24E-01
3	0.01524	5.50E-01	8.25E-01
2	0.00762	5.87E-01	8.80E-01
1	0.0	7.71E-01	9.71E-01

(b) Pitch Angle

ORIGINAL PAGE IS
OF POOR QUALITY

TABLE VII (Continued)

J	Y	I =	1	2
	X =	0.0	0.50042	
20	0.43511	0.0	-1.66E-01	
19	0.45957	0.0	-1.67E-01	
18	0.43404	0.0	-1.32E-01	
17	0.40851	0.0	-1.41E-01	
16	0.38298	0.0	-1.16E-01	
15	0.35745	0.0	-8.16E-02	
14	0.33191	0.0	1.87E-02	
13	0.30638	0.0	8.74E-02	
12	0.28085	0.0	2.62E-01	
11	0.25532	0.0	5.35E-01	
10	0.22979	1.01E+00	8.23E-01	
9	0.20425	1.01E+00	9.84E-01	
8	0.17872	1.01E+00	1.02E+00	
7	0.15319	1.01E+00	1.02E+00	
6	0.12766	1.01E+00	1.02E+00	
5	0.10213	1.01E+00	1.02E+00	
4	0.07660	1.01E+00	1.03E+00	
3	0.05106	1.01E+00	1.03E+00	
2	0.02553	1.01E+00	1.03E+00	
1	0.0	1.01E+00	1.03E+00	

(e) u/u_0

ORIGINAL PAGE IS
OF POOR QUALITY

TABLE VII (Continued)

		I =	1	2
		X =	0.0	0.50042
J	Y			
20	0.48511	0.0		-2.43E-03
19	0.45957	0.0		-3.72E-02
18	0.43404	0.0		-5.49E-02
17	0.40851	0.0		0.0
16	0.38298	0.0		0.0
15	0.35745	0.0		-1.22E-01
14	0.33191	0.0		0.0
13	0.30638	0.0		-4.43E-02
12	0.28085	0.0		4.01E-02
11	0.25532	0.0		8.12E-02
10	0.22979	4.54E-02	6.44E-02	
9	0.20425	3.37E-02	4.70E-02	
8	0.17872	1.38E-02	2.67E-02	
7	0.15319	4.73E-03	1.69E-02	
6	0.12766	3.65E-03	1.39E-02	
5	0.10213	2.50E-03	1.29E-02	
4	0.07660	5.74E-03	1.48E-02	
3	0.05106	9.69E-03	1.48E-02	
2	0.02553	1.03E-02	1.58E-02	
1	0.0	1.36E-02	1.75E-02	

(d) v/u_0

ORIGINAL PAGE IS
OF POOR QUALITY.

TABLE VII (Continued)

J	Y	X	I	2
20	0.48511	0.0		5.80E-07
19	0.45957	0.0		5.84E-07
18	0.43404	0.0		-9.21E-03
17	0.40851	0.0		-1.23E-02
16	0.38298	0.0		-1.42E-02
15	0.35745	0.0		-1.00E-02
14	0.33191	0.0		-1.13E-07
13	0.30638	0.0		-5.26E-07
12	0.28085	0.0		-1.58E-06
11	0.25532	0.0		-3.22E-06
10	0.22979	-6.11E-06		-4.96E-06
9	0.20425	-6.10E-06		-5.93E-06
8	0.17872	-6.08E-06		-6.15E-06
7	0.15319	-6.08E-06		-6.14E-06
6	0.12766	-6.07E-06		-6.16E-06
5	0.10213	-6.08E-06		-6.17E-06
4	0.07660	-6.08E-06		-6.19E-06
3	0.05106	-6.08E-06		-6.19E-06
2	0.02553	-6.07E-06		-6.20E-06
1	0.0	-6.07E-06		-6.21E-06

(e) w/u_0

ORIGINAL PAGE IS
OF POOR QUALITY

TABLE VIII

VELOCITY DATA FOR SWIRL VANE ANGLE $\phi = 45^\circ$ [SIDE-WALL EXPANSION
ANGLE $\alpha = 90^\circ$ WITH CONTRACTION BLOCK AT $L/D = 2$]

	I	2	3	4
X	0.0	0.14935	0.29845	0.4780
Y				
J				
20	0.14478	0.0	1.82E+02	3.60E+02
19	0.13716	0.0	1.82E+02	3.60E+02
18	0.12554	0.0	1.95E+02	3.60E+02
17	0.12192	0.0	1.87E+02	3.60E+02
16	0.11430	0.0	1.87E+02	3.60E+02
15	0.10668	0.0	1.81E+02	3.60E+02
14	0.09906	0.0	3.60E+02	3.60E+02
13	0.09144	0.0	3.60E+02	3.60E+02
12	0.08382	0.0	3.60E+02	3.60E+02
11	0.07620	0.0	3.60E+02	3.60E+02
10	0.06858	3.60E+02	3.60E+02	3.60E+02
9	0.06096	3.60E+02	3.60E+02	3.60E+02
8	0.05334	3.60E+02	3.60E+02	3.60E+02
7	0.04572	3.60E+02	3.60E+02	3.60E+02
6	0.03810	3.60E+02	3.60E+02	3.60E+02
5	0.03048	3.60E+02	3.60E+02	3.60E+02
4	0.02286	3.60E+02	3.60E+02	3.60E+02
3	0.01524	3.60E+02	3.60E+02	3.60E+02
2	0.00762	3.60E+02	3.60E+02	3.60E+02
1	0.0	3.60E+02	3.60E+02	3.60E+02

(a) Yaw Angle

ORIGINAL PAGE IS
OF POOR QUALITY

TABLE VIII (Continued)

J	Y	I =	1	2	3	4
	X =	0.0	0.14935	0.25645	0.44780	
20	0.14473	0.0	0.0	-4.18E+01	-2.89E+01	
19	0.13716	0.0	0.0	0.0	-3.59E+01	
18	0.12554	0.0	0.0	-2.02E+01	5.39E+01	
17	0.12192	0.0	-4.13E+01	3.87E+01	5.18E+01	
16	0.11430	0.0	-4.02E+01	3.16E+01	4.32E+01	
15	0.10608	0.0	0.0	3.46E+01	3.41E+01	
14	0.09906	0.0	-3.00E+01	2.16E+01	2.90E+01	
13	0.09144	0.0	1.09E+01	1.65E+01	1.87E+01	
12	0.08382	0.0	1.12E+01	1.11E+01	1.32E+01	
11	0.07620	0.0	7.89E+00	7.59E+00	1.07E+01	
10	0.06858	3.83E+00	4.63E+00	5.59E+00	8.33E+00	
9	0.05096	2.63E+00	2.85E+00	4.17E+00	6.53E+00	
8	0.05334	1.32E+00	1.82E+00	2.89E+00	5.02E+00	
7	0.04572	5.82E-01	1.28E+00	2.08E+00	4.10E+00	
6	0.03810	1.16E-01	9.90E-01	1.54E+00	3.29E+00	
5	0.03048	1.92E-02	6.32E-01	1.13E+00	2.58E+00	
4	0.02286	2.97E-01	7.95E-01	9.83E-01	2.15E+00	
3	0.01524	4.67E-01	8.64E-01	8.71E-01	1.60E+00	
2	0.00762	6.01E-01	8.12E-01	8.00E-01	1.25E+00	
1	0.0	8.38E-01	9.03E-01	8.27E-01	1.41E+00	

(b) Pitch Angle

ORIGINAL PAGE IS
OF POOR QUALITY

TABLE VIII (Continued)

J	I =	1	2	3	4
	X =	0.0	0.50042	1.00000	1.50042
20	Y	0.0	-7.26E-02	3.80E-02	-8.77E-02
19		0.0	-8.30E-02	2.01E-02	-8.18E-02
18		0.0	-8.25E-02	4.66E-02	3.83E-02
17		0.0	-6.32E-02	5.40E-02	6.19E-02
16		0.0	-6.36E-02	8.74E-02	1.03E-01
15		0.0	-4.50E-02	1.20E-01	1.66E-01
14		0.0	1.81E-02	2.16E-01	2.18E-01
13		0.0	1.13E-01	3.06E-01	3.25E-01
12		0.0	2.84E-01	4.21E-01	4.09E-01
11		0.0	5.68E-01	5.85E-01	5.09E-01
10		1.03E+00	8.55E-01	7.54E-01	6.29E-01
9		1.02E+00	1.03E+00	8.67E-01	7.14E-01
8		1.01E+00	1.04E+00	9.56E-01	7.95E-01
7		1.00E+00	1.04E+00	9.98E-01	8.71E-01
6		1.01E+00	1.04E+00	1.01E+00	9.13E-01
5		1.00E+00	1.04E+00	1.02E+00	9.38E-01
4		1.01E+00	1.04E+00	1.02E+00	9.56E-01
3		1.00E+00	1.04E+00	1.02E+00	9.61E-01
2		1.00E+00	1.04E+00	1.02E+00	9.68E-01
1		1.01E+00	1.04E+00	1.02E+00	9.71E-01

(c) u/u_c

ORIGINAL PAGE IS
OF POOR QUALITY

TABLE VIII (Continued)

J	I	1	2	3	4
20	0.48511	0.0	0.0	-3.40E-02	-4.93E-02
19	0.45957	0.0	0.0	0.0	-6.01E-02
18	0.43404	0.0	0.0	-1.72E-02	5.26E-02
17	0.40851	0.0	-5.61E-02	4.32E-02	7.87E-02
16	0.38298	0.0	-5.41E-02	5.37E-02	9.65E-02
15	0.35745	0.0	0.0	8.25E-02	1.13E-01
14	0.33191	0.0	-1.04E-02	8.55E-02	1.21E-01
13	0.30638	0.0	2.16E-02	9.32E-02	1.10E-01
12	0.28085	0.0	5.63E-02	8.26E-02	9.57E-02
11	0.25532	0.0	7.88E-02	7.79E-02	9.63E-02
10	0.22979	6.90E-02	7.22E-02	7.37E-02	5.21E-02
9	0.20425	4.68E-02	5.16E-02	6.31E-02	8.18E-02
8	0.17872	2.34E-02	3.30E-02	4.83E-02	6.98E-02
7	0.15319	6.69E-03	2.32E-02	3.62E-02	6.25E-02
6	0.12766	2.03E-03	1.79E-02	2.72E-02	5.25E-02
5	0.10213	3.36E-04	1.51E-02	2.02E-02	4.23E-02
4	0.07650	5.22E-03	1.44E-02	1.75E-02	3.59E-02
3	0.05106	8.19E-03	1.57E-02	1.56E-02	2.69E-02
2	0.02553	1.05E-02	1.47E-02	1.43E-02	2.12E-02
1	0.0	1.47E-02	1.64E-02	1.48E-02	2.38E-02

(d) v/u_0

ORIGINAL PAGE IS
OF POOR QUALITY

TABLE VIII (Continued)

	I	2	3	4
	I =	0.50042	1.00000	1.50042
	X =	0.0		
J	Y			
20	0.46511	0.0	-2.53E-03-2.29E-07-1.61E-02	
19	0.45957	0.0	-2.90E-03-1.21E-07-1.50E-02	
18	0.43404	0.0	-2.21E-02-2.81E-07-2.31E-07	
17	0.40851	0.0	-8.21E-03-3.25E-07-3.73E-07	
16	0.38298	0.0	-8.26E-03-5.26E-07-6.19E-07	
15	0.35745	0.0	-7.86E-04-7.21E-07-1.00E-06	
14	0.33191	0.0	-1.09E-07-1.30E-06-1.31E-06	
13	0.30638	0.0	-6.79E-07-1.85E-06-1.96E-06	
12	0.28085	0.0	-1.71E-06-2.54E-06-2.47E-06	
11	0.25532	0.0	-3.42E-06-3.52E-06-3.07E-06	
10	0.22979	-6.21E-06-5.15E-06-4.54E-06-3.79E-06		
9	0.20425	-6.14E-06-6.23E-06-5.22E-06-4.30E-06		
8	0.17872	-6.10E-06-6.24E-06-5.76E-06-4.79E-06		
7	0.15319	-6.05E-06-6.25E-06-6.01E-06-5.25E-06		
6	0.12766	-6.06E-06-6.25E-06-6.10E-06-5.50E-06		
5	0.10213	-6.04E-06-6.25E-06-6.16E-06-5.65E-06		
4	0.07660	-6.06E-06-6.25E-06-6.16E-06-5.76E-06		
3	0.05106	-6.05E-06-6.26E-06-6.16E-06-5.79E-06		
2	0.02553	-6.05E-06-6.26E-06-6.17E-06-5.83E-06		
1	0.0	-6.06E-06-6.27E-06-6.17E-06-5.85E-06		

(e) w/
u₀

ORIGINAL PAGE IS
OF POOR QUALITY

TABLE IX

VELOCITY DATA FOR SWIRL VANE ANGLE
 $\phi = 45^\circ$ [SIDE-WALL EXPANSION ANGLE
 $\alpha = 90^\circ$ WITH CONTRACTION BLOCK]

AT $L/D = 1$

J	Y	I =	1	2
19	0.13716	0.0	0.14935	2.50E+01
18	0.12954	0.0		2.58E+01
17	0.12192	0.0		2.80E+01
16	0.11430	0.0		3.46E+01
15	0.10668	0.0		5.14E+01
14	0.09906	0.0		7.76E+01
13	0.09144	0.0		1.00E+02
12	0.08382	0.0		1.12E+02
11	0.07620	0.0		1.17E+02
10	0.06858	3.30E+01		1.18E+02
9	0.06096	3.34E+01		1.17E+02
8	0.05334	3.10E+01		1.15E+02
7	0.04572	3.54E+01		1.12E+02
6	0.03810	4.14E+01		1.08E+02
5	0.03048	7.76E+01		1.04E+02
4	0.02286	9.74E+01		9.74E+01
3	0.01524	1.02E+02		9.56E+01
2	0.00762	1.08E+02		6.00E+01
1	0.0	5.40E+00		-2.00E-01

(a) Yaw Angle

ORIGINAL PAGE IS
OF POOR QUALITY

TABLE IX (Continued)

	I =	1	2
	X =	0.0	0.14935
J	Y		
19	0.13716	0.0	1.32E+01
18	0.12954	0.0	5.08E+00
17	0.12192	0.0	3.64E+00
16	0.11430	0.0	-2.65E-01
15	0.10668	0.0	-7.18E+00
14	0.09906	0.0	-1.10E+01
13	0.09144	0.0	-5.81E+00
12	0.08382	0.0	-2.82E+00
11	0.07620	0.0	-3.11E+00
10	0.06858	1.19E+01	-3.30E+00
9	0.06096	1.16E+01	-3.59E+00
8	0.05334	1.01E+01	-4.39E+00
7	0.04572	6.98E+00	-6.04E+00
6	0.03810	3.59E+00	-7.58E+00
5	0.03048	-2.13E+01	-1.21E+01
4	0.02286	-1.69E+01	-1.87E+01
3	0.01524	-1.49E+01	-3.39E+01
2	0.00762	-1.87E+00	0.0
1	0.0	-1.03E+01	-4.15E+01

(b) Pitch Angle

ORIGINAL PAGE IS
OF POOR QUALITY

TABLE IX (Continued)

	I =	1	2
J	Y	X = 6.0	0.50042
19	0.45957	0.0	7.54E-01
18	0.43404	0.0	8.17E-01
17	0.40851	0.0	7.01E-01
16	0.38298	0.0	5.06E-01
15	0.35745	0.0	2.59E-01
14	0.33191	0.0	6.80E-02
13	0.30638	0.0	-6.79E-02
12	0.28085	0.0	-1.84E-01
11	0.25532	0.0	-2.53E-01
10	0.22979	1.53E+00	-2.86E-01
9	0.20425	1.68E+00	-2.85E-01
8	0.17872	1.81E+00	-2.68E-01
7	0.15319	1.32E+00	-2.27E-01
6	0.12766	3.58E-01	-1.73E-01
5	0.10213	2.14E-02	-1.16E-01
4	0.07660	-2.18E-02	-4.67E-02
3	0.05106	-3.62E-02	1.63E-02
2	0.02553	-4.79E-02	4.43E-02
1	0.0	1.39E-01	9.80E-02

(c) u/u_0

C-2

ORIGINAL PAGE IS
OF POOR QUALITY

TABLE IX (Continued)

	I =	1	2
	X =	0.0	0.50042
J	Y		
19	0.45957	0.0	2.02E-01
18	0.43404	0.0	8.06E-02
17	0.40851	0.0	5.06E-02
16	0.38298	0.0	-2.84E-03
15	0.35745	0.0	-5.23E-02
14	0.33191	0.0	-6.15E-02
13	0.30638	0.0	-3.98E-02
12	0.28085	0.0	-2.44E-02
11	0.25532	0.0	-3.02E-02
10	0.22979	3.86E-01	-3.46E-02
9	0.20425	4.12E-01	-3.94E-02
8	0.17872	3.76E-01	-4.90E-02
7	0.15319	1.99E-01	-6.47E-02
6	0.12766	2.99E-02	-7.51E-02
5	0.10213	-3.88E-02	-1.03E-01
4	0.07660	-5.15E-02	-1.23E-01
3	0.05106	-4.63E-02	-1.43E-01
2	0.02553	-5.02E-03	0.0
1	0.0	-2.54E-02	-8.68E-02

(d) v/u_0

ORIGINAL PAGE IS
OF POOR QUALITY

TABLE IX (Continued)

J	Y	I = 1 x = 0.0	Z 0.50042
19	0.45957	0.0	4.18E-01
18	0.43404	0.0	3.95E-01
17	0.40851	0.0	3.73E-01
16	0.38298	0.0	3.49E-01
15	0.35745	0.0	3.24E-01
14	0.33191	0.0	3.09E-01
13	0.30638	0.0	3.85E-01
12	0.28085	0.0	4.59E-01
11	0.25532	0.0	4.90E-01
10	0.22979	9.95E-01	5.29E-01
9	0.20425	1.11E+00	5.58E-01
8	0.17872	1.09E+00	5.80E-01
7	0.15319	9.40E-01	5.68E-01
6	0.12766	3.16E-01	5.38E-01
5	0.10213	9.72E-02	4.63E-01
4	0.07660	1.04E-01	3.59E-01
3	0.05106	1.70E-01	2.12E-01
2	0.02553	1.46E-01	7.67E-02
1	0.0	1.31E-02	3.42E-04

(e) w/u_0

ORIGINAL PAGE IS
OF POOR QUALITY.

TABLE X

VELOCITY DATA FOR SWIRL VANE ANGLE $\phi = 45^\circ$ [SIDE-WALL
EXPANSION ANGLE $\alpha = 90^\circ$ WITH CONTRACTION
BLOCK AT $L/D = 2$]

J	Y	I =	1	2	3	4
	X =	0.0	0.14935	0.25845	0.44780	
19	0.15716	0.0	4.50E+01	3.67E+01	6.30E+01	
18	0.12954	0.0	2.32E+01	4.06E+01	6.26E+01	
17	0.12192	0.0	2.62E+01	4.76E+01	6.26E+01	
16	0.11430	0.0	3.48E+01	5.44E+01	6.18E+01	
15	0.10608	0.0	4.00E+01	6.14E+01	6.22E+01	
14	0.09905	0.0	5.26E+01	6.92E+01	6.22E+01	
13	0.09144	0.0	1.13E+02	7.60E+01	6.28E+01	
12	0.08382	0.0	1.21E+02	8.10E+01	6.36E+01	
11	0.07620	0.0	1.24E+02	8.40E+01	6.40E+01	
10	0.06858	0.0	1.24E+01	8.60E+01	6.58E+01	
9	0.06096	0.0	1.24E+02	8.72E+01	6.64E+01	
8	0.05334	0.0	1.23E+02	8.62E+01	6.70E+01	
7	0.04572	0.0	1.20E+02	8.64E+01	6.80E+01	
6	0.03810	0.0	1.16E+02	8.70E+01	6.92E+01	
5	0.03048	0.0	1.14E+02	8.40E+01	6.80E+01	
4	0.02286	0.0	1.10E+02	8.04E+01	6.56E+01	
3	0.01524	0.0	1.02E+02	7.38E+01	5.96E+01	
2	0.00762	0.0	9.90E+01	6.28E+01	4.72E+01	
1	0.0	0.0	1.95E+02	1.28E+02	4.56E+01	1.56E+01

(a) Yaw Angle

ORIGINAL PAGE IS
OF POOR QUALITY

TABLE X (Continued)

J	I	2	3	4
19	0.13716	0.0	8.00E+00	4.36E+00
18	0.12954	0.0	2.56E+00	7.18E+00
17	0.12192	0.0	1.05E+00	1.02E+01
16	0.11430	0.0	-5.32E+00	-1.35E+01
15	0.10668	0.0	-1.81E+01	-1.51E+01
14	0.09906	0.0	-3.00E+00	-1.55E+01
13	0.09144	0.0	1.52E+00	1.55E+01
12	0.08382	0.0	3.14E+00	1.59E+01
11	0.07620	0.0	2.68E+00	1.26E+01
10	0.06858	1.23E+01	1.65E+00	1.03E+01
9	0.06096	1.20E+01	1.98E+00	8.71E+00
8	0.05334	1.04E+01	4.58E-01	-7.87E+00
7	0.04572	7.75E+00	2.09E+00	6.87E+00
6	0.03810	6.05E+00	5.03E+00	-7.31E+00
5	0.03048	2.15E+01	-6.78E+00	-7.19E+00
4	0.02286	3.13E+01	1.12E+01	1.25E+01
3	0.01524	-3.41E+01	-3.00E+01	-1.50E+01
2	0.00762	5.27E+01	0.0	2.86E+01
1	0.0	3.00E+01	0.0	-3.46E+01

(b) Pitch Angle

14-58861-1000-101 (Rev. 10-69)

ORIGINAL PAGE IS
OF POOR QUALITY

TABLE X (Continued)

	I	2	3	4
X =	0.0	0.50042	1.00000	1.50042
J	Y			
19	0.45957	0.0	8.08E-01	8.27E 01
18	0.43404	0.0	8.20E-01	5.29E-01
17	0.40851	0.0	6.68E-01	4.33E-01
16	0.38298	0.0	4.15E-01	3.40E 01
15	0.35745	0.0	1.98E-01	2.58E-01
14	0.33191	0.0	1.26E-02	1.84E 01
13	0.30638	0.0	1.49E-01	1.24E 01
12	0.28085	0.0	2.34E-01	8.19E-02
11	0.25532	0.0	2.82E-01	5.61E-02
10	0.22979	1.53E+00	2.96E-01	3.93E 02
9	0.20425	1.57E+00	3.01E 01	2.94E 02
8	0.17872	1.76E+00	2.89E 01	4.11E-02
7	0.15319	1.27E+00	2.55E-01	4.07E-02
6	0.12766	3.28E-01	1.91E-01	3.43E-02
5	0.10213	2.65E-03	1.54E-01	6.91E-02
4	0.07660	8.01E-02	1.03E-01	8.85E 02
3	0.05106	-9.80E-02	3.60E-02	1.24E-01
2	0.02553	-5.90E-02	9.07E-03	1.32E 01
1	0.0	0.05E-02	2.90E-02	1.40E 01

(c) u/u_0

ORIGINAL PAGE IS
OF POOR QUALITY

TABLE X (Continued)

J	Y	1	2	3	4
19	0.45957	0.0	1.25E-01	3.19E-02	1.56E-02
18	0.43404	0.0	3.97E-02	6.78E-02	-6.29E-03
17	0.40851	0.0	1.39E-02	1.16E-01	-2.32E-02
16	0.38298	0.0	4.70E-02	1.40E-01	3.36E-02
15	0.35745	0.0	-6.48E-02	-1.45E-01	-4.79E-02
14	0.33191	0.0	-1.46E-02	1.43E-01	4.54E-02
13	0.30638	0.0	1.03E-02	1.41E-01	5.00E-02
12	0.28085	0.0	2.48E-02	-1.27E-01	-5.16E-02
11	0.25532	0.0	2.33E-02	1.20E-01	4.93E-02
10	0.22979	3.95E-01	1.50E-02	-1.02E-01	-5.10E-02
9	0.20425	4.22E-01	1.01E-02	-9.25E-02	-5.13E-02
8	0.17872	5.52E-01	4.25E-03	8.58E-02	6.19E-02
7	0.15319	2.08E-01	-1.88E-02	-7.81E-02	-6.92E-02
6	0.12766	4.40E-02	3.81E-02	8.42E-02	7.32E-02
5	0.10213	2.47E-02	5.85E-02	8.23E-02	9.24E-02
4	0.07660	-7.74E-02	-5.88E-02	-1.17E-01	-9.49E-02
3	0.05106	-5.07E-02	-9.98E-02	-1.18E-01	1.13E-01
2	0.02555	-8.49E-02	0.0	-1.58E-01	-1.06E-01
1	0.0	3.58E-02	0.0	1.49E-01	5.97E-02

(d) v/u_0

ORIGINAL PAGE IS
OF POOR QUALITY.

TABLE X (Continued)

	I	1	2	3	4
K		0.0	0.50042	1.00000	1.50042
J	Y				
19	0.45957	0.0	3.77E-01	4.56E-01	5.02E-01
18	0.43404	0.0	3.52E-01	4.54E-01	5.25E-01
17	0.40851	0.0	3.29E-01	4.75E-01	5.38E-01
16	0.38298	0.0	4.83E-01	4.75E-01	5.35E-01
15	0.35745	0.0	1.55E-01	4.73E-01	5.51E-01
14	0.33191	0.0	2.77E-01	4.83E-01	5.68E-01
13	0.30638	0.0	3.57E-01	4.94E-01	5.91E-01
12	0.28085	0.0	3.87E-01	5.17E-01	6.12E-01
11	0.25532	0.0	4.11E-01	5.34E-01	6.36E-01
10	0.22979	9.58E-01	4.32E-01	5.62E-01	6.76E-01
9	0.20425	1.07E+00	4.46E-01	6.03E-01	7.02E-01
8	0.17872	1.11E+00	4.46E-01	6.19E-01	7.19E-01
7	0.15319	8.43E-01	4.45E-01	6.47E-01	7.27E-01
6	0.12766	2.53E-01	3.89E-01	6.55E-01	7.55E-01
5	0.10213	5.33E-02	3.46E-01	6.57E-01	6.54E-01
4	0.07660	9.89E-02	4.79E-01	5.23E-01	5.96E-01
3	0.05106	6.70E-02	1.69E-01	4.20E-01	4.43E-01
2	0.02553	2.47E-02	5.73E-02	2.58E-01	2.42E-01
1	0.0	1.40E-02	3.74E-02	1.43E-01	6.14E-02

(e) w/u_0

ORIGINAL PAGE IS
OF POOR QUALITY

TABLE XI

VELOCITY DATA FOR SWIRL VANE ANGLE
 $\phi = 70^\circ$ [SIDE-WALL EXPANSION ANGLE
 $\alpha = 90^\circ$ WITH CONTRACTION
BLOCK AT $L/D = 1$]

J	Y	I = 1	2
19	0.13716	0.0	5.48E+01
18	0.12954	0.0	6.04E+01
17	0.12192	0.0	6.74E+01
16	0.11430	0.0	7.44E+01
15	0.10668	0.0	8.18E+01
14	0.09906	0.0	8.76E+01
13	0.09144	0.0	9.18E+01
12	0.08382	0.0	9.40E+01
11	0.07620	0.0	9.56E+01
10	0.06858	4.36E+01	9.40E+01
9	0.06096	3.86E+01	9.38E+01
8	0.05334	5.44E+01	9.34E+01
7	0.04572	5.54E+01	9.38E+01
6	0.03810	1.16E+02	9.52E+01
5	0.03048	1.13E+02	9.78E+01
4	0.02286	1.02E+02	1.04E+02
3	0.01524	9.72E+01	1.16E+02
2	0.00762	1.02E+02	1.36E+02
1	0.0	1.20E+02	1.63E+02

(a) Yaw Angle

ORIGINAL PAGE IS
OF POOR QUALITY

TABLE XI (Continued)

	I =	1	2
	X =	0.0	0.14935
J	Y		
19	0.13716	0.0	5.53E+00
18	0.12954	0.0	-1.43E+00
17	0.12192	0.0	-3.81E+00
16	0.11430	0.0	5.45E+00
15	0.10668	0.0	-7.11E+00
14	0.09906	0.0	-7.58E+00
13	0.09144	0.0	-7.83E+00
12	0.08382	0.0	-7.63E+00
11	0.07620	0.0	-6.30E+00
10	0.06858	4.42E+00	-5.69E+00
9	0.06096	1.46E+00	-5.10E+00
8	0.05334	-8.60E+00	4.81E+00
7	0.04572	-1.43E+01	-5.35E+00
6	0.03810	-6.23E+00	-6.16E+00
5	0.03048	-6.92E+00	-7.34E+00
4	0.02286	-1.51E+01	-1.05E+01
3	0.01524	-2.11E+01	-1.47E+01
2	0.00762	-2.83E+01	-1.79E+01
1	0.0	-4.39E+01	-1.58E+01

(b) Pitch Angle

REPRODUCED FROM
OF POOR QUALITY

TABLE XI (Continued)

J	Y	I = 1	2
19	0.45957	0.0	8.01E-01
18	0.43404	0.0	6.29E-01
17	0.40851	0.0	4.76E-01
16	0.38298	0.0	3.21E-01
15	0.35745	0.0	1.70E-01
14	0.33191	0.0	5.02E-02
13	0.30638	0.0	-4.00E-02
12	0.28085	0.0	-9.36E-02
11	0.25532	0.0	-1.41E-01
10	0.22979	3.14E+00	-1.05E-01
9	0.20425	2.72E+00	-1.02E-01
8	0.17872	9.99E-01	-9.12E-02
7	0.15319	-8.40E-02	-9.64E-02
6	0.12766	-3.79E-01	-1.15E-01
5	0.10213	-2.68E-01	-1.41E-01
4	0.07660	-1.06E-01	-1.54E-01
3	0.05106	-5.49E-02	-2.44E-01
2	0.02553	-6.98E-02	-3.06E-01
1	0.0	-7.83E-02	-3.71E-01

(c) w/u_0

ORIGINAL PAGE IS
OF POOR QUALITY

TABLE XI (Continued)

J	Y	X = 0.0	I = 1	2
19	0.45957	0.0	0.50042	1.44E-01
18	0.43404	0.0		-3.17E-02
17	0.40851	0.0		-8.16E-02
16	0.38298	0.0		1.14E-01
15	0.35745	0.0		-1.49E-01
14	0.33191	0.0		-1.68E-01
13	0.30638	0.0		-1.75E-01
12	0.28085	0.0		-1.80E-01
11	0.25532	0.0		-1.59E-01
10	0.22979	3.36E-01		-1.50E-01
9	0.20425	8.85E-02		-1.37E-01
8	0.17872	-2.60E-01		-1.29E-01
7	0.15319	-2.27E-01		-1.36E-01
6	0.12766	-9.38E-02		-1.37E-01
5	0.10213	-8.32E-02		-1.33E-01
4	0.07660	-1.40E-01		-1.44E-01
3	0.05106	-1.69E-01		-1.47E-01
2	0.02553	-1.81E-01		-1.37E-01
1	0.0	-1.52E-01		-1.10E-01

(d) v/u_0

ORIGINAL PAGE IS
OF POOR QUALITY

TABLE XI (Continued)

I =		1	2
X =		0.0	0.50042
J	Y		
19	0.45957	0.0	1.14E+00
18	0.43404	0.0	1.11E+00
17	0.40851	0.0	1.13E+00
16	0.38298	0.0	1.15E+00
15	0.35745	0.0	1.18E+00
14	0.33191	0.0	1.20E+00
13	0.30638	0.0	1.27E+00
12	0.28085	0.0	1.34E+00
11	0.25532	0.0	1.44E+00
10	0.22979	2.99E+00	1.50E+00
9	0.20425	2.17E+00	1.54E+00
8	0.17872	1.40E+00	1.53E+00
7	0.15319	8.88E-01	1.45E+00
6	0.12766	7.70E-01	1.27E+00
5	0.10213	6.31E-01	1.03E+00
4	0.07660	5.06E-01	7.54E-01
3	0.05106	4.34E-01	5.04E-01
2	0.02553	3.28E-01	2.95E-01
1	0.0	1.37E-01	1.16E-01

(e) w/u_0

ORIGINAL PAGE IS
OF POOR QUALITY

TABLE XII

VELOCITY DATA FOR SWIRL VANE ANGLE $\phi = 70^\circ$
[SIDE-WALL EXPANSION ANGLE $\alpha = 90^\circ$ WITH
CONTRACTION BLOCK AT $L/D = 2$]

J	X	Y	1	2	3	4
19	0.13716	0.0	0.0	4.56E+01	7.18E+01	7.10E+01
18	0.12954	0.0	0.0	5.74E+01	7.18E+01	7.10E+01
17	0.12192	0.0	0.0	6.46E+01	7.30E+01	7.26E+01
16	0.11430	0.0	0.0	7.38E+01	7.40E+01	7.40E+01
15	0.10668	0.0	0.0	8.16E+01	7.54E+01	7.44E+01
14	0.09906	0.0	0.0	8.88E+01	7.62E+01	7.58E+01
13	0.09144	0.0	0.0	9.36E+01	7.76E+01	7.74E+01
12	0.08382	0.0	0.0	9.62E+01	7.90E+01	7.88E+01
11	0.07620	0.0	0.0	9.76E+01	8.02E+01	8.00E+01
10	0.06858	4.36E+01	9.80E+01	9.80E+01	8.18E+01	8.18E+01
9	0.06096	3.84E+01	9.80E+01	9.80E+01	8.40E+01	8.38E+01
8	0.05334	5.24E+01	9.80E+01	9.80E+01	8.72E+01	8.56E+01
7	0.04572	5.38E+01	9.90E+01	9.90E+01	8.98E+01	8.76E+01
6	0.03810	1.17E+02	9.96E+01	9.96E+01	9.36E+01	9.14E+01
5	0.03048	1.14E+02	1.01E+02	1.01E+02	9.70E+01	9.88E+01
4	0.02286	1.03E+02	1.03E+02	1.03E+02	1.02E+02	1.09E+02
3	0.01524	9.26E+01	1.05E+02	1.05E+02	1.10E+02	1.29E+02
2	0.00762	8.80E+01	1.12E+02	1.12E+02	1.23E+02	1.56E+02
1	0.0	9.00E+01	1.33E+02	1.33E+02	1.54E+02	1.84E+02

(a) Yaw Angle

ORIGINAL PAGE IS
OF POOR QUALITY

TABLE XII (Continued)

	I	1	2	3	4
X	=	0.0	0.14935	0.29845	0.44760
Y	J				
19	0.13716	0.0	3.70E+00	3.16E+00	4.05E+00
18	0.12954	0.0	-2.41E+00	-1.11E+00	8.67E-01
17	0.12192	0.0	-4.61E+00	-2.13E+00	-2.35E-01
16	0.11430	0.0	-6.11E+00	-2.77E+00	-8.45E-01
15	0.10668	0.0	-7.58E+00	-2.85E+00	-1.71E+00
14	0.09906	0.0	-8.04E+00	-3.21E+00	-2.35E+00
13	0.09144	0.0	-7.48E+00	-3.52E+00	-3.44E+00
12	0.08382	0.0	-6.88E+00	-3.63E+00	-4.18E+00
11	0.07620	0.0	-6.16E+00	-4.34E+00	-5.43E+00
10	0.06858	5.42E+00	-5.44E+00	-4.45E+00	-6.32E+00
9	0.06096	2.53E+00	-5.05E+00	-5.78E+00	-6.70E+00
8	0.05334	-6.99E+00	-5.08E+00	-7.14E+00	-8.11E+00
7	0.04572	-1.33E+01	-5.47E+00	-6.53E+00	-1.06E+01
6	0.03810	-6.38E+00	-6.41E+00	-1.17E+01	-1.55E+01
5	0.03048	-7.35E+00	-8.10E+00	-1.56E+01	-2.02E+01
4	0.02286	-1.51E+01	-1.23E+01	-1.72E+01	-2.93E+01
3	0.01524	-2.26E+01	-1.95E+01	-2.48E+01	-3.30E+01
2	0.00762	-2.93E+01	-3.00E+01	-3.64E+01	-3.65E+01
1	0.0	-3.84E+01	-4.84E+01	-4.91E+01	-5.73E+01

(b) Pitch Angle

ORIGINAL PAGE IS
OF POOR QUALITY

TABLE XII (Continued)

J	Y	I = 1	2	3	4
	X =	0.0	0.50042	1.00000	1.50042
19	0.45557	0.0	8.54E-01	3.79E-01	3.98E-01
18	0.43404	0.0	6.86E-01	3.99E-01	4.09E-01
17	0.40851	0.0	5.08E-01	3.82E-01	3.83E-01
16	0.38298	0.0	3.20E-01	3.66E-01	3.68E-01
15	0.35745	0.0	1.65E-01	3.47E-01	3.66E-01
14	0.33191	0.0	2.39E-02	3.36E-01	3.45E-01
13	0.30638	0.0	-7.65E-02	3.13E-01	3.16E-01
12	0.29085	0.0	-1.39E-01	2.89E-01	2.87E-01
11	0.25532	0.0	-1.78E-01	2.60E-01	2.64E-01
10	0.22979	3.10E+00	-1.54E-01	2.21E-01	2.17E-01
9	0.20425	2.71E+00	-2.00E-01	1.61E-01	1.63E-01
8	0.17872	1.07E+00	-1.59E-01	7.18E-02	1.09E-01
7	0.15319	-5.94E-02	-2.15E-01	4.74E-03	5.30E-02
6	0.12766	-3.85E-01	-2.66E-01	-7.44E-02	-2.49E-02
5	0.10213	-2.89E-01	-2.00E-01	-1.20E-01	-1.18E-01
4	0.07660	-1.18E-01	-1.79E-01	-1.63E-01	-1.72E-01
3	0.05106	-1.91E-02	-1.48E-01	-1.89E-01	-2.72E-01
2	0.02553	1.24E-02	-1.27E-01	-1.55E-01	-3.18E-01
1	0.0	7.04E-07	-1.17E-01	-2.11E-01	-3.26E-01

(c) u/u_0

ORIGINAL PAGE IS
OF POOR QUALITY

TABLE XII (Continued)

	I =	1	2	3	4
	X =	0.0	0.50042	1.00000	1.50042
J	Y				
19	0.45957	0.0	8.53E-02	6.70E-02	6.74E-02
18	0.43404	0.0	-5.36E-02	-2.48E-02	1.90E-02
17	0.40851	0.0	-9.55E-02	-4.86E-02	-5.25E-03
16	0.38258	0.0	-1.23E-01	-6.42E-02	-1.97E-02
15	0.35745	0.0	-1.50E-01	-6.85E-02	-4.07E-02
14	0.33191	0.0	-1.62E-01	-7.89E-02	-5.77E-02
13	0.30638	0.0	-1.60E-01	-8.98E-02	-8.73E-02
12	0.28085	0.0	-1.55E-01	-1.02E-01	-1.08E-01
11	0.25532	0.0	-1.45E-01	-1.16E-01	-1.44E-01
10	0.22979	4.06E-01	-1.33E-01	-1.22E-01	-1.69E-01
9	0.20425	1.53E-01	-1.27E-01	-1.56E-01	-1.77E-01
8	0.17872	-2.15E-01	-1.27E-01	-1.84E-01	-2.02E-01
7	0.15319	-2.12E-01	-1.31E-01	-2.13E-01	-2.38E-01
6	0.12766	-9.62E-02	-1.39E-01	-2.45E-01	-2.82E-01
5	0.10213	-5.31E-02	-1.49E-01	-2.74E-01	-2.84E-01
4	0.07660	-1.42E-01	-1.79E-01	-2.35E-01	-2.98E-01
3	0.05106	-1.75E-01	-1.98E-01	-2.54E-01	-2.80E-01
2	0.02553	-1.99E-01	-1.98E-01	-2.61E-01	-2.59E-01
1	0.0	-1.76E-01	-1.93E-01	-2.71E-01	-2.49E-01

(d) v/u_0

ORIGINAL PAGE IS
OF POOR QUALITY

TABLE XII (Continued)

J	Y	I =	1	2	3	4
	X =	0.0	0.50042	1.00000	1.50042	
19	0.45957	0.0	1.05E+00	1.15E+00	1.16E+00	1.16E+00
18	0.43404	0.0	1.07E+00	1.21E+00	1.19E+00	1.19E+00
17	0.40851	0.0	1.07E+00	1.25E+00	1.22E+00	1.22E+00
16	0.38298	0.0	1.10E+00	1.28E+00	1.28E+00	1.28E+00
15	0.35745	0.0	1.12E+00	1.33E+00	1.31E+00	1.31E+00
14	0.33191	0.0	1.14E+00	1.37E+00	1.36E+00	1.36E+00
13	0.30638	0.0	1.22E+00	1.42E+00	1.42E+00	1.42E+00
12	0.28085	0.0	1.28E+00	1.49E+00	1.45E+00	1.45E+00
11	0.25532	0.0	1.33E+00	1.50E+00	1.50E+00	1.50E+00
10	0.22979	2.95E+00	1.38E+00	1.53E+00	1.51E+00	1.51E+00
9	0.20425	2.15E+00	1.42E+00	1.53E+00	1.50E+00	1.50E+00
8	0.17872	1.39E+00	1.42E+00	1.47E+00	1.41E+00	1.41E+00
7	0.15319	8.94E-01	1.36E+00	1.36E+00	1.27E+00	1.27E+00
6	0.12766	7.70E-01	1.22E+00	1.18E+00	1.02E+00	1.02E+00
5	0.10213	6.62E-01	1.03E+00	9.74E-01	7.65E-01	7.65E-01
4	0.07660	5.12E-01	7.59E-01	7.42E-01	5.00E-01	5.00E-01
3	0.05106	4.22E-01	5.39E-01	5.18E-01	3.36E-01	3.36E-01
2	0.02553	3.54E-01	3.19E-01	2.96E-01	1.44E-01	1.44E-01
1	0.0	2.22E-01	1.26E-01	1.05E-01	-2.05E-02	-2.05E-02

(e) w/u_0

ORIGINAL PAGE IS
OF POOR QUALITY.

TABLE XIII
CHARACTERISTICS OF FLOWFIELDS IN TERMS OF THE
EFFECTS OF SWIRL VANE ANGLE FOR SIDE-WALL
EXPANSION ANGLE $\alpha = 90^\circ$

Vane Angle (deg.)	U_{in} (m/sec)	Re_d	CTRZ (x/D)	CRZ (x/D)	W_{max} (r/D)
0	15.7	150,000		2.1	
38	10.5	100,000	1.6		0.2
45	12.6	120,000	1.5		0.2
60	8.84	84,000	1.3		0.25
70	5.57	53,000	1.2		0.3

ORIGINAL PAGE IS
OF POOR QUALITY

TABLE XIV
SAMPLE ALPHANUMERIC HEADINGS

10000	COMPUTED MASS FLOW RATE
10040	COMPUTED MEAN AXIAL VELOCITY
10050	U VELOCITY
10060	V VELOCITY
10070	W VELOCITY
10080	TOTAL VELOCITY MAGNITUDE
10090	DIMENSIONLESS U VELOCITY
10100	DIMENSIONLESS V VELOCITY
10110	DIMENSIONLESS W VELOCITY
10120	DIMENSIONLESS TOTAL VELOCITY
10121	PROBE PITCH ANGLE (DEG.)
10123	PROBE YAW ANGLE (DEG.)
10125	P(NORTH) - P(SOUTH) (VOLTS)
10127	P(CENTER) - P(WEST) (VOLTS)
10128	MEAS. INLET MASS FLOW RATE
10129	MEAS. INLET AXIAL VELOCITY
10130	MEAS. INLET DYNAMIC PRESSURE
10131	MEAS. PITCH PRESSURE COEFF.
10132	AXIAL FLUX OF ANGULAR MOMENTUM

ORIGINAL PAGE IS
OF POOR QUALITY

TABLE XV
SAMPLE CALIBRATION DATA

10133	-3.76	58.	2.42
10140	-2.81	54.	1.86
10150	-2.23	50.	1.59
10160	-1.72	45.	1.35
10170	-1.31	40.	1.19
10180	-1.00	35.	1.11
10190	-.75	30.	1.02
10200	-.59	25.	.95
10210	-.47	20.	.91
10220	-.35	15.	.87
10230	-.21	10.	.85
10240	-.063	5.	.88
10250	.09	0.	.89
10260	.23	-5.	.89
10270	.38	-10.	.89
10280	.52	-15.	.89
10290	.66	-20.	.90
10300	.82	-25.	.93
10310	1.00	-30.	.96
10320	1.23	-35.	1.04
10330	1.49	-40.	1.10
10340	1.83	-45.	1.24
10350	2.24	-50.	1.40
10360	2.65	-54.	1.59
10370	3.4	-58.	2.04

ORIGINAL PAGE IS
OF POOR QUALITY.

TABLE XVI
SAMPLE MEASUREMENT DATA

10380	0.0		19	.335	
10390	0.0	354.6		-.007	-.018
10400	.3	251.8		.003	.021
10410	.6	258.0		.015	.029
10420	.9	262.6		.016	.028
10430	1.2	282.4		.007	.010
10440	1.5	318.6		-.004	.205
10450	1.8	324.6		-.299	2.450
10460	2.1	329.0		-.917	4.308
10470	2.4	326.6		-1.010	3.953
10480	2.7	327.0		-.865	3.255
10490	3.0				
10500	3.3				
10510	3.6				
10520	3.9				
10530	4.2				
10540	4.5				
10550	4.8				
10560	5.1				
10570	5.4				
10580	5.88		19	.335	
10590	0.0	360.2		.019	.012
10600	.3	300.0		.036	.007
10610	.6	274.4		.060	.051
10620	.9	262.6		.081	.130
10630	1.2	256.0		.094	.213
10640	1.5	252.2		.089	.290
10650	1.8	248.2		.088	.338
10660	2.1	245.2		.078	.367
10670	2.4	243.0		.067	.352
10680	2.7	241.6		.059	.324
10690	3.0	243.0		.049	.277
10700	3.3	248.2		.037	.219
10710	3.6	260.0		.035	.138
10720	3.9	282.4		.038	.093
10730	4.2	308.6		.046	.156
10740	4.5	325.4		.033	.338
10750	4.8	332.0		-.012	.568
10760	5.1	334.2		-.049	.749
10770	5.4	331.0		-.219	.727
10780	//				
END OF DATA					

TABLE XVII
SAMPLE AUXILIARY GEOMETRIC QUANTITY OUTPUT

EXPANSION ANGLE(DEG.) =	9.000E+01
SWIRL VANE ANGLE(DEG.) =	4.500E+01
INLET RADIUS(M) =	7.461E-02
COMBUSTOR RADIUS(M) =	1.492E-01
LAMINAR VISCOSITY(KG/M/SEC) =	1.800E-05
DENSITY(KG/CU. M) =	1.168E+00

*****=>***	MEAS. INLET MASS FLOW RATE
I =	1 2
X =	0.0 0.14935
	2.76E-01 2.76E-01

*****	COMPUTED MASS FLOW RATE
I =	1 2
X =	0.0 0.14935
	2.85E-01 2.91E-01

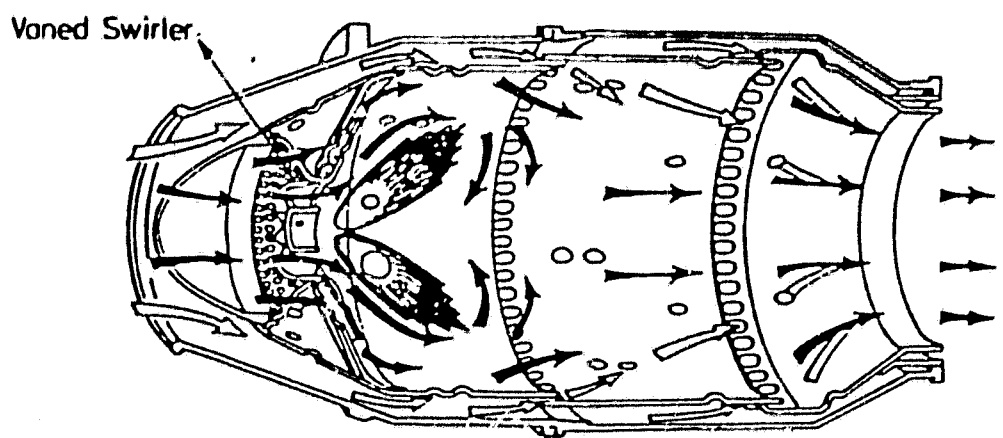
*****	MEAS. INLET AXIAL VELOCITY
I =	1 2
X =	0.0 0.14935
	1.35E+01 1.35E+01

*****	COMPUTED MEAN AXIAL VELOCITY
I =	1 2
X =	0.0 0.14935
	3.49E+00 3.57E+00

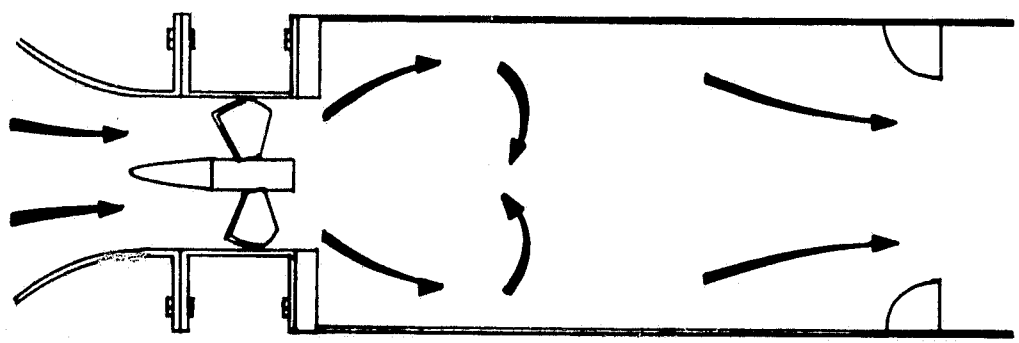
*****	AXIAL FLUX OF ANGULAR MOMENTUM
I =	1 2
X =	0.0 0.14935
	3.65E-02 3.47E-02

APPENDIX B

FIGURES



(a). Typical Axisymmetric Combustion Chamber of a Gas Turbine Engine



(b). Simplified Test Section

Figure 1. Typical Axisymmetric Gas Turbine Combustion Chamber

ORIGINAL PAGE IS
OF POOR QUALITY

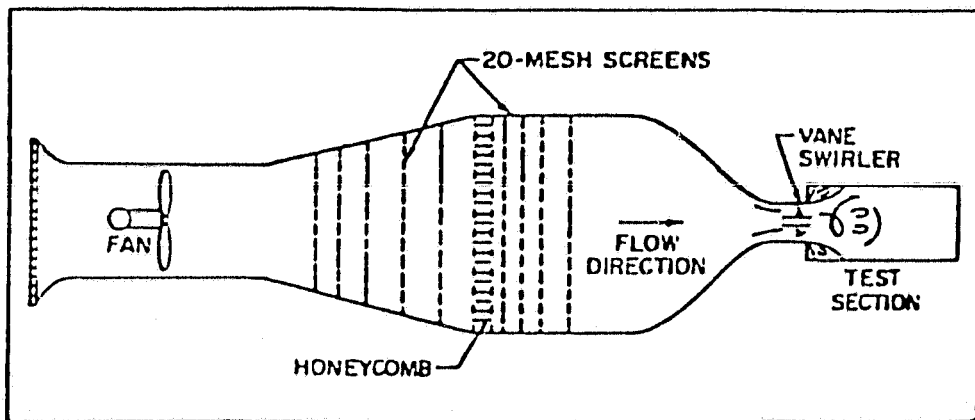


Figure 2. Schematic of Overall Flow Facility

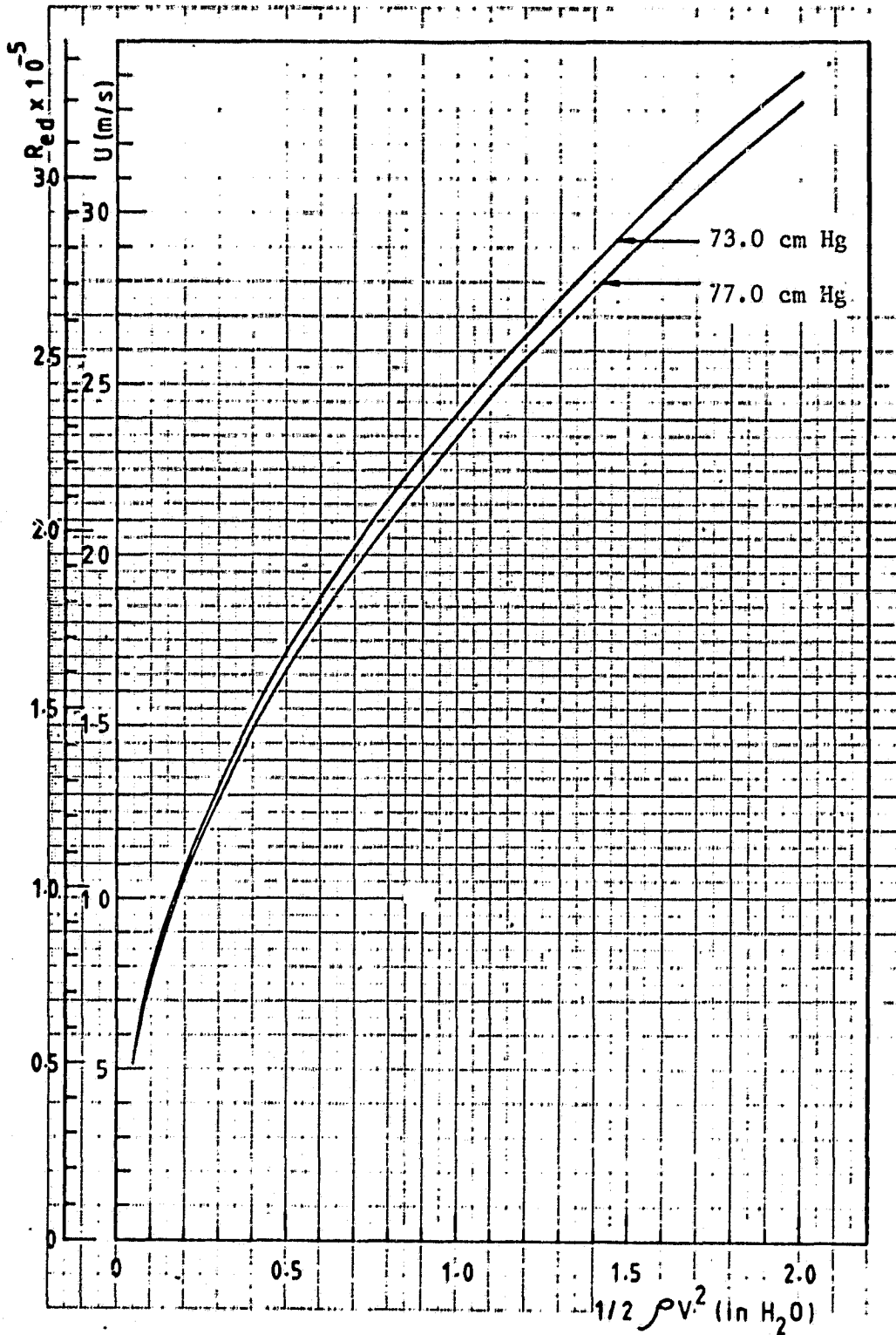


Figure 3. Dynamic Pressure Conversion Characteristic

ORIGINAL PAGE IS
OF POOR QUALITY.

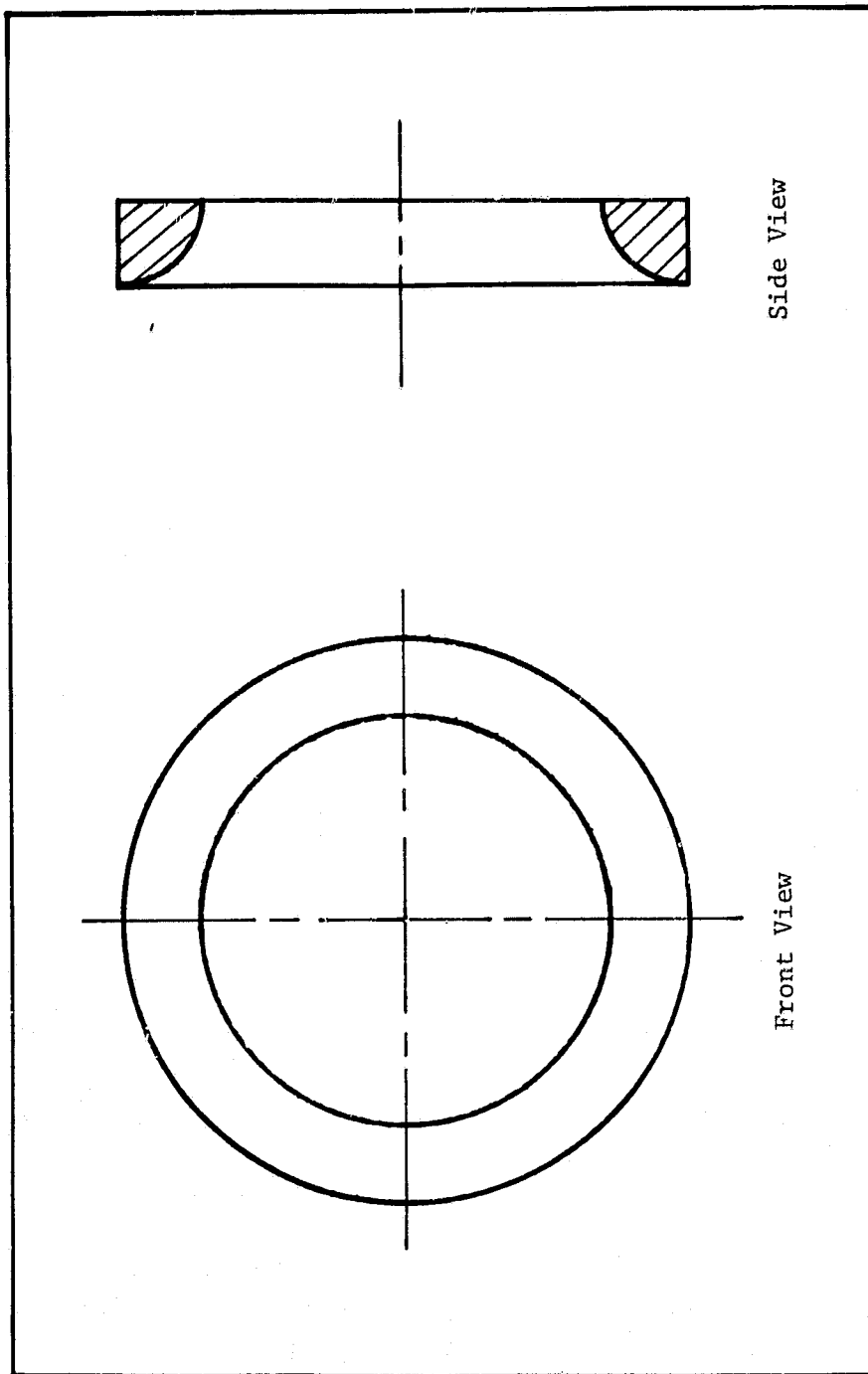


Figure 4. Contraction Block

- Notation
1. Pitot static probe
 2. Swirler
 3. Expansion block
 4. Five-hole pitot probe
 5. Switching valve
 6. Pressure transformer
 7. Contraction block
 8. Voltmeter
 9. Integrating voltmeter
 10. Micro-manometer

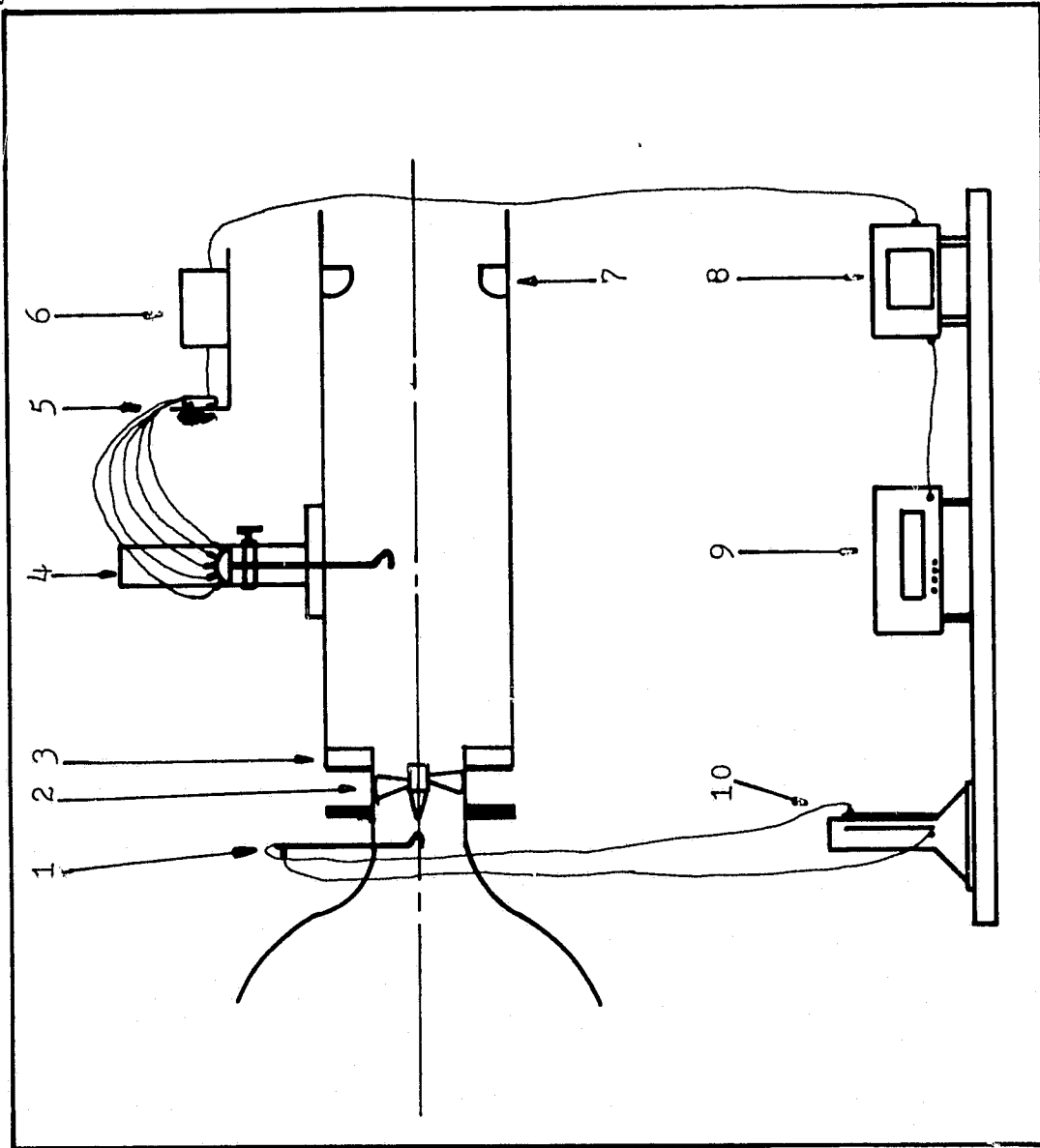


Figure 5 Apparatus for Mean Velocity Measurements

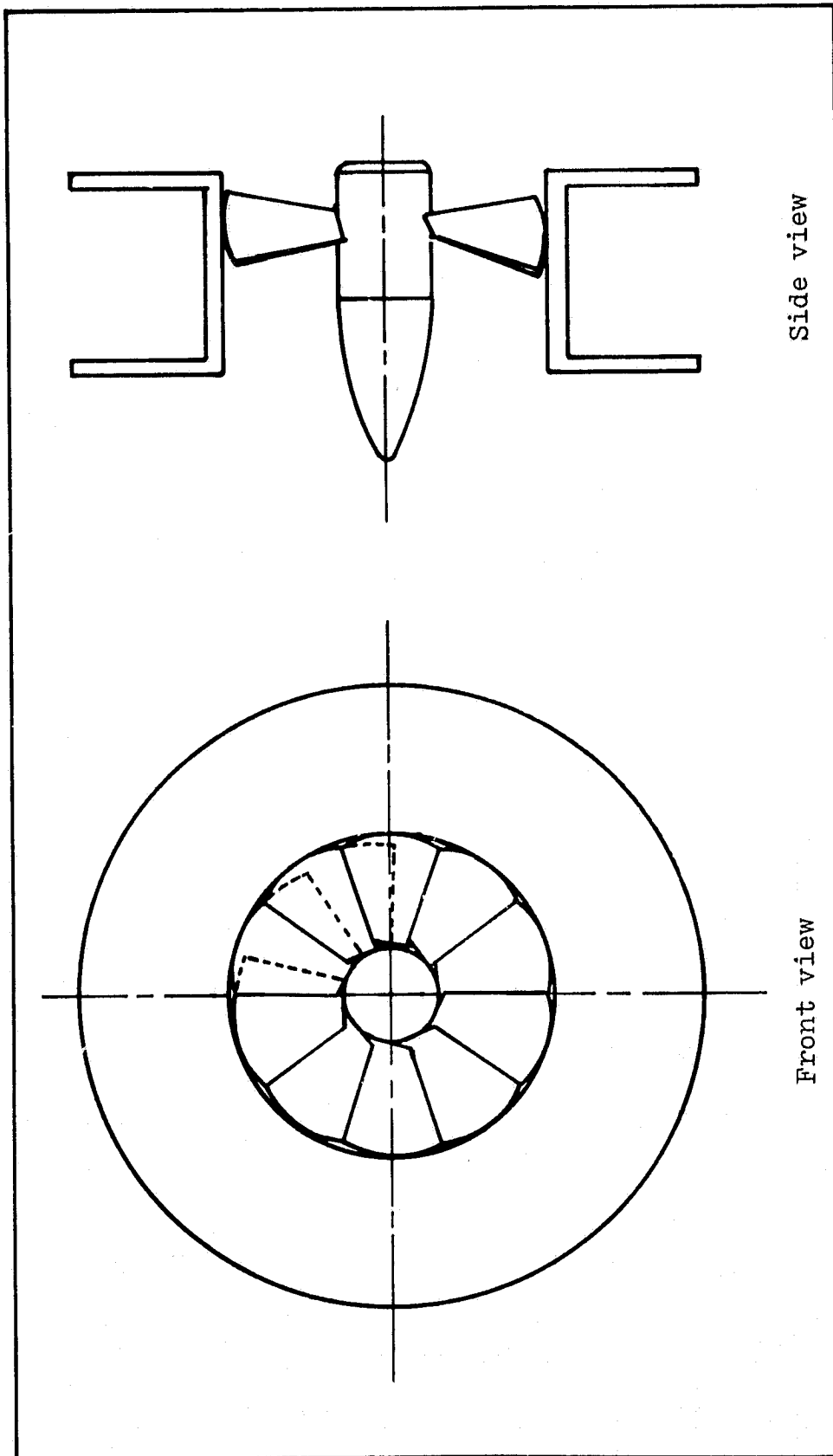


Figure 6. Swirler

ORIGINAL PAGE IS
OF POOR QUALITY

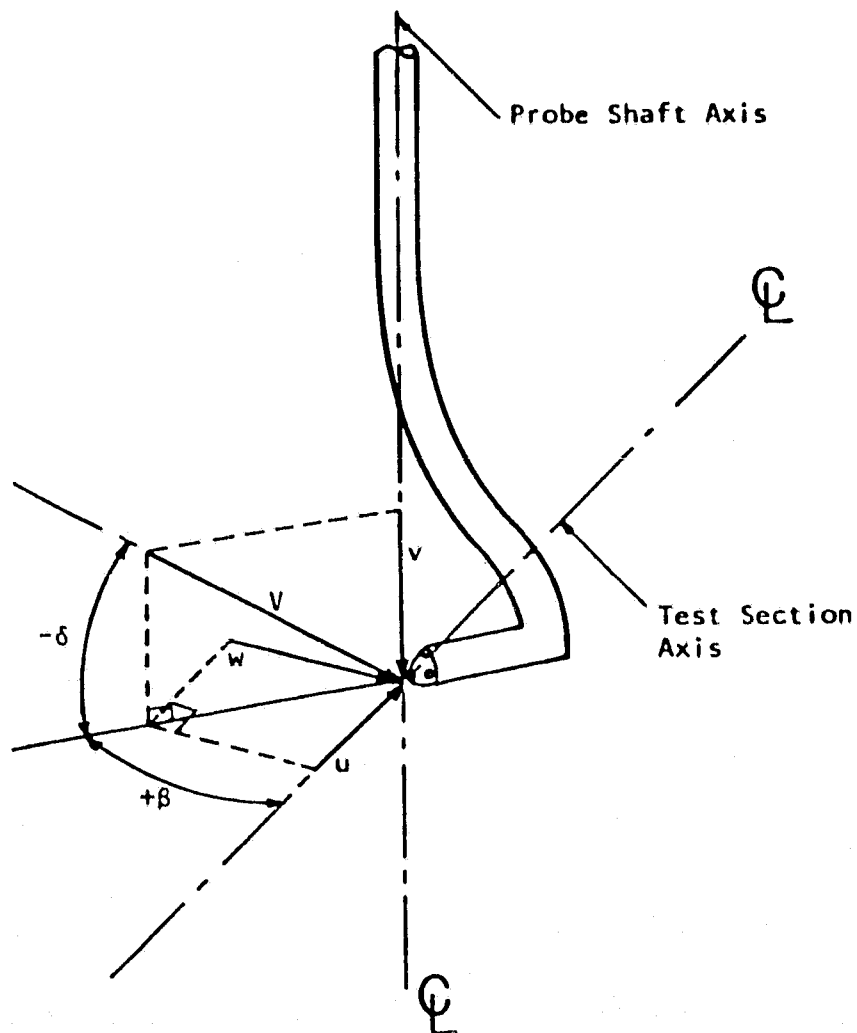


Figure 7. Velocity Components and Flow Direction Angles
Associated with Five-Hole Pitot Measurements

ORIGINAL PAGE IS
OF POOR QUALITY

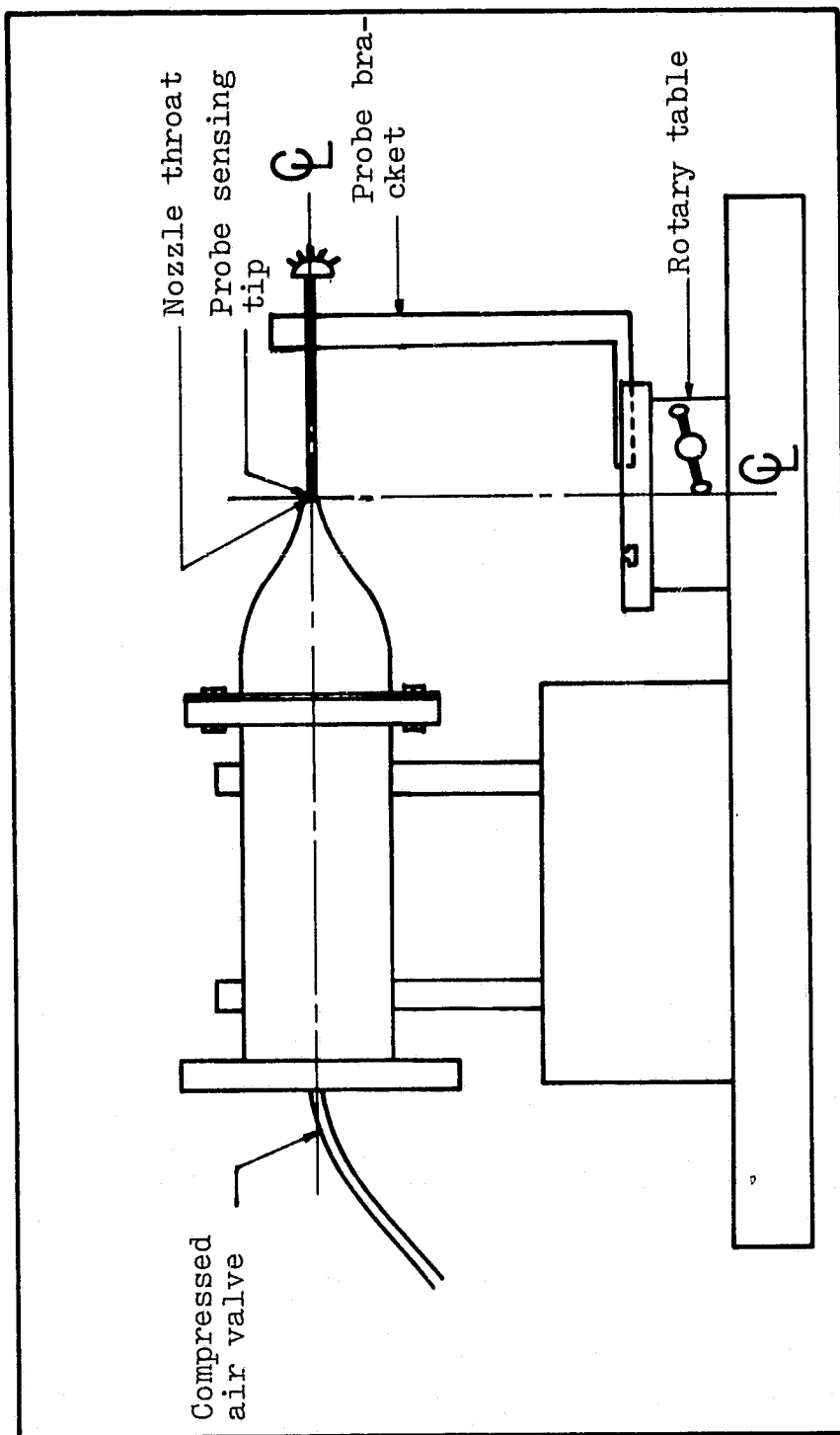


Figure 8. Calibration Apparatus

ORIGINAL PAGE IS
OF POOR QUALITY

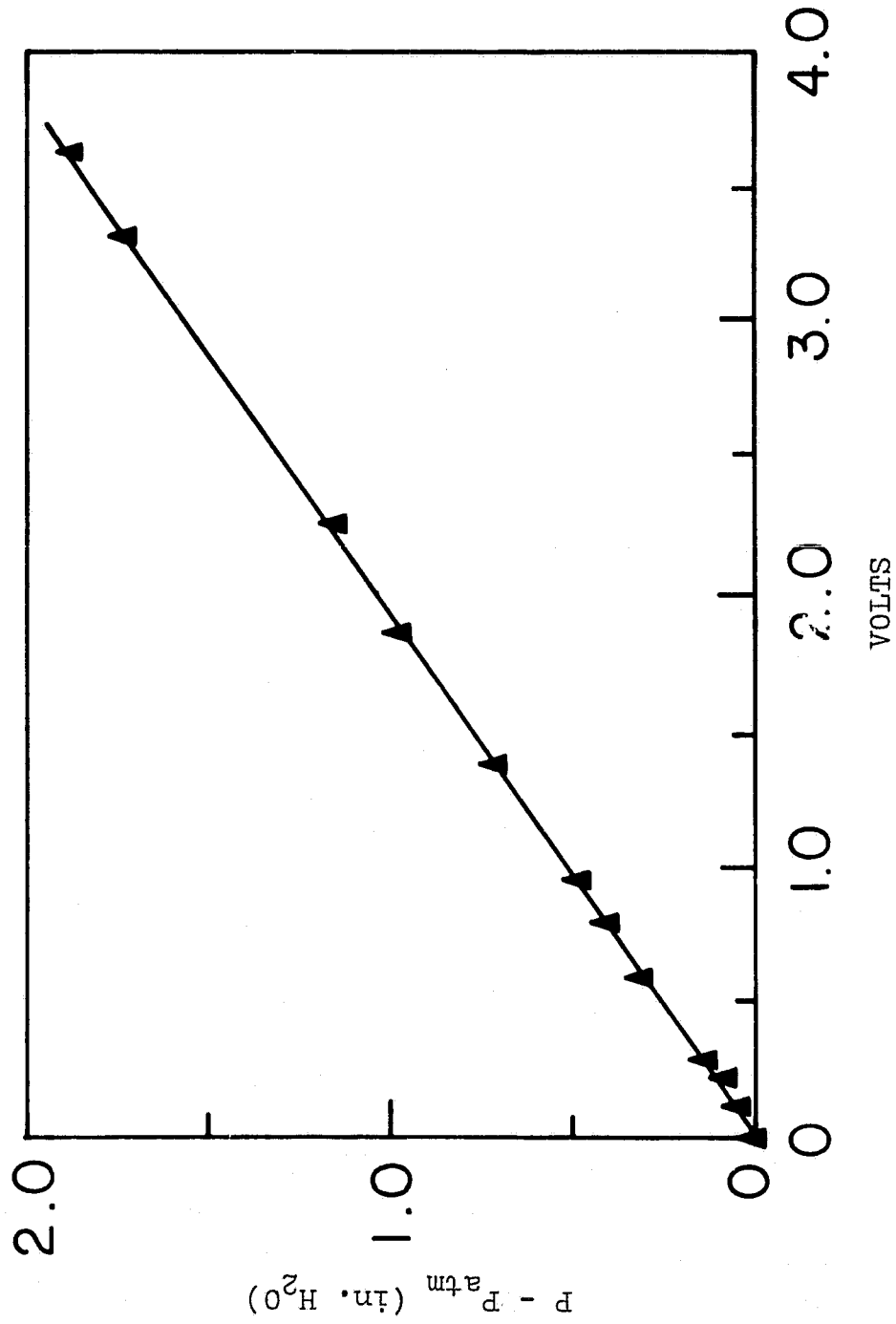
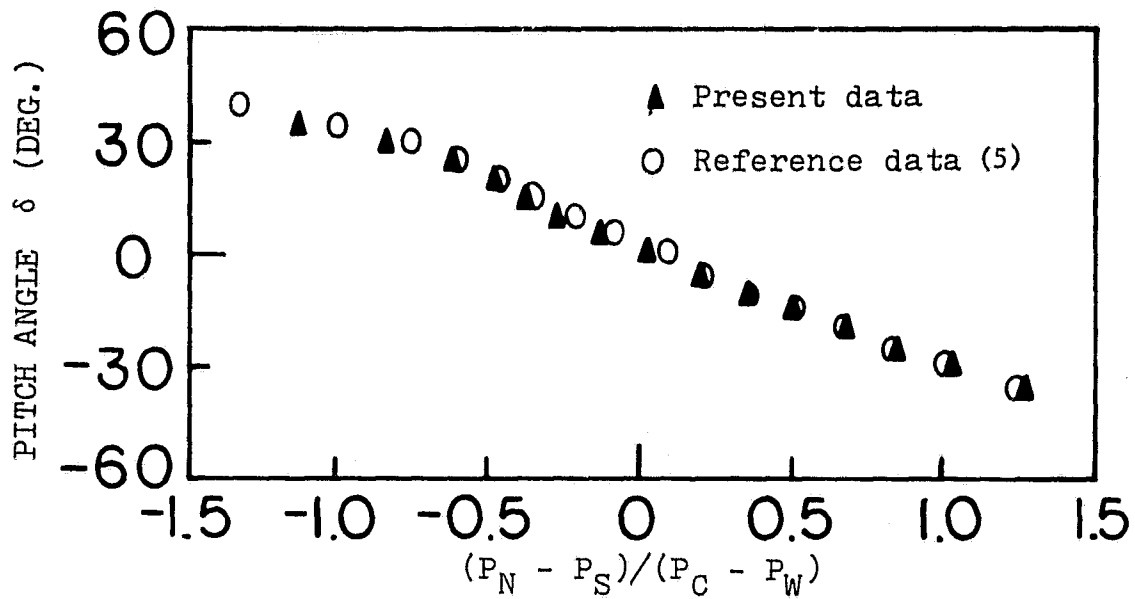
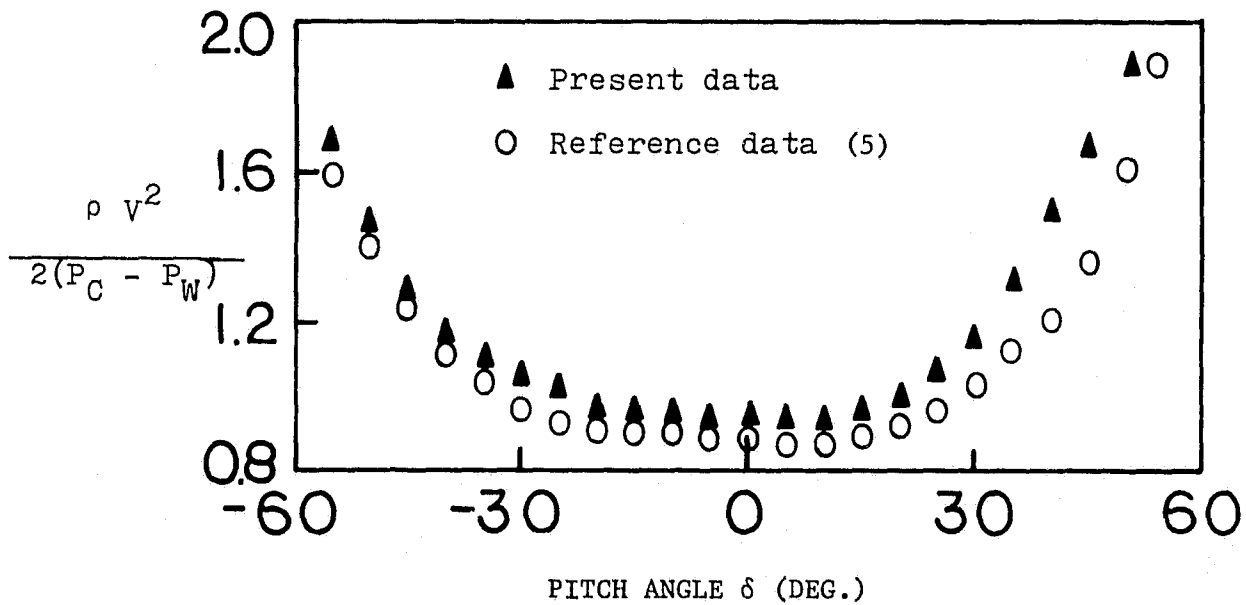


Figure 9. Voltage Output Calibration Characteristic for Voltmeter

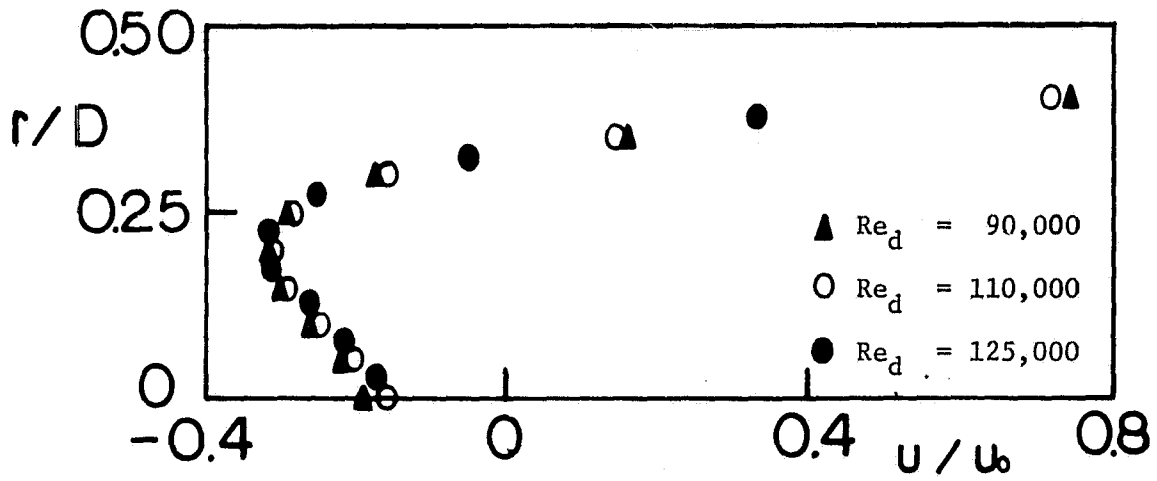


(a) Pitch Angle Calibration Characteristic

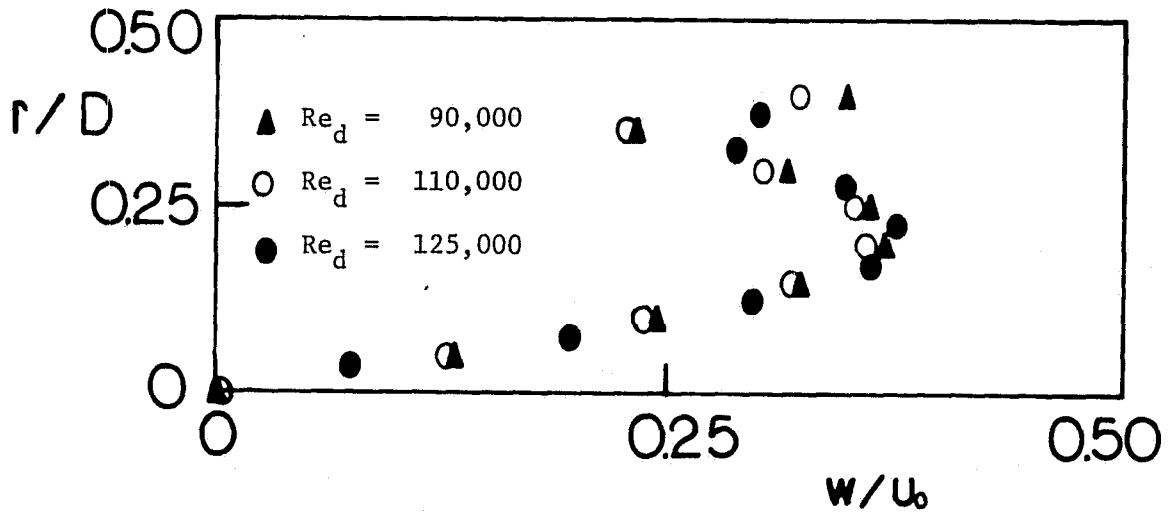


(b) Velocity Coefficient Calibration Characteristic

Figure 10. Calibration Characteristics for Five-Hole Pitot Probe

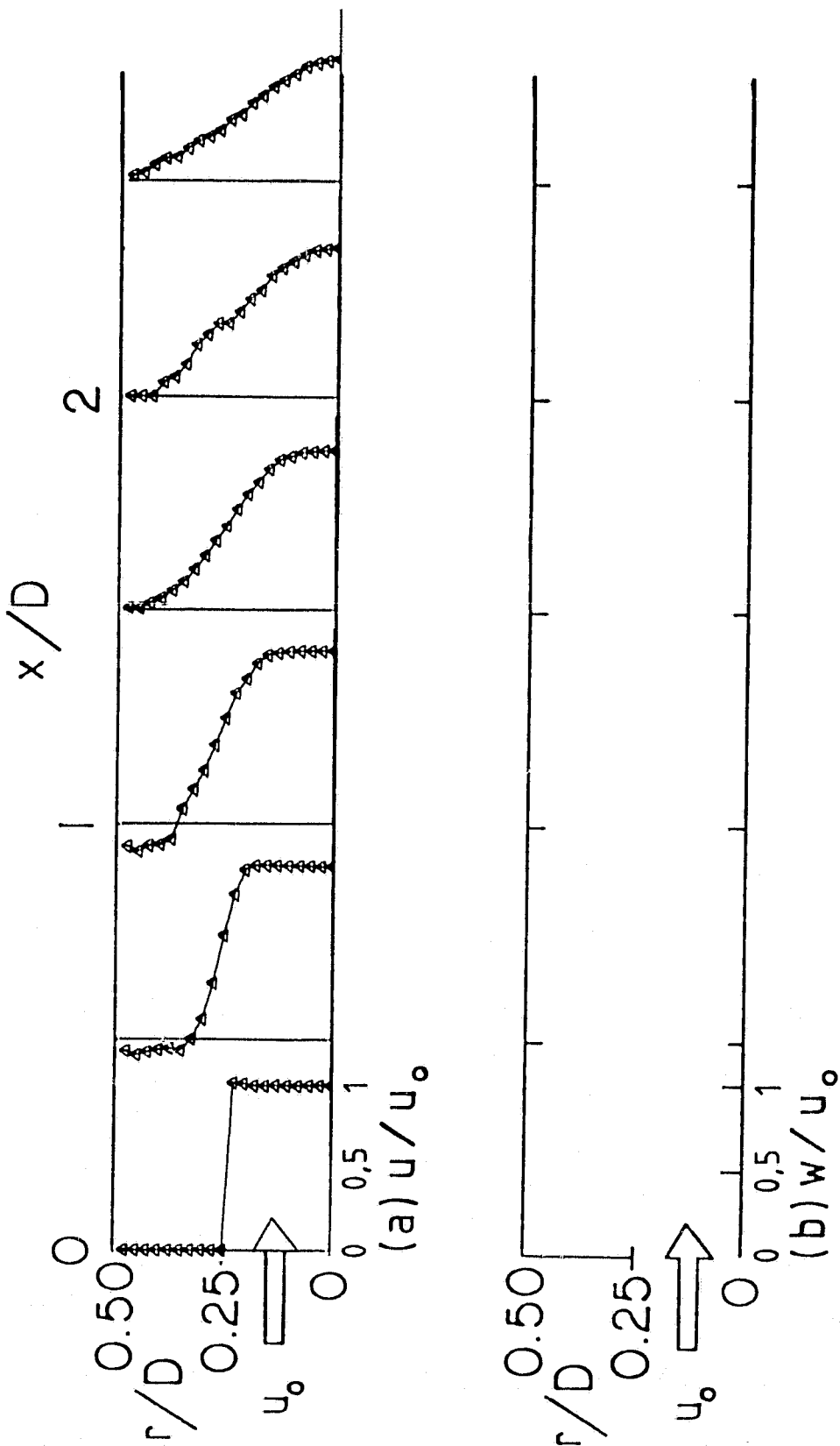


(a) Axial Velocity



(b) Swirl Velocity

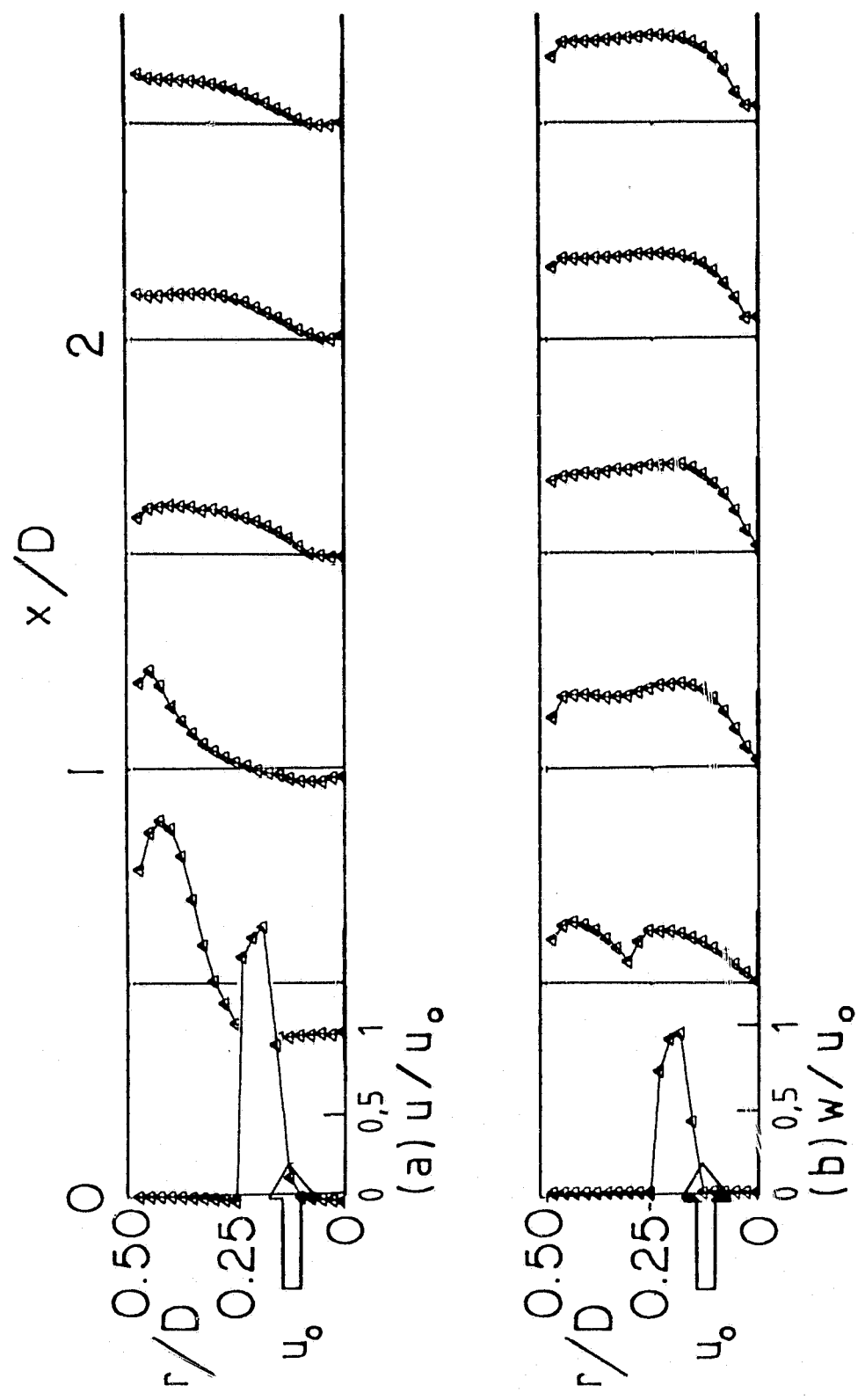
Figure 11. Flowfield Independence of Reynolds Number for Side-Wall Expansion. Angle $\alpha = 90^\circ$ and Swirl Vane Angle $\phi = 45^\circ$ at Axial Station $x/D = 0.5$.



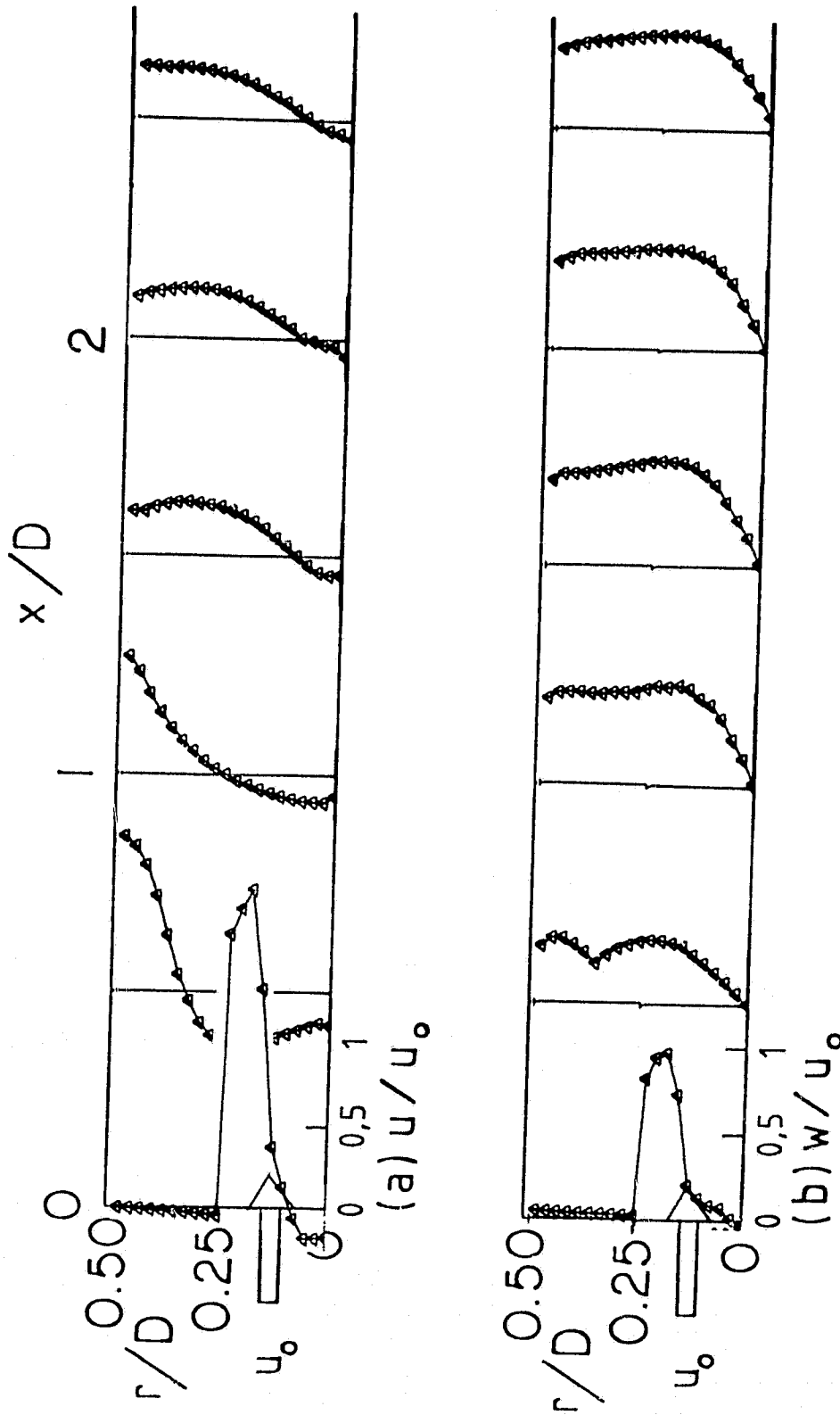
(a) Swirl Vane Angle $\phi = 0^\circ$

Figure 12. Velocity Profiles for Side-Wall Expansion Angle $\alpha = 90^\circ$ without Contraction Block

ORIGINAL PAGE IS
OF POOR QUALITY

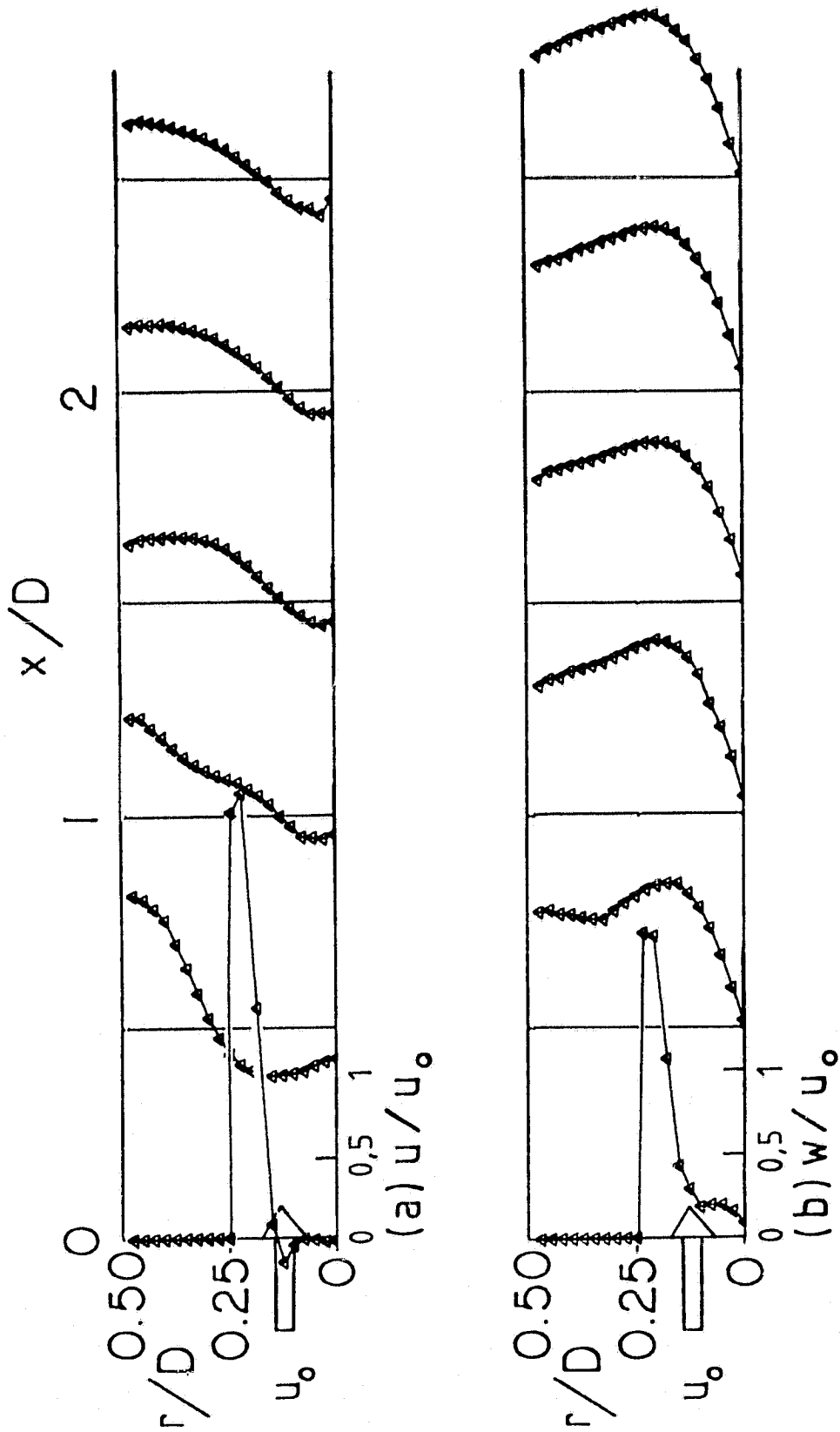


(b) Swirl Vane Angle $\phi = 38^\circ$
Figure 12 (Continued)



(c) Swirl Vane Angle $\phi = 45^\circ$

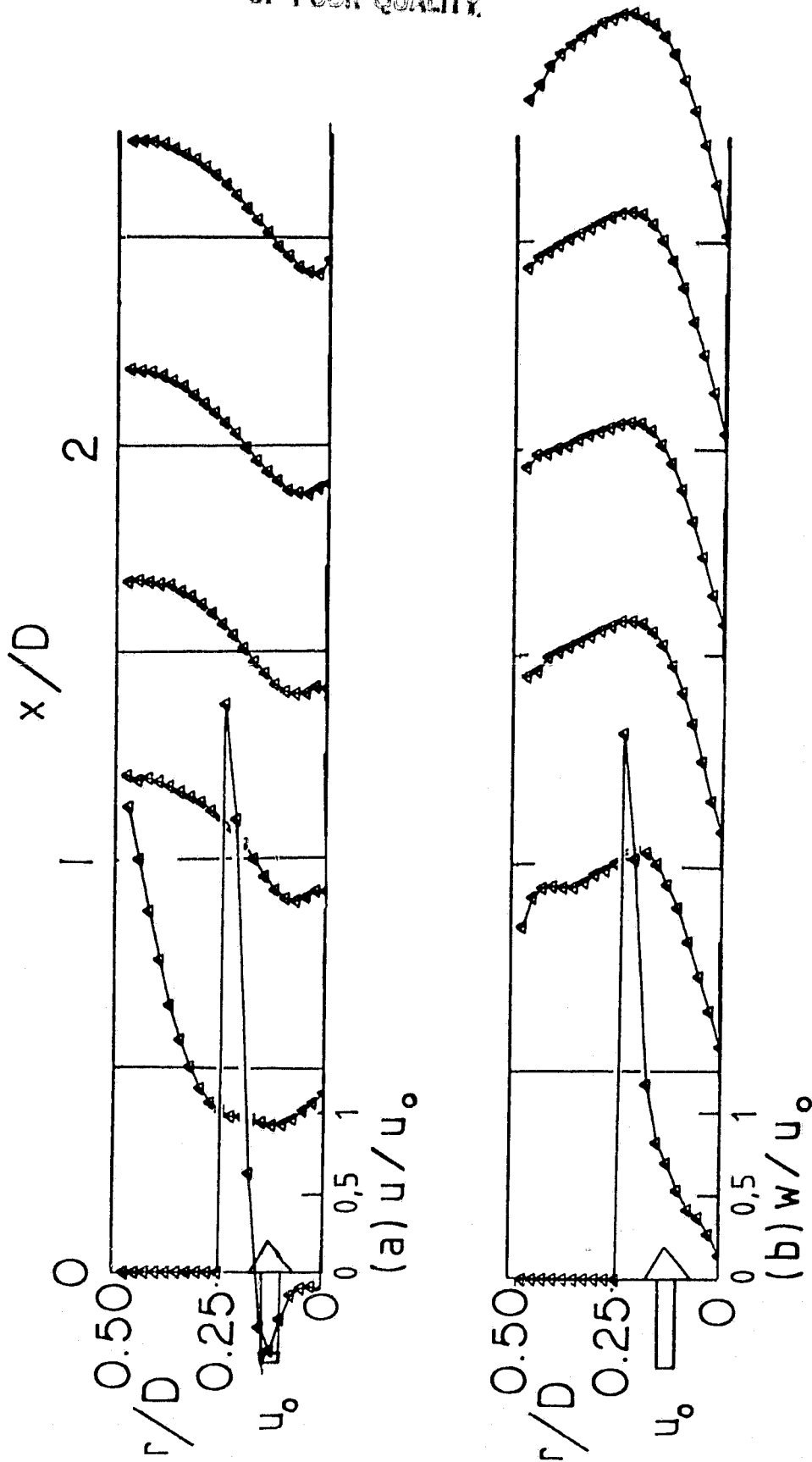
Figure 12 (Continued)



(d) Swirl Vane Angle $\phi = 60^\circ$

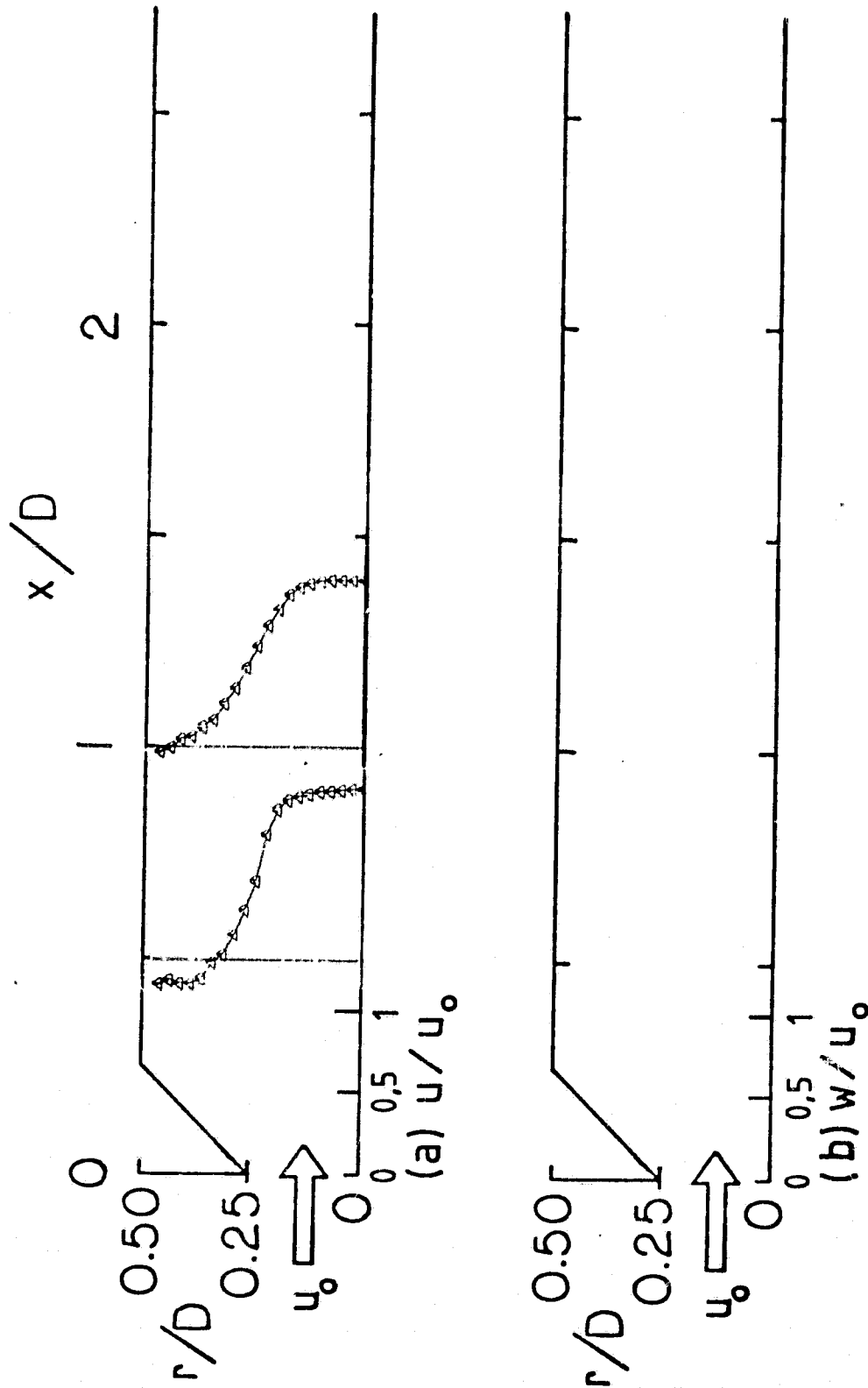
Figure 12 (Continued)

ORIGINAL COPY
OF POOR QUALITY



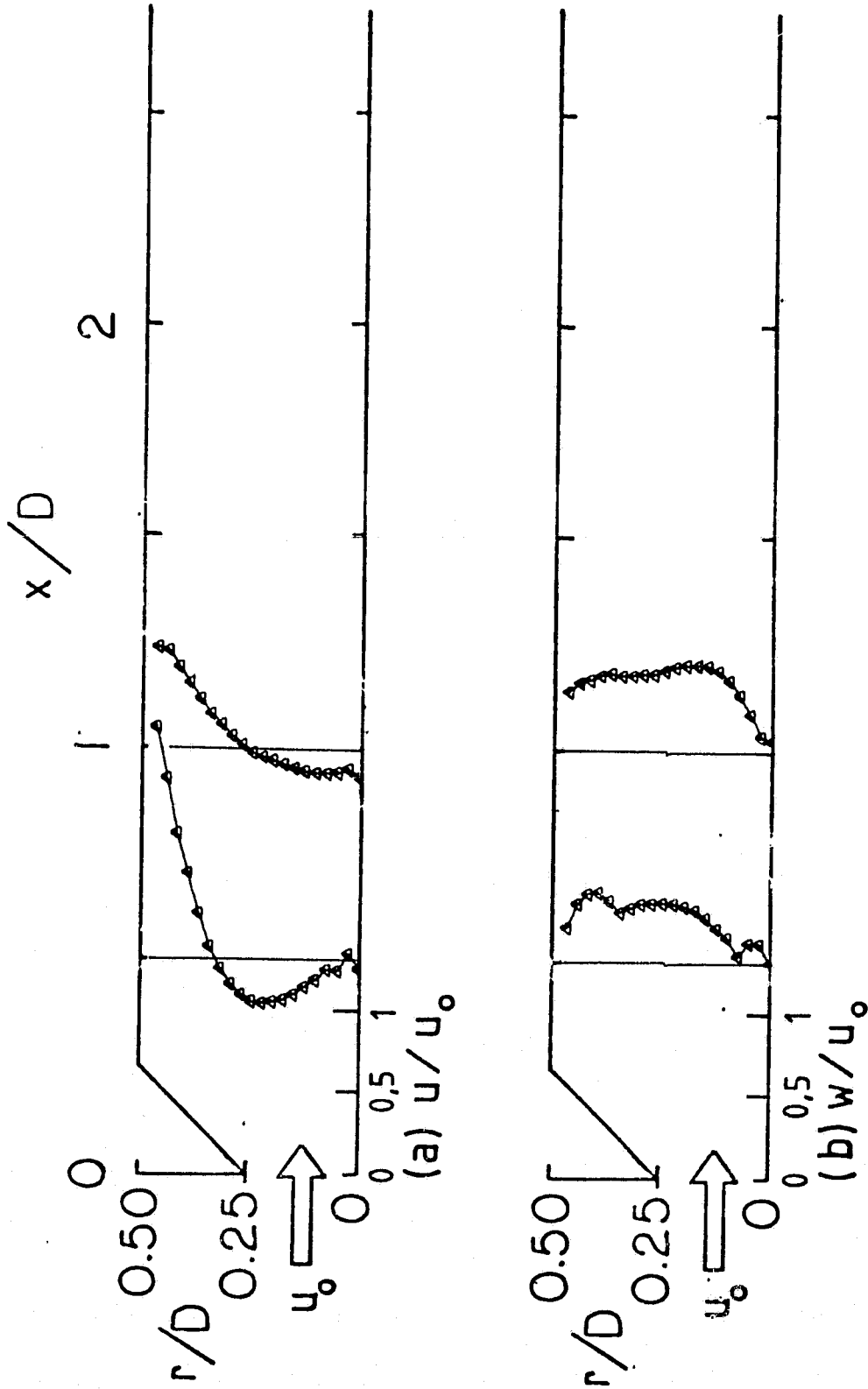
(e) Swirl Vane Angle $\phi = 70^\circ$

Figure 12 (Continued)



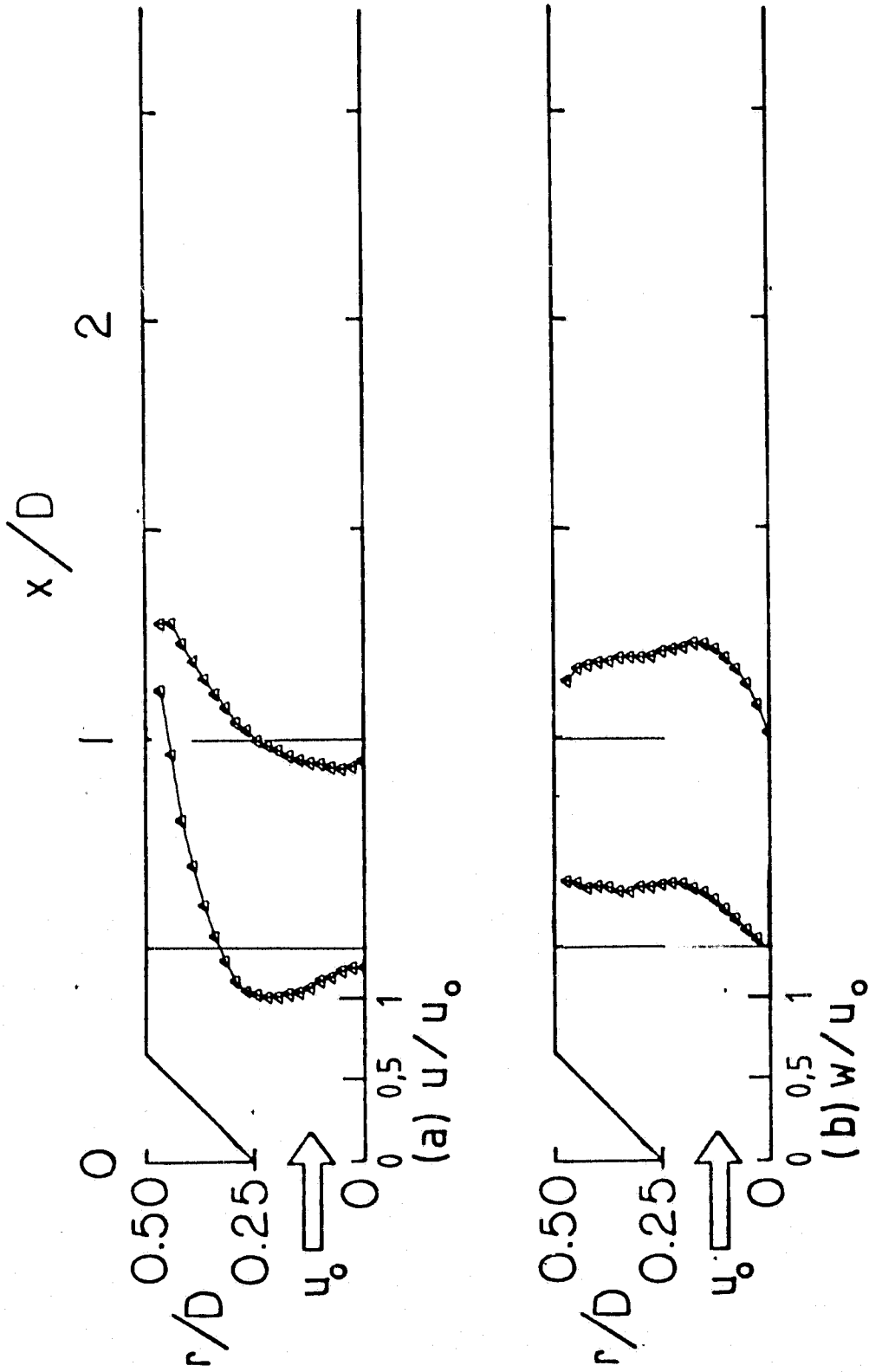
(a) Swirl Vane Angle $\phi = 0^\circ$

Figure 13. Velocity Profiles for Side-Wall Expansion Angle $\alpha = 45^\circ$ without Contraction Block

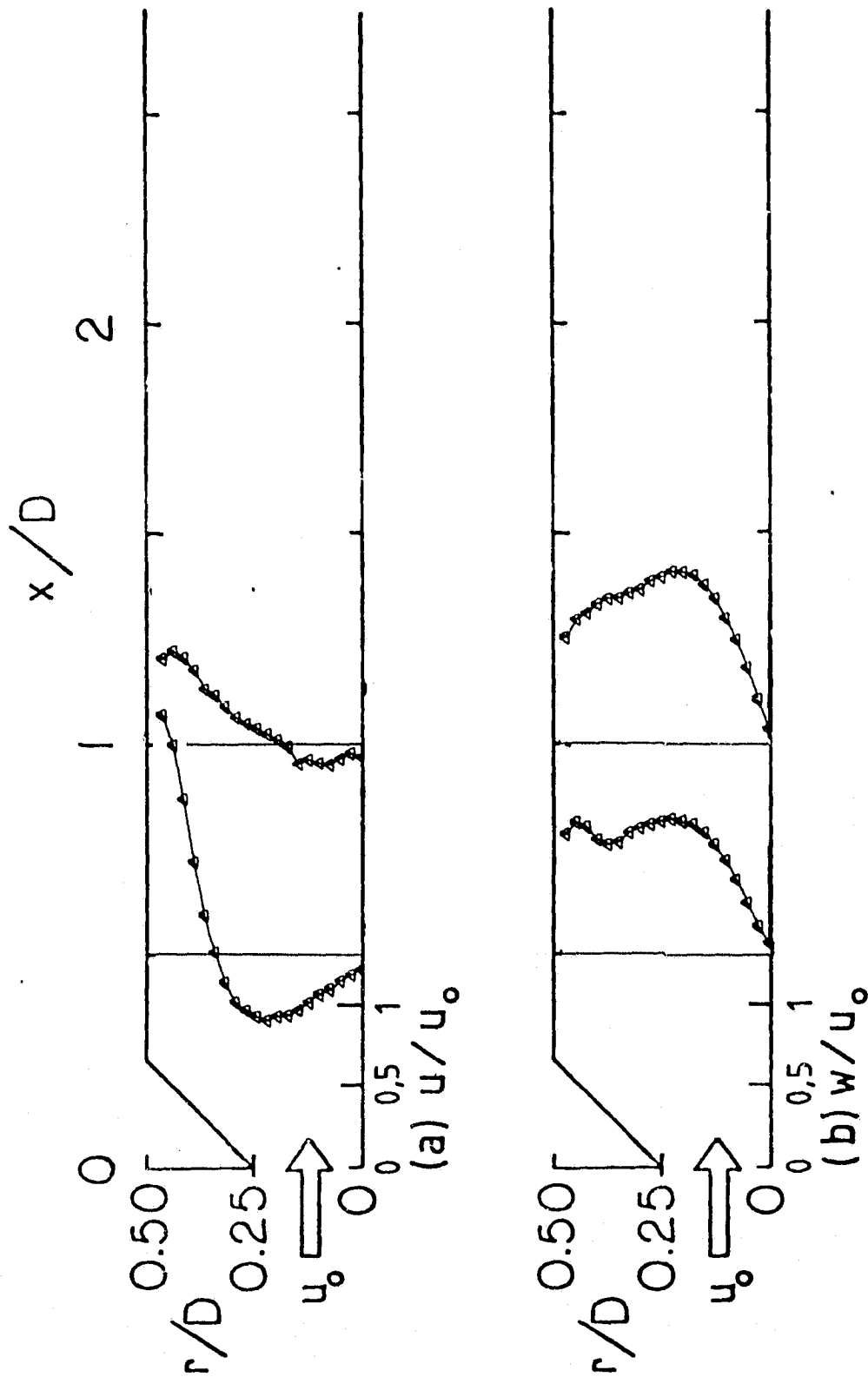


(b) Swirl Vane Angle $\phi = 38^\circ$

Figure 13 (Continued)

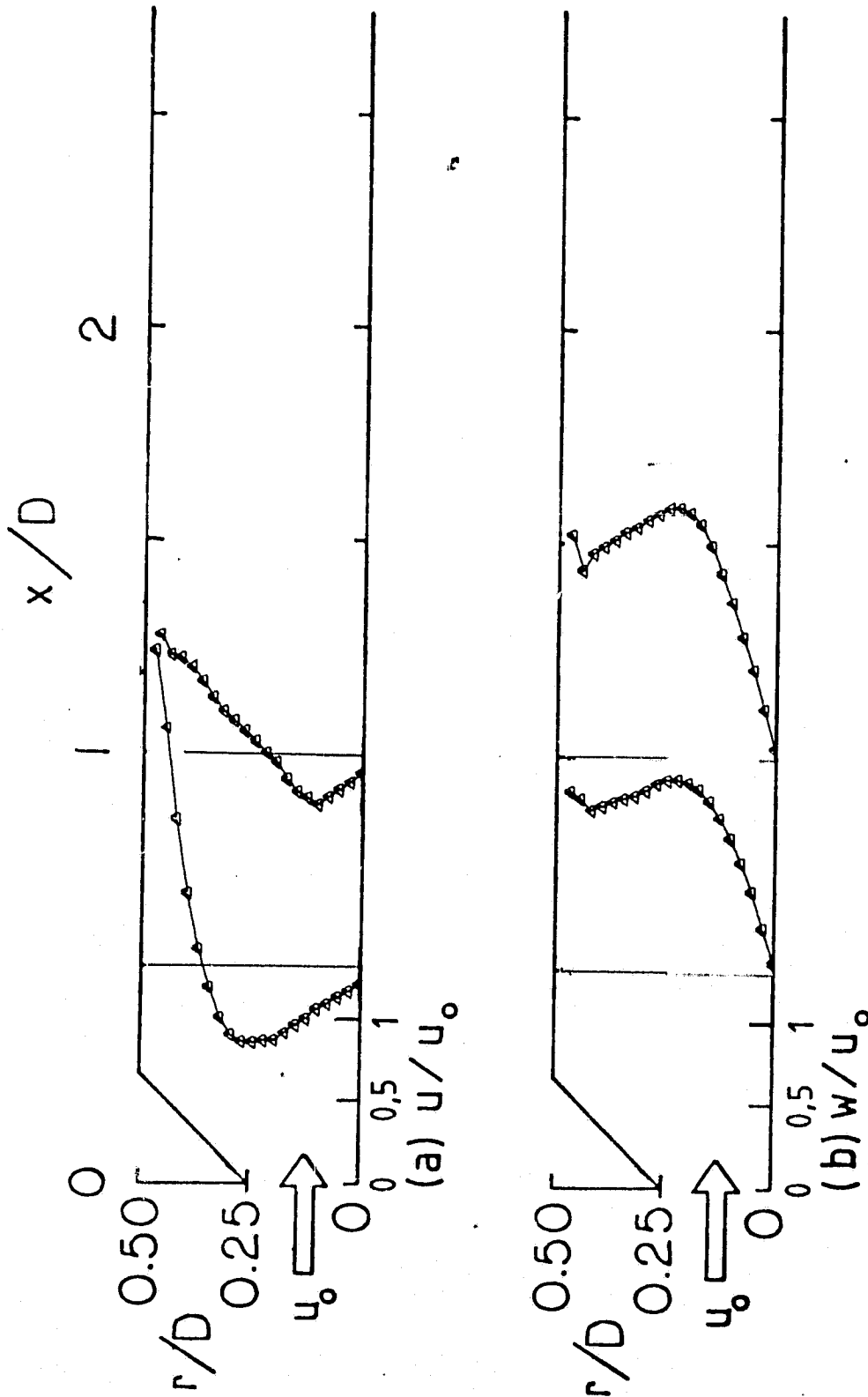


ORIGINAL PAGE IS
OF POOR QUALITY



(d) Swirl Vane Angle $\phi = 60^\circ$

Figure 13 (Continued)



(e) Swirl Vane Angle $\phi = 70^\circ$

Figure 13 (Continued)

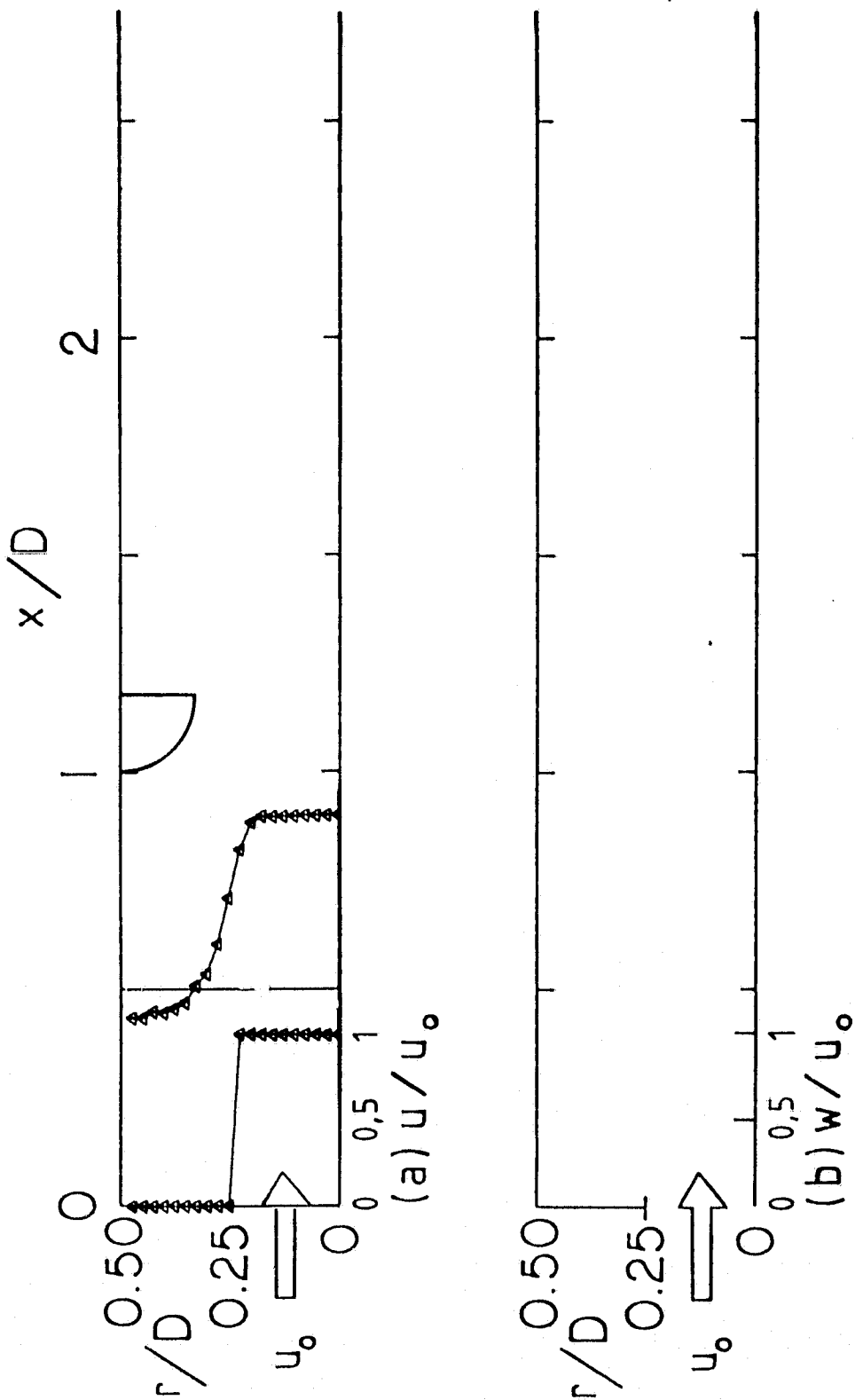
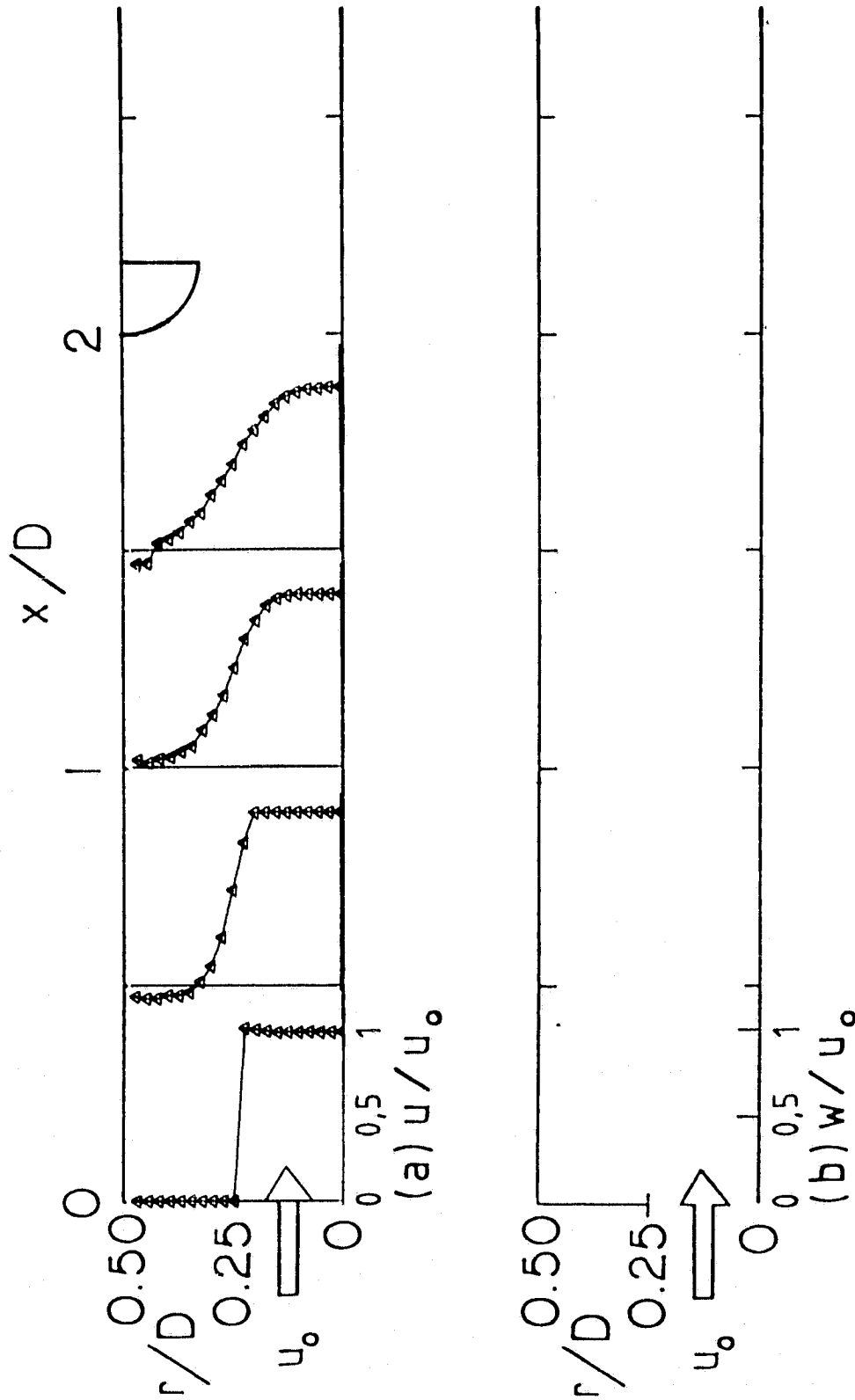
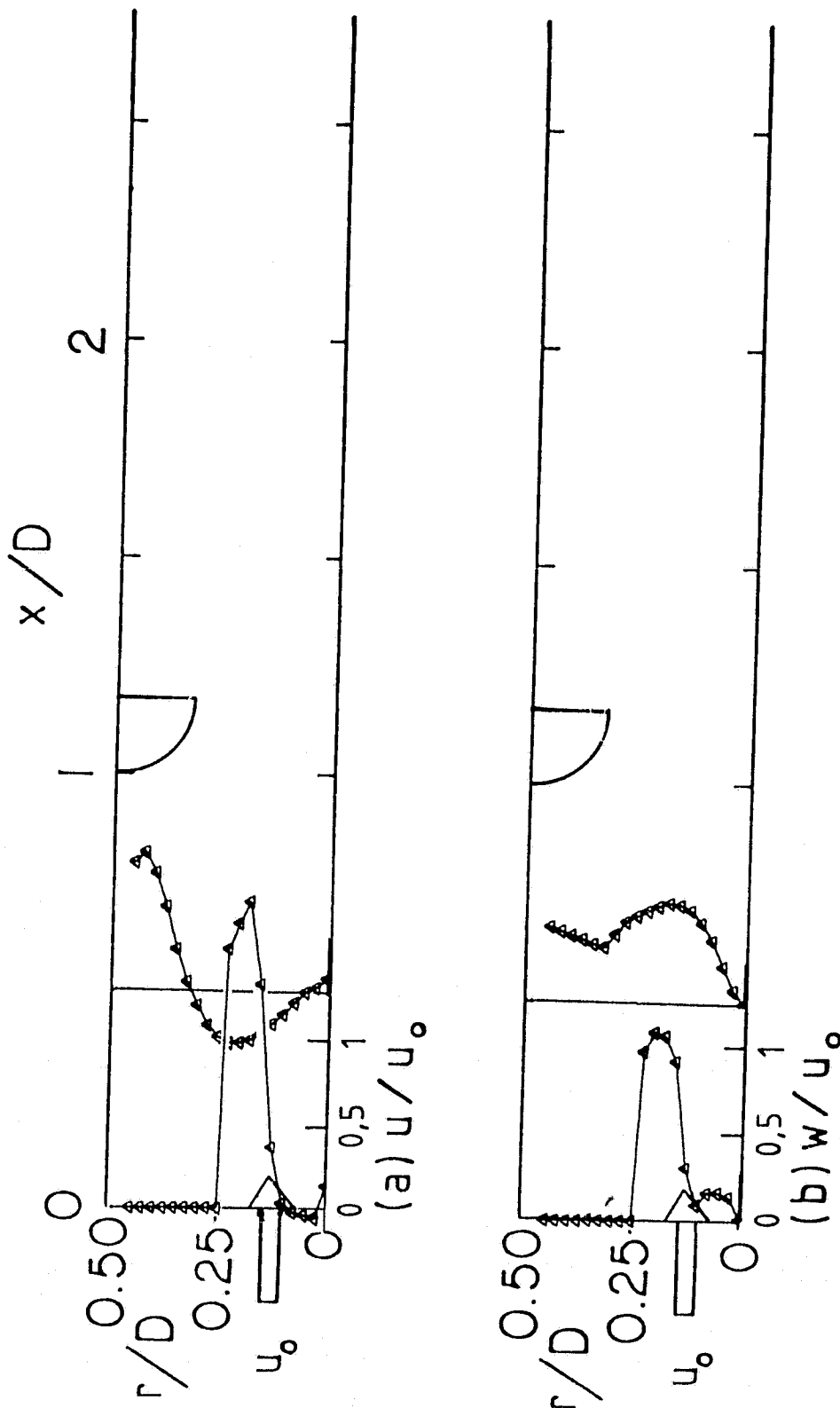


Figure 14. Velocity Profiles for Swirl Vane Angle $\phi = 0^\circ$ with Contraction Block

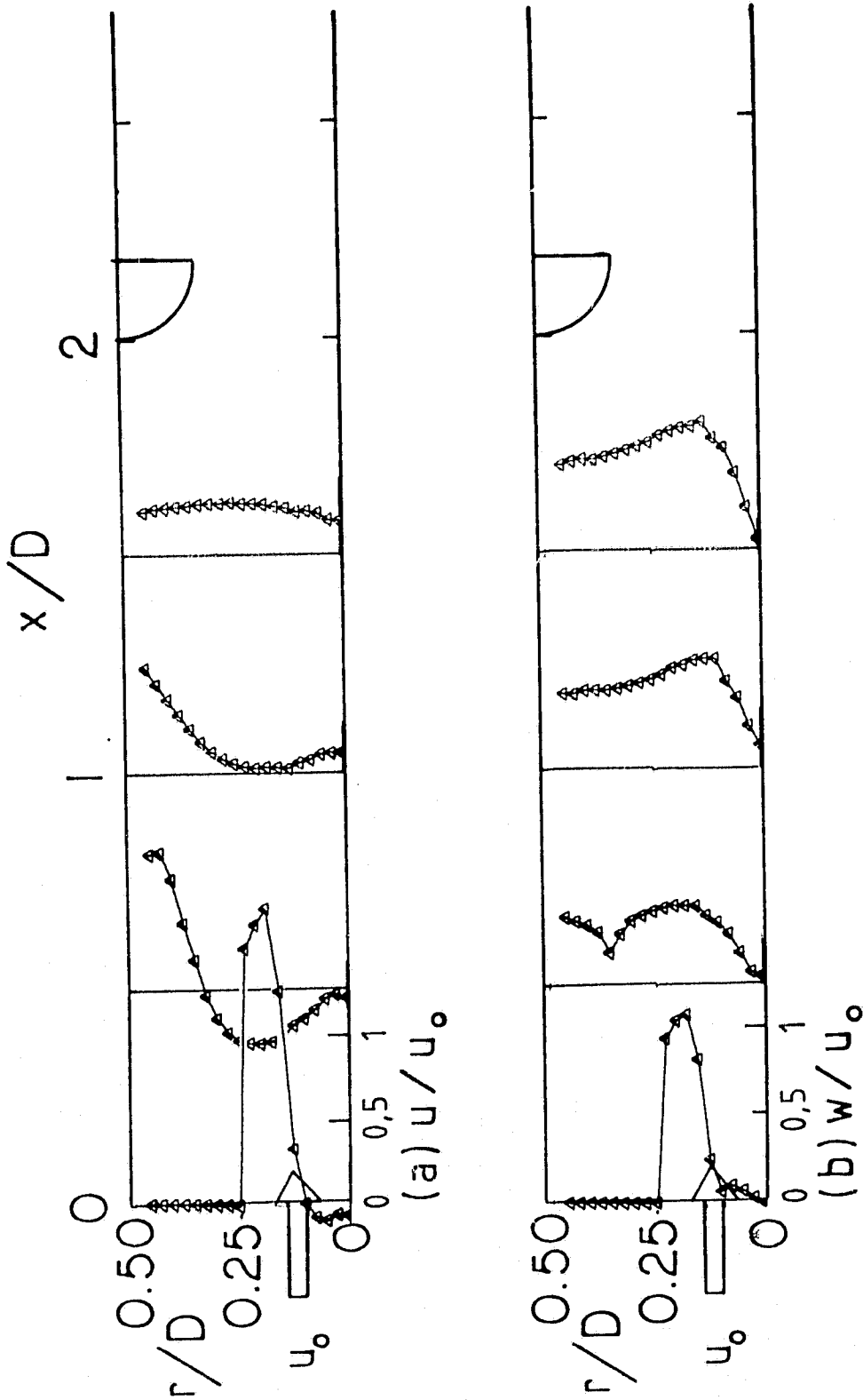


(b) $L/D = 2.0$

Figure 14 (Continued)

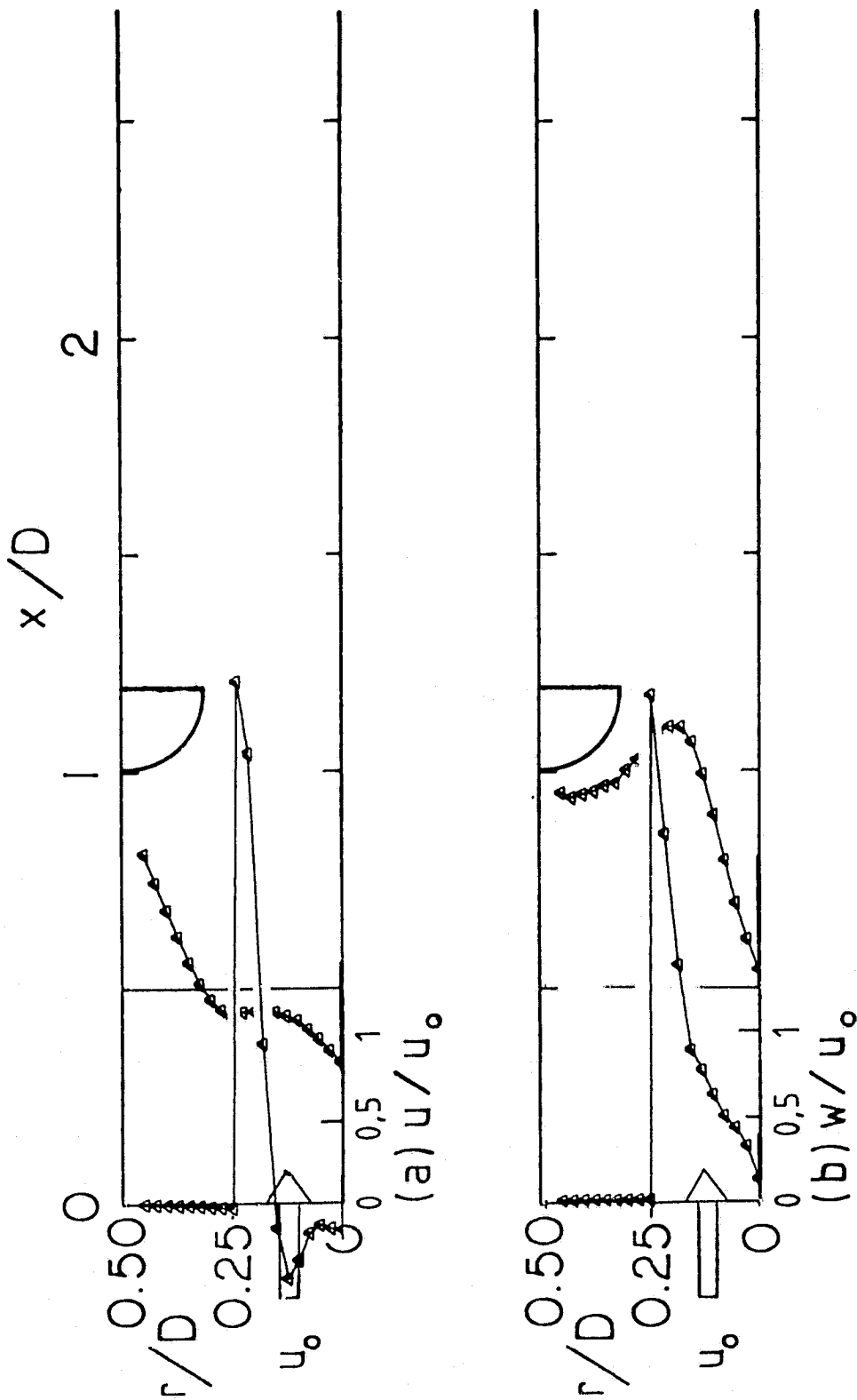


(a) $L/D = 1.0$
Figure 15. Velocity Profiles for Swirl Vane Angle $\phi = 45^\circ$ with Contraction Block



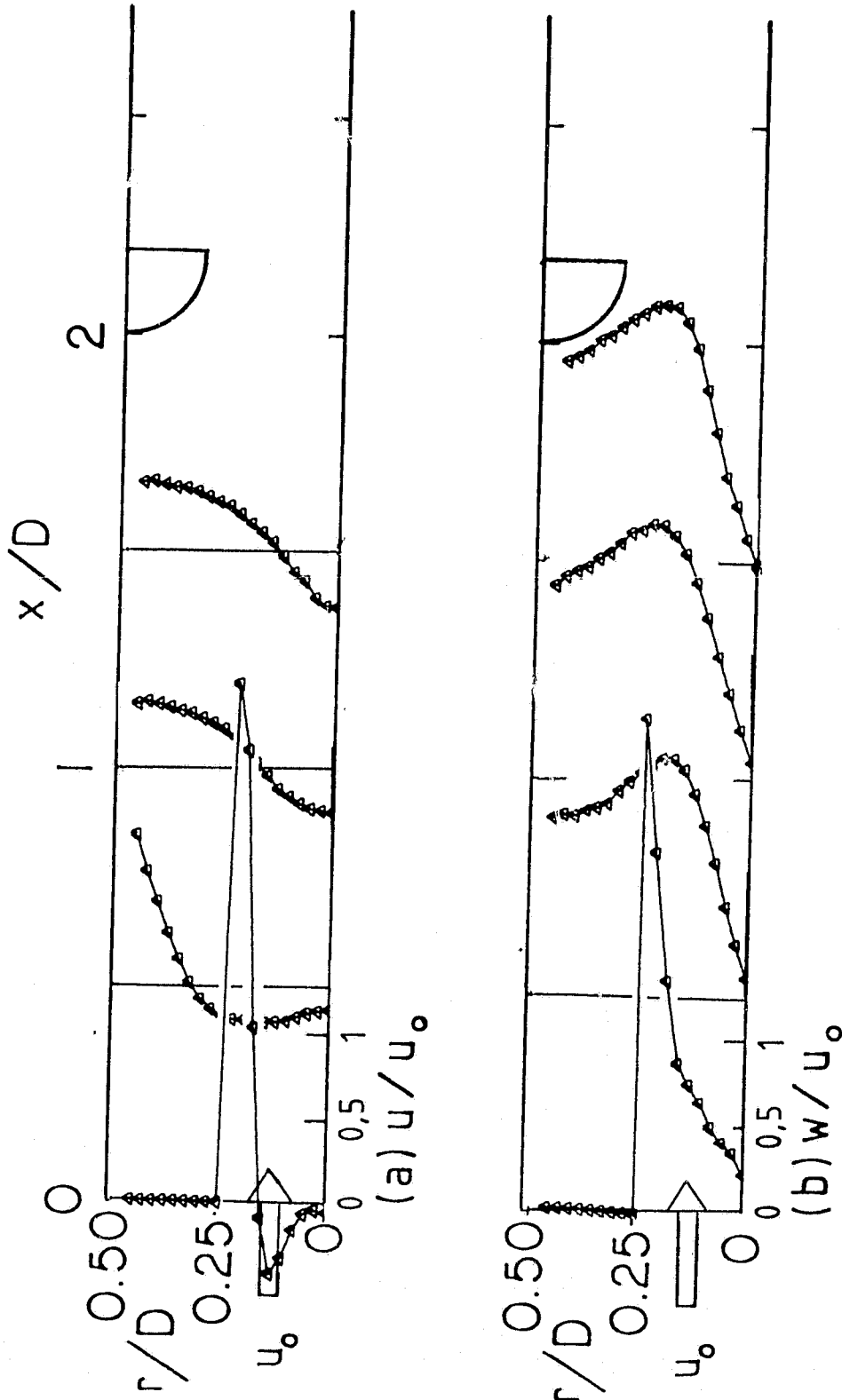
(b) $L/D = 2.0$

Figure 15 (Continued)



(a) $L/D = 1.0$

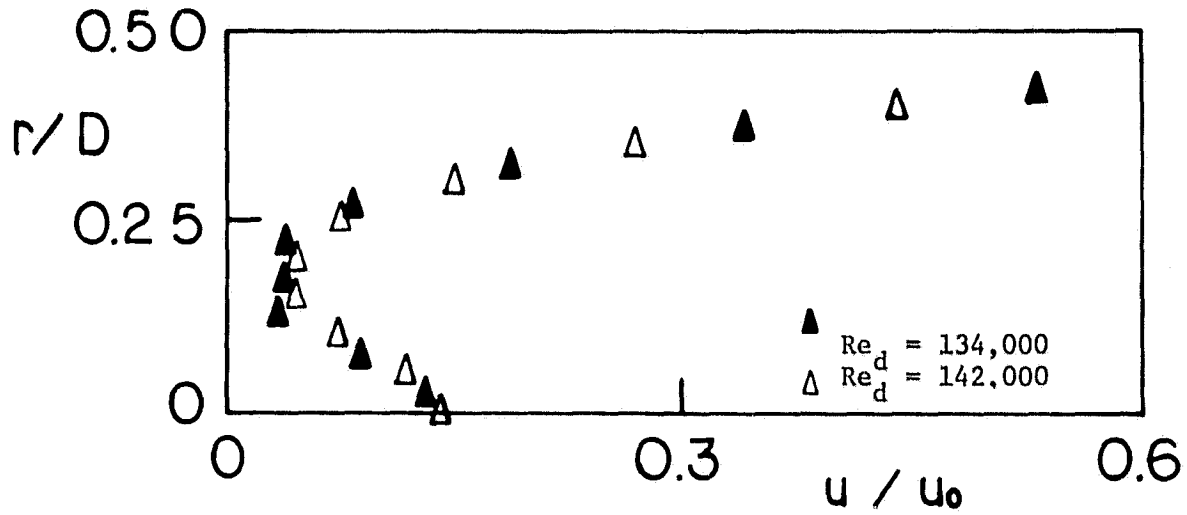
Figure 16. Velocity Profiles for Swirl Vane Angle $\phi = 70^\circ$ with Contraction Block



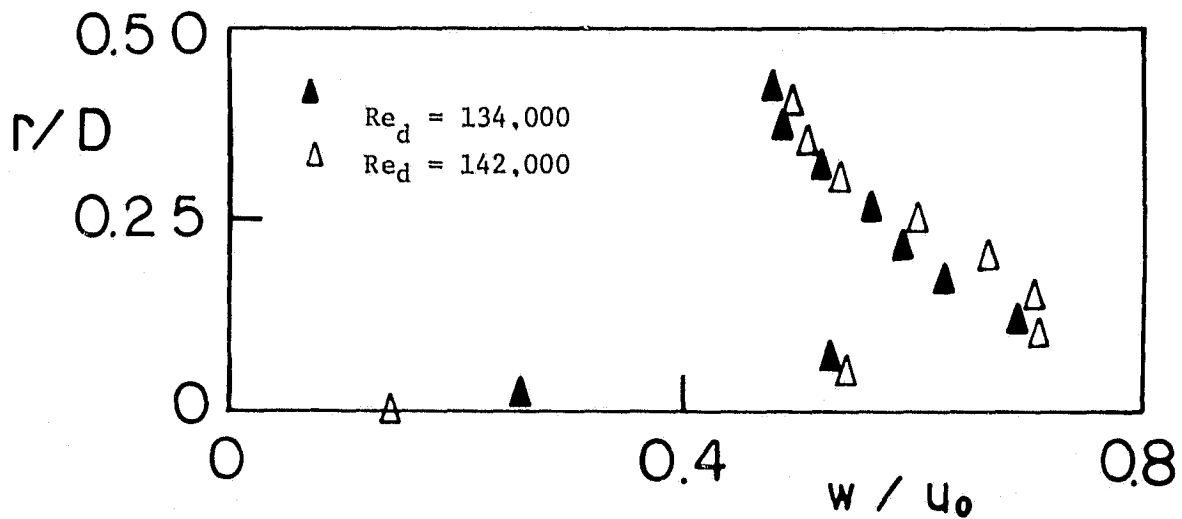
(b) $L/D = 2.0$

Figure 16 (Continued)

ORIGINAL PAGE IS
OF POOR QUALITY



(a) Axial Velocity



(b) Swirl Velocity

Figure 17. Repeatability of Five-Hole Pitot Probe Measurement for Side-Wall Expansion Angle $\alpha = 90^\circ$ and Swirl Vane Angle $\phi = 45^\circ$ with Contraction Block at $L/D = 2.0$ at $x/D = 1.0$

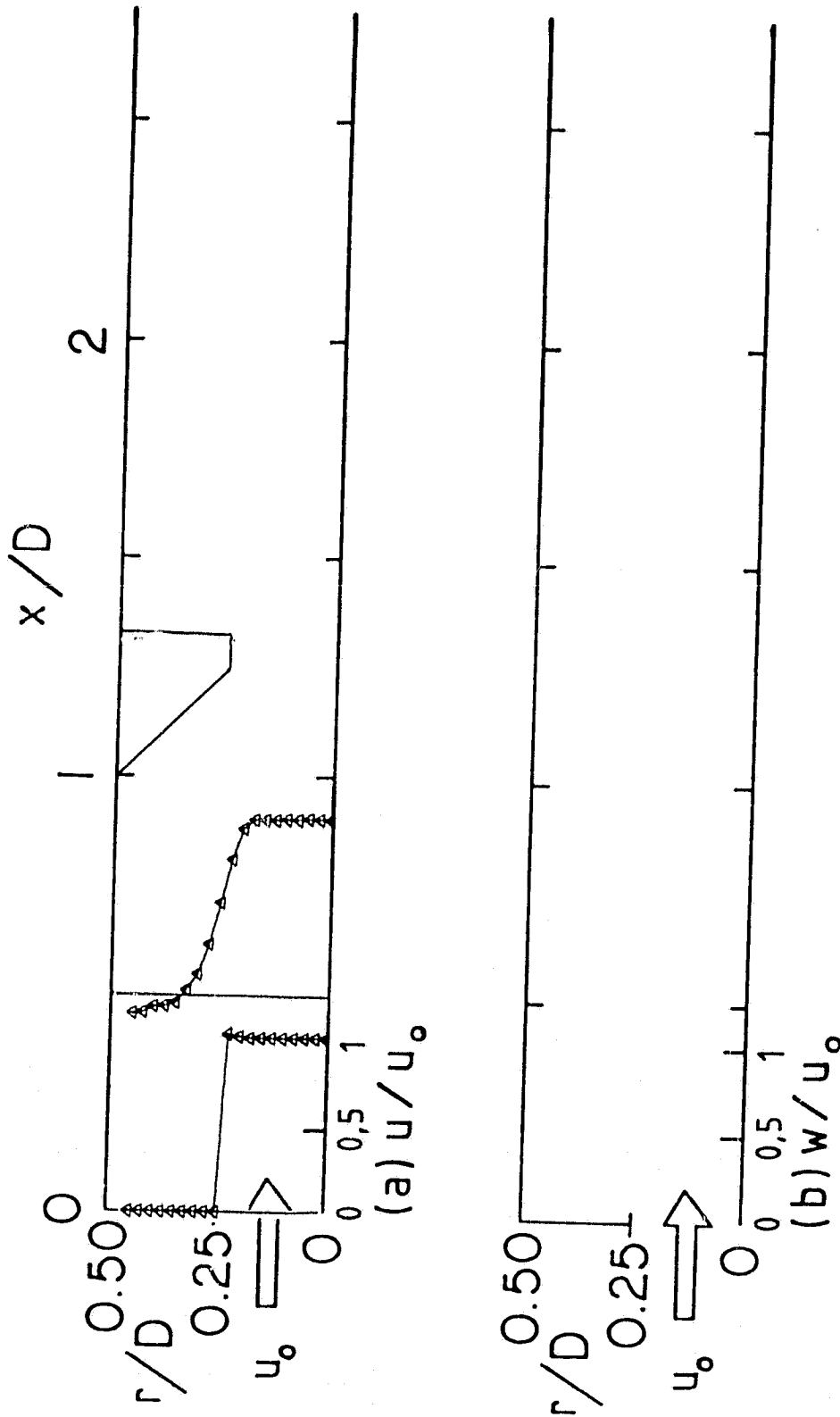
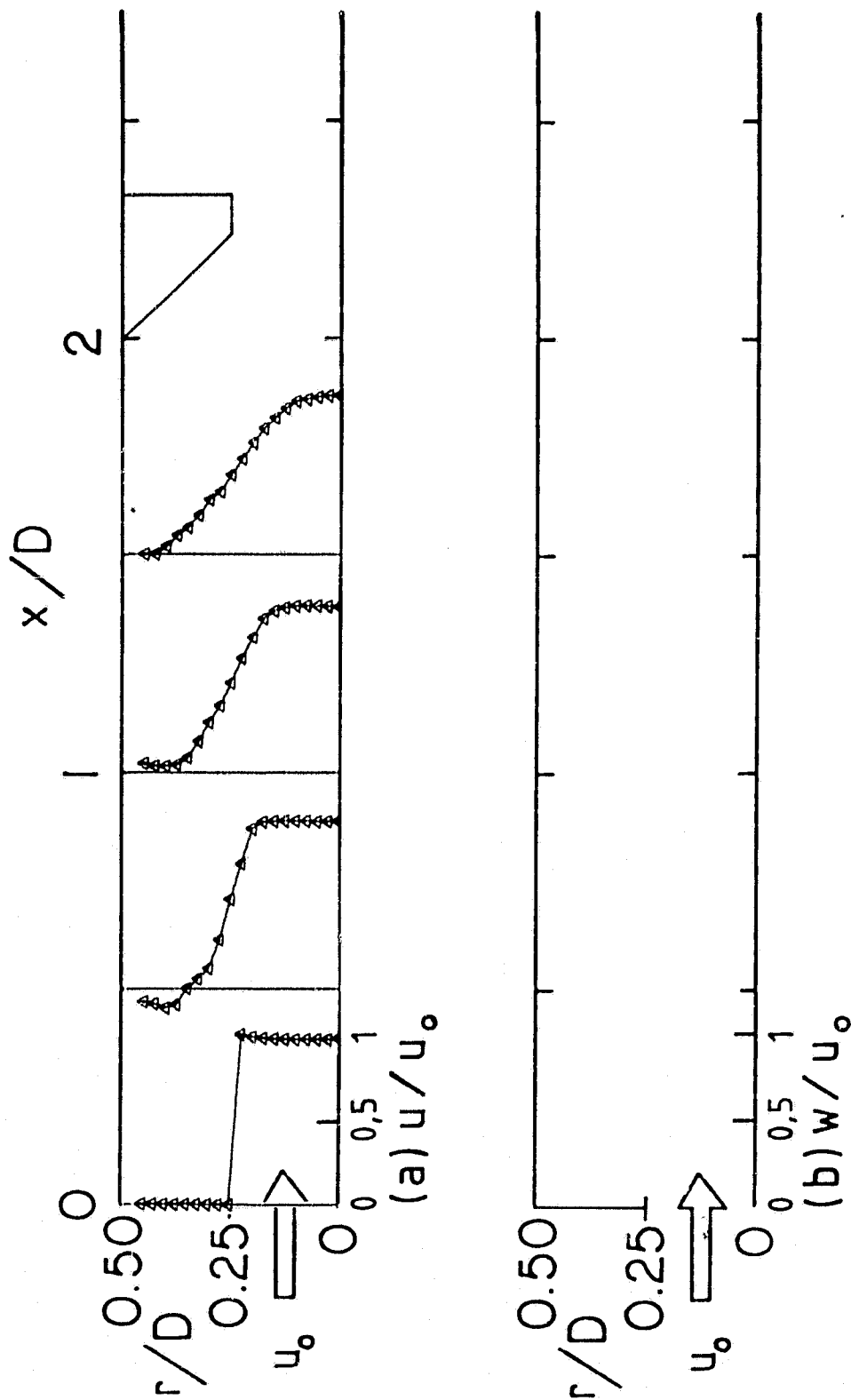


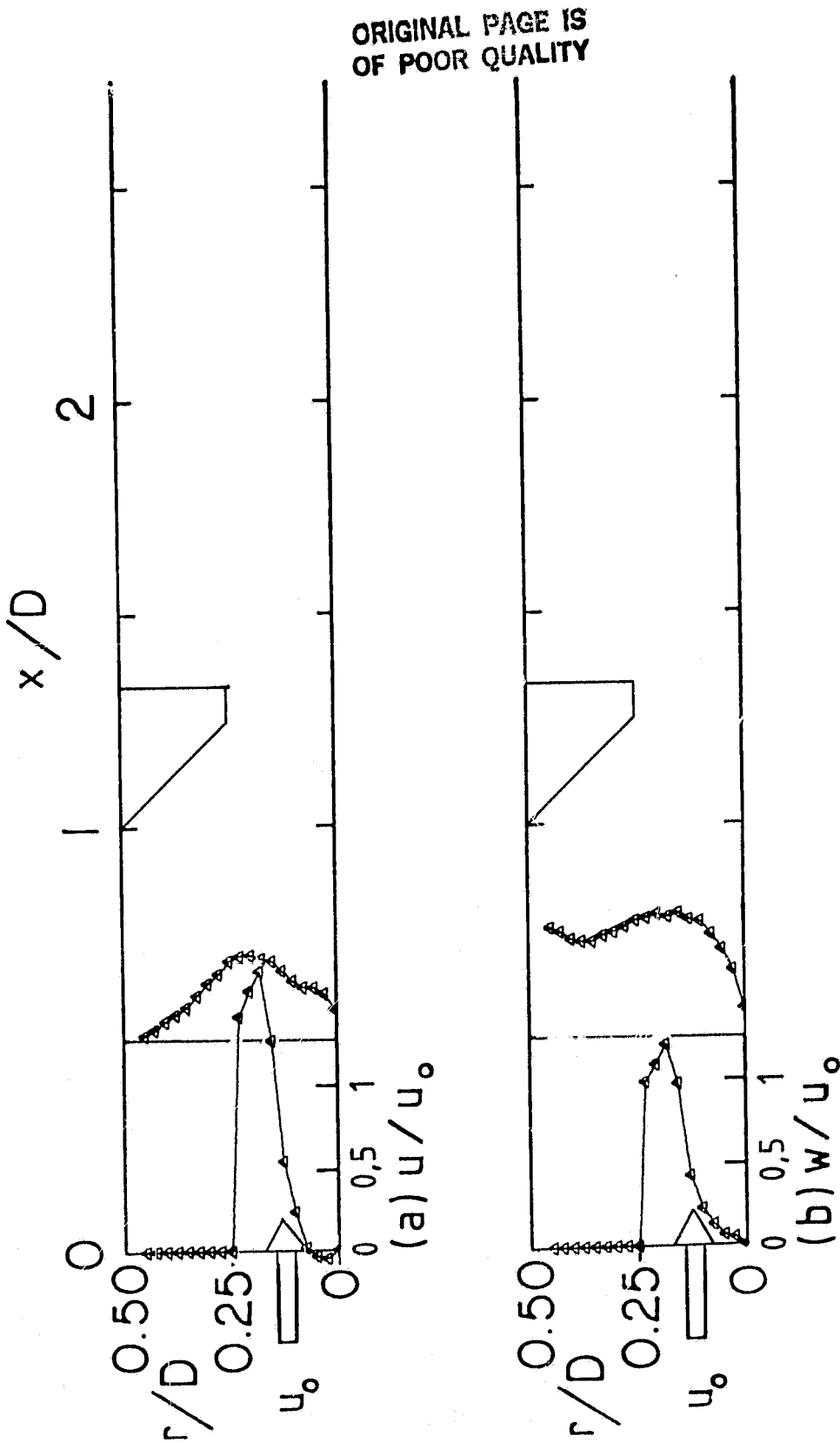
Figure 18. Velocity Profiles for Swirl Vane Angle $\phi = 0^\circ$ with Strong Contraction Nozzle.

(a) $L/D = 1.0$



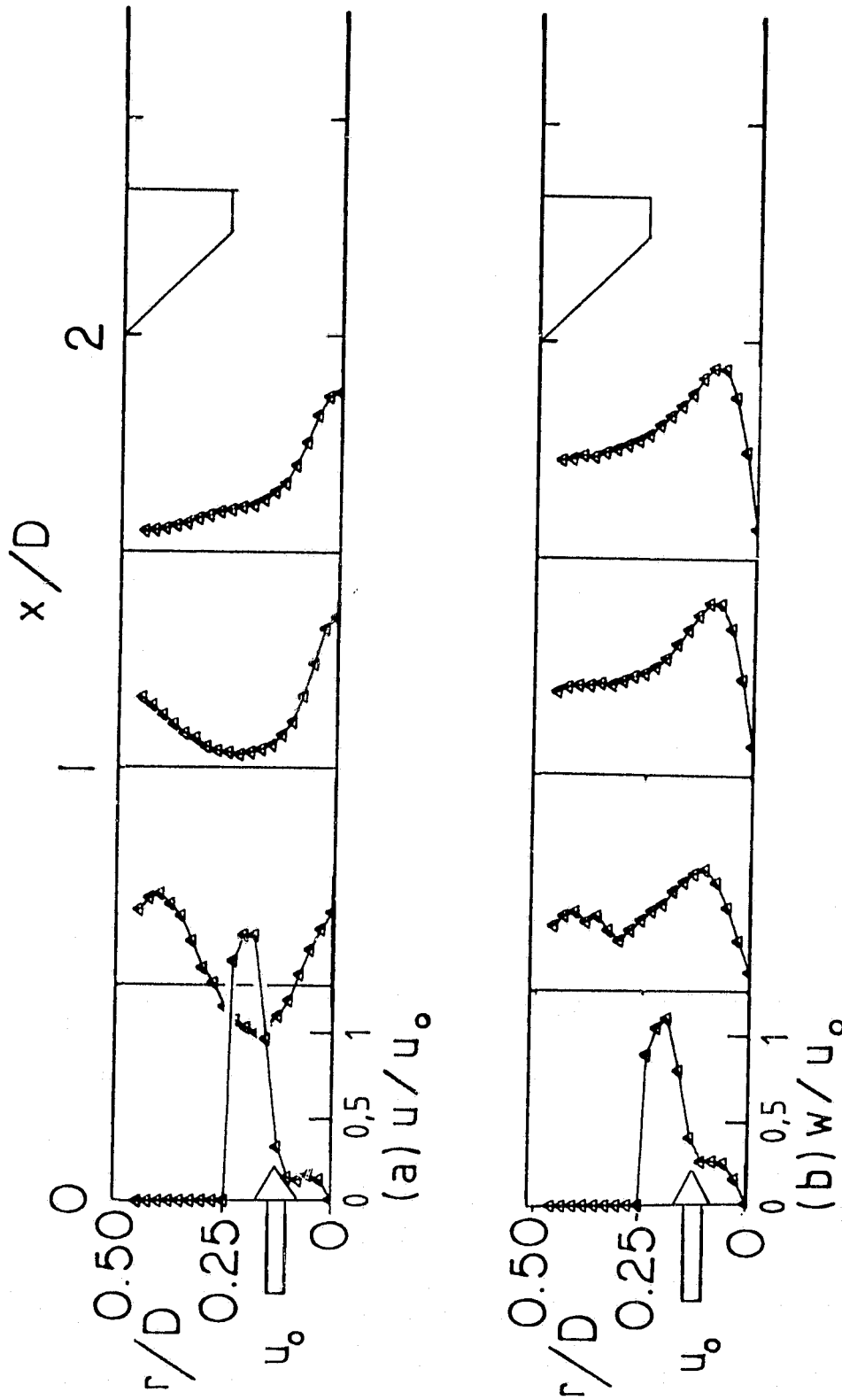
(b) $L/D = 2.0$

Figure 18 (Continued)



(a) $L/D = 1.0$

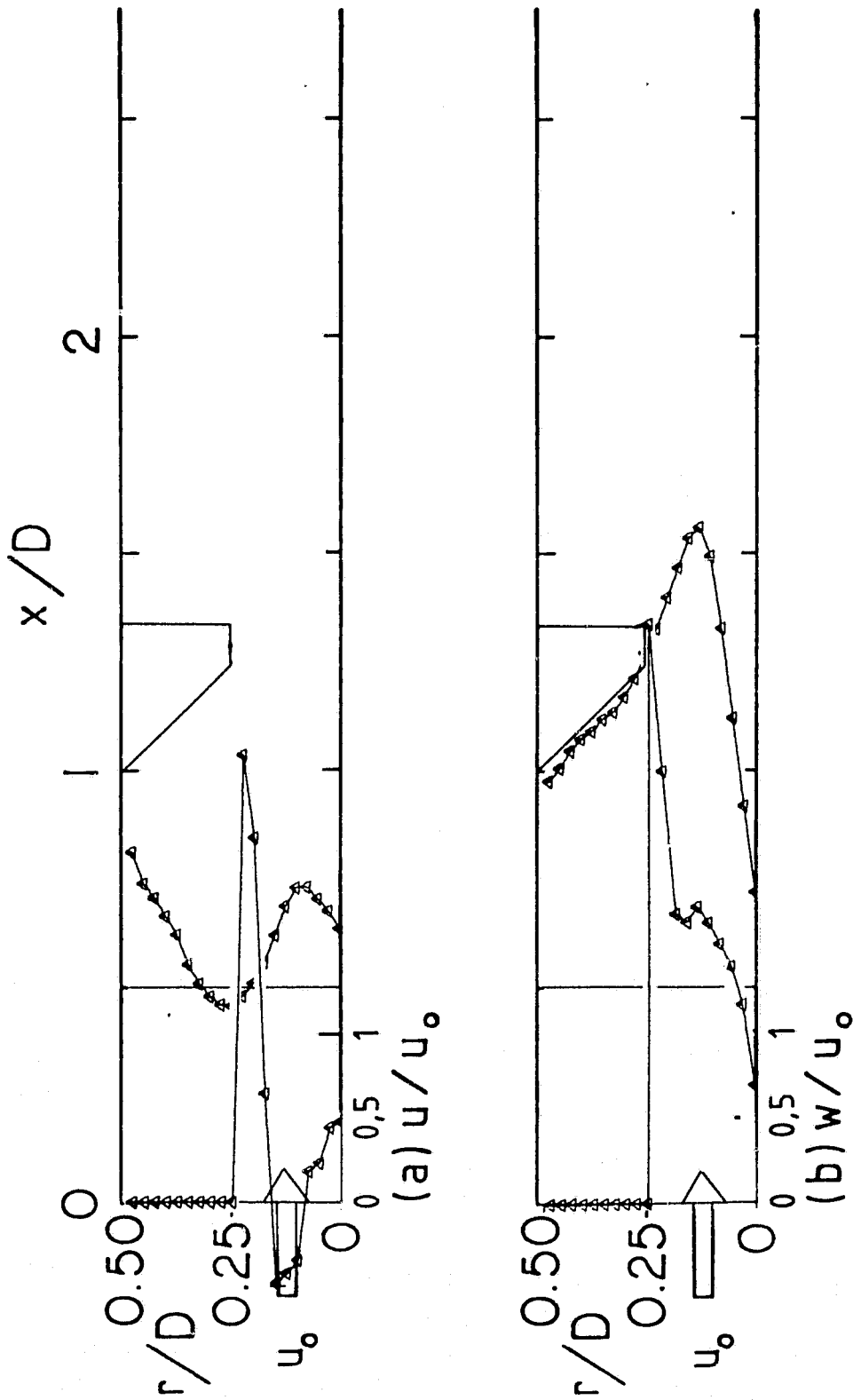
Figure 19. Velocity Profiles for Swirl Vane Angle $\phi = 45^\circ$ with Strong Contraction Nozzle.



(b) $L/D = 2.0$

Figure 19 (Continued)

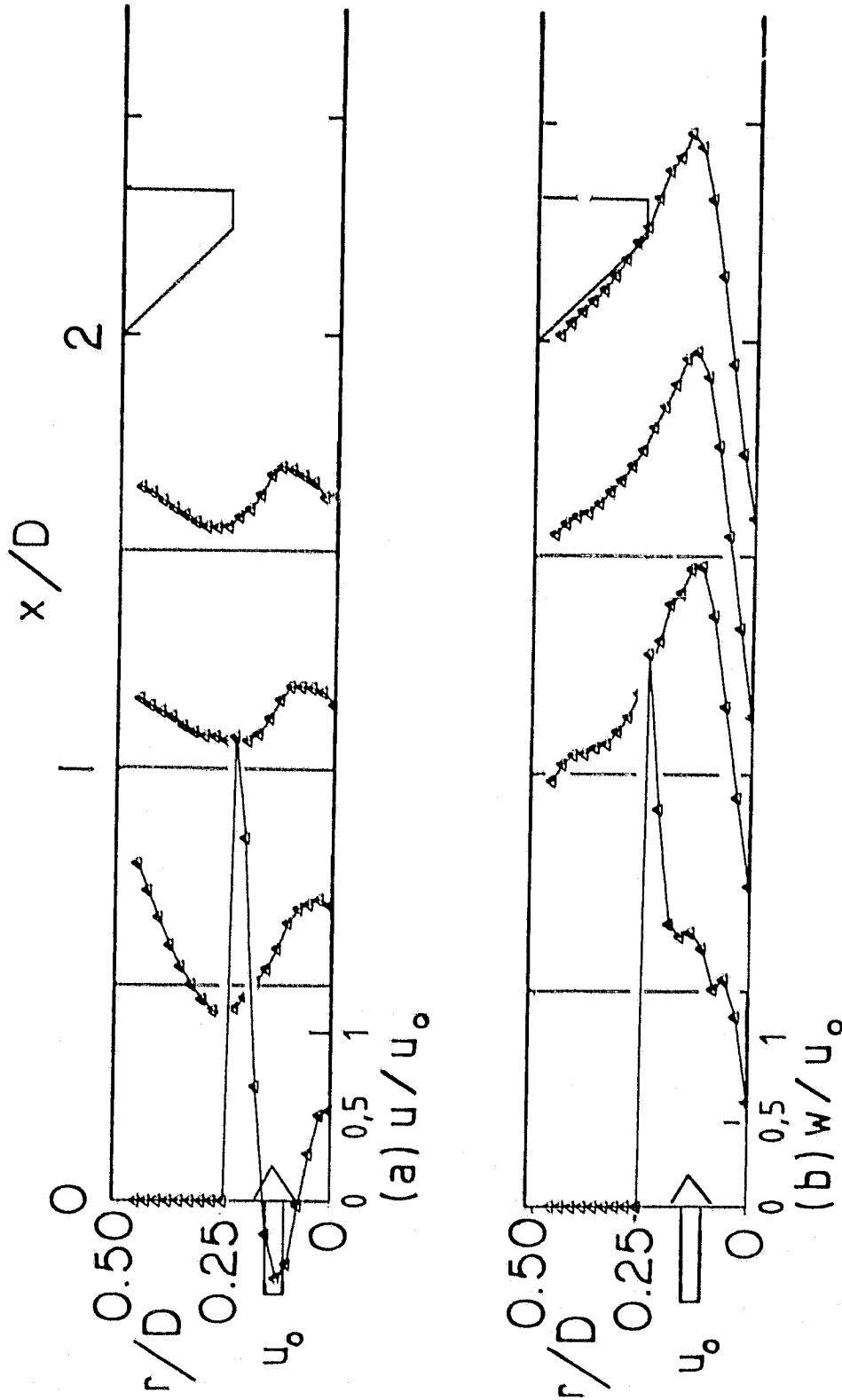
ORIGINAL PAGE IS
OF POOR QUALITY.



(a) $L/D = 1.0$

Figure 20. Velocity Profiles for Swirl Vane Angle $\phi = 70^\circ$ with Strong Contraction Nozzle.

ORIGINAL PAGE IS
OF POOR QUALITY



(b) $L/D = 2.0$

Figure 20 (Continued)

ORIGINAL PAGE IS
OF POOR QUALITY

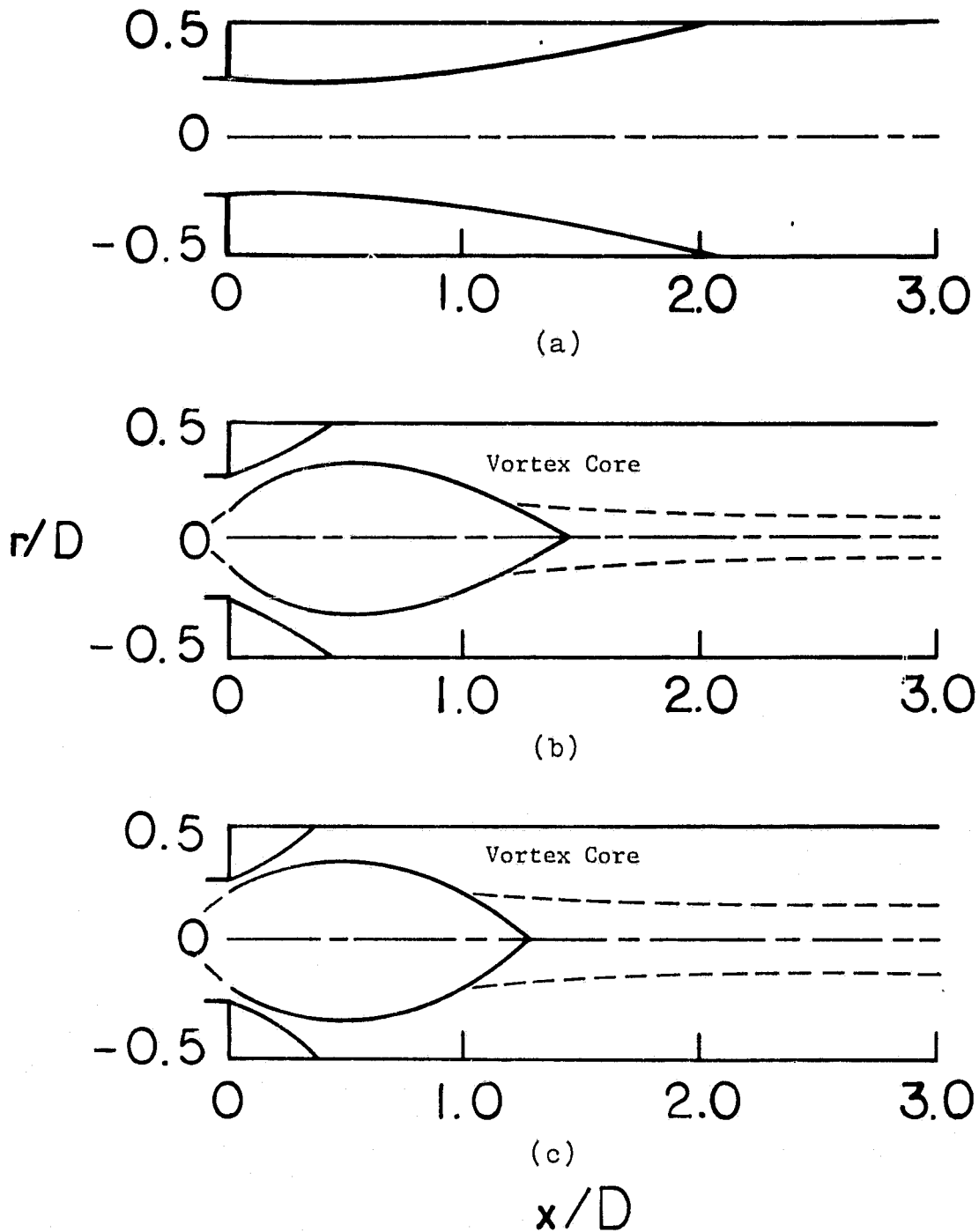


Figure 21. Artistic Impressions of Dividing Streamline without Contraction Block for Side-Wall Expansion Angle $\alpha = 90^\circ$ and Swirl Vane Angle: (a) $\phi = 0^\circ$ (b) $\phi = 45^\circ$ and (c) $\phi = 70^\circ$.

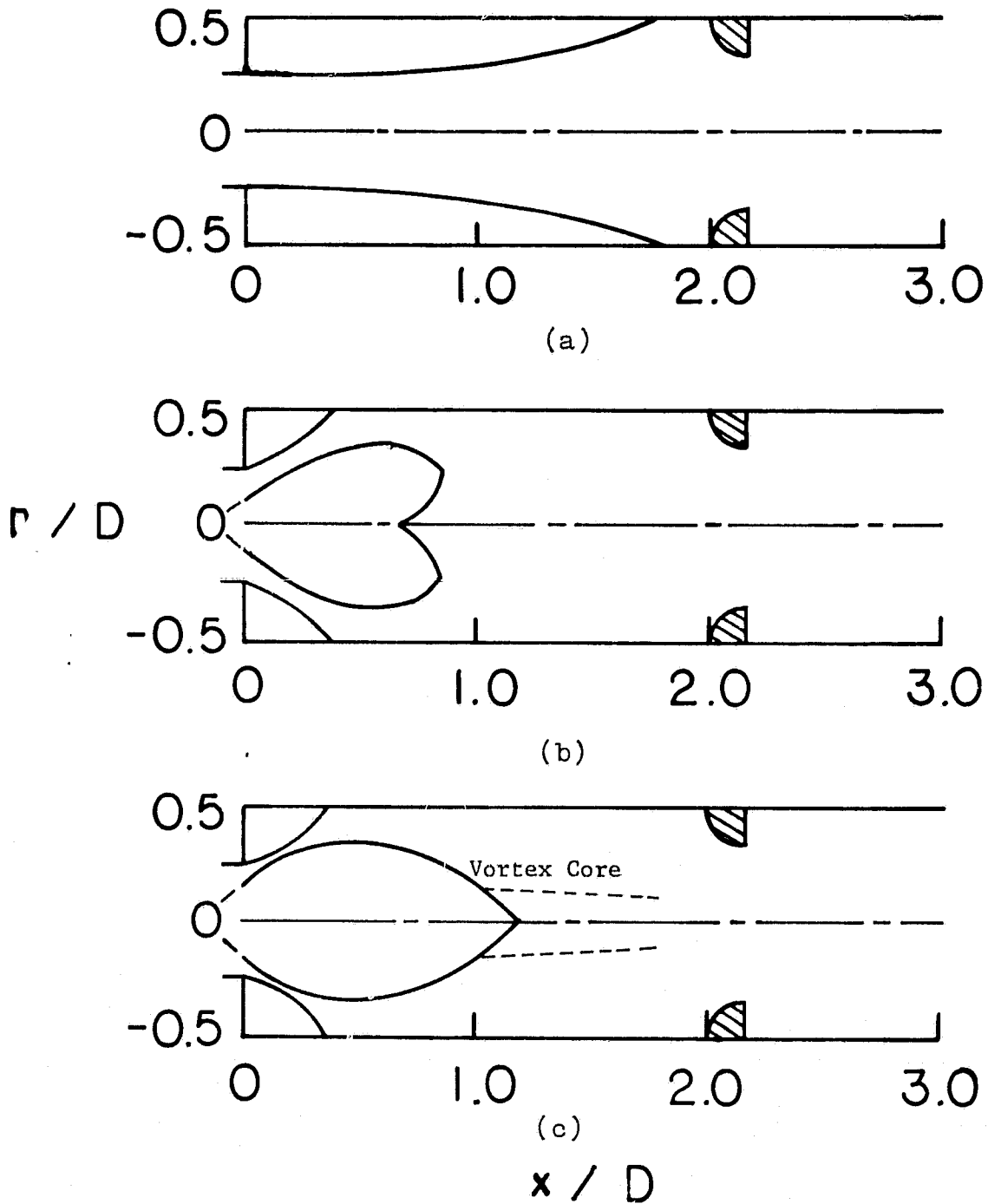


Figure 22. Artistic Impressions of Dividing Streamlines with Contraction Block at $L/D = 2.0$ for Side-Wall Expansion Angle $\alpha = 90^\circ$ and Swirl Vane Angle: (a) $\phi = 0^\circ$ (b) $\phi = 45^\circ$ (c) $\phi = 70^\circ$.

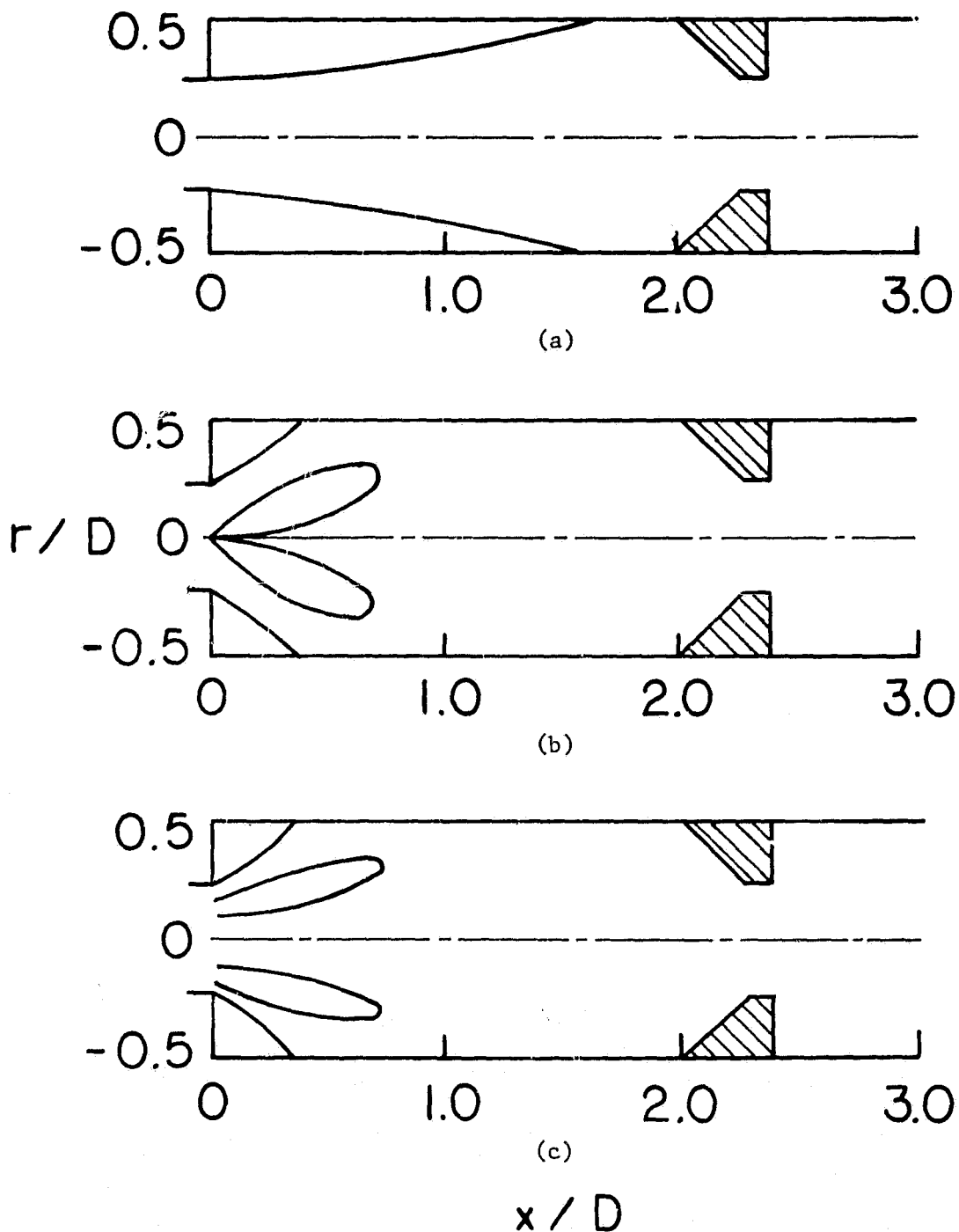


Figure 23. Artistic Impressions of Dividing Streamlines with Contraction Block at $L/D = 2.0$ for Side-Wall Expansion Angle $\alpha = 90^\circ$ and Swirl Vane Angle: (a) $\phi = 0^\circ$ (b) $\phi = 45^\circ$ (c) $\phi = 70^\circ$.

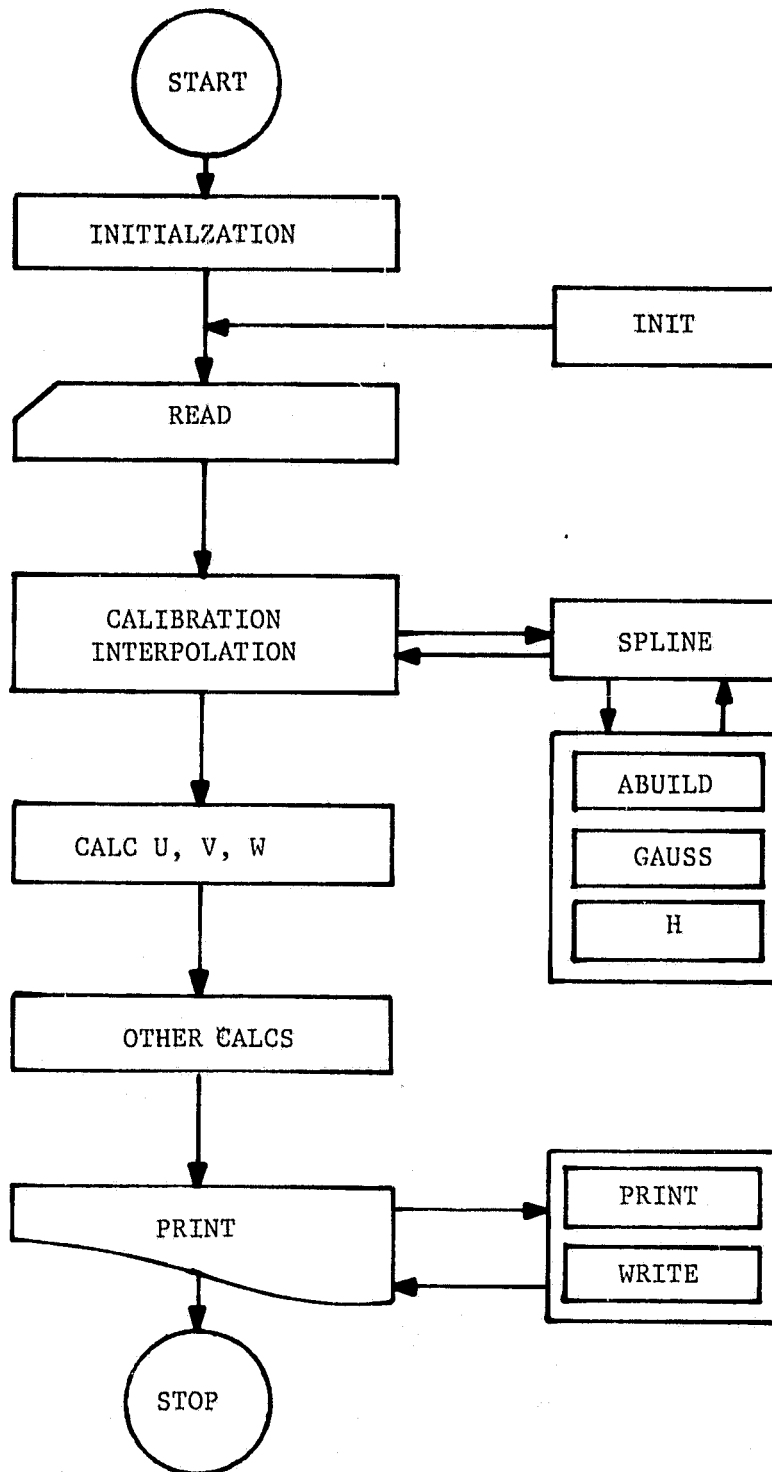


Figure 24. Flow Chart of Data Reduction Computer Program.

APPENDIX C

USER'S GUIDE TO FIVE-HOLE PITOT PROBE DATA
REDUCTION COMPUTER PROGRAM

A FORTRAN computer program to reduce five-hole pitot probe measurement data was written by Rhode (5). The data reduction program consists of one main subprogram, two functions and five subroutines. A cubic spline interpolation technique is employed to interpolate calibration data. This user's guide emphasizes the basic mathematical concepts together with analytical and numerical methods employed in this program. For user's convenience, sample input and output are given. The flow chart of this program is shown in Figure 24.

1. MAIN Subprogram

MAIN characterizes the particular conditions being investigated. Entire solution procedure is controlled by MAIN. So, it is the section of the program to which a user will devote most of his attention. It is divided into four chapters, each with a specific task, and a description of the individual chapters of MAIN now follows.

CO Preliminaries

Dimension and common are followed by input logical parameters, which activate, when specified as TRUE, certain special features of program. IWRITE writes solutions onto allocated disk storage and DIAGNS activates diagnostic write statements. Some geometric parameters

are specified as user input values. Input read statement for alphanumeric headings is given. Initialization of all variables to be zero by calling subroutine INIT is followed by two input read statements, which read calibration and raw measurement data.

C1 Data Reduction

This is a main part to reduce raw measurement data. Data reduction consists of a cubic spline interpolation of calibration data and calculations of u, v and w velocity components. A pitch coefficient is calculated by $(P_N - P_S)/(P_C - P_W)$. With the calculated pitch coefficient, a pitch angle δ is obtained from the corresponding calibration characteristic by calling function SPLINE. The corresponding velocity coefficient C for the resulting pitch angle δ is also obtained by calling function SPLINE once again.

IDID is a parameter to define calibration ranges. If pitch angle δ or velocity coefficient C is out of the calibration range $[-3.759 \leq (P_N - P_S)/(P_C - P_W) \leq 3.399, |\delta| \leq 58]$, respectively, the corresponding value is taken to be zero with IDID = 0.

With the above obtained information, three velocity components and magnitude of the total velocity vector are calculated from

$$V = \left[\frac{2}{\rho} (P_C - P_W) \cdot C \right]^{1/2} \quad (\text{A3.1})$$

$$u = V \cos \delta \cos \beta \quad (\text{A3.2})$$

$$v = V \sin \delta \quad (\text{A3.3})$$

$$w = V \cos \delta \sin \beta. \quad (\text{A3.4})$$

C2 Auxiliary Calculations

This part consist of calculations of geometric quantities and nondimensionizations of velocities. A mass flow rate and axial flux of angular momentum are calculated by a finite difference integration method as following:

$$\text{mass flow rate} = \sum_i u_i \Delta A_i \quad (\text{A3.5})$$

and

$$\text{axial flux of angular momentum} = \sum_i \rho u_i w_i r_i^2 \Delta r_i \quad (\text{A3.6})$$

Mean axial velocity is calculated by

$$\text{mean axial velocity} = \sum u_i \Delta A_i / A$$

A nozzle inlet axial velocity is obtained from the conversion of the measured dynamic static pressure (inch H₂O) at the nozzle throat into the corresponding velocity (m/sec). All velocities are nondimensionized by the nozzle inlet axial velocity.

C3 Output

All reduced data are printed out according to a standard format by calling subroutines WRITE and PRINT.

2. INIT Subroutine

In this subroutine, all variables are initialized to be zero even though some are set to obviously nonzero values. All variables in the subprogram MAIN communicate with those in the subroutine INIT through common statements.

3. SPLINE Function

A cubic spline data fitting technique (25) is employed to interpolate pitch angle δ and velocity coefficient C from the corresponding calibration characteristics. For a certain x value, which lies between the points (X_i, Y_i) and (X_{i+1}, Y_{i+1}) , a cubic polynomial equation can be written by

$$Y = a_i (X - X_i)^3 + b_i (X - X_i)^2 + c_i (X - X_i) + d_i \quad (\text{A3.7})$$

with application of the proper end point conditions, it reduces to

$$h_{i-1} S_{i-1} + 2(h_{i-1} + h_i) S_i + h_i S_{i+1} = b \left(\frac{Y_{i+1} - Y_i}{h_i} - \frac{Y_i - Y_{i-1}}{h_{i-1}} \right) \quad (\text{A3.8})$$

$$h_i = X_{i+1} - X_i \quad (\text{A3.9})$$

During the foregoing procedures, the coefficients are also reduced as

$$a_i = (S_{i+1} - S_i) / [6h_i] \quad (\text{A3.10})$$

$$b_i = S_i / 2 \quad (\text{A3.11})$$

$$c_i = \frac{Y_{i+1} - Y_i}{h_i} - \frac{2h_i S_i + h_i S_{i+1}}{6} \quad (\text{A3.12})$$

$$d_i = Y_i \quad (\text{A3.13})$$

The equation (A3.8) forms $(n - 2)$ equations for n unknowns. Two more equations needed to solve n unknowns are obtained when the conditions

pertaining to the end intervals are specified. Linear extrapolation techniques is employed to obtain the end point conditions. The relations for end conditions of the whole curve are at the left end:

$$S_1 = \frac{(h_1 + h_2) S_2 - h_1 S_3}{h_2} \quad (\text{A3.14})$$

and the right end:

$$S_n = \frac{(h_{n-2} + h_{n-1}) S_{n-1} - h_{n-1} S_{n-2}}{h_{n-2}} \quad (\text{A3.15})$$

Finally, n equations including two conditions are obtained for n unknowns.

With the above mathematic concept in mind, one can follow the calculation steps employed in this program. Two calibration and raw measurement data in MAIN communicate with those in SPLINE through parameters X, FX and X1. A Parameter A is an array for the coefficients of n simultaneous cubic polynomial equations. The $(n-2)$ by $(n-2)$ components of an array A are built by calling the subroutine ABUILD. The end point components $A(1,J)$ and $A(N,J)$ are built in the function SPLINE. The Gauss-Jordan elimination method is employed to solve $(n-2)$ equations for $(n-2)$ unknowns simultaneously. These solutions are translated back to the SPLINE by a parameter A.

With the obtained solutions, the coefficient of a cubic polynomial equation are calculated by equations (A3.10) through (A3.13). Finally, an interpolation is achieved by substituting the known coefficient values into the equation (A3.7). An interpolated value is translated back to the MAIN through a variable SPLINE.

4. H Function

This function calculates the interval ΔX_i between the points (X_i, Y_i) and (X_{i+1}, Y_{i+1}) .

5. ABUILD Subroutine

This routine builds an $(n-2)$ by $(n-2)$ array for the coefficients of a cubic polynomial equation. This forms a tridiagonal matrix with a column vector of $(n-2)$ components. The notation employed here is as follows:

$$a_{i,i-1} = h_{i-1}$$

$$a_{i,i} = 2(h_{i-1} + h_i)$$

$$a_{i,i+1} = h_i$$

and

$$a_{i,n+1} = 6 \left(\frac{Y_{i+1} - Y_i}{h_i} - \frac{Y_i - Y_{i-1}}{h_{i-1}} \right)$$

6. GAUSS Subroutine

This routine solves $(n-2)$ equations simultaneously with a Gauss-Jordan elimination method. Solutions are stored in the $a_{i,n+1}$.

7. PRINT and WRITE Subroutines

The tasks of subroutines PRINT and WRITE are to print out the values of a 2-D array PHI, together with associated heading HEAD, the last parameter of the call list. The only difference between PRINT

and WRITE is that WRITE is used to print out one line and PRINT is used to print out multiple lines at a time. The first two parameters of the call list, ISTART and JSTART, are usually 1 and 1, so that all internal and external values are printed to help diagnostics.

8. Sample Input

Alphanumeric headings, calibration data and raw measurement data are read by input read statements. Sample input data are given for the sample case of side-wall expansion angle $\alpha = 90$ degrees, swirl vane angle $\phi = 45$ degrees and contraction nozzle located $L/D = 1$.

(a) Alphanumeric headings: These alphanumeric headings are used to accompany the output descriptively. Nineteen lines of such headings are read in via the first read statement. The current alphanumeric headings are given in Table XIV.

(b) Calibration Data: Calibrations are done for pitch angle and velocity coefficient characteristics. Calibration input data consist of pitch coefficient $(P_N - P_S)/(P_C - P_W)$ and velocity coefficient $\rho V^2/[2(P_C - P_W)]$ for 24 different pitch angles δ . Sample calibration input data are tabulated in Table XV. This table consists of pitch coefficient in the first column, corresponding pitch angle in the second and corresponding velocity coefficient in the third.

(c) Measurement Data: Sample raw measurement data are given for two axial stations in Table XVI. Nineteen radial traverse measurement data are taken at each axial station. For each axial station, axial distance (inch), maximum number of radial positions and dynamic pressure (in H_2O) are read as shown in lines 10380 and 10580 of Table XVI. Lines 10390 to 10570 are measurement data for the axial station

$x/D = 0,0$ and lines 10590 to 10770 are for the axial station $x/D = 0,5$. The input measurement data consists of four column input data; the first is for radial measurement point (inch), the second for measured flow angle ($360,0 - \beta$ degree), the third for $P_N - P_S$ (volt) and the fourth for $P_C - P_W$ (volt).

9. Sample Output

Typical output consists of yaw angle, pitch angle and three velocity components. The corresponding output for the sample input data just described is given in Table VI, as described earlier in Section 4.1. In this table, I and J denote the axial and radial station number, respectively. Also X and Y denote the normalized axial and radial station by the test section diameter, respectively. Yaw angle β and pitch angle δ are given in degrees. These velocity components are values normalized by the nozzle inlet axial velocity deduced from the pitot static pressure probe located upstream of the inlet to the test section, as described in Section 2.1.

As auxiliary output, geometric specifications and quantities are printed out in front of the typical output. Geometric specifications include expansion angle (degree). Swirl vane angle (degree), inlet radius (m) and combustor radius (m). On the other hand, flow quantities include mass flow rate (kg/s), nozzle inlet axial velocity (m/s), mean axial velocity (m/s) and axial flux of angular momentum (N.m). In each of these items, data relevant to each axial station are presented - these may be different with different axial stations and depend on the particular run conditions at the time of each tranverse. Output for the sample input data is given in Table XVII.

ORIGINAL PAGE IS
OF POOR QUALITY

144

```
C      SUBROUTINE MAIN
C
C *****
C
C      A COMPUTER PROGRAM FOR DATA REDUCTION OF FIVE-HOLE PITOT
C      MEASUREMENTS IN TURBULENT, SWIRLING, RECIRCULATING, FLOW
C      IN COMBUSTOR GEOMETRIES
C
C      VERSION OF JULY, 1982
C
C      H K YOON
C      MECHANICAL AND AEROSPACE ENGINEERING
C      OKLAHOMA STATE UNIVERSITY
C      STILLWATER, OK      74078
C
C *****
CHAPTER 0 0 0 0 0 0 PRELIMINARIES 0 0 0 0 0 0 0 0
C
      DIMENSION HEDM(9),HEDUMN(9),HEDNMS(9),HEDCMW(9),
      #HEDU(9),HEDV(9),HEDW(9),HEDVT(9),HEDUST(9),
      #HEDVST(9),HEDWST(9),HEDVTS(9),HEDDEL(9),HEDBET(9),
      #HEDMMF(9),HEDMIV(9),HEDMIF(9),HEDMPF(9),HEDAM(9)
C
      COMMON
      #/CALIB/CPITCH(26),CDELTA(26),CVELCF(26)
      #/MEASUR/RBETA(48,24),RPNMFS(48,24),RPCMPW(48,24),NDATA(48)
      #      ,MAXJPT,RDNPRS(48)
      #/GEOM/X(48),R(24),XND(48),RND(24),DYPS(24),DYNP(24),
      #      SNS(24),NSTATN,XINCHS(48),RINCHS(24)
      #/CALC/VTOTAL(48,24),U(48,24),V(48,24),W(48,24),
      #      VTSTAR(48,24),USTAR(48,24),VSTAR(48,24),WSTAR(48,24),
      #      PICHCF(48,24),VELCF(48,24),DELTA(48,24),BETA(48,24),
      #ANGMOM(48), UMEAN(48),MASS(48),MASFLO(48),UIN(48)
      REAL MASS,MASFLO
      LOGICAL IWRITE,DIAGNS
C ----- SET IWRITE=.TRUE. FOR WRITING SOLN. ON DISK STORAGE
C ----- SET DIAGNS=.TRUE. TO ACTIVATE DIANOSTIC WRITE STATEMENT
C ----- NSTATN IS NO. OF AXIAL STATIONS FOR WHICH DATA IS
C           SUPPLIED
C ----- MAXJPT IS MAX. NO. OF RADIAL POSITIONS FOR ALL AXIAL
C           STATIONS
C ----- CPITCH IS CALIBRATION PITCH COEFF.
C ----- CDELTA IS CALIBRATION PITCH ANGLE(DEG.)
C ----- CVELCF IS CALIBRATION VELOCITY COEFF.
C ----- NCAL IS NO. OF CALIBRATION POINTS
C ----- XINCHS IS AXIAL POSITION(IN.) OF EACH PARTICULAR RADIAL
C           TRAVERSE
C ----- NDATA IS NO. OF RADIAL LOCATIONS FOR WHICH DATA IS
C           SUPPLIED FOR EACH PARTICULAR RADIAL TRAVERSE
C ----- RDNPRS IS MEASURED DYNAMIC PRESSURE ENTERING THE
C           SWIRLER
C ----- RBETA IS MEASURED FLOW ANGLE(DEG.) WHERE YAW
C           ANGLE BETA = 360.0 - RBETA
C ----- RDNPRS IS MEASURED VOLTS FOR PNORTH - PSOUTH
C           DIFF. PRESSURE
C ----- RPCMPW IS MEASURED VOLTS FOR PCENTER - PWEST
C           DIFF. PRESSURE
C ----- PICHCF IS REDUCED VALUE FOR PITCH COEFF.
C ----- DELTA IS REDUCED VALUE FOR PITCH ANGLE(DEG.)
C ----- VELCF IS REDUCED VALUE FOR VELOCITY COEFF.
C ----- BETA IS REDUCED VALUE FOR PROBE YAW ANGLE(DEG.)
C ----- VTOTAL IS TOTAL VECTOR VELOCITY MAGNITUDE(M/SEC)
C ----- U IS AXIAL VELOCITY (M/SEC)
C ----- V IS RADIAL VELOCITY (M/SEC)
C ----- W IS SWIRL VELOCITY(M/SEC)
C ----- VTSTAR IS DIMENSIONLESS TOTAL VELOCITY
C ----- USTAR IS DIMENSIONLESS AXIAL VELOCITY
C ----- VSTAR IS DIMENSIONLESS RADIAL VELOCITY
C ----- WSTAR IS DIMENSIONLESS SWIRL VELOCITY
```

```

C ----- ALL PRIMARY USER INPUTS ARE LOCATED HERE
      IWRITE=.TRUE.
      DIAGNS=.FALSE.
      ALPHA=90.
      PHI=45.
      VISCOS=1.8E-5
      NSTATN=2
      MAXJPT=19
      FATM=75.1
      TATM=20.
      IT=48
      JT=24
      RLARGE=1.75/(2.0*39.37)
      RSMALL=R LARGE/2.0
      READ(5,205) HEDM,HEDUMN,HEDU,HEDV,HEDW,
      *   HEDVT,HEDUST,HEDVST,HEDWST,HEDVTS,HEDDEL,HEDBET,
      †HEDNMS,HEDCMW,HEDMMF,HEDMIV,HEDMIP,HEDMPP,HEDAM
      205 FORMAT(9A4)
C -----INITIALIZE VARIABLES TO ZERO
      CALL INIT
C -----READ FIVE-HOLE PITOT CALIBRATION DATA
      NCAL=25
      DO 10 I=1,NCAL
      READ(5,210) CPITCH(I),CDELTA(I),CVELCF(I)
      10 CONTINUE
      210 FORMAT(3F10.5)
      IF(DIAGNS) WRITE(6,400) (CPITCH(I),I=1,25)
      IF(DIAGNS) WRITE(6,400) (CDELTA(I),I=1,25)
      IF(DIAGNS) WRITE(6,400) (CVELCF(I),I=1,25)
      400 FORMAT(///,1X,13(F8.4,1X),//,5X,12(F8.4))
C -----READ RAW MEASURED DATA TO BE REDUCED
      DO 30 I=1,NSTATN
      READ(5,230) XINCHS(I),NDATA(I),RDNFRS(I)
      JPTS=NDATA(I)
      DO 20 J=1,JPTS
      READ(5,220) RINCHS(J),RBETA(I,J),RPNMPS(I,J),RPCMPW(I,J)
      20 CONTINUE
      30 CONTINUE
C -----CONVERT X AND R FROM INCHES TO METERS
      DO 35 I=1,NSTATN
      X(I)=XINCHS(I)*0.0254
      JPTS=NDATA(I)
      DO 32 J=1,JPTS
      R(J)=RINCHS(J)*0.0254
      32 CONTINUE
      35 CONTINUE
      220 FORMAT(4F10.5)
      230 FORMAT(1F10.5,1I10,1F10.5)
      IF(DIAGNS) WRITE(6,470) (NDATA(I),I=1,NSTATN)
      IF(DIAGNS) WRITE(6,450) (X(I),I=1,NSTATN)
      IF(DIAGNS) WRITE(6,500) (R(J),J=1,JPTS)
      DO 37 I=1,NSTATN
      IF(DIAGNS) WRITE(6,500) (RBETA(I,J),J=1,JPTS)
      IF(DIAGNS) WRITE(6,500) (RPNMPS(I,J),J=1,JPTS)
      IF(DIAGNS) WRITE(6,500) (RPCMPW(I,J),J=1,JPTS)
      37 CONTINUE
      450 FORMAT(///,40X,1(F8.4,1X))
      500 FORMAT(///,20X,10(F8.4))
C
CHAPTER 1 1 1 1 1 DATA REDUCTION 1 1 1 1 1
C
      470 FORMAT(///,40X,1(I8,1X))
C -----CALC PICHCF AND INTERPOLATE FOR DELTA FROM
C ----- PITOT CALIBRATION CURVE
      IDID=0
      DO 50 I=1,NSTATN
      JPTS=NDATA(I)
      DO 40 J=1,JPTS
      IF((RPCMPW(I,J).EQ.0.0).AND.(RPNMPS(I,J).EQ.0.0))
      *   GO TO 38

```

```

PICHCF(I,J)=RPNMPS(I,J)/(RPCMPW(I,J)+1.E-6)
IF((PICHCF(I,J).GT.3.399).OR.(PICHCF(I,J).LT.-3.759))
  GO TO 38
  IF(IDID.EQ.0) DELTA(I,J)=SPLINE(CPITCH,
  CDELTA,NCAL,PICHCF(I,J))
  IF(IDID.GT.0) DELTA(I,J)=SP(CPITCH,CDELTA,
  NCAL,PICHCF(I,J))
  IDID=1
  GO TO 40
38 CONTINUE
  DELTA(I,J)=0.0
  WRITE(6,850) I,J
850 FORMAT(20X,'PICHCF IS OUT OF RANGE OF CALIBRATION AT I=
  ',I3,' AND J=',I3)
  40 CONTINUE
  50 CONTINUE
C-----INTERPOLATE FOR VELCF FROM PITOT CALIBRATION DATA
  IDID=0
  DO 80 I=1,NSTATN
  JPTS=NDATA(I)
  DO 70 J=1,JPTS
  IF((RPCMPW(I,J).EQ.0.0).AND.(RPNMPS(I,J).EQ.0.0))
  GO TO 65
  IF((ABS(DELTA(I,J))).GT.58.0) GO TO 65
  IF(IDID.EQ.0) VELCF(I,J)=SPLINE(CDELTA,
  CVELCF,NCAL,DELTA(I,J))
  IF(IDID.GT.0) VELCF(I,J)=SP(CDELTA,CVELCF,
  NCAL,DELTA(I,J))
  IDID=1
  GO TO 70
65 CONTINUE
  VELCF(I,J)=0.0
  WRITE(6,870) I,J
870 FORMAT(20X,'DELTA IS OUT OF RANGE OF CALIBRATION DATA
  AT I=',I3,' AND J=',I3)
  70 CONTINUE
  80 CONTINUE
  DO 85 I=1,NSTATN
  IF(DIAGNS) WRITE(6,500) (PICHCF(I,J),J=1,JPTS)
  IF(DIAGNS) WRITE(6,500) (DELTA(I,J),J=1,JPTS)
  IF(DIAGNS) WRITE(6,500) (VELCF(I,J),J=1,JPTS)
  85 CONTINUE
C-----CALC MAGNITUDE OF TOTAL MEAN VELOCITY VECTOR AND
C-----U, V, & W COMPONENTS
  RHO=PATH*(136.0/0.102)/(287.0*(TATM+273.0))
  PI=3.14159
  DO 100 I=1,NSTATN
  JPTS=NDATA(I)
  DO 90 J=1,JPTS
  BETA(I,J)=360.-RBETA(I,J)
  IF((RPCMPW(I,J).EQ.0.0).AND.(RPNMPS(I,J).EQ.0.0))
  BETA(I,J)=0.0
  VTOTAL(I,J)=SQRT(ABS(2.0/RHO*VELCF(I,J)*RPCMPW(I,J)*133.9))
  U(I,J)=VTOTAL(I,J) * COS(DELTA(I,J)*PI/180.0) *
  COS(BETA(I,J)*PI/180.0)
  V(I,J)=VTOTAL(I,J) * SIN(DELTA(I,J)*PI/180.0)
  W(I,J)=VTOTAL(I,J) * COS(DELTA(I,J)*PI/180.0) *
  SIN(BETA(I,J)*PI/180.0)
  90 CONTINUE
  100 CONTINUE
  IF(DIAGNS) WRITE(6,500)(VTOTAL(I,J),J=1,JPTS)
  IF(DIAGNS) WRITE(6,500)(U(I,J),J=1,JPTS)
  IF(DIAGNS) WRITE(6,500)(V(I,J),J=1,JPTS)
  IF(DIAGNS) WRITE(6,500)(W(I,J),J=1,JPTS)
CHAPTER 2 2 2 2 2 2 AUXILIARY CALCULATIONS 2 2 2 2 2
C
  DO 130 I=1,NSTATN
C-----CALC GEOMETRIC QUANTITIES
  JPTS=NDATA(I)

```

```
JPTSM1=JPTS-1
DYPS(1)=0.0
DYNP(JPTS)=2.0*(RLARGE-R(JPTS))
DO 110 J=1,JPTSM1
DYNP(J)=R(J+1)-R(J)
DYPS(J+1)=DYNP(J)
110 CONTINUE
DO 115 J=1,JPTS
SNS(J)=0.5*(DYNP(J)+DYPS(J))
115 CONTINUE
IF(DIAGNS) WRITE(6,500) (DYNP(J),J=1,JPTS)
IF(DIAGNS) WRITE(6,500) (SNS(J),J=1,JPTS)
FLOW=0.0
WMOM=0.0
DO 120 J=1,JPTS
WMOM=WMOM+RHO*R(J)**2*SNS(J)*U(I,J)*W(I,J)
FLOW=FLOW+2.*PI*R(J)*SNS(J)*U(I,J)
IF(DIAGNS) WRITE(6,900) J,FLOW,WMOM,RHO
900 FORMAT(/,/,I5,4(F12.4,2X))
120 CONTINUE
ANGMOM(I)=WMOM
MASS(I)=RHO*FLOW
UMEAN(I)=MASS(I)/(RHO*PI*RLARGE**2)
130 CONTINUE
IF(DIAGNS) WRITE(6,450) (UMEAN(I),I=1,NSTATN)
IF(DIAGNS) WRITE(6,450) (MASS(I),I=1,NSTATN)
C-----NONDIMENSIONALIZE VELOCITIES
DO 150 I=1,NSTATN
XND(I)=X(I)/(2.0*RLARGE)
JPTS=NDATA(I)
UIN(I)=(SQRT(2.0/RHO*RINPRS(I)*249.08))*(6.312/5.94)**2
MASFLO(I)=2.0*PI*RHO*UIN(I)*RSMALL**2/2.0
DO 140 J=1,JPTS
VTSTAR(I,J)=VTOTAL(I,J)/UIN(I)
USTAR(I,J)=U(I,J)/UIN(I)
VSTAR(I,J)=V(I,J)/UIN(I)
WSTAR(I,J)=W(I,J)/UIN(I)
140 CONTINUE
150 CONTINUE
DO 160 J=1,MAXJPT
RND(J)=R(J)/(2.0*RLARGE)
160 CONTINUE
C
CHAPTER 3 3 3 3 3 OUTPUT 3 3 3 3 3 3
C
IF(.NOT. IWRITE) GO TO 165
WRITE(11) X
WRITE(11) R
WRITE(11) U
WRITE(11) V
WRITE(11) W
165 CONTINUE
WRITE(6,311)
WRITE(6,325) ALPHA
WRITE(6,330) PHI
WRITE(6,335) RSMALL
WRITE(6,340) RLARGE
WRITE(6,355) VISCOS
WRITE(6,360) RHO
C
CALL WRITE(1,1,NSTATN,1,IT,JT,X,R,MASFLO,HEDMMF)
CALL WRITE(1,1,NSTATN,1,IT,JT,X,R,MASS,HEDM)
CALL WRITE(1,1,NSTATN,1,IT,JT,X,R,UIN,HEDMIV)
CALL WRITE(1,1,NSTATN,1,IT,JT,X,R,UMEAN,HEDUMN)
CALL WRITE(1,1,NSTATN,1,IT,JT,X,R,ANGMOM,HEDAM)
CALL PRINT(1,1,NSTATN,MAXJPT,IT,JT,X,R,U,HEDU)
CALL PRINT(1,1,NSTATN,MAXJPT,IT,JT,X,R,V,HEDV)
CALL PRINT(1,1,NSTATN,MAXJPT,IT,JT,X,R,W,HEDW)
CALL PRINT(1,1,NSTATN,MAXJPT,IT,JT,X,R,DELTA,HEDDEL)
CALL PRINT(1,1,NSTATN,MAXJPT,IT,JT,X,R,BETA,HEDRET)
CALL PRINT(1,1,NSTATN,MAXJPT,IT,JT,X,R,VTOTAL,HEDVT)
```

ORIGINAL PAGE IS
OF POOR QUALITY

148

```

CALL PRINT(1,1,NSTATN,MAXJPT,IT,JT,XND,RND,USTAR,HEDUST)
CALL PRINT(1,1,NSTATN,MAXJPT,IT,JT,XND,RND,VSTAR,HEDVST)
CALL PRINT(1,1,NSTATN,MAXJPT,IT,JT,XND,RND,WSTAR,HEDWST)
CALL PRINT(1,1,NSTATN,MAXJPT,IT,JT,XND,RND,VTSTAR,HEDVTS)
CALL PRINT(1,1,NSTATN,MAXJPT,IT,JT,XINCHS,RINCHS,RPNMPS
# ,HEDNMS)
CALL PRINT(1,1,NSTATN,MAXJPT,IT,JT,XINCHS,RINCHS,RPCMPW
# ,HEDCMW)
CALL WRITE(1,1,NSTATN,1,IT,JT,XINCHS,RINCHS,RDNPRS,HEDMIP)
CALL PRINT(1,1,NSTATN,MAXJPT,IT,JT,XINCHS,RINCHS,PICHCF
# ,HEDMFP)
STOP
C-----FORMAT STATEMENTS
311 FORMAT(1H1,T37,'AXISYMMETRIC,ISOTHERMAL, GT COMBUSTOR
# FLOWFIELD MEASUREMENTS',//,T53,'USING A FIVE-HOLE
# PITOT PROBE')
325 FORMAT(////,T40,'EXPANSION ANGLE(DEG.) =' ,T77,1PE13.3)
330 FORMAT(//,T40,'SWIRL VANE ANGLE(DEG.) =' ,T77,1PE13.3)
335 FORMAT (//,T40,'INLET RADIUS(M) =' ,T77,1PE13.3)
340 FORMAT(//,T40,'COMBUSTOR RADIUS(M) =' ,T77,1PE13.3)
355 FORMAT(//,T40,'LAMINAR VISCOSITY(KG/M/SEC) =' ,T77,1PE13.3)
360 FORMAT(//,T40,'DENSITY(KG/CU. M) =' ,T77,1PE13.3,////)
END
C
SUBROUTINE INIT
C*****
C
COMMON
# /MEASUR/RBETA(48,24),RPNMPS(48,24),RPCMPW(48,24),NDATA(48)
# ,MAXJPT,RDNPRS(48)
# /GEOM/X(48),R(24),XND(48),RND(24),DYFS(24),DYNP(24),
# SNS(24),NSTATN,XINCHS(48),RINCHS(24)
# /CALC/VTOTAL(48,24),U(48,24),V(48,24),W(48,24),
# VTSTAR(48,24),USTAR(48,24),VSTAR(48,24),WSTAR(48,24),
# PICHCF(48,24),VELCF(48,24),DELTA(48,24),BETA(48,24),
# ANGMOM(48),UMEAN(48),MASS(48),MASFLO(48),UIN(48)
REAL MASS,MASFLO
C
DO 20 I=1,NSTATN
MASFLO(I)=0.0
MASS(I)=0.0
ANGMOM(I)=0.0
UMEAN(I)=0.0
UIN(I)=0.0
DO 10 J=1,MAXJPT
VTOTAL(I,J)=0.0
U(I,J)=0.0
V(I,J)=0.0
W(I,J)=0.0
VTSTAR(I,J)=0.0
USTAR(I,J)=0.0
VSTAR(I,J)=0.0
WSTAR(I,J)=0.0
RBETA(I,J)=0.0
BETA(I,J)=0.0
RPNMPS(I,J)=0.0
RPCMPW(I,J)=0.0
PICHCF(I,J)=0.0
VELCF(I,J)=0.0
DELTA(I,J)=0.0
10 CONTINUE
20 CONTINUE
RETURN
END
C
FUNCTION SPLINE(X,FX,N,X1)
C*****
C CUBIC SPLINE CURVE FITTING IN 2 DIMENSIONAL DATA PLANE
C INPUT VALUES :
C X,FX DATA ARRAYS, ONE DIMENSIONAL, X IN INCREASING ORDER

```

```

C      N          NUMBER OF DATA POINTS IN X, MAX 26
C      X1         POINT OF INTEREST, WHERE F(X1) IS TO BE FOUND
C
C      RETURN VALUE :
C      SPLINE OR SP = F(X1)
C      THIS ROUTINE ACTIVATES ROUTINE ABUILD, H, AND GAUSS.
C      FOR INTERPOLATION OF A LARGE NUMBER OF DATA POINTS, FUNCTION
C      SPLINE MAY BE CALLED ONLY ONCE , AND SUBSEQUENT CALLS MAY US
C
C      ENTRY POINT SP.
C*****
C      DIMENSION X(1), FX(1), A(26,27)
C-----CONSTRUCT SPLINE MATRIX
      NF1=N+1
      DO 10 I=1, N
      DO 10 J=1, NF1
10     A(I,J)=0.
      NM1=N-1
      DO 20 I=2, NM1
20     CALL ABUILD(X, FX, A, N, I)
      A(1,1)=H(X,2)
      A(1,2)=-H(X,1)-H(X,2)
      A(1,3)=H(X,1)
      NM2=N-2
      A(N,NM2)=H(X,NM1)
      A(N,NM1)=-H(X,NM2)-H(X,NM1)
      A(N,N)=H(X,NM2)
C-----FIND SECOND DERIVATIVES
      CALL GAUSS(A, N, NF1)
      ENTRY SP(X, FX, N, X1)
C-----FIND F(X1)
      DO 40 I=1, NM1
      IP1=I+1
      IF(X1 .EQ. X(I)) GO TO 50
      IF(X1 .LT. X(I) .AND. X1 .GT. X(IP1)) GO TO 41
      IF(X1 .GT. X(I) .AND. X1 .LT. X(IP1) ) GO TO 41
40     CONTINUE
      IF(X1 .EQ. X(N)) GO TO 60
      WRITE(6, 42) X1
42     FORMAT(' X1=', G14.7, ' OUT OF INTERPOLATION RANGE,
      # RETURNED VALUE=0')
      SF=0.
      SPLINE= 0.
      STOP
41     CONTINUE
      IP1=I+1
      HI=H(X,I)
      HX=X1-X(I)
      AI = (A(IP1,NF1)-A(I,NF1))/(6.*HI)
      BI = A(I,NF1)/2.
      CI = (FX(IP1)-FX(I))/HI-(2.*HI*A(I,NF1)+HI*A(IP1,NF1))/6.
      DI = FX(I)
      SPLINE=AI*HX**3+BI*HX**2+CI*HX+DI
      SP=SPLINE
      RETURN
C
C      50     CONTINUE
      SPLINE=FX(I)
      SP=SPLINE
      RETURN
C
C      60     CONTINUE
      SPLINE=FX(N)
      SP=SPLINE
      RETURN
      END
C
C      FUNCTION H(X,I)
C*****
C      CALCULATE DELTA X WHICH IS USUALLY CALLED AS H.
C*****

```

```

DIMENSION X(1)
IP1=I+1
H=X(IP1)-X(I)
RETURN
END

C
SUBROUTINE ABUILD(X, F, A, N, I)
C*****
C CONSTRUCT SPLINE MATRIX FOR FINDING 2ND DERIVATIVES.
C*****
DIMENSION X(1), F(1), A(26,27)
IM1=I-1
IP1=I+1
NP1=N+1
HI=H(X,I)
HIM1=H(X,IM1)
A(I,IM1)=HIM1
A(I,I)=2.*(HIM1+HI)
A(I,IP1)=HI
A(I,NP1)=( (F(IP1)-F(I))/HI - (F(I)-F(IM1))/HIM1 ) *6.
RETURN
END

C
SUBROUTINE GAUSS(A, N, NP1)
C*****
C GAUSS-JORDAN ELIMINATION
C*****
DIMENSION A(26,27)
NM1 = N-1
DO 3 L=1, NM1
LP1=L+1
DO 3 I=LP1,N
CONST=A(I,L)/A(L,L)
DO 3 J=L, NP1
3 A(I,J)=A(I,J)-CONST*A(L,J)
DO 6 I=1, NM1
IP1=I+1
DO 6 L=IP1,N
CONST=A(I,L)/A(L,L)
DO 6 J=I, NP1
6 A(I,J)=A(I,J)-CONST*A(L,J)
DO 10 I=1, N
A(I,NP1)=A(I,NP1)/A(I,I)
10 A(I,I)=1.
RETURN
END

C
SUBROUTINE PRINT(ISTART,JSTART,NI,NJ,IT,JT,X,Y,PHI,HEAD)
CA*****
C
DIMENSION PHI(IT,JT),X(IT),Y(JT),HEAD(9),STORE(48)
ISKIP=1
JSKIP=1
WRITE(6,110)HEAD
ISTA=ISTART-12
100 CONTINUE
ISTA=ISTA+12
IEND=ISTA+11
IF(NI.LT.IEND)IEND=NI
WRITE(6,111)(I,I=ISTA,IEND,ISKIP)
WRITE(6,114)(X(I),I=ISTA,IEND,ISKIP)
WRITE(6,112)
DO 101 JJ=JSTART,NJ,JSKIP
J=JSTART+NJ-JJ
DO 120 I=ISTA,IEND
A=PHI(I,J)
IF(ABS(A).LT.1.E-20) A=0.0
120 STORE(I)=A
101 WRITE(6,113)J,Y(J),(STORE(I),I=ISTA,IEND,ISKIP)
IF(IEND.LT.NI)GO TO 100
RETURN

```



```

110 FORMAT(1H0,17(2H*-),7X,9A4,7X,17(2H-*))
111 FORMAT(1H0,13H      I =      ,I2,11I9)
112 FORMAT(8H0 J      Y)
113 FORMAT(I3,OPF8.5,1X,1F12E9.2)
114 FORMAT(11H      X = ,F8.5,11F9.5)
      END

C
      SUBROUTINE WRITE(ISTART,JSTART,NI,NJ,IT,JT,X,Y,PHI,HEAD)
C *****
C
      DIMENSION PHI(IT),X(IT),Y(JT),HEAD(9),STORE(48)
      ISKIP=1
      JSKIP=1
      WRITE(6,110)HEAD
      ISTA=ISTART-12
100 CONTINUE
      ISTA=ISTA+12
      IEND=ISTA+11
      IF(NI.LT.IEND)IEND=NI
      WRITE(6,111)(I,I=ISTA,IEND,ISKIP)
      WRITE(6,114)(X(I),I=ISTA,IEND,ISKIP)
      DO 101 JJ=JSTART,NJ,JSKIP
      J=JSTART+NJ-JJ
      DO 120 I=ISTA,IEND
      A=PHI(I)
      IF(ABS(A).LT.1.E-20) A=0.0
120 STORE(I)=A
      101 WRITE(6,113) (STORE(I),I=ISTA,IEND,ISKIP)
      IF(IEND.LT.NI)GO TO 100
      RETURN
110 FORMAT(1H0,17(2H*-),7X,9A4,7X,17(2H-*))
111 FORMAT(1H0,13H      I =      ,I2,11I9)
113 FORMAT(12X,1F12E9.2)
114 FORMAT(11H      X = ,F8.5,11F9.5)
C
      END

```

VITA

Hyung Kee Yoon

Candidate for Degree of

Master of Science

Thesis: FIVE-HOLE PITOT PROBE TIME-MEAN VELOCITY MEASUREMENTS IN
CONFINED SWIRLING FLOWS

Biographical:

Personal Data: [REDACTED], the son
of Mr. and Mrs. In S. Yoon.

Education: Graduated from Sung Nam High School, Seoul, Korea, in
March, 1973; received Bachelor of Engineering degree in
Mechanical Engineering from Korea University, March, 1980;
completed requirements for the Master of Science degree at
Oklahoma State University in July, 1982.

Professional Experience: Research assistant, School of Mechanical
and Aerospace Engineering, Oklahoma State University,
Stillwater, Oklahoma, 1981-present.

Honor Society: Phi Kappa Phi

Professional Society: AIAA

APPENDIX B

ANNULAR VANE SWIRLER PERFORMANCE

ANNULAR VANE SWIRLER PERFORMANCE

Glenn F. Sander

School of Mechanical and Aerospace Engineering

Oklahoma State University

SUMMARY

The present study clarifies swirler performance characteristics as an aid to understanding and computer modeling of gas turbine combustor flowfields. The swirler under study is annular with 10 adjustable vanes and a hub to swirler diameter ratio of 0.25. Measurements of time-mean axial, radial, and tangential velocities at the swirler exit plane for a range of blade swirl angles ϕ from 0 to 70 degrees show clearly the effects of centrifugal forces, recirculation zones, and blade stall on the combustor inlet velocity profiles.

INTRODUCTION

The problem of optimizing gas turbine combustion chamber design is complex, due to the many conflicting design requirements. In an effort to reduce development time and cost, computer simulation techniques are being used to study the effect of geometry changes on the flowfield inside combustor designs.^{1,2} Accuracy of predictions from a computer model is strongly dependent on the inlet boundary conditions used, which are primarily determined by the swirler and its performance at different vane angle settings. In previous studies,¹ the velocity boundary conditions at the inlet to the model combustor were approximated by idealized flat profiles for axial and swirl

velocity, with radial velocity assumed to be zero. However, measurements taken close to swirler outlets show that the profiles produced are quite nonuniform as found elsewhere³ and at Oklahoma State University.⁴

In the present study, the objective was to make velocity measurements as close as possible to the swirler exit, so as to define better the performance characteristics of the swirler. A range of swirl-blade angles ϕ from 0 (no swirler present) to 70 degrees is being considered, with 0, 45 and 70 degrees being highlighted. Previous velocity measurements at the inlet to the test section on the same test facility⁴ were obtained with expansion blocks attached to the exit of the swirl pack, thus being 3.2 cm downstream of the swirler exit plane. In the present study, these blocks were removed so as to allow measurements directly at the swirler exit plane and give a better indication of the actual performance of the swirler.

EQUIPMENT AND PROCEDURE

The swirler is annular with a hub one-fourth the inside diameter of the swirler housing, with hub and housing diameters of 3.75 and 15.0 cm, respectively. The 10 vanes (or blades) are attached to shafts which pass through the housing wall and allow individual adjustment of each blade's angle. The blades are wedge-shaped to give a constant pitch-to-chord ratio of approximately one, which should give good turning efficiency.⁵

The time-mean velocity components are measured with a five-hole pitot probe, which allows determination of the magnitude and direction of the mean velocity vector simultaneously. The probe is mounted in a traversing mechanism which allows it to be translated vertically and rotated about the yaw axis. Tubing from the probe's five pressure taps is routed through selector valves to a differential pressure transducer, and the resulting pressure difference values are read directly from an integrating digital voltmeter. The pressure data are reduced by a computer program to yield

nondimensionalized u , v , and w velocity components, which are then plotted in the form of profiles. Details appear in Ref. 4.

RESULTS

Velocity profiles for a number of flowfields have been compiled for both radial and aximuthal traverses, and some sample results are presented below:

1. Radial Profiles

Figure 1 shows radial profiles of axial and swirl velocity running from the swirler centerline to twice the swirler exit radius [$r/D = 0.5$ where D is the test section diameter used in associated studies] for three values of blade angle ϕ : zero (no swirler), 45, and 70 degrees. The nonswirling case has a nearly-flat axial velocity profile, as expected. All velocities shown are normalized with respect to the mean exit axial velocity, measured independently. However, for the 45 degree case, both profiles vary from zero at the hub to a maximum at or near the rim of the swirler in an almost linear fashion. This is due to centrifugal forces on the rotating air, resulting in much of the flow leaving near the outer boundary. Note the low velocities for $r/D < 0.1$ approximately; they are probably an effect of the central recirculation zone extending upstream enough to obstruct the inlet flow.

The 70 degree profile shows strong reverse flow in the range in the central region showing that the central recirculation zone now extends upstream past the exit plane. The maximum velocity at the outer edge is approximately three times the inlet velocity and the velocity gradients across the profile are quite large. The positive axial velocity adjacent to the hub is probably the result of the slight clearance between the blades and the hub, allowing a thin layer of nonswirling air to pass directly through the swirler.

2. Azimuthal Profiles

Figure 2 shows the azimuthal or θ -variation of axial, radial and swirl velocities for the case of $\phi = 45$ degrees. Similar results occur at other swirl angles. The profiles span an angle of 48 degrees, more than the 36 degrees between successive blades. The measurements were taken at a constant radial distance of $r/D = 0.20$.

The profiles all show significant variation with azimuthal position, which can be attributed to several causes. Among them are blade stall from using flat blades at a high angle of attack, not enough blade overlap (pitch/chord ratio too high), and wakes from blunt trailing edges. The radial component is seen to be of the same order of magnitude as the axial and swirl components, and also shows the greatest variation.

CONCLUSIONS

Assumptions of flat axial and swirl profiles with radial velocity equal to zero are progressively less realistic as the swirler blade angle ϕ increases. At moderate swirl $\phi = 45$ degrees, linearly increasing profiles of u and w with radius are appropriate with v nonzero. At strong swirl $\phi = 70$ degrees, even more spiked profiles are appropriate with most of the flow leaving the swirler near its outer edge. Nonaxisymmetry prevails in all swirl cases investigated.

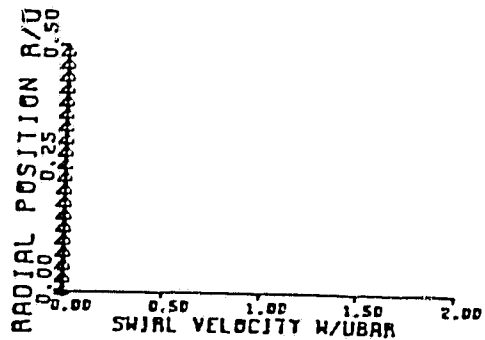
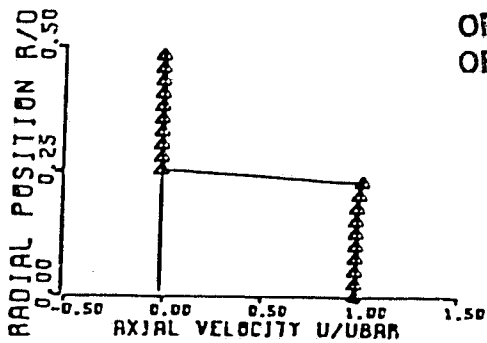
ACKNOWLEDGMENT

The author wishes to express his gratitude to NASA and AFWAL for support under Grant No. NAG 3-74 and to Dr. D. G. Lilley for his advice and encouragement.

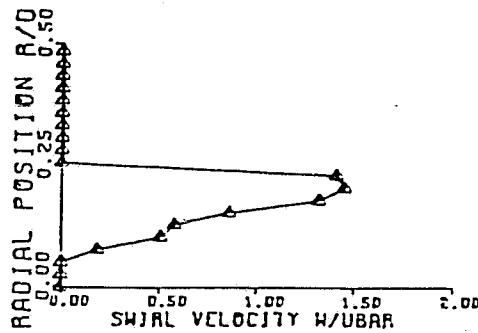
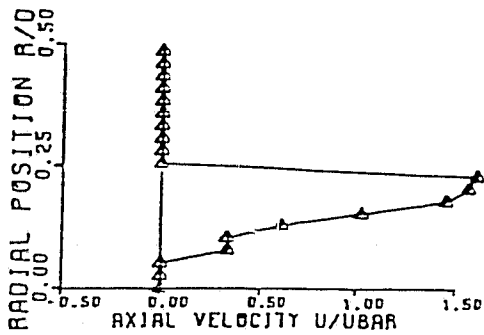
REFERENCES

1. Rhode, D. L., Lilley, D. G., and McLaughlin, D. K., "On the Prediction of Swirling Flowfields Found in Axisymmetric Combustor Geometries," ASME Symposium on Fluid Mechanics of Combustion Systems, Boulder, CO, June 22-24, 1981, pp. 257-266. Journal of Fluids Engineering, 1982 (in press).
2. Serag-Eldin, M. A., and Spalding, D. G., "Computations of Three-Dimensional Gas-Turbine Combustion Chamber Flows," Transactions ASME, Journal of Engineering for Power, Vol. 101, 1979, pp. 326-336.
3. Mathur, M. L., and MacCallum, N. R. L., "Swirling Air Jets Issuing from Vane Swirlers. Part 1: Free Jets," Journal of the Institute of Fuel, Vol 40, May 1967, pp. 214-225.
4. Rhode, D. L., Lilley, D. G., and McLaughlin, D. K., "Mean Flowfields in Axisymmetric Combustor Geometries with Swirl," AIAA Paper No. 82-0177, Orlando, FL, Jan. 11-14, 1982.
5. Gupta, A. K., Lilley, D. G., and Syred, N. "Swirl Flows." Abacus Press, Tunbridge Wells, England, 1982 (in press).

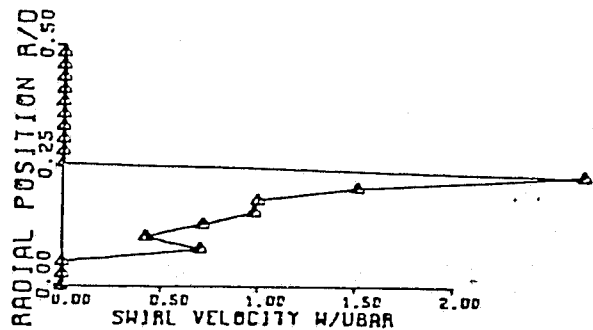
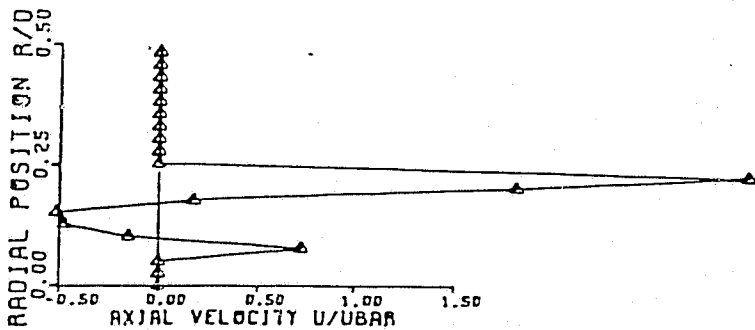
ORIGINAL PAGE IS
OF POOR QUALITY



(a) $\phi = 0^\circ$ (No Swirler)



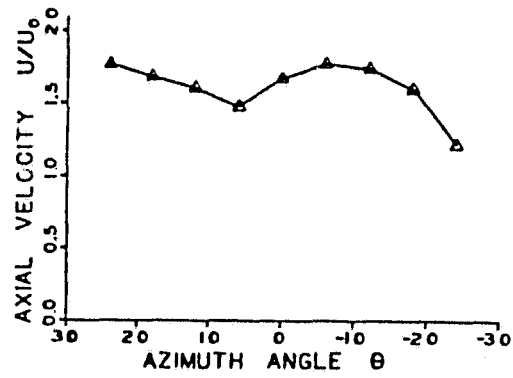
(b) $\phi = 45^\circ$



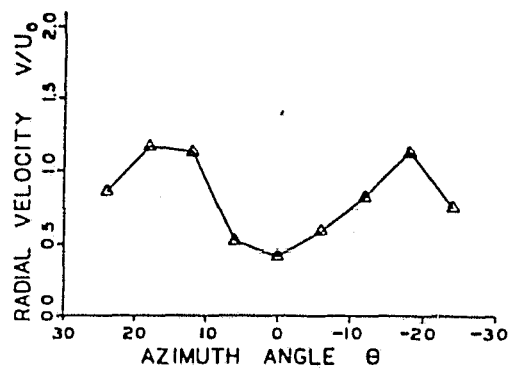
(c) $\phi = 70^\circ$

Fig. 1 Radial Profiles of Axial and Swirl Velocity at Swirler Exit Plane for Swirl Cases: (a) $\phi = 0^\circ$, (b) $\phi = 45^\circ$, and (c) $\phi = 70^\circ$.

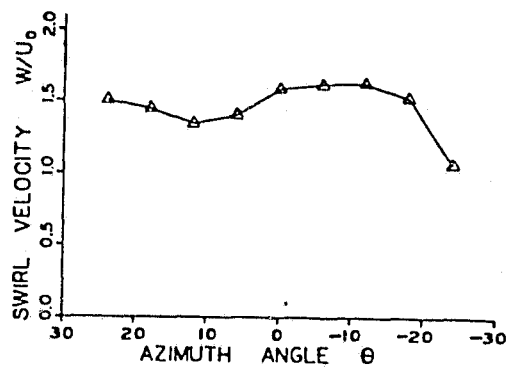
ORIGINAL PAGE IS
OF POOR QUALITY.



(a) Axial Velocity



(b) Radial Velocity



(c) Swirl Velocity

Fig. 2 Azimuthal Profiles of (a) Axial Velocity, (b) Radial Velocity, and (c) Swirl Velocity at Swirler Exit Plane for Swirl Case $\phi = 45^\circ$.

APPENDIX C

CONFINED SWIRLING FLOW PREDICTIONS:

EFFECT OF SWIRL AND INLET PROFILE ASSUMPTIONS

CONFINED SWIRLING FLOW PREDICTIONS:
EFFECT OF SWIRL AND INLET PROFILE ASSUMPTIONS

M. T. Abujelala and D. G. Lilley

School of Mechanical and Aerospace Engineering
Oklahoma State University
Stillwater, OK 74078

TABLE OF CONTENTS

<u>CONTENTS</u>	<u>Page</u>
SUMMARY	ii
1. INTRODUCTION	1
2. TYPES OF INLET BOUNDARY CONDITIONS CONSIDERED	2
3. RESULTS AND DISCUSSION	4
3.1 Effect of Inlet Velocity Profiles	4
3.2 Effect of Swirl Vane Angles on Flowfield Patterns	6
3.3 Convergence Rates	7
3.4 Effect of Inlet Turbulence Energy	8
4. CONCLUSIONS	10
5. REFERENCES	11
6. FIGURE LIST	13
FIGURES	
7. TABLE LIST	38
TABLES	

SUMMARY

The present contribution provides numerical predictions of turbulent swirling recirculating confined flows using various inlet velocity starting conditions for the case of swirl vane angle equal to 45 degrees. The validity of flowfield predictions resulting from the choice of inlet profiles is assessed by comparing the predicted velocity profiles with corresponding experimental velocity profiles. Results demonstrate that realistic predictions are forthcoming only from the inclusion of realistic axial, radial and swirl velocity profiles as inlet conditions, and that considerable errors occur if unrealistic idealized inlet conditions are used. Predictions are then exhibited for a range of swirl strengths [$\phi = 0, 38, 60$ and 70 degrees] using measured inlet axial, radial and swirl velocity profiles in each case. The ensuing flowfields are characterized via velocity profiles and streamline patterns, and illustrate the large-scale effects of inlet swirl on flowfields.

1. INTRODUCTION

The governing differential equations of swirling recirculating flows are elliptic, and solutions depend strongly on the boundary conditions applied around the flow domain. It is important to define adequately the boundary conditions, especially the inlet velocity profiles. Predictions given in Ref. 1 have been obtained by using flat inlet axial and swirl velocity profiles in which the swirl velocity magnitude is deduced from the swirl vane angle ϕ . In Refs. 2 and 3 the initial values of the components of mean axial and swirl velocity were taken from experimental data, while the radial component of mean velocity was assumed negligible. On the other hand, Ref. 4 assumes the swirl velocity profile to be that of solid body rotation.

The present contribution provides numerical predictions of the velocity field for a swirling confined jet flow through a vane swirler, expanding into a larger chamber with diameter ratio $D/d = 2$. A swirl vane angle of 45 degrees is selected to evaluate, via comparison with time-mean flow measurements, the predictions using various types of inlet axial, radial and swirl velocity profiles. This illustrates their effect on the flowfield, and dramatizes the need to use realistic inlet boundary conditions in predictive studies and turbulence modeling improvements. Also, predictions of the velocity field for a complete range of swirl vane angles (0, 38, 60 and 70 degrees) using the best measured inlet velocity profiles are exhibited. They illustrate the large-scale effects of inlet swirl on flowfields.

2. TYPES OF INLET BOUNDARY CONDITIONS CONSIDERED

In all cases considered, the kinetic energy of turbulence k and its dissipation rate are specified as in general accepted ways.⁵ The total time-mean velocity magnitude has been used in specifying k . Four possible specifications of the inlet velocities are considered:

1. Flat inlet axial and swirl velocities with radial velocity zero are assumed. That is, both u and w are constant valued:

$$u_0 = \text{constant}$$

$$w_0 = u_0 \tan \phi$$

where ϕ is the best estimate of the constant flow turn angle, slightly less than the swirl vane angle. [When $\phi_{\text{blades}} = 45$ deg. it has been found experimentally that $\phi_{\text{flow}} = 42$ deg.].

2. As Case 1, except that the inlet swirl velocity profile is assumed to be that of solid body rotation:

$$u_0 = \text{constant}$$

$$w_0 = w_{m,0} \cdot r/R$$

where $w_{m,0}$ is the maximum orifice value of w which occurs at the outer edge $r = R$ of the inlet. The value of $w_{m,0}$ is so chosen as to maintain the swirl number S the above as Case 1 for similarity purposes as is now described. Defining

$$G = w_{m,0}/u_0$$

it can be shown⁵ that S and G are related via

$$S = (G/2)/[1 - (G/2)^2].$$

For a given flat profile flow angle $\phi = \phi_{\text{flow}}$, it can also be shown^{6,7} that approximately:

$$S = 2/3 \tan \phi.$$

Thus the equivalent swirl number jet with different inlet profile types can be deduced.

3. Measured inlet axial and swirl velocities are used⁸ with radial velocity assumed to be zero.
4. Measured inlet axial, radial and swirl velocity values are used, taking data from recent five-hole pitot-probe data in close vicinity of the swirler exit.⁸ The measured data are linearly interpolated to fit into the computer code as shown in Table 1.

3. RESULTS AND DISCUSSION

Predicted results are obtained via the STARPIC computer program,⁹ developed at Oklahoma State University as an advanced version of the Imperial College, London, TEACH computer code.¹⁰ The present version includes the calculation of swirl velocity, and incorporates its effect on wall functions. Currently the standard k- ϵ turbulence model is employed, with minor changes as in Ref. 1. Sudden and gradual expansions can be accommodated easily. It has already been used¹ for tentative predictions using the profiles of Case 1 described in Section 2.

Predictions are first discussed which deal with the flow through inlet swirl guide vanes of angle $\phi = 45$ degrees, which impart a flow angle of approximately $\phi = 42$ degrees to the flow, although this varies a little with radial location. Various types of inlet profile assumptions are considered and their similarities and differences are noted. Predictions are then presented for flowfields with four other swirl strengths using measured inlet flow velocity profiles for axial, radial and swirl velocity in each case. To aid convergence, the solution for each value of ϕ [0, 38, 45, 60 and 70 deg.] is used for the initial starting values for the next higher value of ϕ . [This includes the predictions for the specific case of $\phi = 45$ deg. discussed at length in Section 3.1]. The convergence criteria in each case are all normalized residual source sums to be less than 0.004 or a maximum of 200 iterations, with results in Table 2 and Figs. 1 through 19 being so generated.

3.1 Effect of Inlet Velocity Profiles

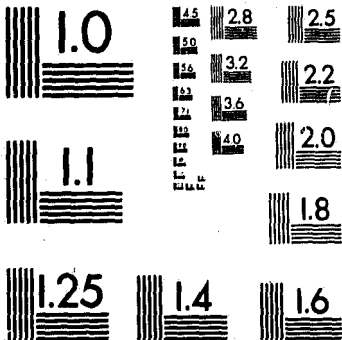
Figure 1 shows the predicted velocity profiles at various downstream axial stations using flat inlet profiles for axial and swirl velocities with inlet radial velocity equal to zero. This is Case 1 of Section 2. For purpose of comparison with the experimental data, the averaged flow angle

value is used instead of $\phi = 45$ degrees. The cited value in Ref. 8 is 42 degrees. A central recirculation zone is seen to be more than one chamber diameter in length, and approximately one half of the chamber diameter in diameter, encouraged by centrifugal force. No corner recirculation zone is observed beyond $x/D = 0.5$.

Figure 2 displays the predicted velocity profiles using flat inlet axial velocity profile with the inlet radial velocity is equal to zero. The inlet swirl velocity profile is assumed to be that of solid body rotation for flow angle of 42 deg. This is Case 2 of Section 2. A flow recirculation is observed at the corner of the combustor through $x/D = 0.5$ with a very small recirculation region at the center.

Flowfield prediction using measured inlet axial and swirl velocity profiles⁷ with the assumption that inlet radial velocity is equal to zero are displayed in Fig. 3. Two recirculation zones are predicted, one on the corner and the other being a larger zone located on the axis. The central zone extends downstream up to approximately 1.5 combustor diameters, with maximum core diameter of 0.4 times the chamber diameter. Notice that this is somewhat longer and narrower, with higher reverse velocities, than found in the previous case. The corner zone extends to less than one diameter in length.

Predictions made by using the most realistic measured inlet axial, radial and swirl velocity profiles taken from Ref. 8 are shown in Fig. 4. The corner recirculation zone terminates before $x/D = 0.5$ and a wider central recirculation zone than previously calculated is observed. The flowfield structure is illustrated via streamline plots, which are computer calculated and drawn, as shown in Fig. 5. A three-dimensional representation of the predicted axial velocity is given in Fig. 6, so as to aid in visualizing flow zones.



MICROCOPY RESOLUTION TEST CHART
 NATIONAL BUREAU OF STANDARDS
 STANDARD REFERENCE MATERIAL 1010a
 (ANSI and ISO TEST CHART No. 2)

Figure 7 displays the measured axial and swirl velocity profiles using a five-hole pitot probe for the corresponding inlet flow swirl case.¹¹ A larger central recirculation zone which extends downstream more than two chamber diameters is observed. The flow fills the larger chamber rapidly because of centrifugal effects, and no corner recirculation zone is seen in the velocity profiles shown, although flow visualization studies reveal a corner zone of length approximately 0.4 chamber diameters. From comparison of the predicted velocity profiles with the measured velocity profiles, it can be seen that flowfield predictions following the most realistic inlet velocity specifications give best agreement with the data, see Figs. 4 and 7.

3.2 Effect of Swirl Vane Angle on Flowfield Patterns

The velocity field predictions for swirl vane angles of 0, 38, 60 and 70 degrees using the obtained more realistic inlet velocity profile are displayed in Figs. 8, 9, 10, and 11. The streamline patterns are computed and plotted as shown in Figs. 12, 13, 14, and 15 and the flowfield construction is shown in Figs. 16, 17, 18, and 19. The following results can be drawn from these figures:

1. The higher the swirl strength, the higher the centrifugal force, hence the larger the central recirculation zone core diameter;
2. The stronger the swirl strength, the longer the central zone extends downstream;
3. The corner recirculation zone size reduces sharply as swirl strength increases

Recirculation zone lengths are dramatically affected as the degree of swirl increases. Discrepancies seen on comparing predictions with corresponding flowfield data obtained with a five-hole pitot probe¹¹ indicate typically longer corner and center zones predicted than measured. This may be

because of poor probe sensitivity in turbulent low velocity regions, and/or poor turbulence model performance in these regions. Only further detailed hot-wire and/or laser doppler anemometer measurements and turbulence model development will resolve the inconsistencies. Despite this, the results are in general agreement with the discussion of Ref. 7.

3.3 Convergence Rates

Table 2(a) displays the residual source sums (RSS) after 200 iterations between successive values of ϕ . It can be seen that as the swirl vane angle increases, the RSS increases. This is expected because of the complexity of the flow at the higher swirl strengths. In Part (b) of the table, the effect of inlet velocity profile assumption on the degree of convergence for the $\phi = 45$ deg. case is illustrated via the RSS values. It can be seen that as the degree of nonuniformity in inlet profiles increases, the degree of convergence reduces, with higher RSS values after a given number of iterations. This is generally to be expected.

Table 3 displays the progress toward convergence with more stringent final convergence criteria [all normalized residual source sums to be less than 0.004 or a maximum of 500 iterations]. Part (a) shows normalized residual source sums for u , v , w and mass; Part (b) shows nondimensionalized velocities u/u_0 , v/u_0 and w/u_0 at a monitored field location $(I,J) = (8,8)$. Both parts of the table contain the sequence of five degrees of swirl. It is found that the convergence rate for $\phi = 0$ deg. case is good enough at 200 iterations. The degree of convergence in all the cases can be clearly seen. However, Figs. 20 and 21 give u and w profile plots for the cases $\phi = 45$ and 70 degrees, respectively, after complete convergence, requiring 315 and 500 iterations, respectively. Comparison of these figures with Figs. 4 and 11, which were obtained after 200 iterations between successive swirl cases,

reveals that general field results were good enough after 200 iterations, although the fine detail and turbulence data may clearly require quite stringent convergence criteria.

Figures 22 and 23 display the prediction of the flowfield streamlines pattern for the cases $\phi = 45$ and 70 deg., respectively, obtained after complete convergence, requiring 315 and 500 iterations, respectively. Again, they are comparable with Figs. 5 and 15 which were obtained with a lower number of iterations between successive swirl cases investigated.

3.4 Effect of Inlet Turbulence Energy

Table 4 displays the predicted axial and swirl velocities and turbulence parameters for swirl vane angle $\phi = 45$ deg. at the axial location $x/D = 0.5$. Only the weak degree of convergence was used for those results requiring 200 iterations in each case. Three types of specification of inlet kinetic energy of turbulence k were considered:

1. Inlet k is assumed to be a constant obtained from the average exit axial velocity:

$$k = 0.03 a_{v,0}^2$$

2. Inlet k is allowed to vary with radius and is a function of local inlet time-mean axial velocity at each radial location

$$k = 0.03 u_0^2$$

3. Inlet k is allowed to vary with radius and is a function of local inlet total time-mean velocity at each radial location

$$k = 0.03 (u_0^2 + v_0^2 + w_0^2)$$

The factor 0.03 in these equations is the recommended constant given inlet relative turbulence intensity of 0.245. Specimen predictions using these three inlet k assumptions with realistic inlet velocity values are given in Table 4, Parts a, b, and c, respectively. They illustrate that there is

little change in velocity predictions with changes in the inlet k specification.

4. CONCLUSIONS

A numerical prediction using the standard two-equation $k-\epsilon$ turbulence model and different inlet flow boundary condition assumption has been applied to a confined swirling flow. Inlet flow boundary conditions have been demonstrated to be extremely important in simulating a flowfield via numerical calculations. Predictions with either flat inlet profiles, solid body rotation or zero radial velocity are inappropriate. Predictions are given for a full range of swirl strengths using measured inlet axial, radial and swirl velocity profiles in each case, and predicted velocity profiles and streamline plots illustrate the large-scale effects of inlet swirl on flowfields.

REFERENCES

1. Rhode, D. L., Prediction and Measurements of Isothermal Flowfields in Axisymmetric Combustor Geometries, Ph.D. Thesis, Oklahoma State University, 1981.
2. Sturgess, G. J., and Syed, S. A., Widely-Spread Coaxial Jet, Diffusion Flame Combustor: Isothermal Flow Calculation Using the Two-Equation Turbulence Model, Paper No. AIAA 82-0113, Orlando, Florida, January 11-14, 1982.
3. Habib, M. A., and Whitelaw, J. H., Velocity Characteristics of Confined Coaxial Jets With and Without Swirl, Journal of Fluids Engineering, Vol. 102, March 1980, pp. 47-53.
4. Kubo, I., and Gouldin, F. C., Numerical Calculations of Turbulent Swirling Flow, Journal of Fluids Engineering, Vol. 47, Sept. 1975, pp. 310-315.
5. Chigier, N. A., and Chervinsky, A., Experimental Investigation of Swirling Vortex Motion in Jets, Transactions of the ASME, Journal of Applied Mechanics, Vol. 89, June 1967, pp. 443-451.
6. Beer, J. M., and Chigier, N. A., Combustion Aerodynamics, Applied Science, London and Halstead-Wiley, New York, 1972.
7. Lilley, D. G., Swirl Flows in Combustion: A Review, AIAA Journal, Vol. 15, No. 8, Aug. 1977, pp. 1067-1078.
8. Sander, G. F., Work in Progress, Oklahoma State University, Stillwater, Oklahoma, 1982.
9. Lilley, D. G., and Rhode, D. L., A Computer Code for Swirling Turbulent Axisymmetric Recirculating Flows in Practical Isothermal Combustor Geometries, NASA CR-3442, Feb. 1982.
10. Gosman, A. D., and Pun, W. M., Calculation of Recirculating Flows, Report No. HTS/74/12, Dept. of Mech. Eng., Imperial College, London, 1974.

11. Yoon, H. K., Five-Hole Pitot Probe Time-Mean Velocity Measurements in Confined Swirling Flows, M.S. Thesis, Oklahoma State University, Stillwater, Oklahoma, July 1982.

FIGURE LIST

- Fig. 1 Predicted velocity profiles for swirl vane angle $\phi = 45^\circ$ using flat inlet profiles with $v = 0$.
- Fig. 2 Predicted velocity profiles for swirl vane angle $\phi = 45^\circ$ using flat inlet u profile with solid body rotation w profile with $v = 0$.
- Fig. 3 Predicted velocity profiles for swirl vane angle $\phi = 45^\circ$ using measured inlet u and w profiles with $v = 0$.
- Fig. 4 Predicted velocity profiles for swirl vane angle $\phi = 45^\circ$ using measured inlet u , v and w profiles.
- Fig. 5 Predicted streamlines for swirl vane angle $\phi = 45^\circ$ using measured inlet, u , v and w profiles.
- Fig. 6 Axial velocity representation for swirl vane angle $\phi = 45^\circ$.
- Fig. 7 Measured velocity profiles for swirl vane angle $\phi = 45^\circ$ using five-hole pitot probe. (Ref. 11)
- Fig. 8 Predicted velocity profiles for nonswirling flow using measured inlet u and v profiles.
- Fig. 9 Predicted velocity profiles for swirl vane angle $\phi = 38^\circ$ using measured inlet u , v and w profiles.
- Fig. 10 Predicted velocity profiles for swirl vane angle $\phi = 60^\circ$ using measured inlet u , v and w profiles.
- Fig. 11 Predicted velocity profiles for swirl vane angle $\phi = 70^\circ$ using measured inlet u , v and w profiles.
- Fig. 12 Predicted streamlines for nonswirling flow.
- Fig. 13 Predicted streamlines for swirl vane angle $\phi = 38^\circ$ using measured inlet u , v , and w profiles.
- Fig. 14 Predicted streamlines for swirl vane angle $\phi = 60^\circ$ using measured inlet u , v and w profiles.

- Fig. 15 Predicted streamlines for swirl vane angle $\phi = 70^\circ$ using measured inlet u , v and w profiles.
- Fig. 16 Axial velocity representation for nonswirling flow.
- Fig. 17 Axial velocity representation for swirl vane angle $\phi = 38^\circ$.
- Fig. 18 Axial velocity representation for swirl vane angle $\phi = 60^\circ$.
- Fig. 19 Axial velocity representation for swirl vane angle $\phi = 70^\circ$.
- Fig. 20 Predicted velocity profile for swirl vane angle $\phi = 45^\circ$ using measured inlet u , v and w profiles and high degree of convergence.
- Fig. 21 Predicted velocity profiles for swirl vane angle $\phi = 70^\circ$ using measured inlet u , v and w profiles and high degree of convergence.
- Fig. 22 Predicted streamlines for swirl vane angle $\phi = 45^\circ$ using measured inlet u , v and w profiles and high degree of convergence.
- Fig. 23 Predicted streamlines for swirl vane angle $\phi = 70^\circ$ using measured inlet u , v and w profiles, and high degree of convergence.

ORIGINAL PAGE IS
OF POOR QUALITY

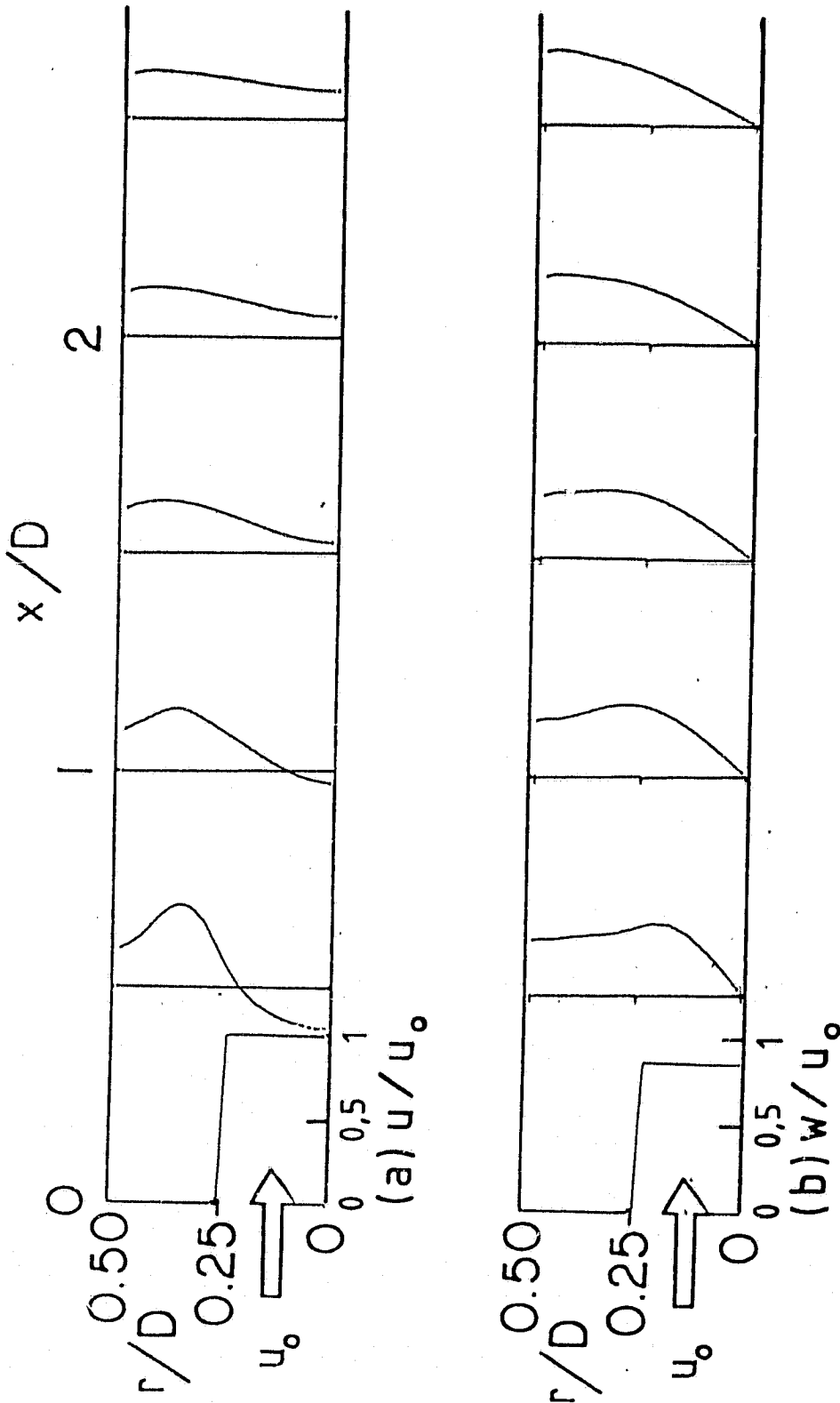


Fig. 1 Predicted velocity profiles for swirl vane angle $\phi = 45^\circ$ using flat inlet profiles with $v = 0$.

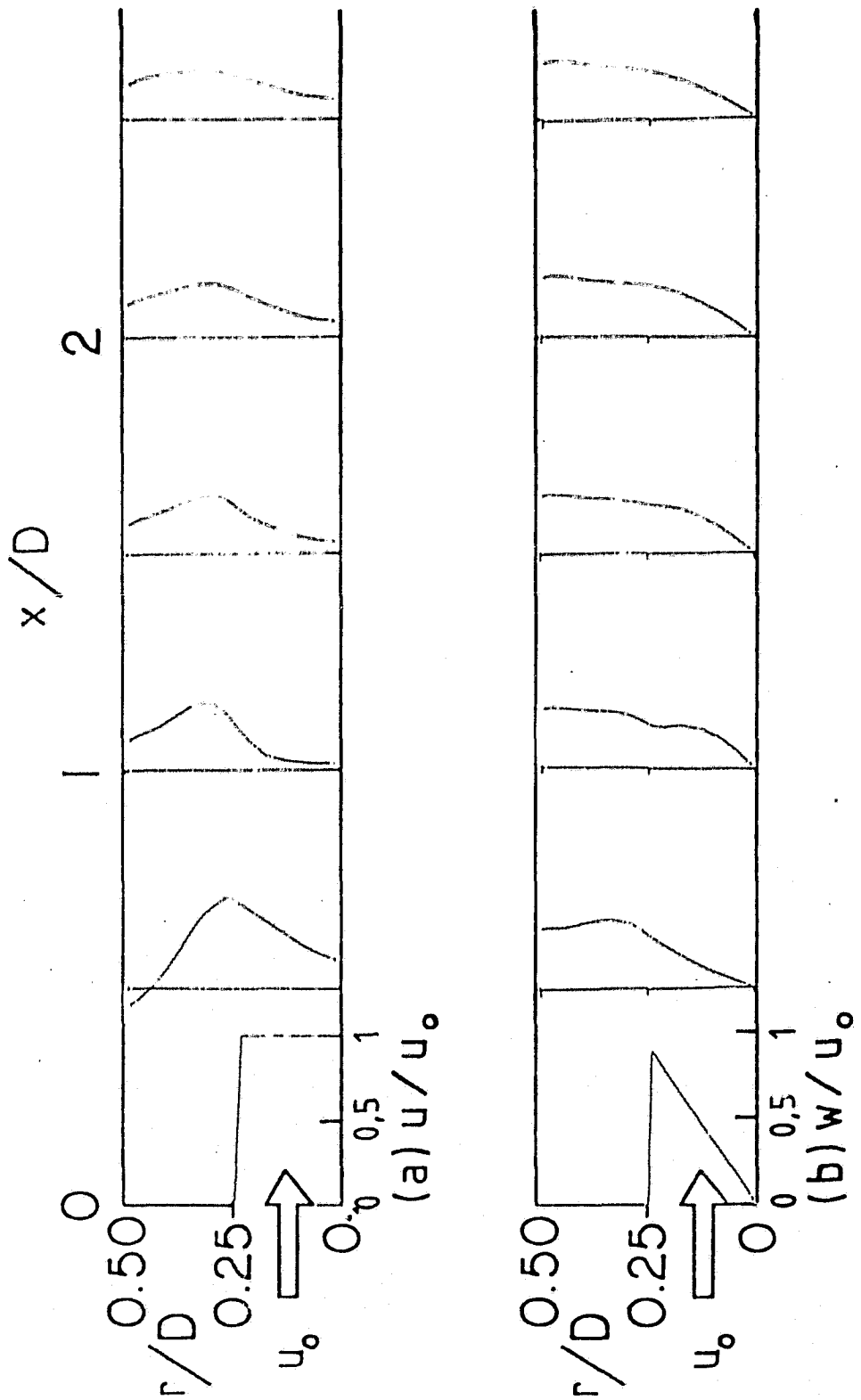


Fig. 2 Predicted velocity profiles for swirl vane angle $\phi = 45^\circ$ using flat inlet u profile with solid body rotation w profile with $v = 0$.

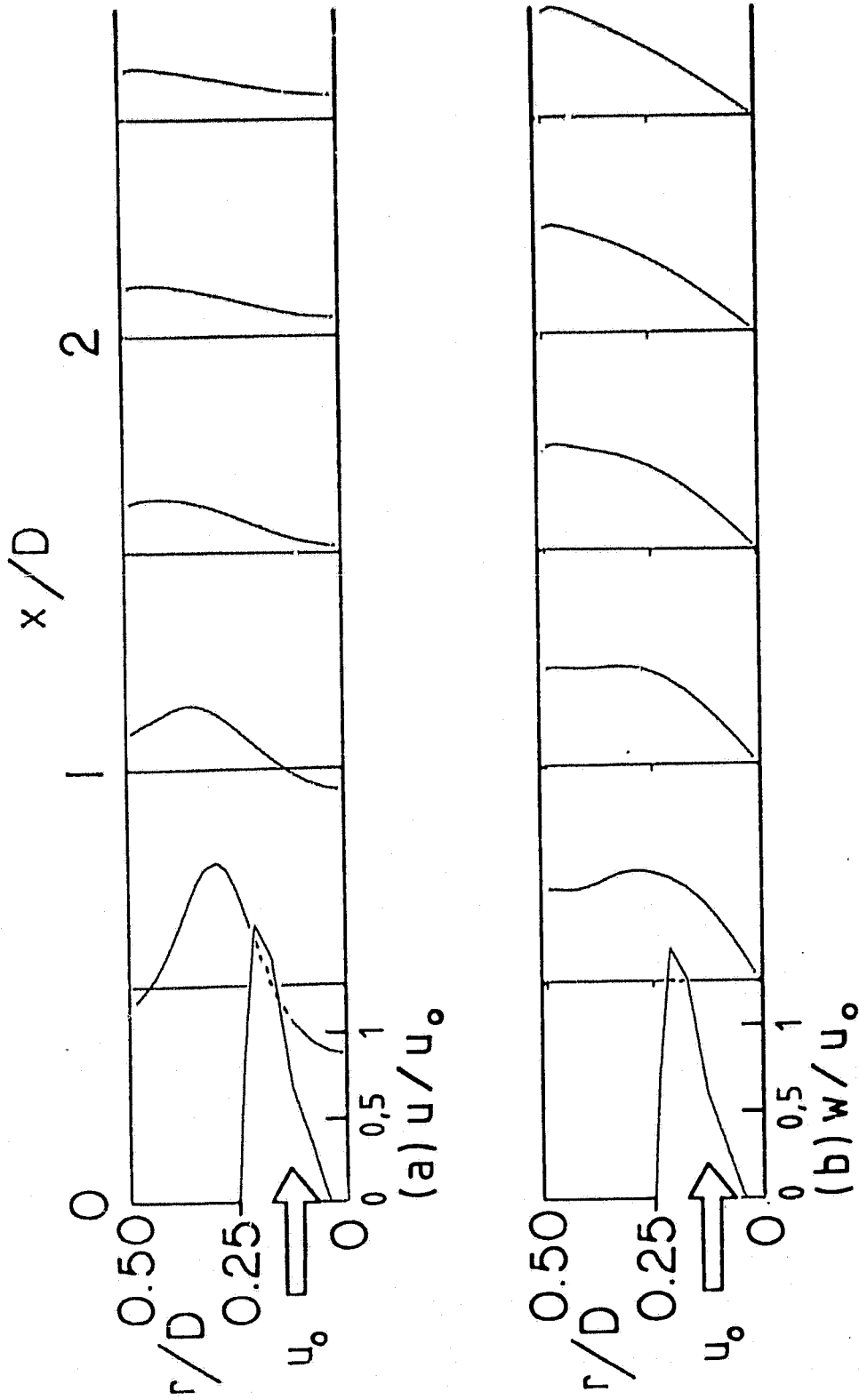


Fig. 3 Predicted velocity profiles for swirl vane angle $\phi = 45^\circ$ using measured inlet u and w profiles with $v = 0$.

CHARACTERISTICS
OF POOR QUALITY

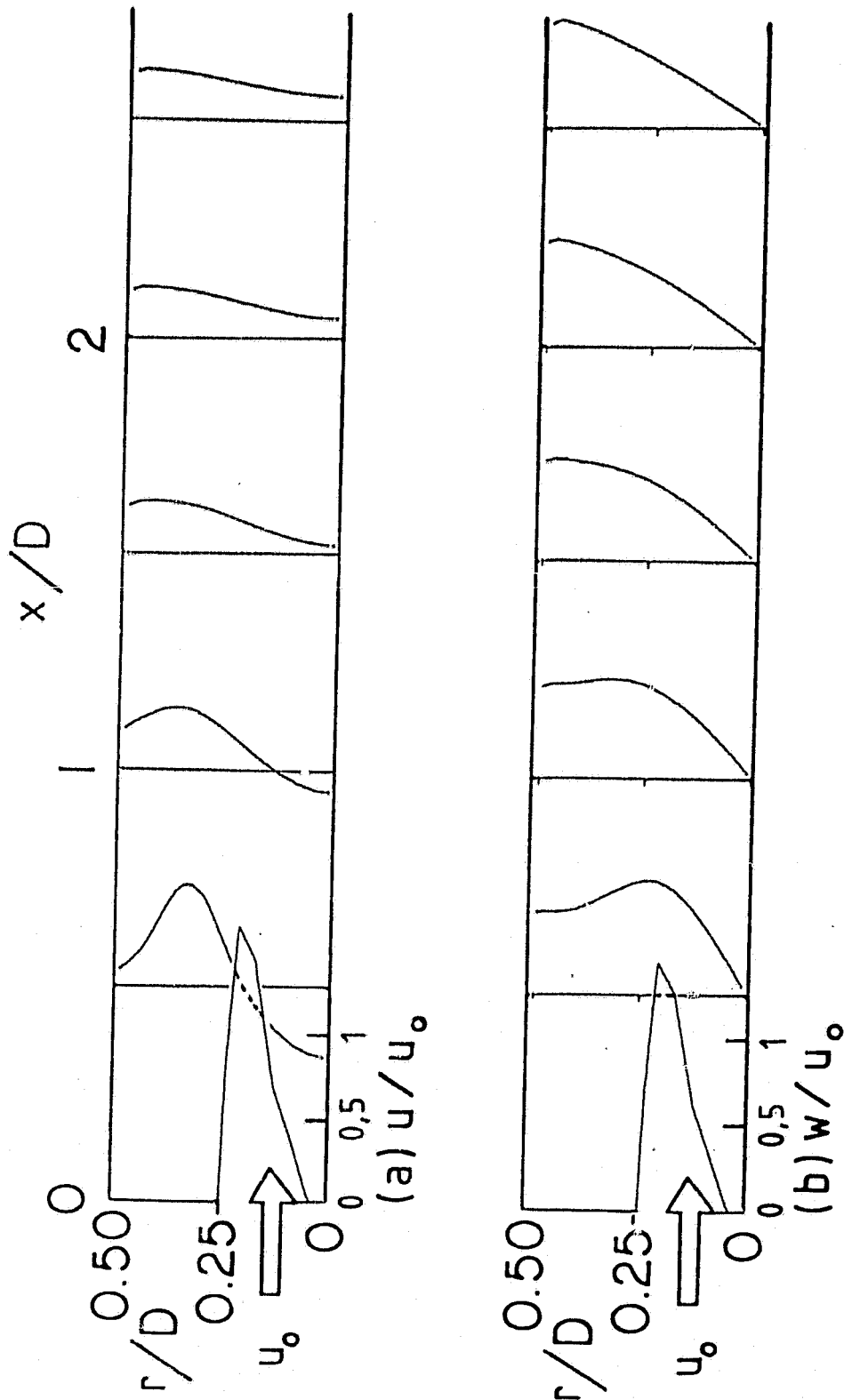


Fig. 4 Predicted velocity profiles for swirl vane angle $\phi = 45^\circ$ using measured inlet u , v and w profiles.

ORIGINAL CASE IS
OF POOR QUALITY.

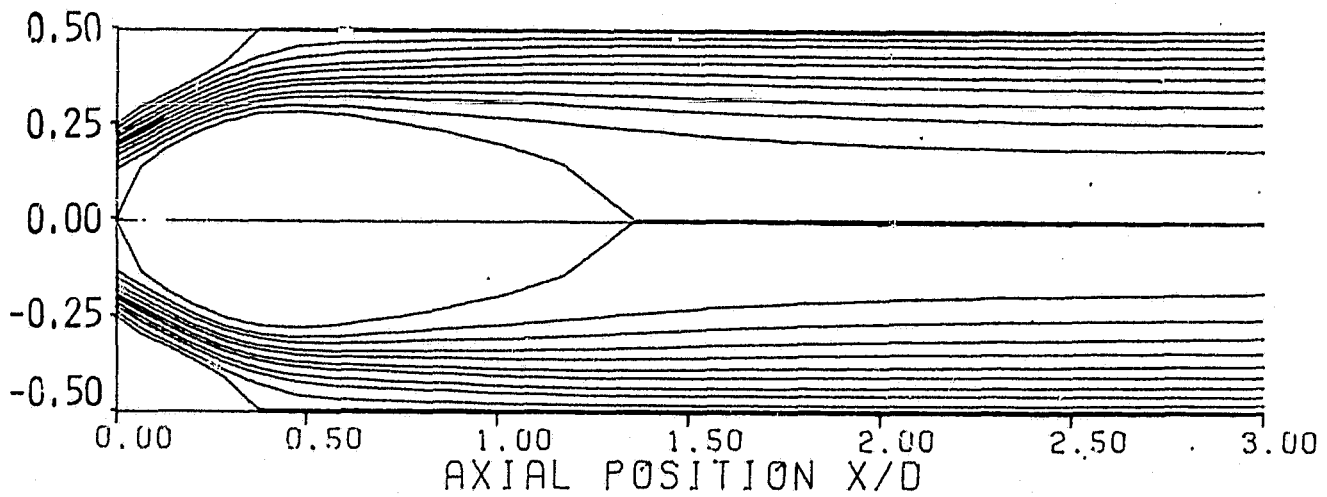


Fig. 5 Predicted streamlines for swirl vane angle $\phi = 45^\circ$ using measured inlet, u, v and w profiles.

ORIGINAL PAGE IS
OF POOR QUALITY

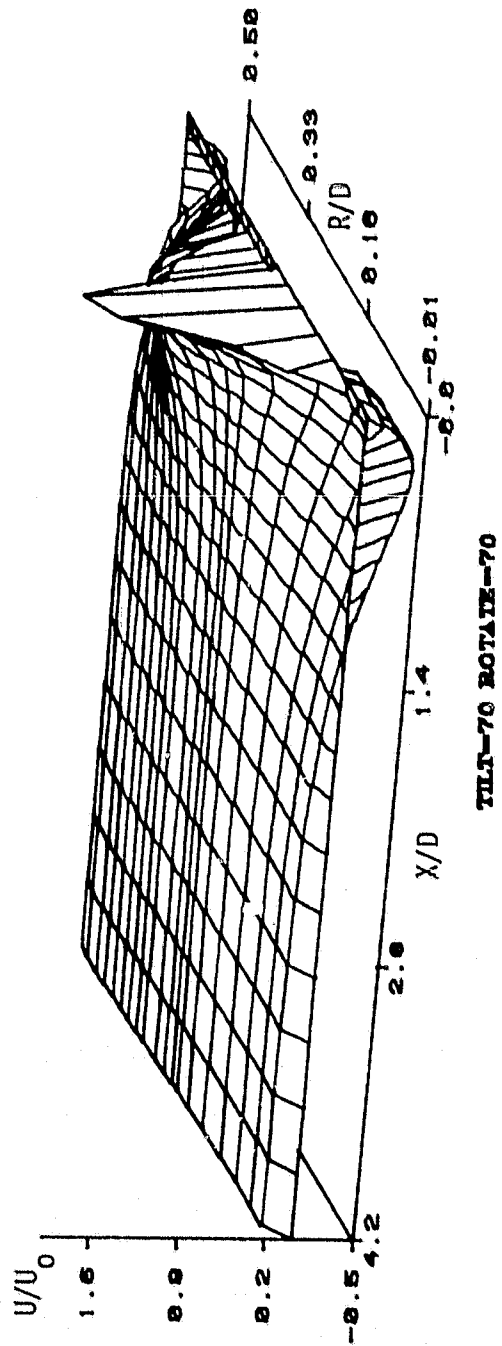


Fig. 6 Axial velocity representation for swirl vane angle $\phi = 45^\circ$.

ORIGINAL PAGE IS
OF POOR QUALITY

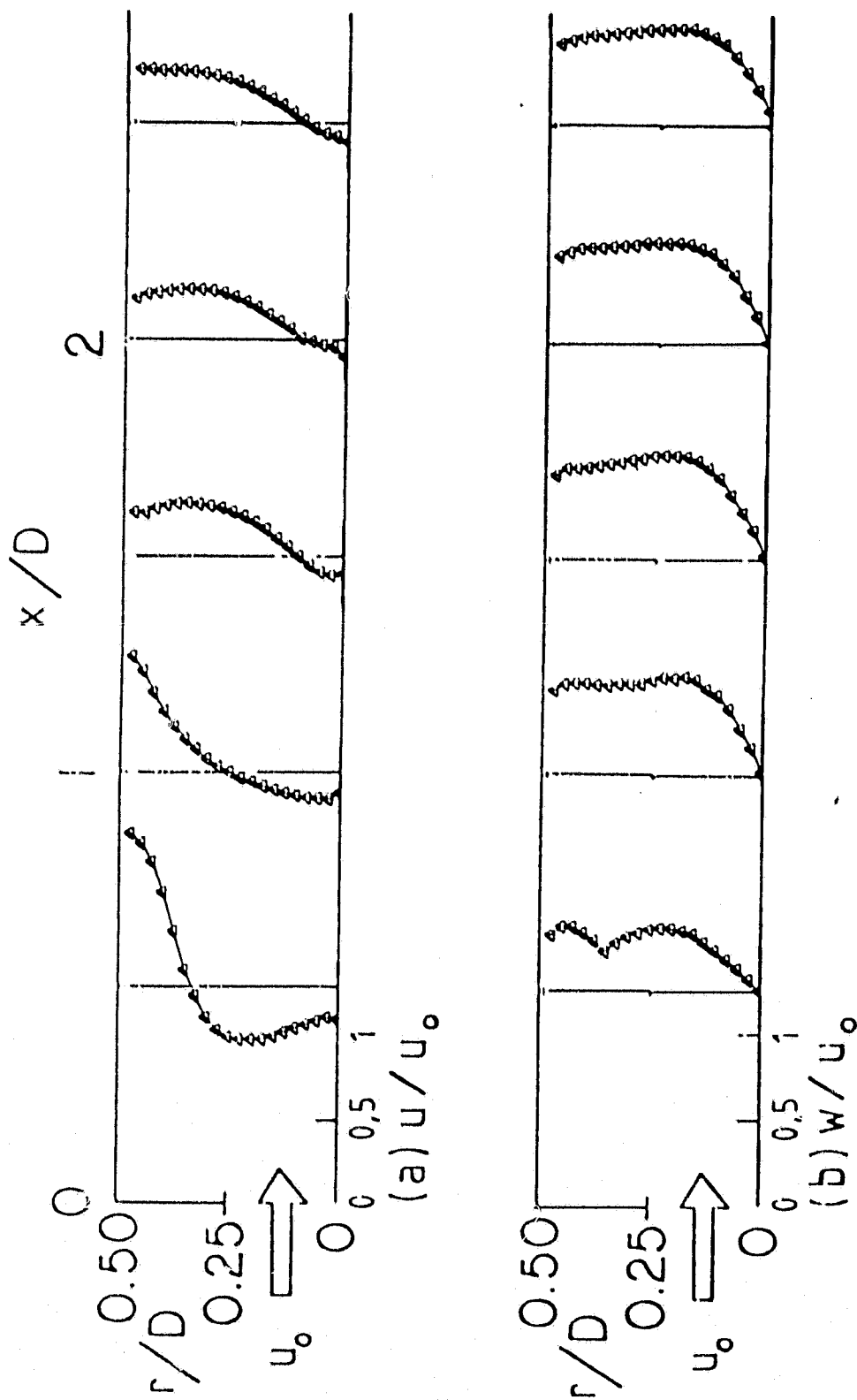


Fig. 7 Measured velocity profiles for swirl vane angle $\phi = 45^\circ$ using five-hole pitot probe. (Ref. 11)

ORIGINAL PAGE IS
OF POOR QUALITY.

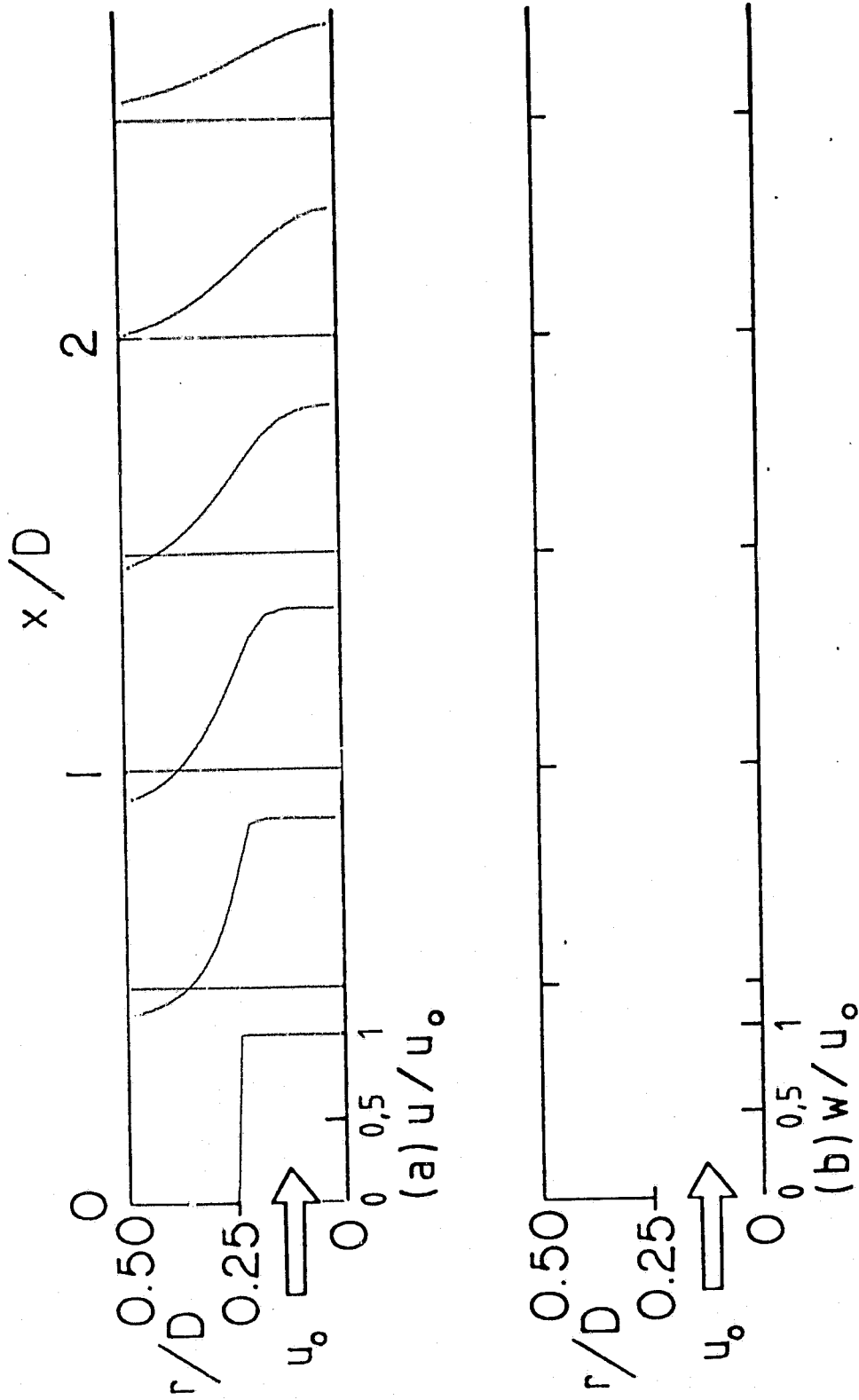


Fig. 8 Predicted velocity profiles for nonswirling flow using measured inlet u and v profiles.

ORIGINAL PAGE IS
OF POOR QUALITY.

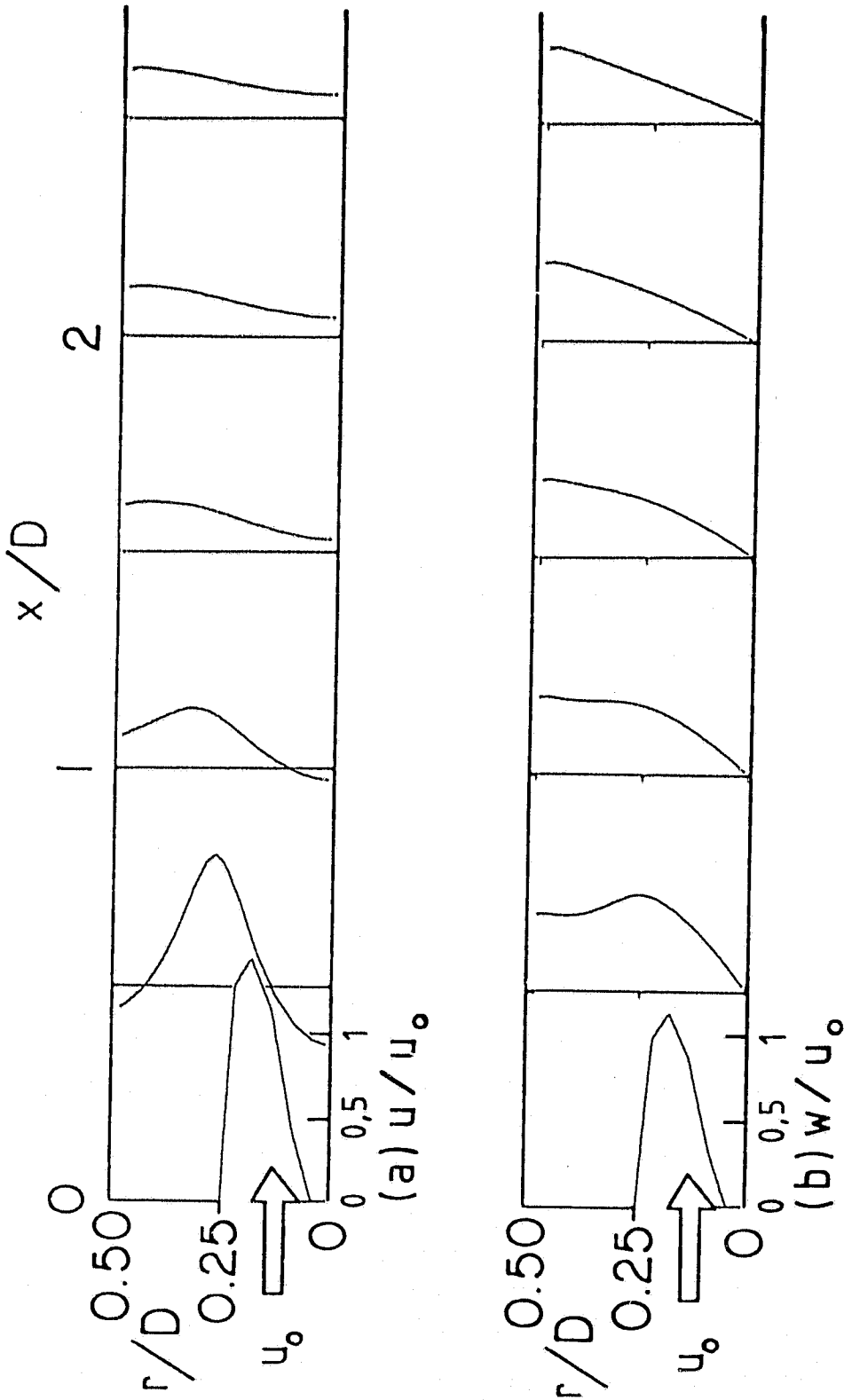


Fig. 9 Predicted velocity profiles for swirl vane angle $\phi = 38^\circ$ using measured inlet u , v and w profiles.

ORIGINAL PAGE IS
OF POOR QUALITY.

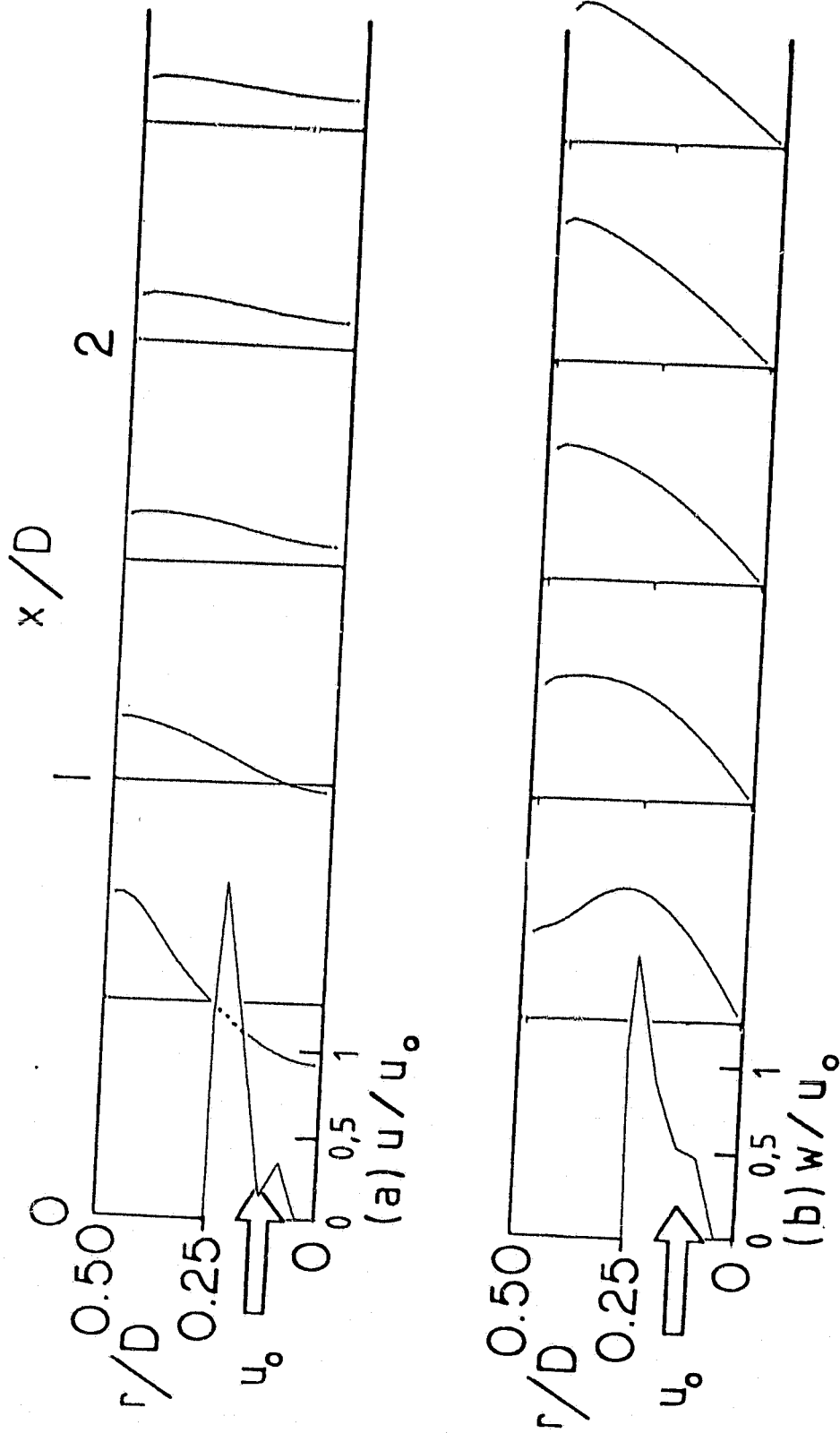


Fig. 10 Predicted velocity profiles for swirl vane angle $\phi = 60^\circ$ using measured inlet u , v and w profiles.

ORIGINAL PAGE IS
OF POOR QUALITY

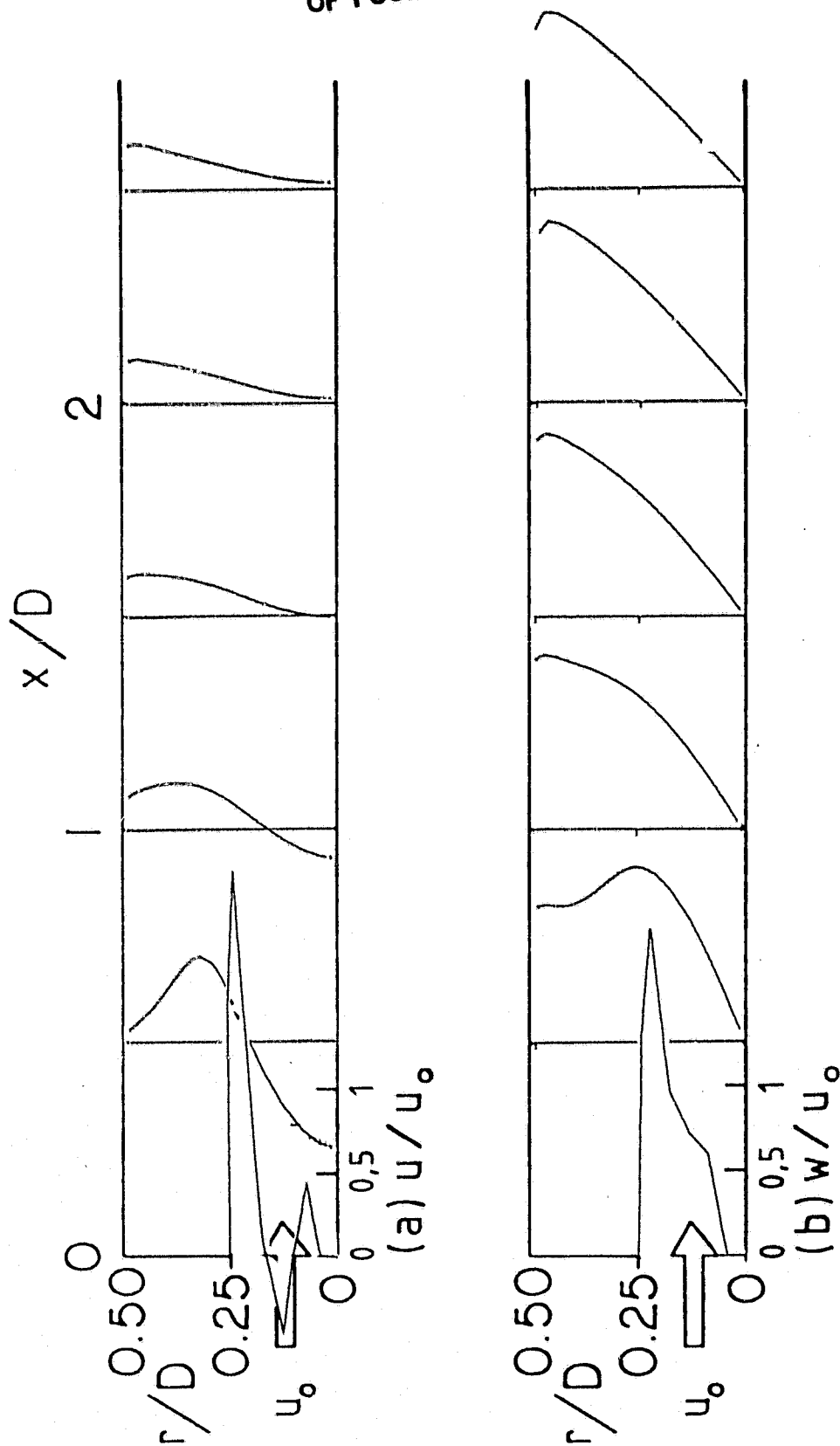


Fig. 11 Predicted velocity profiles for swirl vane angle $\phi = 70^\circ$ using measured inlet u , v and w profiles.

ORIGINAL PAGE IS
OF POOR QUALITY

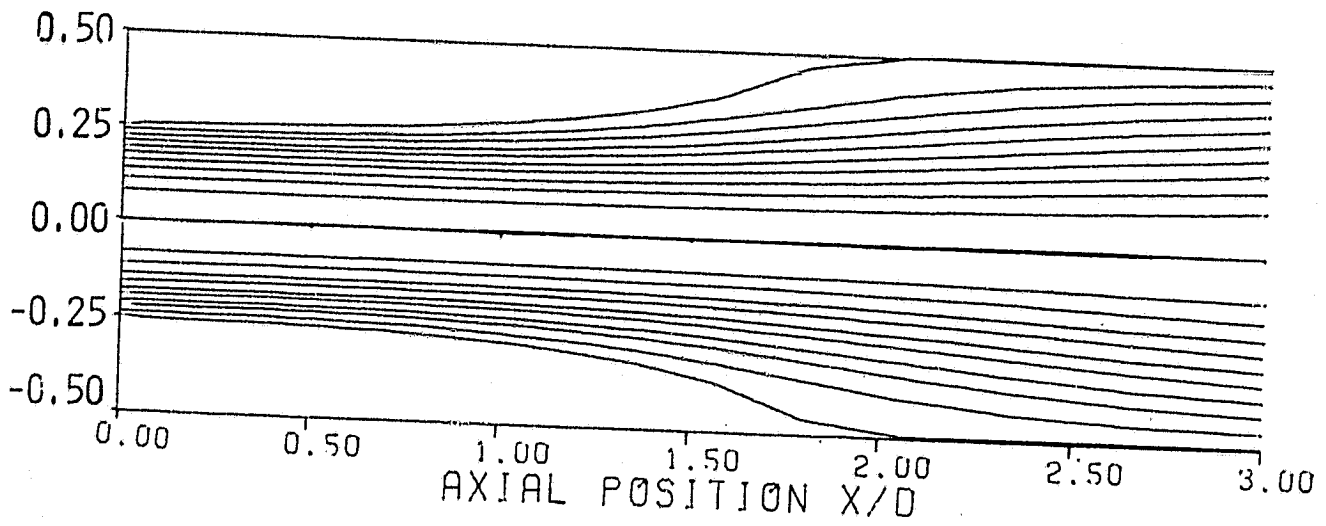


Fig. 12 Predicted streamlines for nonswirling flow.

ORIGINAL PAGE IS
OF POOR QUALITY.

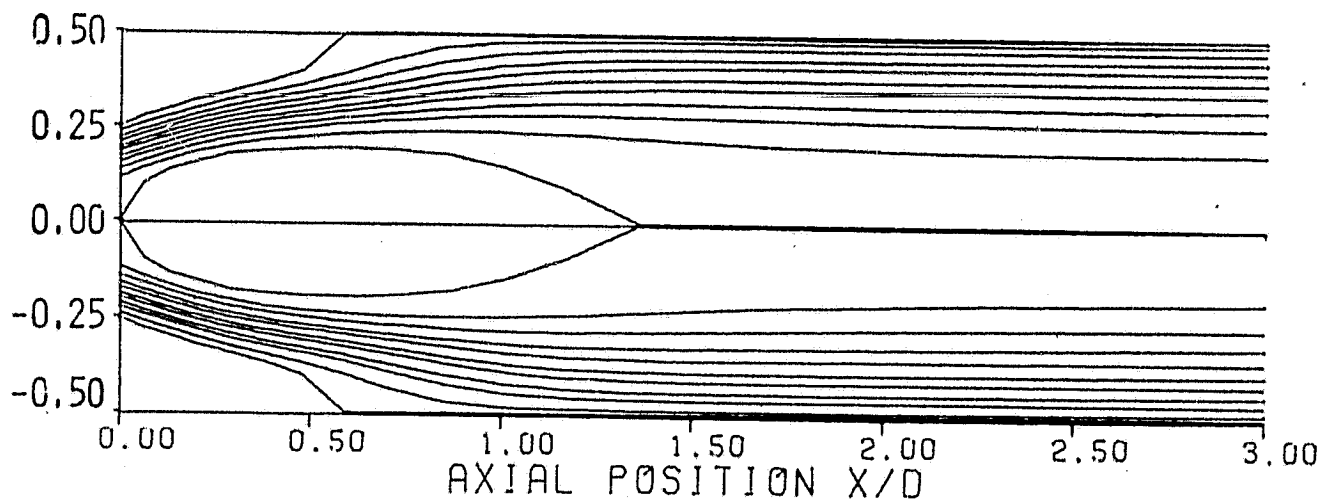


Fig. 13 Predicted streamlines for swirl vane angle $\phi = 38^\circ$ using
measured inlet u, v, and w profiles.

ORIGINAL PAGE IS
OF POOR QUALITY

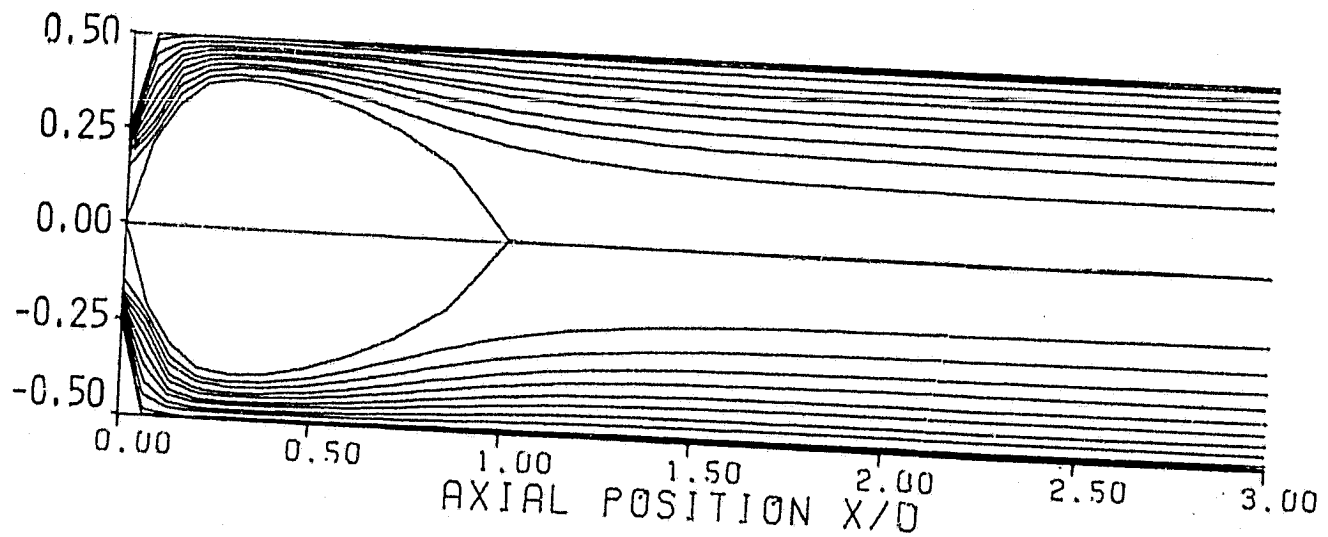


Fig. 14 Predicted streamlines for swirl vane angle $\phi = 60^\circ$ using measured inlet u , v and w profiles.

ORIGINAL PAGE IS
OF POOR QUALITY.

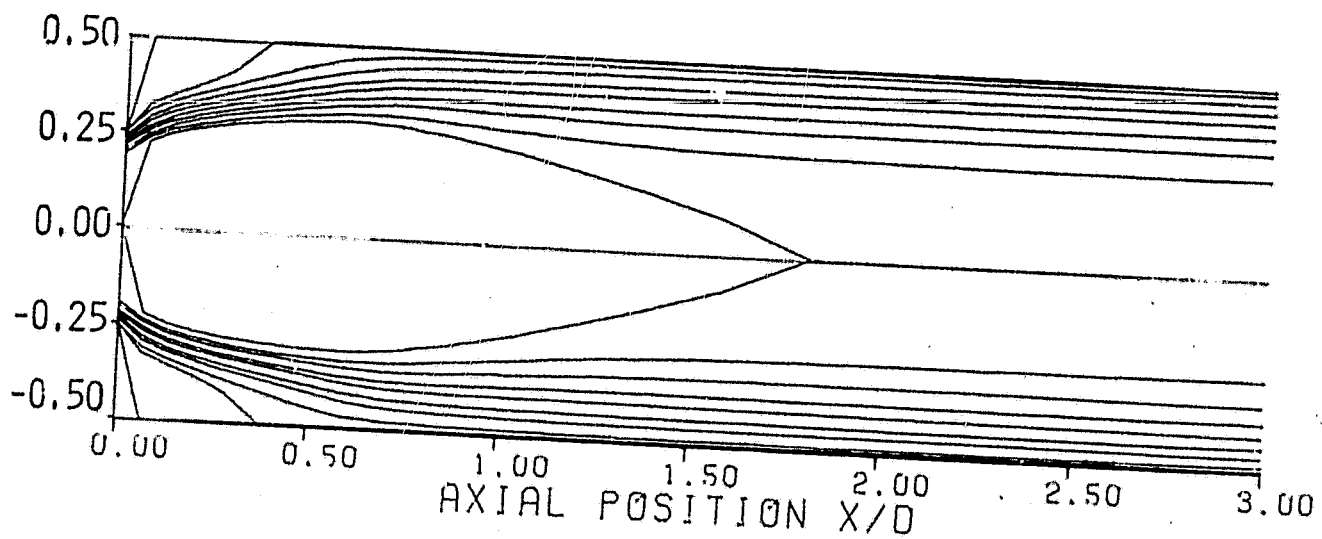


Fig. 15 Predicted streamlines for swirl vane angle $\phi = 70^\circ$ using measured inlet u, v and w profiles.

ORIGINAL PAGE IS
OF POOR QUALITY

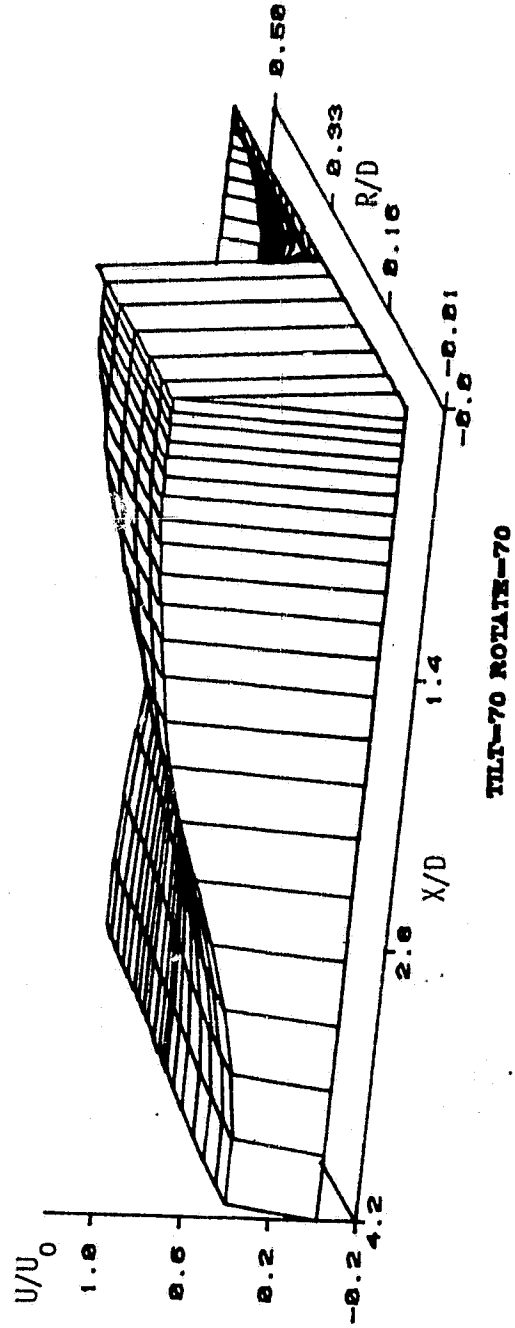


Fig. 16 Axial velocity representation for nonswirling flow.

ORIGINAL PAGE IS
OF POOR QUALITY.

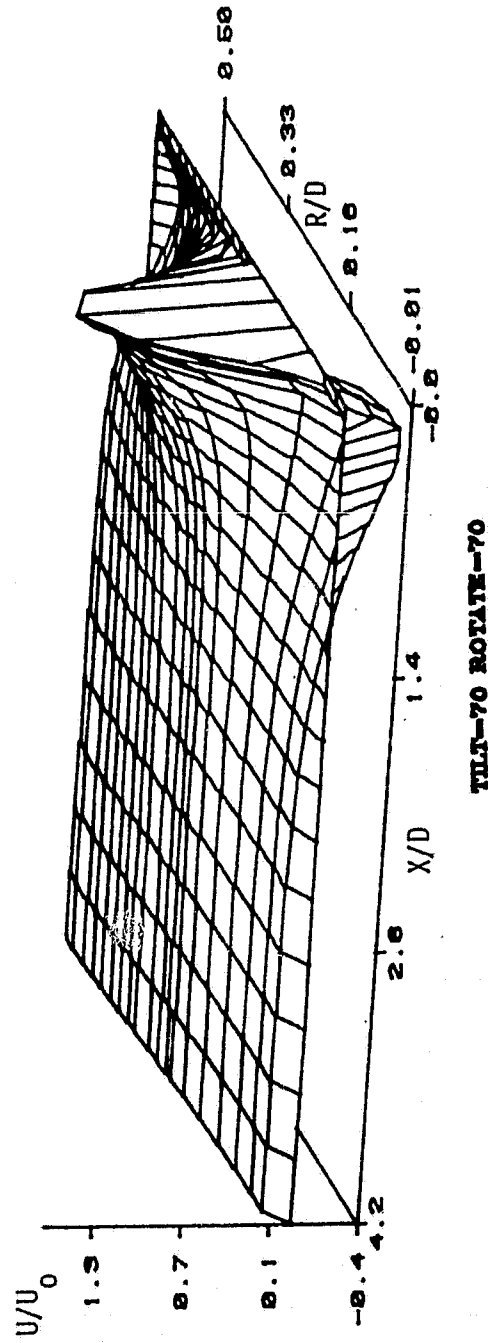


Fig. 17 Axial velocity representation for swirl vane angle $\phi = 38^\circ$.

ORIGINAL PAGE IS
OF POOR QUALITY

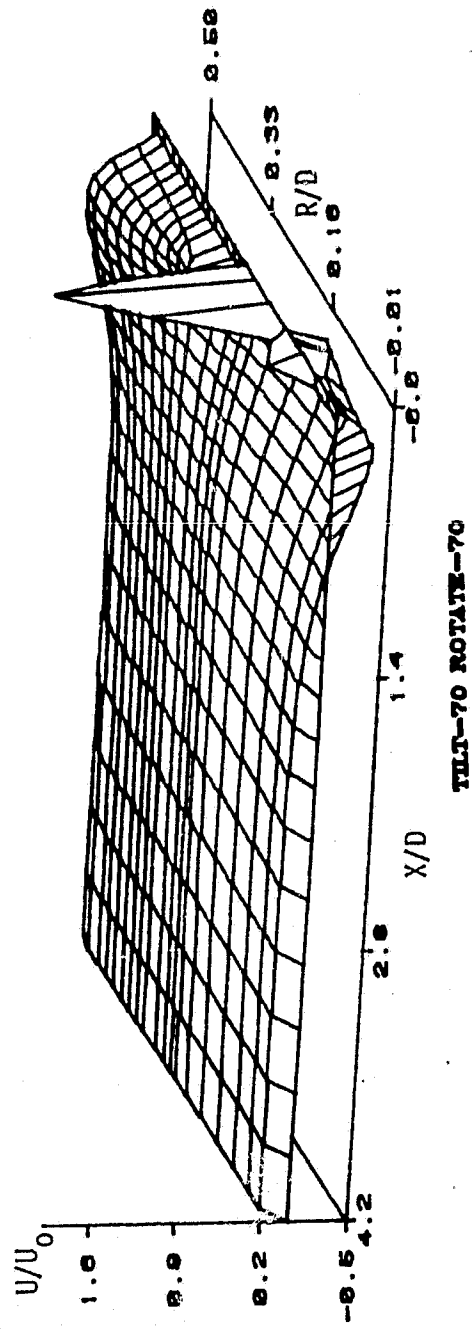


Fig. 18 Axial velocity representation for swirl vane angle $\phi = 60^\circ$.

ORIGINAL PAGE IS
OF POOR QUALITY

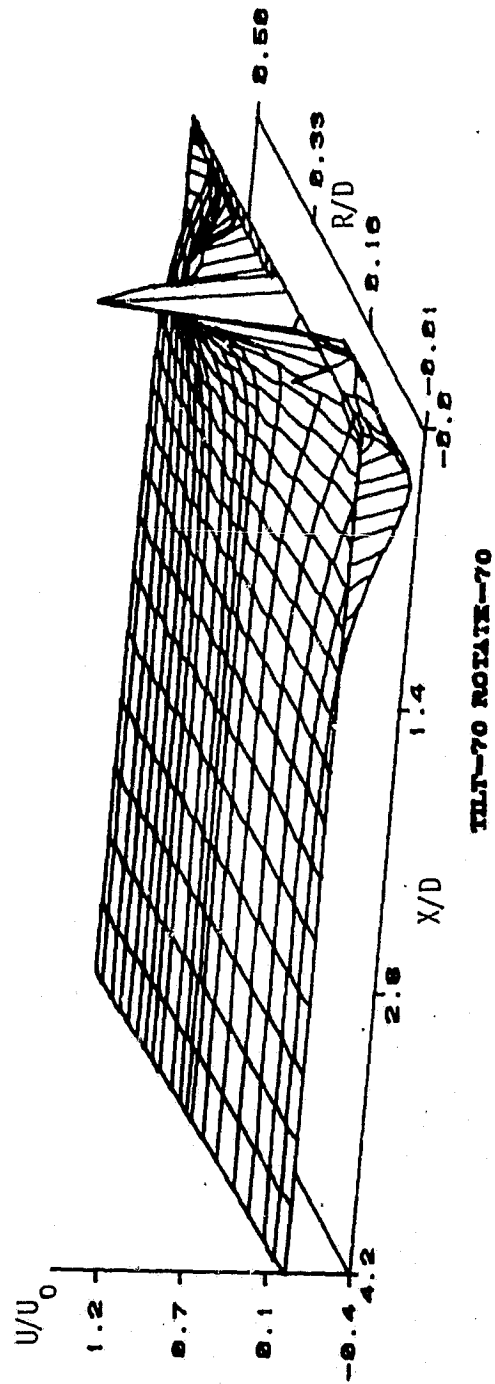


Fig. 19 Axial velocity representation for swirl vane angle $\phi = 70^\circ$.

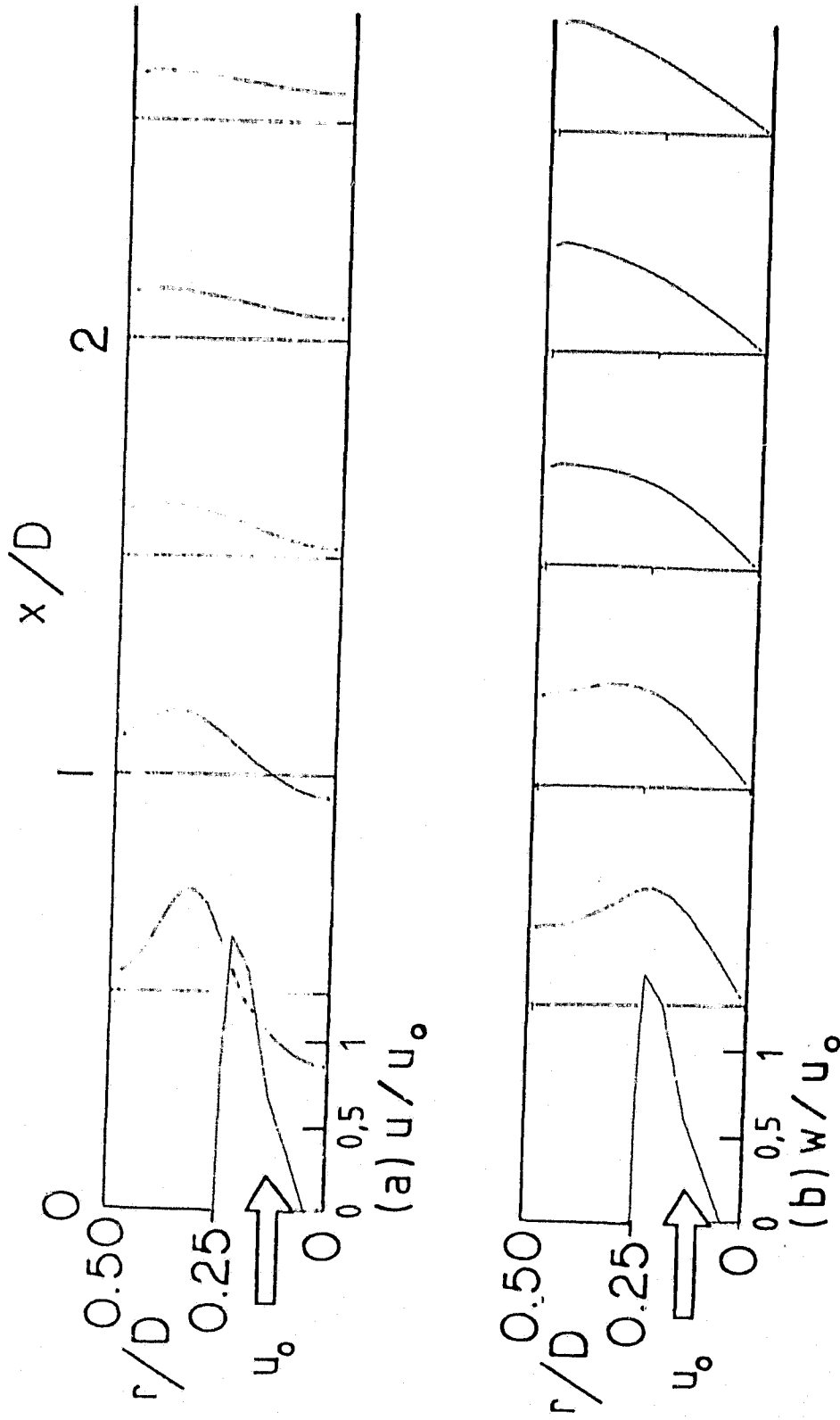


Fig. 20 Predicted velocity profiles for swirl vane angle $\phi = 45^\circ$ using measured inlet u , v and w profiles and high degree of convergence.

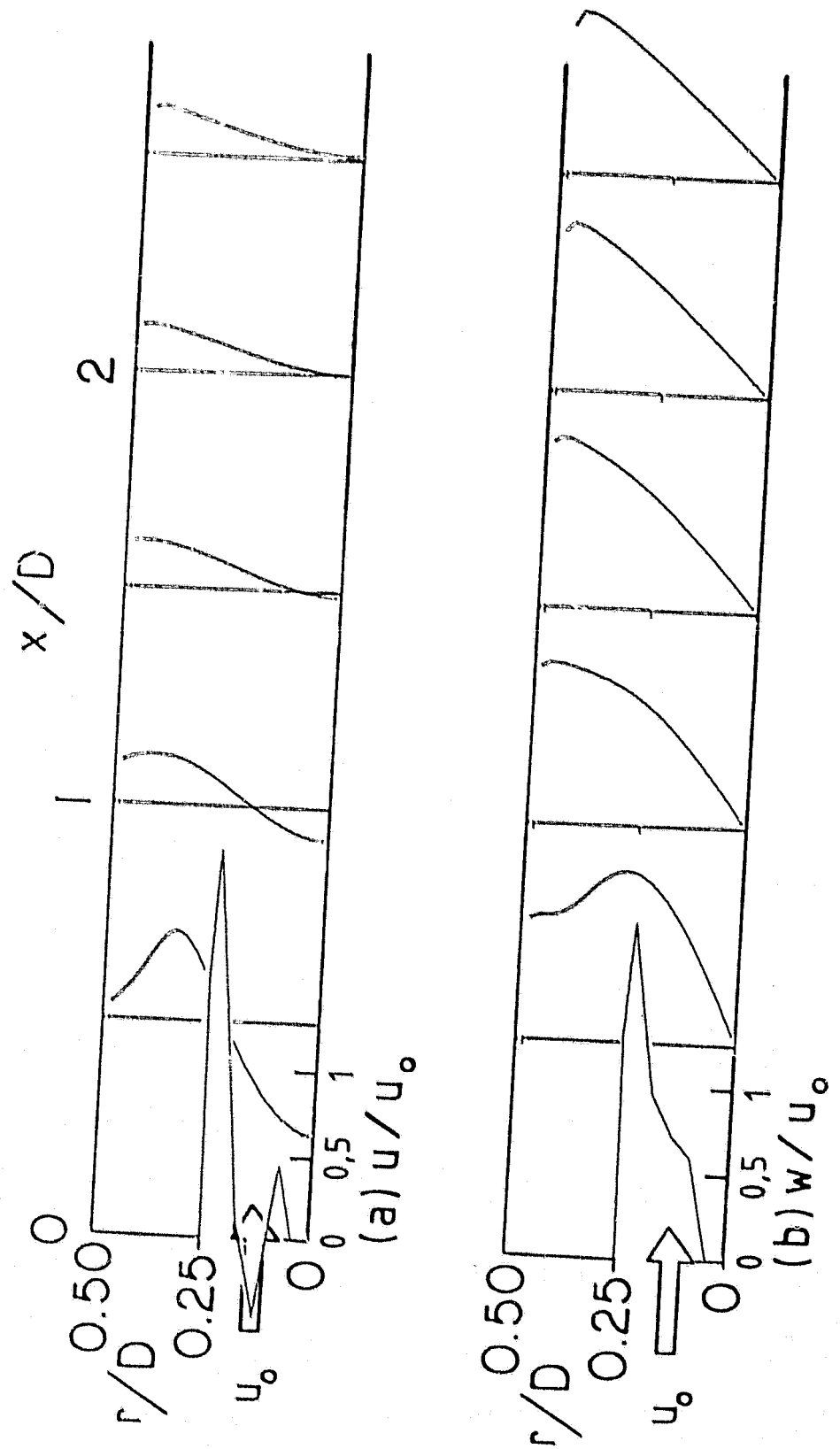


Fig. 21 Predicted velocity profiles for swirl vane angle $\phi = 70^\circ$ using measured inlet u , v and w profiles and high degree of convergence.

ORIGINAL PAGE IS
OF POOR QUALITY

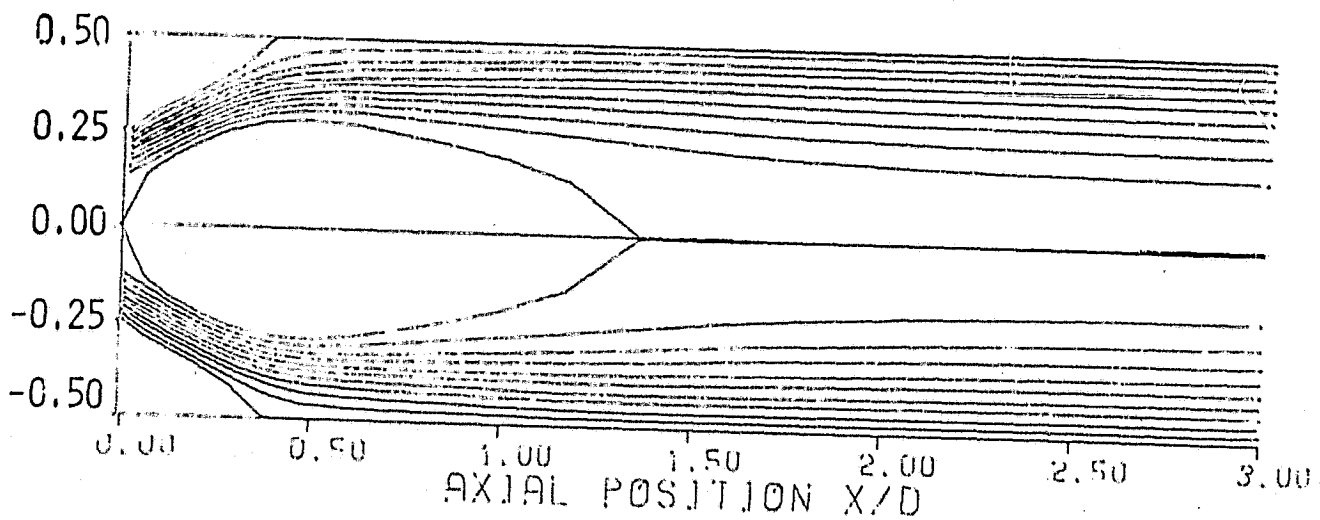


Fig. 22 Predicted streamlines for swirl vane angle $\phi = 45^\circ$ using measured inlet u, v and w profiles and high degree of convergence.

ORIGINAL PAGE IS
OF POOR QUALITY

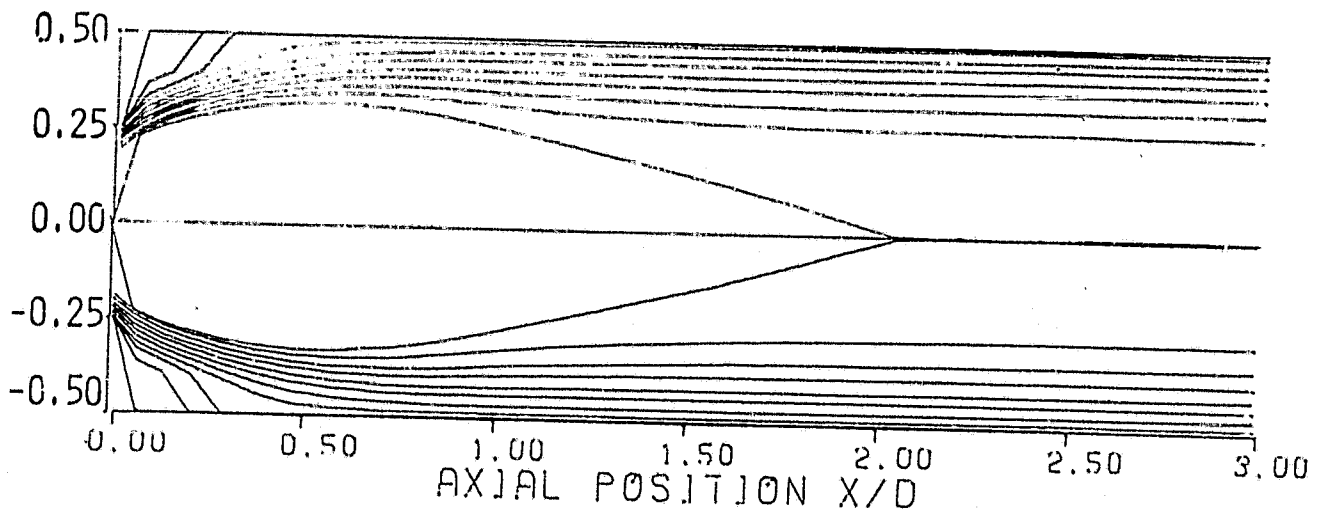


Fig. 23 Predicted streamlines for swirl vane angle $\phi = 70^\circ$ using measured inlet u , v and w profiles, and high degree of convergence.

TABLE LIST

Table 1. Fitting Experimental Data into the Computer Code for Swirl Vane Angle

$$\phi = 45 \text{ deg}$$

- (a) Axial Velocity
- (b) Radial Velocity
- (c) Swirl Velocity

Table 2. Absolute Residual Source Sums After 200 Iterations

- (a) For Different Swirl Vane Angles, with Measured, u, v and w
- (b) For Different Inlet Profile Assumptions for $\phi = 45$ degrees

Table 3. Iteration Toward Convergence

- (a) Normalized Residual Source Sums
- (b) Nondimensional Velocities at Field Location (I, J) = (8, 8)

Table 4. Effect of Inlet Turbulence Parameters on Flowfield Predictions for

$$\phi = 45^\circ \text{ and at } x/D = 0.5$$

- (a) $k = 0.03 u_{av,0}^2$ (constant)
- (b) $k = 0.03 u_0^2$ (varies with radius)
- (c) $k = 0.03 (u_0^2 + v_0^2 + w_0^2)$ (varies with radius)

Table 1. Fitting Experimental Data into the Computer Code for Swirl Vane Angle $\phi = 45$ deg.

Wall Expansion Angle $\alpha = 90$ deg.

Average Inlet Velocity $u_0 = 13.0$ m/s

(a) Axial Velocity

Experimental Data:

J	r/D	u/u_0
11	0.25532	0.000
10	0.22979	1.610
9	0.20425	1.570
8	0.17872	1.450
7	0.15319	1.030
6	0.12766	0.618
5	0.10213	0.327
4	0.07660	0.332
3	0.05106	0.000
2	0.02553	0.000

Interpolated Data:

J	r/D	u/u_0	u (m/s)
8	.2425	0.8085	10.51
7	.215	1.5866	20.63
6	.175	1.3890	18.05
5	.13	0.6560	8.52
4	.085	0.3304	4.29
3	.045	0.000	0.00
2	.0125	0.000	0.00

Table 1 (continued)

(b) Radial Velocity

Experimental Data:

J	R/D	v/u_0
10	0.22979	0.5450
9	0.20425	0.4890
8	0.17872	0.5050
7	0.15319	0.5090
6	0.12766	0.5690
5	0.10213	0.3590
4	0.07660	0.3420
3	0.05106	0.0000
2	0.02553	0.0000

Interpolated Data:

J	R/D	v/u_0	$v(m/s)$
8	0.22875	0.5427	7.05
7	0.19500	0.4948	6.43
6	0.15250	0.5106	6.64
5	0.10750	0.4032	5.24
4	0.06500	0.1867	2.43
3	0.02875	0.0000	0.00
2	0.00000	0.0000	0.00

Table 1 (continued)

(c) Swirl Velocity

Experimental Data:

J	r/D	w/u ₀
11	0.25532	0.000
10	0.22979	1.410
9	0.20425	1.450
8	0.17872	1.320
7	0.15319	0.862
6	0.12766	0.580
5	0.10213	0.508
4	0.07660	0.186
3	0.05106	0.000
2	0.02553	0.000

Interpolated Data:

J	r/D	w/u ₀	w (m/s)
8	0.2425	0.7080	9.20
7	0.2150	1.4334	18.63
6	0.1750	1.2533	16.29
5	0.1300	0.6058	7.88
4	0.0850	0.2919	3.80
3	0.0450	0.0000	0.00
2	0.0125	0.0000	0.00

Table 2. Absolute Residual Source Sums After 200 Iterations

(a) For different swirl vane angles, with measured u, v and w

Swirl Vane Angle ϕ	u	v	w	Mass
0	0.00560	0.00096	0.00500	0.00009
38	0.05060	0.02340	0.13190	0.04280
45	0.02040	0.02200	0.02580	0.00720
60	0.03607	0.02960	0.04286	0.01410
70	0.05322	0.05032	0.09408	0.04622

(b) For different inlet profile assumptions for $\phi = 45$ degrees

Inlet Type	u	v	w	Mass
Flat u and w with v zero	0.00634	0.0048	0.0039	0.0012
Flat u with w solid body rotation and v zero	0.02540	0.0270	0.0313	0.02700
Measured u and w with v zero	0.03509	0.0393	0.0426	0.01055
Measured u, v and w	0.02040	0.0220	0.0258	0.00720

Table 3. Iteration Toward Convergence

(a) Normalized Residual Source Sums.

ϕ^0	U_0 m/s	Iteration Numbers	u	v	w	Mass
0	54.91	200	0.0056	0.00096	0.005	0.0001
38	31.75	200	0.0506	0.0234	0.1319	0.0428
		300	0.0146	0.0029	0.0218	0.0073
		400	0.0053	0.0042	0.0053	0.0027
		430	0.0035	0.0009	0.0039	0.002
45	31.00	200	0.0186	0.0190	0.0183	0.0058
		300	0.0041	0.0040	0.0048	0.0012
		315	0.0035	0.0037	0.0039	0.0005
60	21.96	200	0.0376	0.0296	0.0482	0.0159
		300	0.0184	0.0131	0.0249	0.0085
		400	0.01	0.0065	0.0126	0.0041
		500	0.0048	0.0037	0.0065	0.00156
70	13.20	200	0.0434	0.0352	0.0694	0.0230
		300	0.0165	0.0177	0.0317	0.0177
		400	0.0082	0.0079	0.0151	0.0079
		500	0.0039	0.0044	0.0071	0.0042

Table 3. (Continued)

(b) Nondimensional Velocities at Field Location (I, J) = (8, 8).

ϕ	Iteration Number	u/u_0	v/v_0	w/u_0
0	200	0.705	0.0126	0.0
38	200	0.680	0.035	0.563
	300	0.645	0.027	0.542
	400	0.663	0.030	0.548
	430	0.665	0.031	0.549
45	200	0.199	0.056	0.676
	300	0.170	0.058	0.674
	315	0.169	0.058	0.674
60	200	0.022	0.074	0.690
	300	0.044	0.071	0.653
	400	0.055	0.070	0.663
	500	0.060	0.067	0.646
70	200	0.185	0.063	1.064
	300	0.143	0.066	1.024
	400	0.116	0.068	1.010
	500	0.105	0.069	1.00

Table 4. Effect of Inlet Turbulence Parameters on Flowfield Predictions for $\phi = 45^\circ$ and at $x/D = 0.5$.

(a) $k = 0.03 u_{av,0}^2$ (constant)

r/D	u/u_0	w/u_0	ϵ	k
0.4	0.365	0.49	9050.0	26.5
0.3	0.529	0.606	10939.0	32.4
0.2	0.003	0.635	21025.0	76.2

(b) $k = 0.03 u_0^2$ (varies with radius)

0.4	0.377	0.487	7960.0	22.8
0.3	0.535	0.606	8832.0	25.0
0.2	0.026	0.652	19462.0	69.8

(c) $k = 0.03 (u_0^2 + v_0^2 + w_0^2)$ (varies with radius)

0.4	0.377	0.490	7460.0	21.2
0.3	0.542	0.606	8090.0	23.2
0.2	0.026	0.655	19537.0	71.9

APPENDIX D

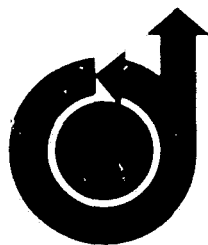
BLUFF-BODY FLAMEHOLDER WAKES:

A SIMPLE NUMERICAL SOLUTION

AIAA-82-1177

Bluff-Body Flameholder Wakes: A Simple Numerical Solution

G.H. Vatistas, S. Lin and C.K. Kwok,
Concordia Univ., Montreal, Canada; and
D.G. Lilley, Oklahoma State Univ.,
Stillwater, OK



AIAA/SAE/ASME
18th Joint Propulsion Conference
June 21-23, 1982/Cleveland, Ohio

BLUFF-BODY FLAMEHOLDER WAKES:
A SIMPLE NUMERICAL SOLUTION

ORIGINAL PAGE IS
OF POOR QUALITY.

G. H. Vatistas*, S. Lin** and C. K. Kwok***
Concordia University, Montreal, Canada

and

D. G. Lilley****
Oklahoma State University, Stillwater, Oklahoma

Abstract

Numerical finite difference predictions are made of recirculation zones behind bluff-body flame stabilizers, showing quantitatively the effects of forebody geometry, blockage ratio, lateral position of the blockage and inlet swirl on the central recirculation zone. A simple transient Navier-Stokes solution algorithm and laminar flow simulation are used with 'free slip' and 'no slip' wall boundary conditions, thus illustrating how a basic approach may be used to solve a sophisticated fluid dynamic problem.

Introduction

The Phenomenon

Flames in combustion chambers are generally stabilized by means of recirculation zones.¹⁻¹⁰ The recirculation zone acts as a continuous heat source by transporting hot combustion products upstream towards the burner and thereby supplying the energy required for ignition. In addition to the stability of the flame, the size and shape of the recirculation zone affects the volumetric heat release rate and the combustion efficiency.

Previous experimental work shows that the recirculation zone can be set up in the wake of a bluff-body such as a stabilizer disk or cone. Alternatively it can be generated by the action of swirl and then, at sufficiently high degrees of swirl, the presence of a central bluff-body is not required. In a divergent nozzle, where the flow remains attached to the wall, the increased radial component of the flow results in an increase in the size of the recirculation eddy. The combined effect of blockage, swirl and divergent nozzle considerably enhances the process. This paper is concerned with nonreacting flows; a schematic of the flow system appears in Fig. 1.

The Problem

To aid the design of combustors with complex geometries, one wishes to characterize this recirculation zone theoretically, both qualitatively and quantitatively. The properties of this zone (length, breadth, reverse mass flow rate, and maximum reverse flow velocity) provide a key to the residence time distribution and time-temperature history of gases in the system, and bear a strong relation to efficiency of, and pollution emanation from, the system.

*Graduate Student, Dept. of Mechanical Engineering, Member AIAA.

**Associate Professor, Dept. of Mechanical Engineering

***Professor, Dept. of Mechanical Engineering

****Associate Professor, School of Mechanical and Aerospace Engineering, Associate Fellow AIAA.

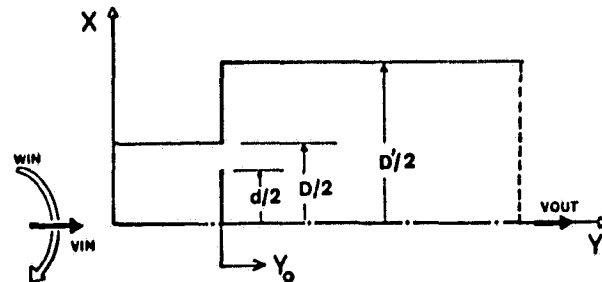


Fig. 1 Schematic of the axisymmetric problem with disk blockage

Mathematically the recirculating flow requires the solution of the full Navier-Stokes equations and a transient time-marching technique is used here. The present investigation omits combustion and treats the turbulence of the flowfield rather crudely: the flow is supposed to behave as a laminar flow with a constant artificially high value ascribed to the viscosity. Even so, it is interesting to see what level of accuracy results from this quite reasonable assumption.

The Present Contribution

Consideration is given here to a primitive, pressure-velocity variable, finite difference code which has been developed to predict 2-D axisymmetric swirling transient flows. The technique used here incorporates the following:

- (i) A finite difference procedure is used in which the dependent variables are the velocity components and pressure, formulated in axisymmetric cylindrical polar coordinates.
- (ii) The pressure is deduced from the continuity equation and the latest velocity field, using a guess-and-correct procedure for the latter.
- (iii) The procedure incorporates displaced grids for the two velocity components, which are placed between the nodes where pressure is stored.

The code is designed for persons with little or no experience in numerical fluid dynamics with the purpose of demonstrating that many useful and difficult problems can be attacked without resorting to large, complicated computer programs and useful qualitative computer experimentation may be performed. As specific complexities can be added easily, the program provides a basis for developing

many new numerical capabilities. The present work has grown out of previous ideas about solving 2-D flows using transient Los Alamos¹¹⁻¹³ and steady state Imperial College¹⁴⁻¹⁵ methods.

Solution Technique

The General Idea

A laminar flow simulation with 'free slip' or 'no slip' wall boundary conditions is used in simplified code, based directly on the SOLA algorithm¹³, suitably extended to include swirl effects. It provides an alternative to more sophisticated codes that are also applicable to the problems of this type.¹⁴⁻¹⁵ It is assumed that the flow is 2-D isothermal, incompressible and axisymmetric, and that material properties are constant. Under these assumptions, the governing equations can be expressed as follows:

$$\frac{\partial u}{\partial x} + \frac{\partial v}{\partial y} + \frac{u}{x} = 0$$

$$\frac{\partial u}{\partial t} + \frac{\partial}{\partial x} (u^2) + \frac{\partial}{\partial y} (vu) + \frac{(u^2 - w^2)}{x} = -\frac{\partial p}{\partial x} + v(\nabla^2 u - \frac{u}{x^2})$$

$$\frac{\partial v}{\partial t} + \frac{\partial}{\partial x} (uv) + \frac{\partial}{\partial y} (v^2) + \frac{uv}{x} = -\frac{\partial p}{\partial y} + v\nabla^2 v$$

$$\frac{\partial w}{\partial t} + \frac{\partial}{\partial x} (uw) + \frac{\partial}{\partial y} (vw) + \frac{2uw}{x} = v(\nabla^2 w - \frac{w}{x^2})$$

where

$$\nabla^2 \phi = \frac{\partial^2 \phi}{\partial x^2} + \frac{\partial^2 \phi}{\partial y^2} + \frac{1}{x} \frac{\partial \phi}{\partial x}$$

Here u , v and w are velocity components in the x ($\equiv r$), y (\equiv symmetry axis) and θ directions, respectively, in accordance with the basic algorithm.¹³

A general grid system covering the domain of interest appears in Fig. 2, illustrating how boundaries and blockages may be located. A single cell of the mesh is enlarged in Fig. 3 which shows the location of each field variable p , u , v and w relative to this (I, J) cell. The pressure and swirl velocity w are located at the center of each cell and the radial and axial velocities are on the boundaries as shown. Thus normal velocities lie directly on the physical boundaries of the solution domain, while the tangential velocities and pressure are displaced half a cell interval inside the flowfield. In this way the exterior fictitious cells are particularly convenient when applying the boundary conditions.

Boundary Conditions

Finite difference equations simulating the differential equations are set up and solved by way of a time-march process applied to cells within the flow domain of interest. Cells touching the boundary thus utilize the value on the boundary (in the case of tangential velocities). Interior normal velocity calculations take the zero normal wall values, the given normal inlet values, or the yet-

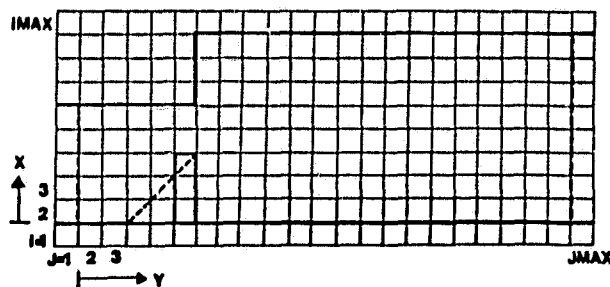


Fig. 2 General grid system covering the flow domain

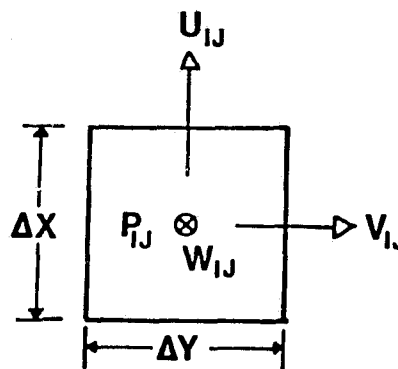


Fig. 3 Arrangement of finite difference variables in a typical cell

to-be-determined outlet values as appropriate during their calculations. Interior tangential velocity calculations adjacent to boundaries use the fictitious values which are placed in the surrounding layer of complementary cells. Specification of these is after each time-step and after each sweep of the cells during the pressure-velocity iteration. With a coarse grid, *free-slip* conditions are appropriate for tangential velocities, and external values are set equal to their associated immediately interior values. On the other hand, with a fine grid computing through the boundary layer, *no-slip* conditions are appropriate for tangential velocities and external values are set equal to the negative of their associated immediately interior values. In the computations shown later, free slip boundary conditions are applied on all wall boundaries except those corresponding to internal obstacles. These are incorporated via blocking out appropriate cells, setting to zero their boundary normal velocities as recommended as a simple approach in Ref. 13. If accuracy demands, more realistic approaches are easy to incorporate. Specification of all velocities at the outlet is via the continuative condition. On the axis of symmetry the usual zero normal velocity and free-slip axial velocity specification are applicable; the swirl velocity is given a definite zero value.

Solution Technique

Numerical solution of the problem is obtained from the time-dependent Navier-Stokes equations, along with initial and boundary conditions, following the Los Alamos SOLA technique.¹³ Each forward time

ORIGINAL PAGE IS
OF POOR QUALITY

step is obtained from the momentum equations, using an explicit scheme with donor cell approach for the convection terms. The newly-calculated velocities will not, in general, satisfy the continuity requirement. So at each step of the march a pressure-velocity correction iteration procedure is applied; iteration continues with overrelaxation until the cell mass imbalance for each cell is less than some prescribed small quantity. Criteria for the stability and accuracy of the algorithm can be found elsewhere,^{13, 16-18} along with further details about the solution technique. Convergence to the approximately steady-state solution is established by taking many forward time-steps.

Sample Computations

Standard Prediction

To demonstrate the capabilities of the solution scheme, predictions are now made and discussed for the case of a blockage located centrally in a sudden expansion chamber, at the expansion plane. In general, the blockage ratio BR is $(d/D)^2 = 0.25$ and the chamber expansion ratio $D'/D = 1.67$. Prechamber length ℓ and subsequent main chamber length L are $0.5 D'$ and $1.05 D'$, respectively. A 12×30 square mesh system [including fictitious cells] overlays the flow domain. A flat inlet axial velocity is imposed, with zero radial velocity. Transient computations are continued until steady state conditions establish themselves, roughly two flowfield resistance times later, corresponding to about 500 time-steps, and requiring about 120 s of CDC Cyber 174 CP time. The number of pressure-velocity iterations required per time-step depends on initial nonuniformities, but typically it is about 200 during early stages of transient computations and decreases to 1 as the steady-state solution is approached.

Predictions are first discussed for the case of a blockage located at the expansion plane, with sizes as just described. Figures 4 and 5 show the predicted recirculation zone size for the case of disk and cone blockages. Each computation in these and all other results shown is determined at the same Reynolds number, so chosen to match only the recirculation zone length for flow over the disk with blockage ratio BR of 0.25. Thus, the time-mean behavior of the turbulent flow is simulated via the use of an artificially large constant value given to laminar viscosity, in a manner reported elsewhere.^{17,18} Comparison with the experimental data of Ref. 10 is used for this single calibration. Nevertheless predicted zone lengths for other geometric configurations are seen to be very good in comparison to the data. As expected, the smaller the blockage forebody geometry cone half-angle [in going from disk with $\alpha = 90^\circ$ to a cone with $\alpha = 45^\circ$] the smaller the recirculation zone becomes. Figure 6 shows mass flow recirculated as a function of distance downstream for the case of a disk blockage with BR = 0.25. Again results compare favorably with the data. Velocity vectors are shown in Fig. 7 where central and corner recirculation zones are clearly evident.

Swirl Effect

The effect of inlet swirl, with flat swirl velocity w given by

$$w_{in} = u_{in} \tan \phi$$

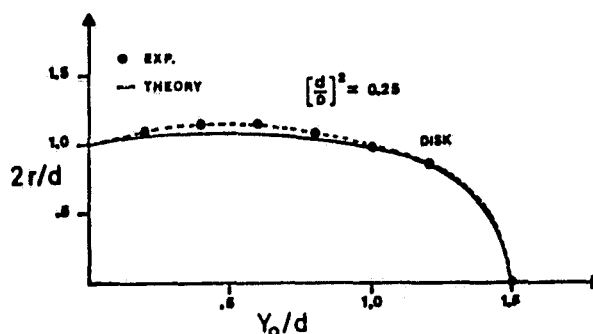


Fig. 4 Predicted and measured recirculation zone size with disk blockage, nonswirling flow [Blockage ratio = 0.25, — predictions, --- experiment¹⁰].

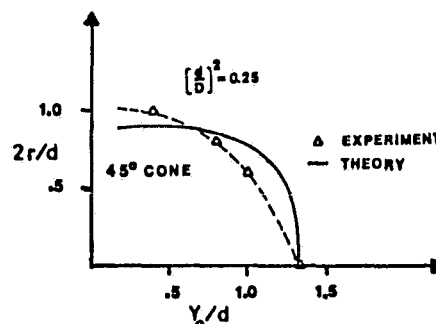


Fig. 5 Predicted and measured recirculation zone size with 45 deg. cone blockage, nonswirling flow [Blockage ratio = 0.25, — predictions, --- experiment¹⁰].

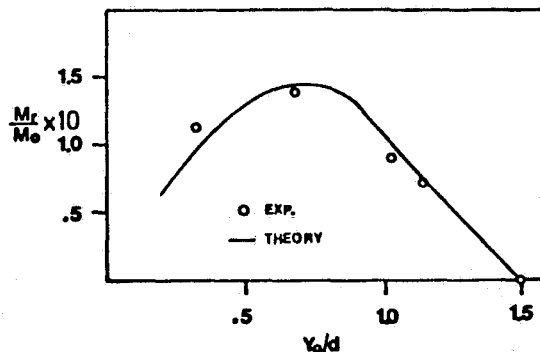


Fig. 6 Reverse mass-flow rate behind disk, nonswirling flow [Blockage ratio = 0.25, — predictions, --- experiment¹⁰].

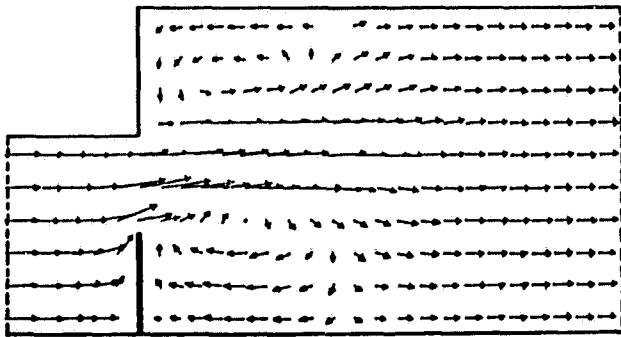


Fig. 7 Predicted velocity vectors with disk blockage and nonswirling flow.

is now considered as a perturbation about the standard disk prediction. This assumes that the inlet flow passes through swirl vanes so imposing a swirl angle ϕ to the axis direction. Recirculation zone size is seen in Fig. 8 to increase as swirl vane angle ϕ increases. This general effect of swirl is well-known, although specific experimental data in the present configuration are not available. Corresponding velocity vector plots for the $\phi = 60^\circ$ case are given in Fig. 9. In comparison with Fig. 7 for nonswirling flow, an increase in central recirculation zone length and a decrease in corner recirculation length are evident. These facts are well-known to combustion engineers.^{19,20} In the present case, strong centrifugal effects have also encouraged recirculation prior to the disk. Similar swirl predictions, albeit without central blockages, are available using more complex turbulent computer codes.^{21,22}

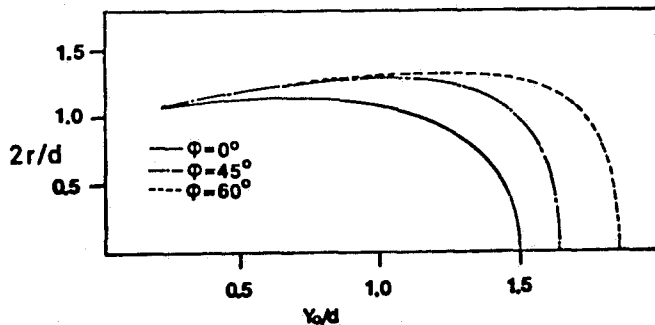


Fig. 8 Effect of swirl on recirculation zone boundary behind disk blockage [Blockage ratio = 0.25]

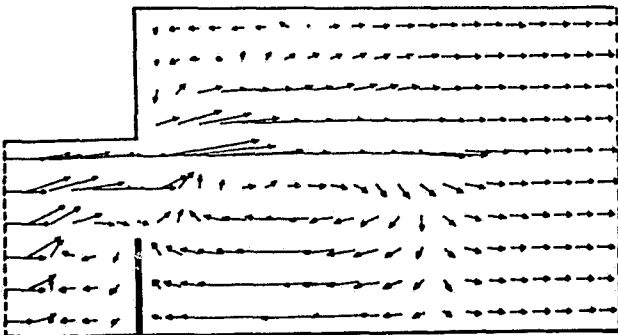


Fig. 9 Predicted velocity vectors with disk blockage and swirling flow with $\phi = 60^\circ$

Blockage Ratio Effect

Changes in disk diameter are accompanied by corresponding inverse changes in inlet axial velocity, so as to maintain the same Reynolds number based on disk size. However the velocity passing the blockage is then affected by available flow area, which is related to the inverse square of disk diameter. Prediction of blockage ratio $BR = (d/D)^2$ effect on central recirculation zone length [normalized with respect to particular disk diameter d] is given in Fig. 10 for nonswirling flow. Corresponding experimental data are very well predicted.

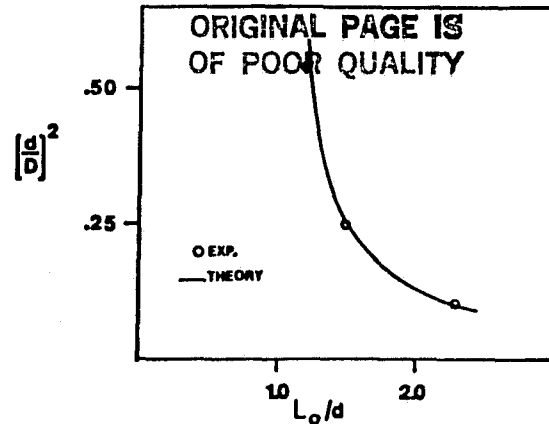


Fig. 10 Effect of blockage ratio on recirculation zone length behind disk blockage

Lateral Position Effect

The effect of lateral position of disk blockage [with blockage ratio $BR = 0.25$] is illustrated via velocity vector plots in Figs. 11 and 12, which show qualitatively the effect of upstream and downstream movements, respectively, of the blockage under nonswirling conditions. In the former case, higher velocities pass the disk and occur near the expansion corner, giving rise to larger central and corner recirculation zones than those seen in Fig. 7. In the latter case, lower velocities with an outward radial component pass the disk and occur near the expansion corner, giving rise to smaller central and corner recirculation zones than those seen in Fig. 7. Finally, Fig. 13 shows recirculation zone boundaries with respect to the disk location for the three axial locations considered.

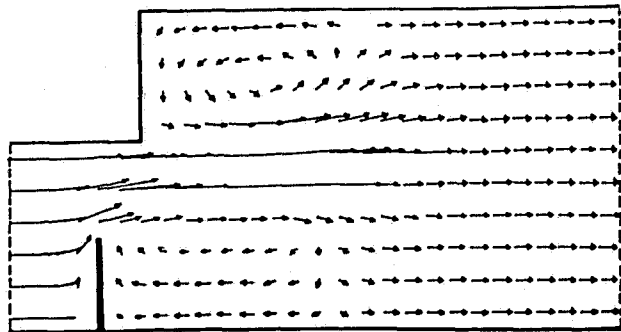


Fig. 11 Predicted velocity vectors with upstream located disk blockage and nonswirling flow

ORIGINAL PAGE IS
OF POOR QUALITY

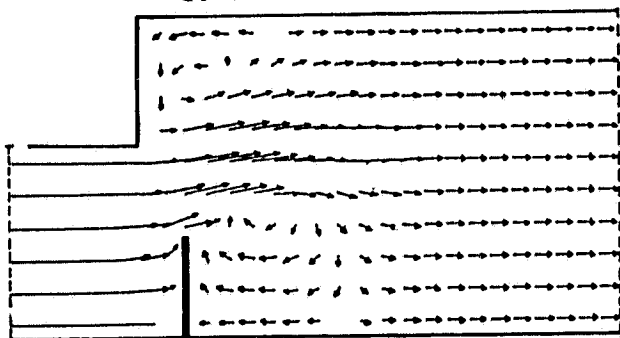


Fig. 12 Predicted velocity vectors with downstream located disk blockage and nonswirling flow

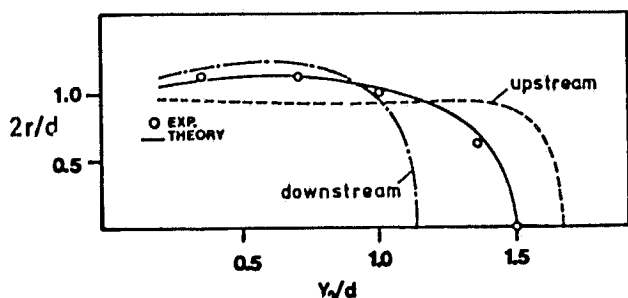


Fig. 13 Effect of blockage location on recirculation zone boundary behind disk blockage [Blockage ratio = 0.25]

Conclusions

Predictions of recirculation zones behind bluff-body flame stabilizers are now possible, showing the effects of complex geometric configurations on the size, shape, and reverse mass flow rate in subsequent recirculation zones. These recirculation eddies are now amenable to numerical solution via the simplified laminar flow finite difference technique presented here. Clearly the prediction of trends given in this paper take another step towards providing designers of practical equipment with useful qualitative results more cheaply and quickly than currently possible by more complex analytical and experimental means.

References

1. Beér, J. M., On the Stability and Combustion Intensity of Pressure Jet Oil Flames. *Combustion*, Vol. 37, 1965, pp. 27-44.
2. Carmody, T., Establishment of the Wake Behind a Disk. *Trans. ASME 86D, J. Basic Eng.*, Vol. 4, 1964, pp. 869-882.
3. Fail, R., Lawford, J. A., and Eyre, R. C. W., Low Speed Experiments on the Wake Characteristics of Flat Plates Normal to an Air Stream. *ARC RLM No. 3120*, 1959.
4. Winterfeld, G., On Processes of Turbulent Exchange Behind Flameholders. 10th Symp. (Int.) on Combustion, The Comb. Inst., Pittsburgh, PA, 1965, pp. 1265-1275.

5. Lefebvre, A. H., Ibrahim, A. R. A. F., and Benson, N. C., Factors Affecting Fresh Mixture Entrainment in Bluff-Body Stabilized Flames. *Combustion and Flame*, Vol. 10, 1966, pp. 231-239.
6. Chigier, N. A., and Beér, J. M., The Flow Region Near the Nozzle in Double Concentric Jets. *J. Basic Eng.*, Vol. 4, 1964, pp. 797-804.
7. Chigier, N. A., and Gilbert, J. L., Recirculation Eddies in the Wake of Flameholders. *J. Inst. Fuel*, Vol. 12, 1968, pp. 105-112.
8. Ullrich, M., *Forschung auf dem Gebiete des Ingenieurwesens*, 1959, pp. 165-181, 1960, pp. 19-28.
9. Patrick, M. A., Ph.D. Thesis, Sheffield Univ., England, 1965.
10. Davies, T. W., and Beér, J. M., Flow in the Wake of Bluff-Body Flame Stabilizers. 13th Symp. (Int.) on Comb., The Comb. Inst., Pittsburgh, PA, 1971, pp. 631-638.
11. Harlow, F. H., and Weisich, J. E., Numerical Calculation of Time-Dependent Viscous Incompressible Flow of Fluid with Free Surface (The MAC Method), *Physics of Fluids*, Vol. 8, 1965, pp. 2182-2189.
12. Amsden, A. A., and Harlow, F. H., The SMAC Method: A Numerical Technique for Calculating Incompressible Fluid Flows, Report LA-4379, Los Alamos Scientific Laboratory, Los Alamos, NM, 1970.
13. Hirt, C. W., Nichols, B. D., and Romero, N. C., SOLA: A Numerical Solution Algorithm for Transient Fluid Flows, Report LA-5882, Los Alamos Scientific Laboratory and the University of California, Los Alamos, NM, 1975.
14. Gosman, A. D., and Pun, W. M., Lecture Notes for Course Entitled "Calculation of Recirculating Flows," Report HTS/74/2, Dept. of Mechanical Engineering, Imperial College, London, 1974.
15. Patankar, S. V., *Numerical Heat Transfer and Fluid Flow*, McGraw-Hill, New York, 1980.
16. Vatistas, G. H., "Computational Flow Prediction in Cyclone Chambers", Masters of Engineering Thesis, Concordia University, Mechanical Engineering Department, 1980.
17. Busnaina, A. A., and Lilley, D. G., Numerical Simulation of Swirling Flow in a Cyclone Chamber. *Proc. ASME Symp. on Fluid Mechanics of Combustion Systems*, Boulder, CO, June 22-24, 1981, pp. 169-178.
18. Busnaina, A. A., and Lilley, D. G., A Simple Finite Difference Procedure for the Vortex Controlled Diffuser. Paper AIAA 82-0109, Orlando, FL, Jan. 11-14, 1982.
19. Lilley, D. G., "Swirl Flows in Combustion: A Review," *AIAA Journal*, Vol. 15, Aug. 1977, pp. 1063-1078.
20. Gupta, A. K., Lilley, D. G., and Syred, N., *Swirl Flows*, Applied Science Publishers, London, 1981.

21. Novick, A. S., Miles, G., and Lilley, D. G.,
 "Numerical Simulation of Combustor Flow Fields,"
 Journal of Energy, Vol. 3, No. 2, March-April
 1979, pp. 95-105.
22. Rhode, D. L., Lilley, D. G., and McLaughlin,
 D. K., On the Prediction of Swirling Flow-
 fields in Axisymmetric Combustor Geometries.
 ASME Journal of Fluids Engrg., 1982 (in press).

**ORIGINAL PAGE IS
 OF POOR QUALITY**

Nomenclature

D	Prechamber diameter
D'	Main chamber diameter
d	Blockage diameter
i, j	Mesh point
ℓ	Prechamber length
L	Main chamber length
L	Length of recirculation zone
p ^o	Ratio of pressure to constant density
r	Radial coordinate
t	Time
u, v, w	Velocity components in x(≡r), y(≡ axial) and θ coordinate directions
x, y, θ	Cylindrical polar coordinates [in radial, axial and swirl directions]
Y _o	Axial coordinate measured from blockage base
ν	Kinematic viscosity
φ	Swirl vane angle

Subscript

in Inlet

Acknowledgment

The authors appreciate support from NRC Canada
 Grant No. A7435 and NASA Lewis Research Center Grant
 No. NAG 3-74.

APPENDIX E

TURBULENCE MEASUREMENTS IN A CONFINED JET
USING A SIX-ORIENTATION HOT-WIRE PROBE TECHNIQUE

AIAA-82-1262

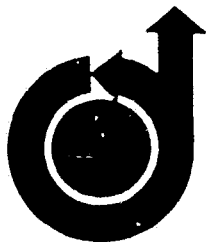
**Turbulence Measurements In A
Confined Jet Using A Six-Orientation
Hot-Wire Probe Technique**

S. I. Janjua and D. K. McLaughlin, Dynamics Technology, Inc.,

Torrance, CA,

T. W. Jackson and D. G. Lilley, Oklahoma State Univ.,

Stillwater, OK



**AIAA/SAE/ASME
18th Joint Propulsion Conference
June 21-23, 1982/Cleveland, Ohio**

**ORIGINAL PAGE IS
OF POOR QUALITY**

**TURBULENCE MEASUREMENTS IN A CONFINED JET USING A
SIX-ORIENTATION HOT-WIRE PROBE TECHNIQUE**

S. I. Janjua* and D. K. McLaughlin**
Dynamics Technology, Inc., Torrance, California

and

T. Jackson† and D. G. Lilley††
Oklahoma State University, Stillwater, OK:

Abstract

The six-orientation single hot-wire technique has been applied to the complex flowfield of a swirling, confined jet. This flowfield, which contains a rapid expansion with resulting recirculation regions, is typical of those found in gas turbine engines and ramjet combustors. The present study focusses on turbulence measurements in such a flowfield in the absence of chemical reaction.

A modification to the six-orientation hot-wire technique developed by King has been made, which incorporates the determination of turbulent shear stresses (in addition to normal stresses) and ensemble averaging of redundant turbulence output quantities. With this technique, flowfield surveys have been performed in both swirling and nonswirling axisymmetric confined jets. Where independent data exist, comparisons have been made which demonstrate the reliability of the technique. Finally, a sensitivity analysis of the data reduction technique has been completed which forms the major ingredient in an uncertainty analysis.

Nomenclature

A, B, C	Calibration constants in Equation 1
AO, BO, CO	Cooling velocity functions in Table 1
D	Test section diameter
d	Inlet nozzle diameter
E	Hot-wire voltage
U	Velocity function for axial velocity
W	Velocity function for azimuthal velocity
V	Velocity function for radial velocity
G	Pitch factor
K	Yaw factor
$K_{z_p z_q}$	Covariance for cooling velocities Z_p , and Z_q
P, Q, R	Selected hot-wire probe positions
Re _d	Inlet Reynolds number
u	Axial velocity
v	Radial velocity
w	Azimuthal (swirl) velocity
$\tilde{u}, \tilde{w}, \tilde{v}$	Three components of velocity in probe coordinates defined by Figure 5
x, r, θ	Axial, radial, azimuthal cylindrical polar coordinates
Z	Effective cooling velocity acting on a wire

α	Side-wall expansion angle
$\gamma_{z_i z_j}$	Correlation coefficient (estimated) between cooling velocities of adjacent wire orientations
σ^2	Variance of a given quantity
ϕ	Inverse function of calibration equation
Φ	Swirl vane angle

Subscripts

1, 2, 3, 4, 5, 6	Refers to the six probe measuring positions
i, j	Dummy indices which take the values 1 to 3
P, Q, R	Refers to the three selected measuring positions
rms	Root-mean-squared quantity

Superscripts

'	Time-mean average
'	Fluctuating quantity

1. Introduction

1.1 The Gas Turbine Combustor Flowfield

Recent emphasis on fuel economy and pollutant suppression has sparked a renewed interest in gas turbine combustor analysis. A typical axisymmetric gas turbine engine combustor is shown in Figure 1. Flowfields within such combustors typically have a rapid expansion and strong swirl imparted to the incoming air, which result in corner and central recirculation regions. The swirling, recirculating, turbulent flows within combustors present one of the more difficult fluid dynamic problems to analyze. This complexity is increased many fold by the processes of combustion and heat transfer within the flowfield. Despite the complexity of combustor flows, significant progress is being made in their analysis.

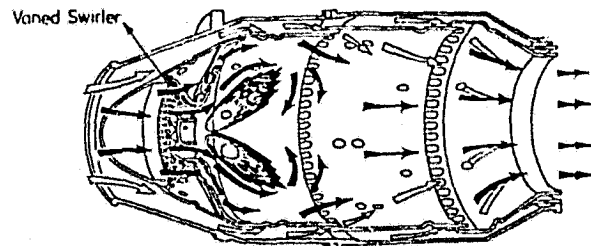


Figure 1. Axisymmetric Combustor of a Gas Turbine Engine

* Research Engineer, Member AIAA
 ** Senior Research Scientist, Member AIAA
 † Graduate Student, Student Member AIAA
 †† Professor, Associate Fellow AIAA

The present paper reports on research which is part of an extensive experimental and computational study of gas turbine flowfields in the absence of combustion. Figure 2 shows the characteristics of the simplified flowfield being investigated. Flow enters through a jet of diameter d into a tube of diameter D , after being expanded through an angle α . Before entering the tube, the flow may be swirled by a swirler located upstream of the inlet plane. Shown schematically are the corner recirculation zone (CRZ) and the central toroidal recirculation zone (CTRZ) which are typically present in these flows.

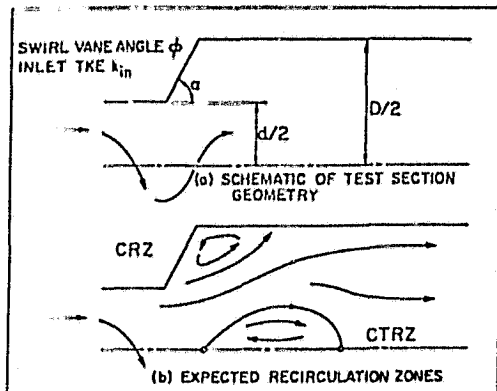


Figure 2. Idealized Combustor Flowfield

The swirling confined jet flowfield shown in Figure 1 is being investigated at Oklahoma State University and at Dynamics Technology, with various methods of approach. Analytically, a computer program (STARPIC) has been assembled which is designed specifically to calculate the swirling confined jet flowfields.² Experimentally, a series of flow visualization experiments coupled with 5-hole pitot probe measurements have been used to characterize the time-mean flowfield.³ Hot-wire measurements of the turbulence properties are also being conducted. This paper reports on the initial results of the hot-wire measurements in the confined jet flowfield.

Several studies on time-mean flowfields of the type just described have been carried out using various turbulence measuring techniques.⁴⁻¹⁰ Unfortunately, most of the techniques used do not give complete and detailed information about the flow in terms of all its time-mean and turbulence quantities. In addition, no experiments have been performed on the specific geometry of the present study in the presence of inlet swirl. To develop further the flowfield computational techniques, including the turbulence modeling, there is a strong need to obtain experimental estimates of the turbulence and mean flow quantities in such flows.

1.2 The Turbulence Measurement Problem

Turbulence measurement in a complex flowfield has always been a complicated problem encountered by engineers. In the past, turbulence phenomena have been discussed by various authors in detail and various methods of turbulence measurements

have been suggested.¹¹⁻¹³ One of the most widely used instruments to obtain turbulence quantities is the hot-wire anemometer, the most common of which is a single hot-wire. When used at a single orientation and in a two-dimensional flow with a predominant flow direction, a single hot-wire can measure the streamwise components of the time-mean velocity and the root-mean-square velocity fluctuation at a particular location in the flowfield. A two-wire probe can be used to determine the time-mean velocities, streamwise and cross stream turbulence intensities, and the cross correlation between the two components of the velocity fluctuations.¹⁴⁻¹⁵

Hot-wire measurements in complex three-dimensional flowfields are considerably more difficult than in one- or two-dimensional flowfields in which the mean flow is predominantly in one direction. To measure the three velocities and their corresponding fluctuating components in a three-dimensional flowfield such as encountered in combustor simulators, there are two methods that can be employed at a point in the flowfield:

- 1) A three-wire probe used with a single orientation.
- 2) A single- or double-wire probe used with multi-orientation.

The three-wire probe technique permits the necessary simultaneous measurements from which three instantaneous velocity components can be determined. The appropriate signal processing can produce estimates of mean velocity components and normal and shear turbulent stresses (such as $\overline{u'^2}$ and $\overline{u'v'}$).

The three-hot-wire probe technique is significantly more complex than the single wire multi-orientation techniques. A multi-dimensional probe drive is required to orient the probe in approximately the mean flow direction. Also, sophisticated signal processing electronics is required to handle the three instantaneous hot-wire voltages. Finally, the three-wire probe typically has less spatial resolution in comparison with a single wire probe.

Multi-orientation of a single hot-wire is a novel way to measure the three components of a velocity vector and their fluctuating components. A method devised by Dvorak and Syred¹⁶ uses a single normal hot-wire oriented at three different positions such that the center one is separated by 45 degrees from the other two. The velocity vector at a location is related to the three orthogonal components using pitch and yaw factors as defined by Jorgensen.¹⁷ The data are obtained in the form of mean and root-mean-square voltages at each orientation. However, the measurements done with a single wire do not supply all the information needed to obtain the turbulence quantities. Therefore, in addition to a single wire, Dvorak and Syred used a cross-wire probe to obtain the covariances between the voltages obtained at adjacent hot-wire orientations.

King¹⁸ modified the technique developed by Dvorak and Syred. His method calls for a normal hot-wire to be oriented through six different positions, each orientation separated by 30 degrees from the adjacent one. Mean and root-mean-square

ORIGINAL PAGE IS OF POOR QUALITY

voltages are measured at each orientation. The data reduction is performed using some assumptions regarding the statistical nature of turbulence, making it possible to solve for the three time-mean velocities, the three normal turbulent stresses, and the three turbulent shear stresses.

1.3 The Scope of the Present Study

In the present study, the six-orientation single normal hot-wire technique is being employed to obtain the turbulence quantities in the combustor simulator confined jet flowfield. Measurements have been carried out for both swirling and nonswirling flow with expansion angles of 90 degrees (sudden expansion) and 45 degrees (gradual expansion). Only the 90 degree angle data are presented here and the Reynolds number of the inlet flow is $\approx 5 \times 10^4$ which is comparable with aircraft combustor flows (although our experiments are performed in nonreacting flows). The data reduction procedure extends King's technique to obtain turbulent shear and normal stresses using six basic response equations representing the six orientations of a normal hot-wire positioned in the flowfield. Certain modifications are made in the procedure to calculate covariances which are an integral part of the data reduction procedure. An uncertainty analysis is performed on the technique which reveals the sensitivity of this technique to various input parameters discussed in the later parts of this paper. Some of the turbulence quantities obtained are compared with measurements performed by Chaturvedi⁵ using a crossed-wire probe in a corresponding flow situation.

2. Experimental Facility and Instrumentation

2.1 Idealized Flowfield

The facility, designed and built at Oklahoma State University, is a simulation of a typical axisymmetric combustion chamber of a gas turbine engine shown in Figure 1. The schematic of the test facility with the idealized flowfield is shown in Figure 3. Ambient air enters the low-speed wind tunnel through a foam air filter. The air then flows through an axial flow fan driven by a 5 h.p. variable drive motor. Thus, the flow rate can be varied for different test conditions. The flow passes through a turbulence management section which has two fine-mesh screens, a 12.7 cm length of packed straws, and five more fine-mesh screens.

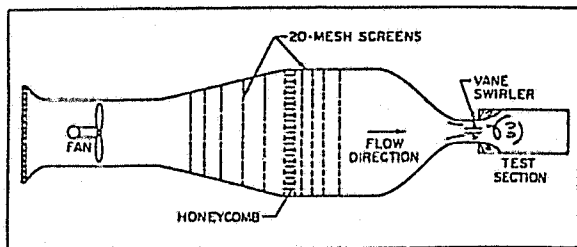


Figure 3. Schematic of the Experimental Facility

The axisymmetric nozzle was designed to produce a minimum adverse pressure gradient on the boundary layer to avoid flow unsteadiness associated with local separation regions. The area ratio of the cross sections of the turbulence management section to that of the nozzle throat is approximately 22.5. The diameter, d , of the nozzle throat is approximately 15 cm.

The test section is composed of a swirler (optional), an expansion block, and a long plexiglass tube. The expansion block, attached after the swirler, is a 30 cm diameter annular disk of wood. At present, there are three expansion blocks, and the appropriate choice gives $\alpha = 90, 70, \text{ or } 45$ degrees. The flow is expanded into a plexiglass tube of diameter, D , of 30 cm, thus giving a diameter expansion ratio (D/d) of 2. The test chamber has no film cooling holes or dilution air holes, and the chamber wall of the test section is a constant diameter pipe.

2.2 Hot-Wire Instrumentation

The anemometer used for the present study is DISA type 55M01, CTA standard bridge. A normal hot-wire probe, DISA type 55P01, is used in the experiments. This probe has two prongs set approximately 3 mm apart which support a 5 μm diameter wire which is gold plated near the prongs to reduce end effects and strengthen the wire. The mean voltage is measured with a Hickok Digital Systems, Model DP100, integrating voltmeter and the root-mean-square voltage fluctuation is measured using a Hewlett Packard, Model 400 HR, AC voltmeter.

The hot-wire is supported in the facility by a traversing mechanism shown schematically in Figure 4. It consists of a base that is modified to mount on the plexiglass tube of the test section at various axial locations. The hot-wire probe is inserted into the tube through a rotary vernier and the base. The rotary vernier is attached to a slide which can traverse across the flow chamber. Thus, it is possible for the probe to be traversed to any radial location at selected downstream locations in the flowfield and to be rotated through 180 degrees.

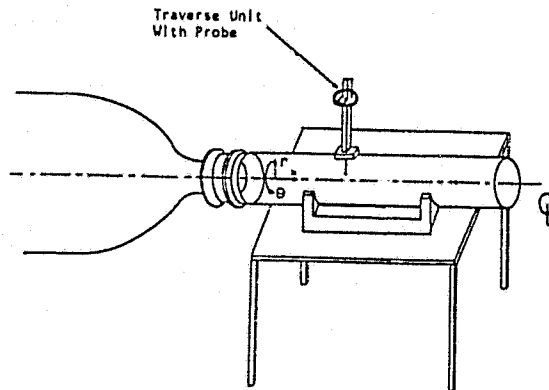


Figure 4. Hot-Wire Probe Mounted on the Test Section

* Provided for information and not necessarily a product endorsement.

2.3 Calibration Nozzle

The hot-wire is calibrated in a small air jet. The facility consists of a compressed air line, which delivers the desired flow rate through a small pressure regulator and a Fisher and Porter Model 10A1735A rotameter. The jet housing consists of an effective flow management section followed by a contoured nozzle with a 3.5 cm diameter throat. A rotary table is used to hold the probe while it is being calibrated in three different orientations.

3. Hot-Wire Data Analysis

3.1 Hot-Wire Response Equations

The six-orientation hot-wire technique requires a single, straight, hot-wire to be calibrated for three different flow directions in order to determine the directional sensitivity of such a probe. The three directions and three typical calibration curves are shown in Figure 5. In these relations, tildes signify components of the instantaneous velocity vector in coordinates on the probe. Each of the three calibration curves is obtained with zero velocity in the other two directions. The calibration curves demonstrate that the hot-wire is most efficiently cooled when the flow is in the direction of the \tilde{u} component, whereas, the wire is most inefficiently cooled when the flow is in the direction of the \tilde{w} component. Each of the calibration curves follows a second order, least square fit of the form:

$$E_i^2 = A_i + B_i \tilde{u}_i^{1/2} + C_i \tilde{u}_i \quad (1)$$

which is an extension of the commonly used King's law. In this equation, A_i , B_i , and C_i are calibration constants and \tilde{u}_i can take on a value of \tilde{u} , \tilde{v} , and \tilde{w} for the three calibration curves, respectively.

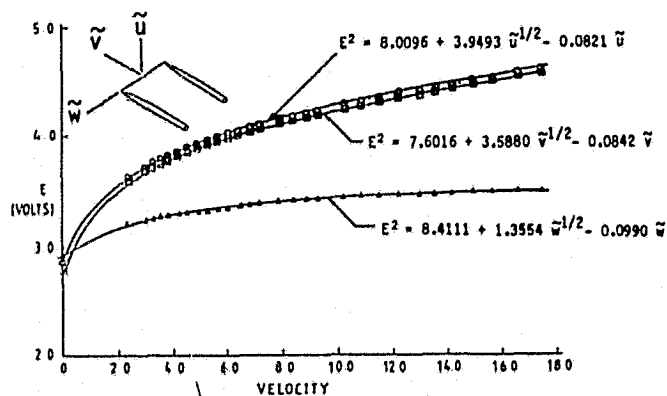


Figure 5. The Three-Directional Hot-Wire Calibration

When the wire is placed in a three dimensional flowfield, the effective cooling velocity experienced by the hot-wire is:

$$Z^2 = \tilde{v}^2 + G^2 \tilde{u}^2 + K^2 \tilde{w}^2 \quad (2)$$

where G and K are the pitch and yaw factors defined by Jorgensen¹⁷ to be:

$$G = \frac{\tilde{v}(\tilde{u} \text{ and } \tilde{w}=0)}{\tilde{u}(\tilde{v} \text{ and } \tilde{w}=0)}, \text{ and}$$

$$K = \frac{\tilde{v}(\tilde{u} \text{ and } \tilde{w}=0)}{\tilde{w}(\tilde{u} \text{ and } \tilde{v}=0)} \quad (3)$$

which are evaluated from the three calibration curves (Figure 5) for a constant value of E^2 . Equation (3) shows that the pitch and yaw factors are calculated with the \tilde{v} component $i = 2$ in equation (1) of the effective cooling velocity as the reference. Therefore, the calibration constants used in equation (1) are the coefficients in the E vs. \tilde{v} calibration of Figure 5., i.e., in a general flowfield:

$$E^2 = A_2 + B_2 Z^{1/2} + C_2 Z$$

with Z as given in Equation (2) above.

Figure 6 shows the pitch and yaw factors as a function of hot-wire voltage determined from the calibration curve of Figure 5. Both factors vary with hot-wire voltage, but the yaw factor is far more sensitive. The sensitivity analysis discussed in the next section demonstrates that uncertainties associated with the varying pitch and yaw factors do not seriously affect the accuracy of the estimated flow quantities.

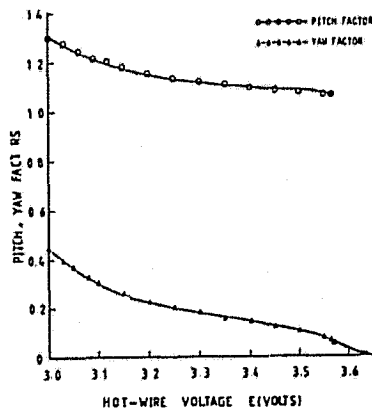


Figure 6. Pitch and Yaw Factors Plotted Against Hot-Wire Mean Effective Voltage

To carry out measurements in the confined jet flowfield, the wire is aligned in the flow in such a way that in the first orientation, the wire is normal to the flow in the axial direction and the probe coordinates coincide with the coordinates of

ORIGINAL PAGE IS
OF POOR QUALITY

the experimental facility. Thus, the six equations for the instantaneous cooling velocities at the six orientations, as given by King¹⁸ are:

$$\begin{aligned} Z_1^2 &= v^2 + G^2 u^2 + K^2 w^2 \\ Z_2^2 &= v^2 + G^2(u \cos 30^\circ + w \sin 30^\circ)^2 \\ &\quad + K^2(w \cos 30^\circ - u \sin 30^\circ)^2 \\ Z_3^2 &= v^2 + G^2(u \cos 60^\circ + w \sin 60^\circ)^2 \\ &\quad + K^2(w \cos 60^\circ - u \sin 60^\circ)^2 \\ Z_4^2 &= v^2 + G^2 w^2 + K^2 u^2 \\ Z_5^2 &= v^2 + G^2(w \sin 120^\circ + u \cos 120^\circ)^2 \\ &\quad + K^2(u \sin 120^\circ - w \cos 120^\circ)^2 \\ Z_6^2 &= v^2 + G^2(w \sin 150^\circ + u \cos 150^\circ)^2 \\ &\quad + K^2(u \sin 150^\circ - w \cos 150^\circ)^2 \end{aligned} \quad (4)$$

Solving simultaneously any three adjacent equations provide expressions for the instantaneous values of the three velocity components, u, w, and v in terms of the equivalent cooling velocities (Z₁, Z₂ and Z₃ for example, when the first three equations are chosen). Thus, the general form of the instantaneous velocity components is given as:

$$\begin{aligned} U &= \left[\left\{ AO + \left(AO^2 + \frac{BO^2}{3} \right)^{1/2} \right\} \frac{1}{(G^2 - K^2)} \right]^{1/2} \\ W &= \left[\left\{ -AO + \left(AO^2 + \frac{BO^2}{3} \right)^{1/2} \right\} \frac{1}{(G^2 - K^2)} \right]^{1/2} \\ V &= \left[CO - \frac{(G^2 + K^2)}{(G^2 - K^2)} \left(AO^2 + \frac{BO^2}{3} \right)^{1/2} \right]^{1/2} \end{aligned} \quad (5)$$

The values of AO, BO and CO depend on the set of the three equations chosen and are given in Table 1 for appropriate equation sets.

TABLE 1

Values of AO, BO, and CO in Various Equation Sets

Equation Set P, Q, R Choice	AO	BO	CO
1, 2, 3	(Z ₂ ² - Z ₃ ²)	(-2Z ₁ ² + 3Z ₂ ² - Z ₃ ²)	(Z ₁ ² - Z ₂ ² + Z ₃ ²)
2, 3, 4	(Z ₂ ² - Z ₃ ²)	(-Z ₂ ² + 3Z ₃ ² - 2Z ₄ ²)	(Z ₂ ² - Z ₃ ² + Z ₄ ²)
3, 4, 5	(Z ₃ ² - 2Z ₄ ² + Z ₅ ²)	(Z ₃ ² - Z ₅ ²)	(Z ₃ ² - Z ₄ ² + Z ₅ ²)
4, 5, 6	(-Z ₅ ² + Z ₆ ²)	(-2Z ₄ ² + 3Z ₅ ² - Z ₆ ²)	(Z ₄ ² - Z ₅ ² + Z ₆ ²)
5, 6, 1	(-Z ₅ ² + Z ₆ ²)	(-Z ₅ ² + 3Z ₆ ² - 2Z ₁ ²)	(Z ₅ ² - Z ₆ ² + Z ₁ ²)
6, 1, 2	(-Z ₆ ² + 2Z ₁ ² - Z ₂ ²)	(-Z ₆ ² + Z ₂ ²)	(Z ₆ ² - Z ₁ ² + Z ₂ ²)

However, these equations cannot be directly used because it is impossible to obtain Z₁, Z₂ and Z₃ at a single instant in time with a single wire

probe. Therefore, Equations (5) must be expressed in terms of mean and root-mean-square values. Equation (1) can be written as:

$$Z_1 = [-B_2 + \{B_2^2 + 4C_2(A_2 - E_1^2)\}^{1/2} / 2C_2]^2 \quad (6)$$

The above equation is in terms of instantaneous velocity Z₁ and instantaneous voltage E₁. In order to obtain an expression for time-mean velocity as a function of time-mean voltage, a Taylor series expansion of Equation (6) can be carried out as follows:

$$Z_1 = Z_1(\bar{E}_1 + E_1') = \phi(\bar{E}_1) + \frac{E_1'}{1!} \frac{\partial \phi}{\partial E_1} + \frac{E_1'^2}{2!} \frac{\partial^2 \phi}{\partial E_1^2} + \dots \quad (7)$$

where $\phi = Z_1(\bar{E}_1)$.

The Taylor series is truncated after second order terms assuming the higher order terms to be relatively small. Time averaging both sides of the above equation and employing the fact that E'₁ = 0, yields:

$$\bar{Z}_1 = \phi + \frac{1}{2} \frac{\partial^2 \phi}{\partial E_1^2} \sigma_{E_1}^2 \quad (8)$$

To obtain $\overline{Z_1^2} = \sigma_{Z_1}^2$, the relationship as given by Hinze¹⁹ is:

$$\overline{Z_1^2} = \sigma_{Z_1}^2 = \text{Expec}[Z_1^2] - (\text{Expec}[Z_1])^2 \quad (9)$$

Using Equation (8) as the basis, Expec[Z₁²] and (Expec[Z₁])² can be evaluated and substituted into Equation (9) to get:

$$\overline{Z_1^2} = \sigma_{Z_1}^2 = \frac{\partial \phi^2}{\partial E_1^2} \sigma_{E_1}^2 - \left(\frac{1}{2} \frac{\partial^2 \phi}{\partial E_1^2} \sigma_{E_1}^2 \right)^2 \quad (10)$$

Thus, Equations (8) and (10) give the mean and variance of effective cooling velocities in terms of the mean and variance of the appropriate voltages.

In a 3-dimensional flow, it is usually desirable to obtain the mean and variance for the individual velocity components in axial, azimuthal, and radial directions, and also their cross correlations. The procedure to obtain the mean and variance of the individual velocity components is the same as for the effective cooling velocities except that u, w and v are functions of three random variables and there are extra terms in the Taylor expansion to account for the covariances of the cooling velocities. Thus, the axial mean velocity component as given by Dvorak and Syred,¹⁶ and King¹⁸ is:

$$\bar{u} = U(\bar{Z}_P, \bar{Z}_Q, \bar{Z}_R) + \frac{1}{2} \sum_{i=1}^3 \frac{\partial^2 U}{\partial Z_i^2} \sigma_{Z_i}^2 + \sum_{i < j}^3 \frac{\partial^2 U}{\partial Z_i \partial Z_j} K_{Z_i Z_j} \quad (11)$$

where K_{Z_iZ_j} is the covariance of the cooling velocities Z_i and Z_j and is defined as:

$$K_{Z_i Z_j} = \frac{1}{T} \int_0^T (Z_i - \bar{Z}_i)(Z_j - \bar{Z}_j) dt \quad (12)$$

Identical expressions for \bar{w} and \bar{v} can also be obtained in terms of W and V , respectively. Derivatives of the form $\partial^2 U / \partial Z_i \partial Z_j$ are determined analytically from equations (5) and Table 1.

Also, the normal stresses are given as:

$$\begin{aligned} \overline{u'^2} &= \sum_{i=1}^3 \left(\frac{\partial U}{\partial Z_i} \right)^2 \sigma_{Z_i}^2 + \sum_{i \neq j}^3 \sum_{i < j}^3 \frac{\partial U}{\partial Z_i} \frac{\partial U}{\partial Z_j} \cdot K_{Z_i Z_j} \\ &- \left[\frac{1}{2} \sum_{i=1}^3 \frac{\partial^2 U}{\partial Z_i^2} \sigma_{Z_i}^2 + \sum_{i < j}^3 \sum_{i < j}^3 \frac{\partial^2 U}{\partial Z_i \partial Z_j} \cdot K_{Z_i Z_j} \right]^2 \quad (13) \end{aligned}$$

with similar expressions for $\overline{w'^2}$ and $\overline{v'^2}$.

Finally, the expressions for shear stresses as given by Dvorak and Syred¹⁶ are of the form:

$$\begin{aligned} \overline{u'v'} &= \sum_{i=1}^3 \frac{\partial U}{\partial Z_i} \frac{\partial V}{\partial Z_i} \sigma_{Z_i}^2 + \sum_{i \neq j}^3 \sum_{i < j}^3 \frac{\partial U}{\partial Z_i} \frac{\partial V}{\partial Z_j} K_{Z_i Z_j} \\ &- \left[\frac{1}{2} \sum_{i=1}^3 \frac{\partial^2 U}{\partial Z_i^2} \sigma_{Z_i}^2 + \sum_{i < j}^3 \sum_{i < j}^3 \frac{\partial^2 U}{\partial Z_i \partial Z_j} \cdot K_{Z_i Z_j} \right] \\ &\cdot \left[\frac{1}{2} \sum_{i=1}^3 \frac{\partial^2 V}{\partial Z_i^2} \sigma_{Z_i}^2 + \sum_{i < j}^3 \sum_{i < j}^3 \frac{\partial^2 V}{\partial Z_i \partial Z_j} \cdot K_{Z_i Z_j} \right] \quad (14) \end{aligned}$$

Expressions for $\overline{u'w'}$ and $\overline{v'w'}$ can also be obtained in a similar manner and are given in Reference 22.

3.2 Calculation of Covariances

Dvorak and Syred¹⁶ used a DISA time correlator (55A06) to find the correlation coefficients between the velocity fluctuations in the three directions. King's approach is to use the information obtained by all six orientations and devise a mathematical procedure to calculate the covariances.

Covariances are calculated using the relationship:

$$K_{Z_i Z_j} = \gamma_{Z_i Z_j} [\sigma_{Z_i}^2 \sigma_{Z_j}^2]^{1/2} \quad (15)$$

where $\gamma_{Z_i Z_j}$ is the correlation coefficient between the two cooling velocities Z_i and Z_j . By definition, the absolute value of the correlation coefficient $\gamma_{Z_i Z_j}$ is always less than 1.

King¹⁸ made certain assumptions to calculate the covariances. However, he observed that at times the calculated value of the correlation coefficient is greater than one at which instance he assigned previously fixed values to the correlation coefficients. He argued that if two wires are separated by an angle of 30 degrees, the fluctuating signals from the wires at the two loca-

tions would be such that their contribution to the cooling of the wire would be related by the cosine of the angle between the wires. This assumption leads to the following three values of the correlation coefficients.

$$\gamma_{Z_P Z_Q} = \cos 30 \approx 0.9 \quad (16)$$

$$\gamma_{Z_Q Z_R} = \cos 30 \approx 0.9$$

To relate $\gamma_{Z_P Z_R}$ with $\gamma_{Z_P Z_Q}$ and $\gamma_{Z_Q Z_R}$, King introduced the following relationship:

$$\gamma_{Z_P Z_R} = \eta \gamma_{Z_P Z_Q} \gamma_{Z_Q Z_R} \quad (17)$$

where η is given a value of 0.8. Hence $\gamma_{Z_P Z_R}$ becomes:

$$\gamma_{Z_P Z_R} = (0.8)(0.9)(0.9) = 0.65 \quad (18)$$

The three covariances are then obtained by substituting the corresponding values of the correlation coefficients into Equation (15).

The present study, however, uses Equations (16) and (18) during the entire data reduction. The reason for this is contained in the results of the sensitivity analysis presented in the next section. This analysis demonstrated that there is not significant error magnification in the data reduction due to the correlation terms.

4. Results of Hot-Wire Measurements

The six-orientation hot-wire technique was employed to measure the turbulence quantities for swirling and non-swirling flow conditions in the confined jet facility described earlier. Also, an extensive sensitivity analysis of the data reduction was conducted to assist the estimation of the uncertainties in the output quantities.

4.1 Uncertainty Analysis

The uncertainty analysis includes a determination of the sensitivity of the six-orientation hot-wire data reduction to various input parameters which have major contributions in the response equations. Pitch and yaw factors (G and K) are used in the response equations described in Section 3 in order to account for the directional sensitivity of the single hot-wire probe. Figure 6 shows the pitch and the yaw factors plotted against the hot-wire mean effective voltage. Both the pitch and yaw factors are functions of the hot-wire mean effective voltage, but the yaw factor is far more sensitive. A one percent increase in the hot-wire voltage reduces the pitch factor by 1.3 percent and the yaw factor by 56 percent. For the present study, the values of these factors are chosen at an average hot-wire voltage experienced in the flowfield. This was appropriate since the output quantities (u , u'_{rms} , $u'v'$, etc) are only weakly dependent on the value of K. This can be seen in the data of Table 2 which summarizes a sensitivity analysis performed on the data reduction program at a

**ORIGINAL PAGE IS
OF POOR QUALITY**

representative position in the flowfield.

Table 2 demonstrates the percent change in the output quantities for a 1 percent change in most of the important input quantities. For the data presented in this table only quantities calculated from the probe orientation combination \bar{Z}_5 , \bar{Z}_6 and \bar{Z}_1 are used, for simplicity. In this swirling flow \bar{Z}_6 was the minimum of the 6 mean effective cooling velocities. King¹⁸ has argued that the probe orientation combination approximately centered around the minimum effective cooling velocity produces more accurate estimates of calculated turbulence quantities, than do the other orientation combinations.

TABLE 2
Effect of Input Parameters on Turbulence Quantities

PARAMETER	% CHANGE IN PARAMETER	% CHANGE IN TIME-MEAN AND TURBULENCE QUANTITIES								
		\bar{u}	\bar{v}	\bar{w}	u'_{rms}	v'_{rms}	w'_{rms}	$u'v'$	$u'w'$	$v'w'$
\bar{E}_1	+1	+16.10	+0.66	+4.98	+15.75	-2.06	+2.75	+6.0	+51.43	+11.94
\bar{E}_5	+1	+2.19	-2.21	+11.49	-6.50	+2.42	+12.88	+4.0	+14.29	+7.46
\bar{E}_6	+1	-10.59	-0.36	-8.50	-1.88	+7.07	-9.54	-6.0	-54.29	-11.94
E^1_{rms}	+1	+0.27	-0.06	+0.14	+1.63	+0.13	+0.39	+2.0	+2.86	+1.49
E^5_{rms}	+1	+0.05	0.0	+0.14	0.0	-0.13	+1.57	0.0	0.0	+1.49
E^6_{rms}	+1	-0.16	+0.18	-0.14	-0.63	+1.03	-1.08	-2.0	-5.71	0.0
S	+1	-1.02	0.0	-1.01	-1.0	0.0	-0.98	-2.0	-2.86	-1.49
K	+1	+0.01	-0.04	+0.01	+0.01	0.0	+0.01	0.0	0.0	0.0
$\gamma_{z_p z_Q}$	+1	+0.05	0.0	+0.14	-0.13	-0.13	-1.77	0.0	-2.86	+1.49
$\gamma_{z_Q z_R}$	+1	+0.21	+0.01	+0.05	-1.63	+0.13	-0.19	0.0	-0.71	+1.49
$\gamma_{z_p z_R}$	+1	-0.16	+0.18	-0.08	+0.13	0.0	+0.69	-2.0	+2.86	0.0

It is not unusual in hot-wire anemometry to have the mean velocity components and turbulence quantities that are measured, be quite sensitive to changes in mean hot-wire voltage. For interpretive purposes, the mean hot-wire voltage variations can be thought of as being either errors in measuring the mean voltage, or shifts in the individual wire calibrations due to contamination or strain 'aging' of the wire. The data of Table 2 demonstrate that the most serious inaccuracies in the measurement and data reduction technique will be in the estimates of turbulent shear stresses, the most inaccurate output term being $u'w'$.

As already discussed in Section 3, an *ad hoc* assumption is made regarding the numerical values of the correlation coefficients used in the deduction of time-mean and turbulence quantities. The results of the sensitivity analysis (Table 2) show the time-mean and turbulence quantities to be relatively insensitive to variations in the correlation coefficients. Therefore, the major *ad hoc* assumption made in the technique does not seem to have a great effect on the output quantities compared to the effect of other input quantities.

As mentioned earlier, turbulence quantities (the output) can be calculated from six combina-

tions of data from adjacent wire orientations. One measure of the uncertainty in the output quantities can be obtained by examining the variance in these quantities calculated from the six different position combinations. Table 3 shows these comparison data for a representative position in the flowfield.* For each of the output quantities, an ensemble mean \bar{x} is calculated together with an ensemble standard deviation σ . The ratio σ/\bar{x} is a measure of the uncertainty in the output quantity. In this table, NR stands for 'not resolved', a problem that occurs when the data reduction program attempts to take the square root of a negative quantity. In addition, quantities which are more than three standard deviations outside the mean are rejected as spurious calculations.

TABLE 3
Scatter Among the Turbulence Quantities When Solved by Six Different Combinations

TURBULENCE QUANTITY	TURBULENCE QUANTITY SOLVED BY SIX COMBINATIONS						MEAN \bar{x}	STANDARD DEVIATION σ	σ/\bar{x}
	1,2,3	2,3,4	3,4,5	4,5,6	5,6,1	6,1,2			
\bar{u}/U_0	0.21	0.20	0.21	0.21	0.19	0.18	0.20	0.01	0.06
\bar{v}/U_0	0.19	NR ^a	0.11	0.17	0.17	0.17	0.14	0.04	0.26
\bar{w}/U_0	0.40	0.39	0.39	0.38	0.37	0.40	0.39	0.01	0.03
u'_{rms}/U_0	0.14	0.14	0.14	0.07	0.08	0.08	0.11	0.03	0.31
v'_{rms}/U_0	0.06	0.11	0.11	0.08	0.08	0.09	0.09	0.02	0.23
w'_{rms}/U_0	0.13	0.16	0.10	0.11	0.10	0.12	0.12	0.02	0.20
$u'v'/U_0^2$	NR ^a	NR ^a	0.012	NR ^a	0.005	0.004	0.007	0.004	0.62
$u'w'/U_0^2$	0.002	0.010	0.002	0.004	0.004	0.008	0.005	0.003	0.72
$v'w'/U_0^2$	0.003	NR ^a	0.003	0.003	0.007	0.001	0.003	0.002	0.58

* Not Resolved

The data in Tables 2 and 3 can be used to produce estimates in the uncertainties of the calculated turbulence quantities. The data suggest that uncertainties on the order of 5 percent are to be expected in the mean velocity component estimates. Normal turbulent stress estimates (u'_{rms} , etc.) have uncertainties on the order of 20 to 30 percent and turbulent shear stress estimates are significantly higher, although most of this is a consequence of taking a product of terms such as u' and v' .

These uncertainty estimates are considered to be somewhat conservative. More accurate estimates are quite difficult to obtain because, to our knowledge, similar measurements have not been performed with any other instrumentation system in this geometry flowfield. Also, comparisons of several representative points with independent measurements suggest that the ensemble averages estimates are typically in closer agreement than are selected sets of three orientations. Therefore, all turbulence estimates presented in this paper are calculated from ensemble averages of six groups of three adjacent wire orientations. Any data not resolved are not included in this averaging. This approach represents a departure from the technique developed by King¹⁸ who typically

* $x/D=1.5$, $r/D=0.25$, $\phi=38$ deg (swirling flow).

ORIGINAL PAGE IS OF POOR QUALITY

selected one group of three orientations from which to calculate his turbulence estimates.

4.2 Results of Flowfield Surveys

Radial distributions of time-mean velocities, turbulent normal stresses and shear stresses are obtained for both nonswirling and swirling conditions, at various axial locations in the flowfield.

Nonswirling Flow. In the confined jet, the experiments have been conducted with expansion angles of 90 degrees (sudden expansion) and 45 degrees (gradual expansion) and the results for both cases are presented in Reference 22. In the interest of brevity, only the data for a 90 degree expansion are presented here.

Figure 7 shows the radial distribution of time-mean axial and radial velocity components at various axial locations. The axial velocity distributions are compared with a similar study performed by Chaturvedi⁵ with a crossed hot-wire probe. Because of the inability of the six-orientation hot-wire technique to determine the sense of the flow direction in a nonswirling flow, the presence of the corner recirculation zone was observed by a sudden increase in the axial velocity closer to the wall.

Figure 8 shows the radial distribution of axial and radial components of the turbulence intensity at various axial locations in the confined jet flowfield. These turbulence intensity components are compared with Chaturvedi's measurements⁵ and reasonable agreement is found. In fact, the agreement in most cases is better than the uncertainty estimates derived from the data reduction sensitivity analysis.

Included on Figure 8 are measured turbulent shear stress component ($\overline{u'v'}/U_0^2$) profiles for the nonswirling confined jet. For the most part, these measurements are in reasonable agreement with those made by Chaturvedi⁵ with a crossed wire probe. The two significant exceptions to the good agreement occur at the furthest upstream and furthest downstream locations. Upstream, at $x/D = 0.5$ the shear layer is very thin and, therefore, matching data from several wire orientations obtained at somewhat different times may be practically difficult. We believe the overly large measured turbulent shear stress on the centerline at the furthest downstream station ($x/D = 3.0$) to be a consequence of the transient nature of the flow. The recirculation regions in the confined jet oscillate somewhat at a low frequency, likely characteristic of the main acoustic modes in the tube. These large scale oscillations can have significant correlated velocity fluctuations (such as $u'v'$).

Swirling Flow The measurements performed in the swirling flow are with $\alpha = 90^\circ$, $\phi = 38^\circ$, and $x/D = 0.5, 1.0, \text{ and } 1.5$. The object of these limited number of experiments was to evaluate the reliability and accuracy of the six-orientation hot-wire technique before making extensive use of the technique.

The hot-wire results in the case of time-mean axial and azimuthal (swirl) velocities shown in Figures 9 and 10, are compared with five-hole pitot probe measurements performed by Rhode³ in the same experimental facility. Agreement among the two studies is fairly good. King¹⁸ suggested a method to determine the sense of the axial velocity. He advised comparing the magnitudes of Z_3 and Z_5 given by Equations 4. In the present flowfield, the swirl velocity is always positive and the two equations giving Z_3 and Z_5 differ only in the sign of axial velocity. Therefore, when Z_5 is greater than Z_3 , the axial velocity is negative, otherwise it is positive. With the proper sense being assigned to the x velocity mean component, the presence of central toroidal recirculation zone is evident in the results of both measurement techniques.

Figure 11 shows the radial distribution of the time-mean radial velocity at various axial locations for a swirl vane angle of 38 degrees and a wall expansion angle of 90 degrees. Flow visualization and five-hole pitot probe measurements performed in Rhode's study³ show the time-mean radial velocity to be negative at axial locations greater than $x/D = 0.5$. In spite of the inability of the six-orientation hot-wire technique to determine the sense of the radial velocity, the data are presented with the appropriate sign change. There is a reasonable agreement among the two studies in measurements of time mean radial velocities except at the initial measurement station.

Figure 12 shows the radial distribution of axial, radial and azimuthal turbulent intensities at three axial locations presented. At axial locations closer to the inlet of the confined jet, the axial turbulence intensity is fairly high, up to 32 percent for $x/D = 0.5$ which is due to the large axial velocity gradients closer to the wall. However, in the case of radial turbulence intensity, the profiles are rather flat. The mean azimuthal velocity also experiences sudden changes in gradients and, hence, the outcome is a large azimuthal turbulence intensity closer to the wall at $x/D = 0.5$.

Figure 13 shows the shear stresses $\overline{u'v'}/U_0^2$, $\overline{u'w'}/U_0^2$, and $\overline{v'w'}/U_0^2$ as a function of radial and axial distance. The sensitivity analysis showed that we should expect large uncertainties associated with evaluation of turbulent shear stresses using the six-orientation technique. Therefore, the reliability of the profiles of these shear stresses shown in Figure 13 is uncertain at this time. Nevertheless, stresses $\overline{u'v'}/U_0^2$ and $\overline{u'w'}/U_0^2$ are found to have large values closer to the wall that one would expect due to steep axial and azimuthal velocity gradients. The fact that we have found no other measurements of this type in a swirling, recirculating flow attests to the fact that accurate measurements in such a flow are quite difficult.

Closure

The six-orientation hot-wire technique is a relatively new method to measure time-mean velocity components and turbulence quantities in complex three-dimensional flowfields. Applied in

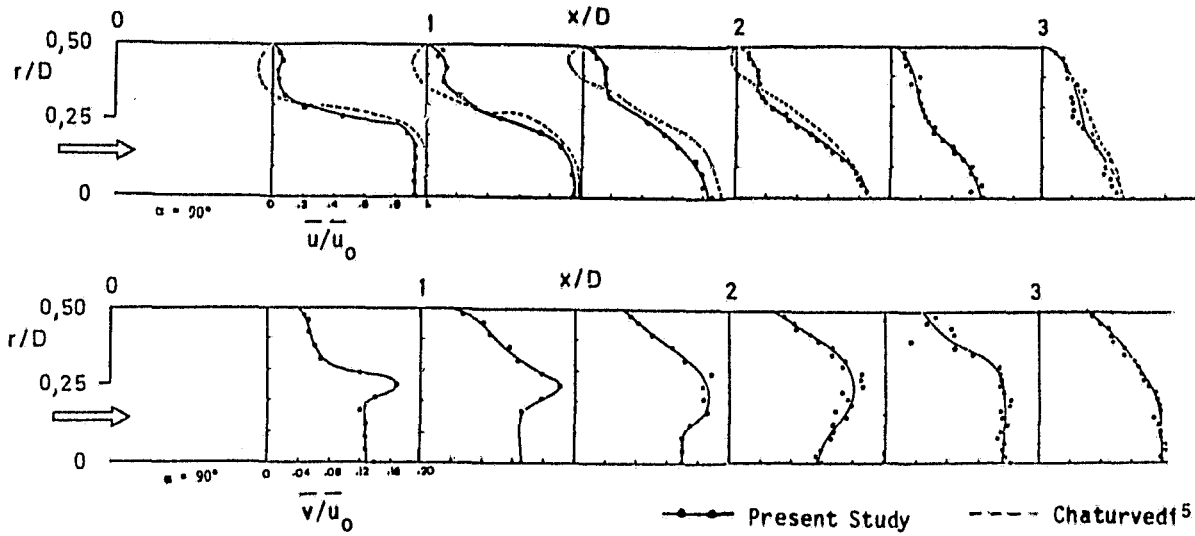


Figure 7. Radial Distributions of Time-Mean Axial and Radial Velocity Components in the Non-Swirling Confined Jet; (Note the Difference in Velocity Scales)

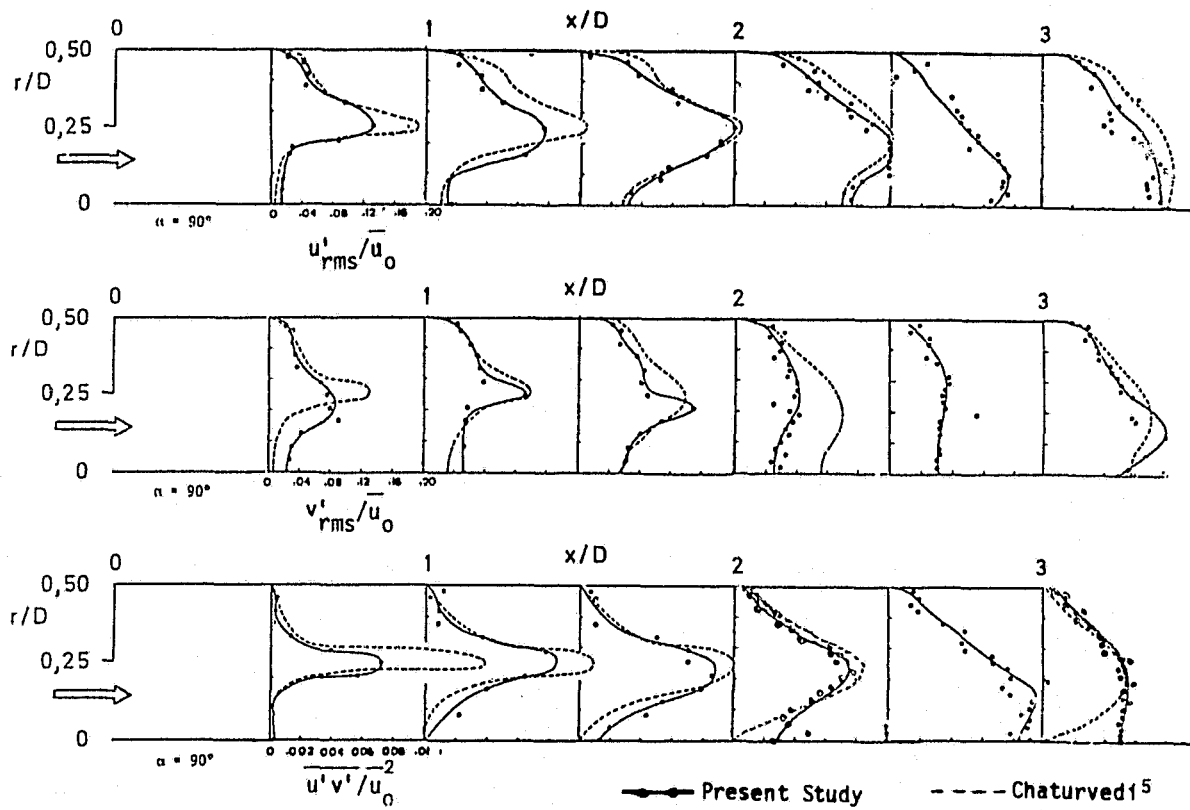


Figure 8. Radial Distributions of Turbulent Intensities $\frac{u'_{rms}}{\bar{u}_0}$, $\frac{v'_{rms}}{\bar{u}_0}$ and shear stress $\frac{u'v'}{\bar{u}_0^2}$

ORIGINAL PAGE IS
OF POOR QUALITY

- Present Study
- △ Rhode et al³
(5-hole pitot probe)

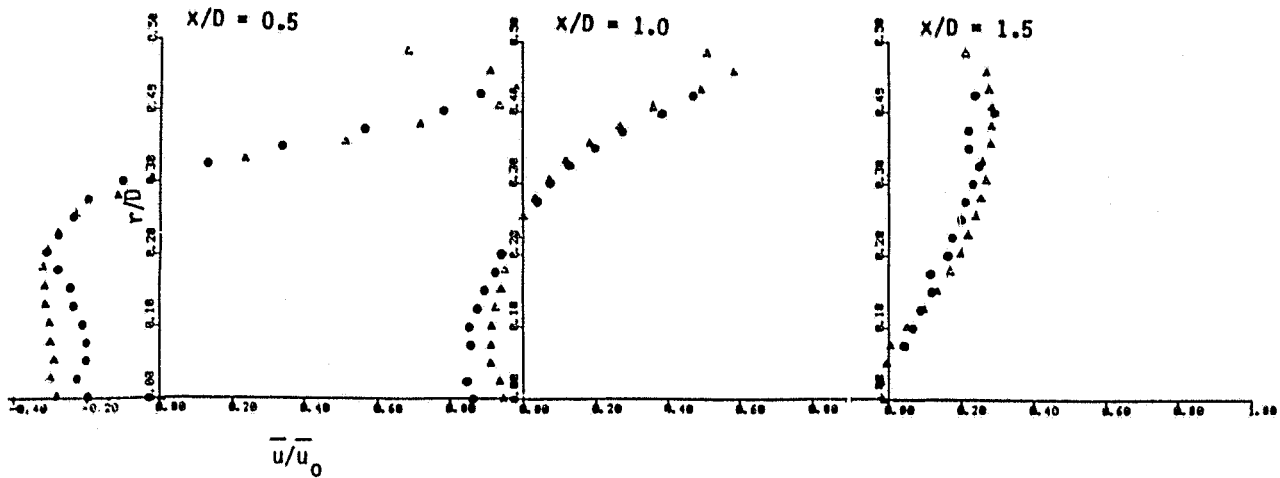


Figure 9. Radial Distribution of Time-Mean Axial Velocity in Swirling Confined Jet for $\alpha = 90^\circ$ and $\phi = 38^\circ$

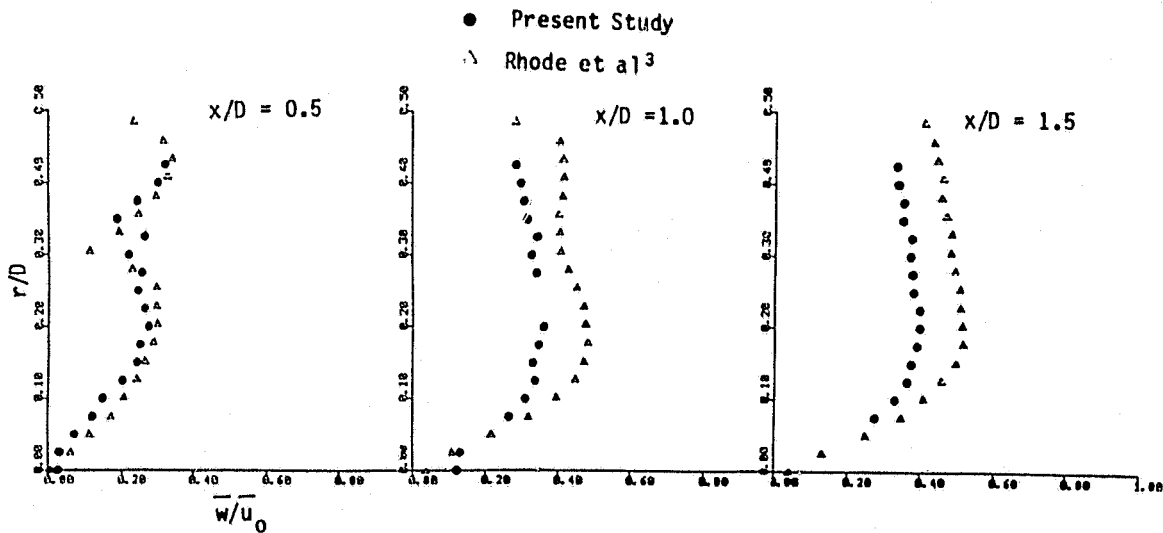


Figure 10. Radial Distribution of Time-Mean Azimuthal Velocity in Swirling Confined Jet for $\alpha = 90^\circ$ and $\phi = 38^\circ$

this study to nonreacting axisymmetric flowfields, measurements of time-mean and root-mean-square voltages at six different orientations contain enough information to obtain the time-mean velocities, turbulence intensities and shear stresses. At each location in the flow, there are six different values of each of the above quantities that can be obtained using six sets of measurements of three adjacent orientations. Ensemble averages of the output quantities from the six combinations of data appear to produce estimates with the best agreement with independent measurements.

Flowfield surveys of both swirling and non-swirling confined jets have been made with the six-orientation single hot-wire technique. These measurements have been used to calculate estimates of the mean velocity components and the normal and shear turbulent stresses. Where independent data exist, comparisons have been made which demonstrate the reliability of the technique.

In addition, a sensitivity analysis of the data reduction technique has been conducted which

ORIGINAL PAGE IS
OF POOR QUALITY

forms the major ingredient in the uncertainty analysis. It is demonstrated that the largest uncertainties are to be expected in the turbulent shear stress estimates. Nevertheless, in non-swirling flows the measured shear stresses are in reasonable agreement with previous measurements made with a crossed-wire probe. In swirling flow, previous similar measurements have not been found. Consequently, the universal accuracy of the mea-

sured technique applied to swirl flows is still an open question.

Acknowledgement:

The authors wish to extend their sincere gratitude to NASA Lewis Research Center and the Air Force Wright Aeronautical Laboratories for support under Grant No. NAG3-74.

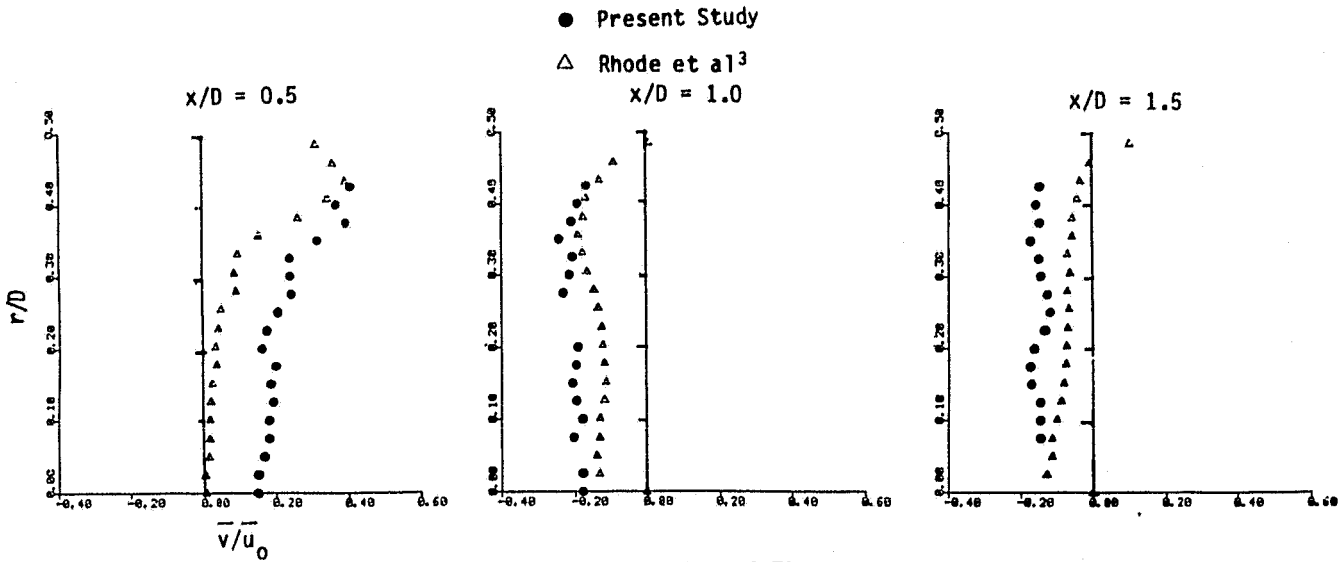


Figure 11. Radial Distribution of Time-Mean Radial Velocity in Swirling Confined Jet for $\alpha = 90^\circ$ and $\phi = 38^\circ$

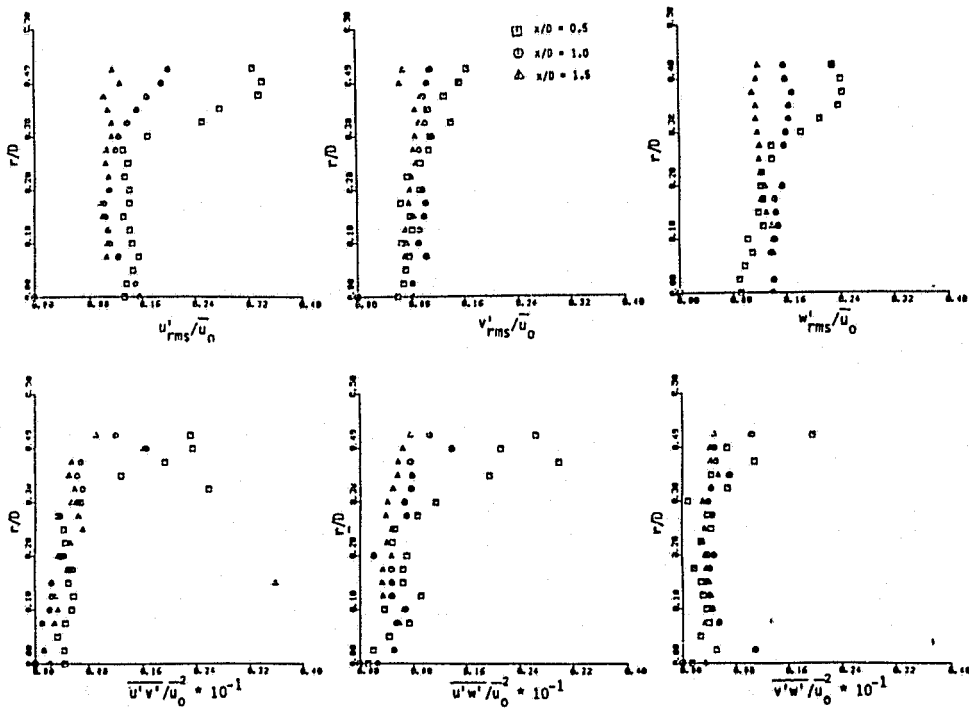


Figure 12. Radial Distribution of Turbulent Shear Stresses $\overline{u'v'}/u_0$, $\overline{u'w'}/u_0$, and $\overline{v'w'}/u_0$ in Swirling Confined Jet for $\alpha = 90^\circ$ and $\phi = 38^\circ$

References

- ¹ Lilley, D.G., "Flowfield Modeling in Practical Combustors: A Review," Journal of Energy, 3, No. 4, 1979.
- ² Lilley, D.G. and Rhode, D.L., "A Computer Code for Swirling Turbulent Axisymmetric Recirculating Flows in Practical Isothermal Combustor Geometries," NASA Contractor Report 3442, February 1982.
- ³ Rhode, D.L., Lilley, D.G. and McLaughlin, D.K., "Mean Flowfields in Axisymmetric Combustor Geometries with Swirl," AIAA Paper No. 82-0177, 1982, AIAA Journal (in press).
- ⁴ Krall, K.M. and Sparrow, E.M., "Turbulent Heat Transfer in the Separated, Reattached, and Redevelopment Regions of a Circular Tube," Journal of Heat Transfer, pp. 131-136, February 1966.
- ⁵ Chaturvedi, M.C., "Flow Characteristics of Axisymmetric Expansions," Proceedings, Journal of the Hydraulic Division, ASCE, 89, No. HY3, pp. 61-92, 1963.
- ⁶ Phaneuf, J.T. and Netzer, D.W., Flow Characteristics in Solid Fuel Ramjets, Report No. NPS-57Nc74081. Prepared for the Naval Weapons Center by the Naval Postgraduate School, Monterey, California, July 1974.
- ⁷ Back, L.H. and Roschke, E.J., "Shear Layer Flow Regimes and Wave Instabilities and Reattachment Lengths Downstream of an Abrupt Circular Channel Expansion," Journal of Applied Mechanics pp. 677-681, September 1972.
- ⁸ Roschke, E.J. and Back, L.H., "The Influence of Upstream Conditions on Flow Reattachment Lengths Downstream of an Abrupt Circular Channel Expansion," Journal of Biomechanics, 9, pp. 481-483, 1976.
- ⁹ Ha Minh, H. and Chassaing, P., "Perturbations of Turbulent Pipe Flow," Proceedings, Symposium on Turbulent Shear Flows, Pennsylvania State University, pp. 13.9-13.17, April 1977.
- ¹⁰ Moon, L.F. and Rudinger, G., "Velocity Distribution in an Abruptly Expanding Circular Duct," Journal of Fluids Engineering, pp. 226-230, March 1977.
- ¹¹ Bradshaw, P., An Introduction to Turbulence and Its Measurement, Pergamon Press, New York, 1971.
- ¹² Beer, J.M. and Chigier, N.A. Combustion Aerodynamics, Halsted Press Division, John Wiley & Sons, Inc., New York, 1972.
- ¹³ Syred, N., Beer, J.M. and Chigier, N.A., "Turbulence Measurements in Swirling Recirculating Flows," Proceedings, Salford Symposium on Internal Flows, London, England: Inst. of Mechanical Engineering, pp. B27-B36, 1971.
- ¹⁴ Wagnanski, I. and Fiedler, H., "Some Measurements in the Self Preserving Jet," Journal of Fluid Mechanics, 38, p. 577, 1969.
- ¹⁵ Pratte, B.D. and Keffer, J.R., "The Swirling Turbulent Jet," Journal of Basic Engineering, 94, pp. 739-748, December 1972.
- ¹⁶ Dvorak, K. and Syred, N., "The Statistical Analysis of Hot Wire Anemometer Signals in Complex Flow Fields," DISA Conference, University of Leicester, 1972.
- ¹⁷ Jorgensen, F.E., "Directional Sensitivity of Wire and Fiber Film Probes," DISA Information No. 11, Franklin Lakes, N.J., pp. 31-37, May 1971.
- ¹⁸ King, C.F., "Some Studies of Vortex Devices - Vortex Amplifier Performance Behavior," Ph.D. Thesis, University College of Wales, Cardiff, Wales, 1978.
- ¹⁹ Hinze, J.O. Turbulence, 2nd Edition, McGraw-Hill, New York, 1975.
- ²⁰ Habib, M.A. and Whitelaw, J.H., "Velocity Characteristics of Confined Coaxial Jets With and Without Swirl," ASME Paper 797-WA/FE-21, New York, N.Y., December 2-7, 1979.
- ²¹ Gupta, A.K. and Lilley, D.G., Flowfield Modeling and Diagnostics, Abacus Press, Tunbridge Wells, England, 1982 (in press).
- ²² Janjua, S.I., "Turbulence Measurements in a Complex Flowfield Using a Six-Orientation Hot-Wire Probe Technique," M.S. Thesis, Oklahoma State University, Stillwater, Oklahoma, December 1981.